Author:
Rubio Denniss, Ana

Title:
The dynamic optical micro-environment

an open platform for the closed-loop control of microscale collectives using light

The Dynamic Optical Micro-Enviroment

An open platform for the closed-loop control of microscale collectives using light

By

ANA MARIA RUBIO DENNISS

Department of Engineering Mathematics
UNIVERSITY OF BRISTOL

A dissertation submitted to the University of Bristol in accordance with the requirements of the degree of DOCTOR OF PHILOSOPHY in the Faculty of Engineering.

MAY 2021

Word count: 37,087

Abstract

The of engineering microscopic collectives such as bacteria, mammalian cells and microrobots has implications from the design of novel biomedical therapies to the development of functional materials. Controlling microagent behaviour is challenging however, due to the limited capabilities of individual agents, lack of straightforward programmability and difficulties in visualisation. To address this, the Dynamic Optical Micro-Environment (DOME) has been developed as a low-cost, modular and open-source device for closed-loop light-based control of microagent systems at both an individual and collective level. The DOME offers an accessible means to study complex multiagent phenomena and implement new behaviours with desired functionalities. This work explores the state-of-the-art regarding light-based microagent control and the current hardware landscape for optical control systems. The DOME is presented, with details of the low-cost fabrication process and characterisation of key specifications. Control over microsystem behaviour using light is demonstrated through the implementation of building blocks towards swarm control in a system of light-responsive *Volvox* agents. Future steps explored include the engineering of cellular collectives, such as biofilms and migrating tissue, as well as the potential for integration of machine learning techniques for the discovery of de novo swarm behaviours.

Dedication and acknowledgements

I would like to acknowledge the wonderful friends and family who supported me though trying times, bringing me laughter and joy even in the hardest moments. I also wish to thank my supervisors, Sabine and Tom, whose encouragement and invaluable mentorship will stay with me always. Above all, I dedicate this work to Elaine and Jose, my parents and greatest source of inspiration. Though I wish you were still here to to see that persevered until the end, I take comfort in knowing that you would be proud.

Author's declaration

I declare that the work in this dissertation was carried out in accordance with the requirements of the University's Regulations and Code of Practice for Research Degree Programmes and that it has not been submitted for any other academic award. Except where indicated by specific reference in the text, the work is the candidate's own work. Work done in collaboration with, or with the assistance of, others, is indicated as such. Any views expressed in the dissertation are those of the author.

SIGNED: Ana Maria Rubio Denniss DATE: 18/05/2021

Table of Contents

List of Tables

List of Figures

Figure **Page**

CHAPTER 1

INTRODUCTION

1.1 Introduction

Controlling the behaviour of microscale systems is a challenging but crucial task across numerous fields, from biomedicine to microrobotics. The limited capabilities intrinsic to microagents make the application of traditional engineering practices difficult, often requiring creative solutions to achieve a desired behaviour. One approach is to use external control to influence microsystem dynamics and to enable the emergence of desired behaviours. To facilitate this, the work detailed in this thesis focuses on the design and fabrication of a device for the optical control of microagent systems. This device, known as the Dynamic Optical Micro-Environment (DOME), provides an open-source platform for closed-loop interaction with microagent systems at an individual and collective level. The DOME combines digital light processing with a custom microscopy set-up to facilitate spatiotemporal light-based control with a resolution of 30×30µm, allowing for the delivery of multi-wavelength illumination to many microagents simultaneously and independently. A closed computational feedback loop enables the system to respond dynamically in real time to changes in a microsystem and alter the optical stimulus accordingly. The device costs just £685 to build, and all design files are freely available online as an open-source project along with all calibration code, with the goal of widening accessibility to collective control techniques at the microscale. In this thesis, the capabilities of the DOME are demonstrated through its use in the implementation of building blocks towards collective control of microscale systems, as depicted schematically in Figure 1.1. To do this, *Volvox* colonies were employed as a model microagent system in which to enact augmented signalling and stigmergy communication channels, as well as to demonstrate phototactic motion control.

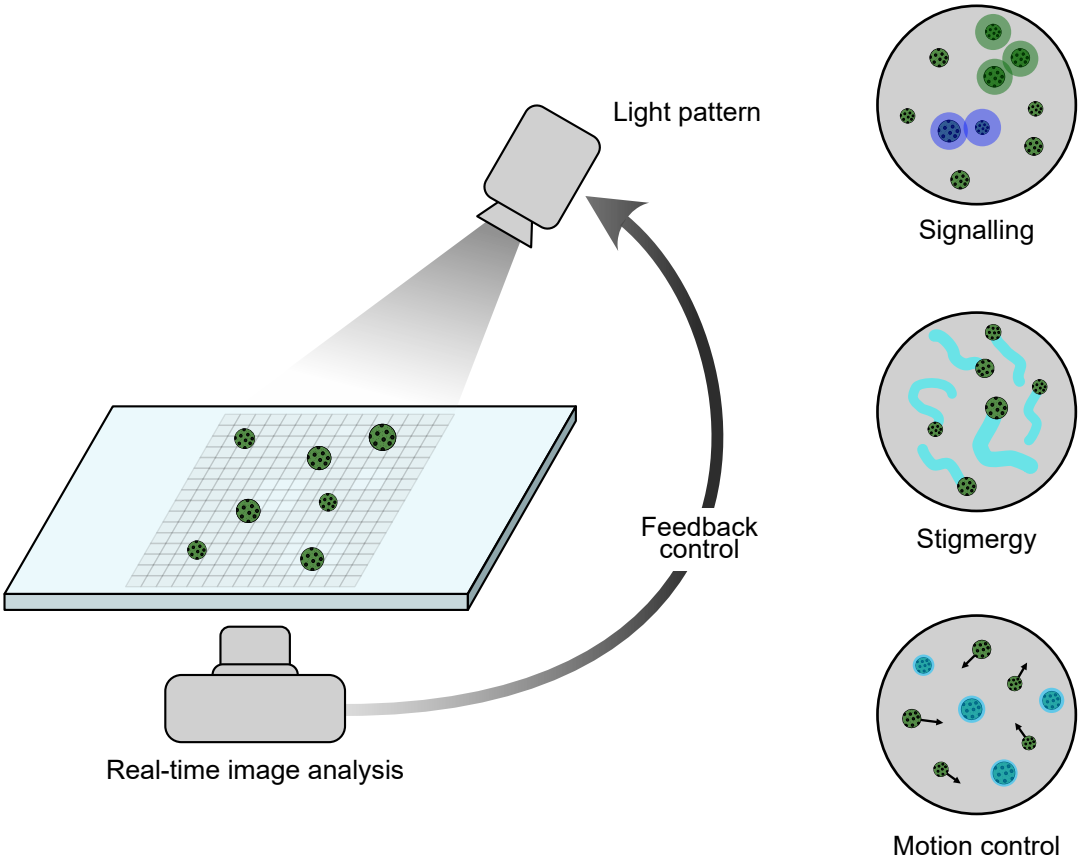

Figure 1.1: **The DOME project.** Schematic representation of the DOME device (left), which provides closed-loop control over microagent systems using localised light patterns. The DOME platform was used in the implementation three building blocks towards swarm control; signalling, stigmergy and motion control (right), all enacted in a living *Volvox* system.

1.2 Motivation

This project was motivated by a desire to control complex microsystems on both an individual and collective level, in this case through the use of light-based interactions. Light is frequently employed as a controller for many types of microagent, yet there is little in the way of unifying technology or practices across this work. In an ever more interdisciplinary research landscape, technological tools that are accessible across specialities are increasingly important. This work aims to provide a platform towards the engineering of microagent systems for the development of novel collective behaviours, and to help widen accessibility to optical control techniques at the microscale.

1.3 Control at the microscale

The ability to engineer the behaviour of microagents such as bacteria, mammalian cells, microparticles and microrobots has wide-reaching implications. For applications such as the design of novel biomedical therapies [89, 278, 356], drug delivery [239, 306, 365], the development of functional materials [15, 184], and environmental remediation [212, 271], the development of effective microagent control strategies is crucial. There are however some significant challenges in the engineering of behaviours at the microscale. These can be summarised as:

1. **Programmability** – In traditional macroscale engineering the actuation, power, and sensing capabilites of an agent are typically achieved using programmable onboard electronic, and computational components. Evidently, these methods are not feasible at the microscale, and so alternative forms of control reliant on various biological, physical and chemical phenomena must be utilised. This is generally achieved through iterative agent design and functionalisation [4, 301, 363] which can be resource intensive, often requiring many rounds of chemical synthesis, molecular engineering or other design processes.

2. **Scalability** – At these very small scales, it is rare for agents to operate solely as individuals. Instead, they tend to form part of wider systems that operate in large numbers such as bacterial colonies [74] or eukaryotic cell collectives [89]. This can make it difficult to develop control processes that are able to address individual agents as well as the collective system, something that is important in the engineering of more complex behaviours.

A step towards addressing the first challenge is to employ an automated external control framework that is capable of controlling microsystems both at a collective and individual level. By providing an external control system, an additional degree of programmability can be lent to otherwise simple agents, allowing the exploration of the conditions and parameters required for the emergence of desired behaviours. To address the second challenge, this system must provide highly localised control in space and time for interaction with individual microagents, and operate an automated, closed-loop scheme to respond rapidly to evolving microsystem dynamics.

1.4 Light as a control mechanism

In the absence of computational programmability, control at the microscale is usually exerted through external methods. Commonly employed techniques are the use of electrical [140, 145], magnetic [102, 359], acoustic [103, 411], or optical [61, 96] interactions to illicit various microagent responses. All these control methods operate in very different ways, and the optimum choice for a given application is fundamentally dependent on the properties of the microagents in question, as well as the desired behavioural outcome. Given that the work detailed here is concerned with the design of a hardware platform for use across many microsystem types, this choice is less

straightforward. Although optical control was ultimately deemed to be the most suitable choice in this context, it is worthwhile to consider the key benefits and potential drawbacks to each. Direct comparisons between different methods are challenging, since important control specifications such as resolution are highly hardware dependent and thus can very significantly. A full review of these methods is outside the scope of this work, however some important characteristics (summarised in Figure 1.2) will be considered here in brief:

- Capability for independent control
- Range of agents that may be controlled through by this method
- Potential damaging effects on agents
- Possibility of multi-channel control using orthogonal control inputs

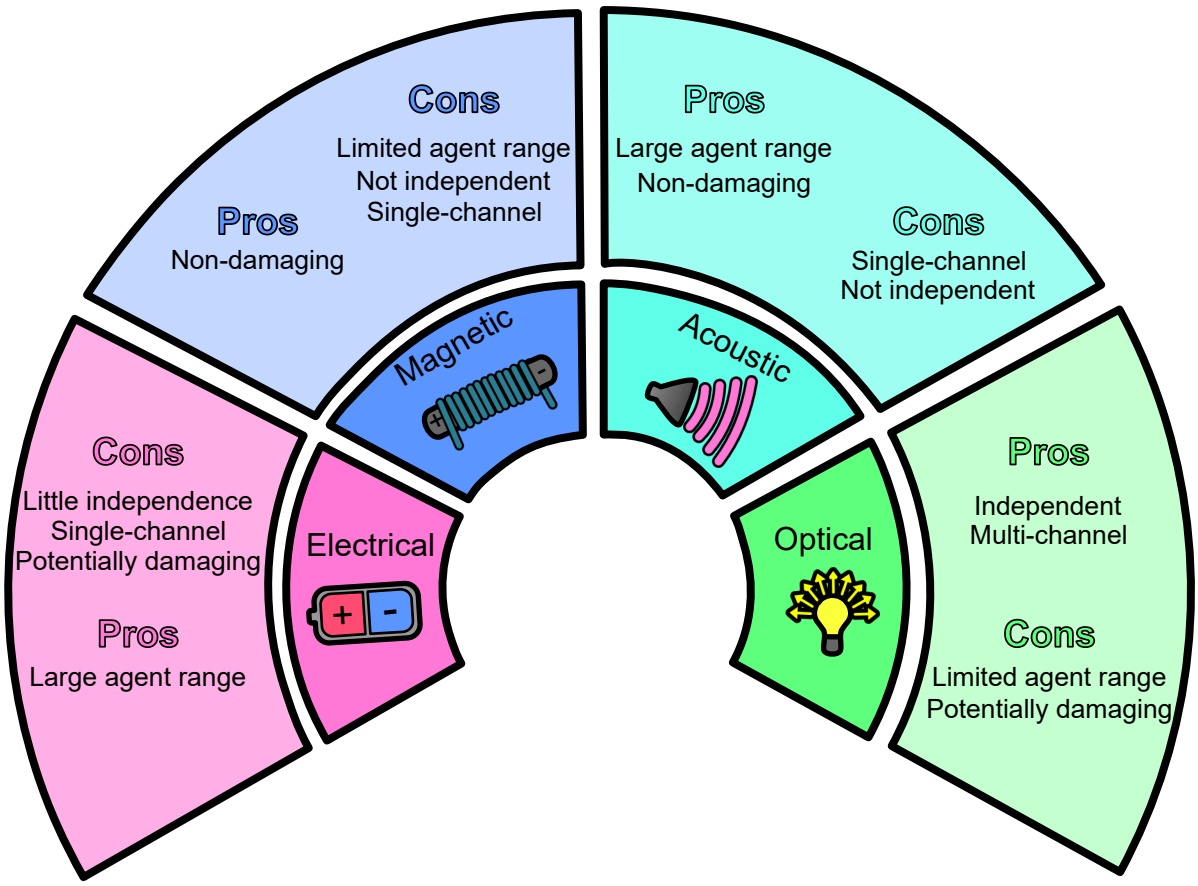

Figure 1.2: **Microagent control methods.** Benefits and drawbacks to commonly employed methods for exerting control over agents at the microscale.

One method of controlling microscale agents is by subjecting them to dielectrophoretic forces generated by the application of non-uniform electric fields [424], through which spatial

manipulation and trapping can be achieved. The specific response of the agent to this force is highly dependent on agent properties such as size, shape and conductivity [316], making dielectrophoresis particularly useful in agent separation and sorting applications [140]. When sufficiently strong electrical fields are applied to organic agents such as bacteria there is the potential for damage to occur. In general however, the field strength required for dielectrophoretic manipulation falls below this level, and thus electric field manipulation is mostly compatible with living biological agents [317]. The use of electric fields to exert control in this way is capable of generating significant local forces that are applicable to a wide variety of organic [264, 329] and inorganic [42, 203] agent types. The primary disadvantage to this method is the difficulty in achieving independent parallel agent control. Although independent control is possible and has been demonstrated, it requires the use of intricate microelectrode arrays and complex control strategies [422].

An alternative control method is the application of magnetic forces, exerted either by an electromagnetic coil or permanent magnet. This is a powerful control mechanism, generating large forces that can result in rapid translational or rotational motion [6]. Magnetic fields are also largely non-damaging to organic matter, making them useful in the context of medicine and biomedical research [143, 436]. Drawbacks to a magnetic control system include the limited agent range, requiring that agents exhibit magnetic properties, as well as the lack of independent control. Given the nature of magnetic fields, it is a great challenge to simultaneously drive multiple homogeneous agents independently, with uncoupled manipulation requiring the use of heterogeneous microagents or techniques such as selective trapping [102, 310, 357].

It is also possible to perform trapping and manipulation of microagents through the use of acoustic waves, with variations in the applied frequency and amplitude resulting in the repositioning of agents in 2 or 3 dimensional space [78, 153]. This technique is highly biocompatible and non-specific, able to work with a wide variety of organic and inorganic agents [103, 220]. However, although parallel control of many agents is possible [297], this control is not independent, and is limited to a single control channel.

For optical control, there are many interaction types that are not tied to direct physical manipulation. Although trapping and manipulation from optical forces is a well established technique [21, 68, 259], many optical control systems instead operate using light as a means to induce some secondary control processes. This is made possible by the many light-responsive mechanisms that exist at the microscale in both organic and inorganic systems, including phototaxis and the generation of local heating. In the case of manipulation via optical forces, a wide range of microagents types may be used, as control is exerted by photonic momentum, however control schemes become complex for agents of larger size [13], non-spherical shape [45] or high-motility [377]. Additionally, high light intensities are required which necessitates the use of focused laser beams and can have damaging effects in some circumstances [39, 325]. Outside of optical trapping, implementations of optical control rely on the use of light-responsive

agents [303] or substrates [385] and thus have a degree of specificity in terms of compatible microsystems. Despite this, there are significant benefits to light-based control, namely the high resolution attainable and the capability for independent agent control. Using high resolution light patterning techniques, many agents can be controlled simultaneously and independently, with maximum resolution dictated by the diffraction limit of the light delivery system used. An additional advantage of optical control compared to the other methods discussed is the capacity for multi-channel control. This means that for microsystems with more than one wavelength specific photoresponse [5, 60, 177], multi-wavelength illumination can facilitate the realisation of multiple orthogonal control modes using a single system. A possible drawback to optical control is the potential for damage, particularly for biological agents through the destructive interaction of light with DNA.

Ultimately, of the control methods considered here, optical control was deemed to be the most suitable around which to develop a control device. Specifically, an optical control scheme for parallel manipulation of light-responsive agents using secondary processes was chosen, as opposed to optical force based direct manipulation. The deciding factor was largely the capability for high resolution and independent agent control compared to other control methods, as this is crucial for achieving the individual and collective level control required. The capacity for multi-channel control is also appealing, as it could allow for the development more complex control schemes, particularly for systems that undergo a reversible change under different light wavelengths. In terms of the potential for agent damage, this typically requires very intense levels of light, and is more common in the UV range than for visible light. The risk of this occurrence can thus be greatly minimised through the selection of appropriate light wavelengths and the modulation of overall intensity. The issue of agent specificity is also much less problematic than for other control methods, such as magnetic manipulation, owing to the abundance of light-responsive processes that occur at the microscale. Some mechanisms by which light can be converted into useful processes for microagent control are represented in Figure 1.3.

One such mechanism is the photothermal effect, through which a material absorbs light and converts it into thermal energy. Incident photons cause the excitation of electrons within the material, which ultimately releases this extra energy as heat. This can be harnessed for the purpose of microagent manipulation in a number of ways, including the deformation of polymer microrobots [303, 370] and the self-propulsion of micromotors by way of local temperature gradient [117, 417]. Photothermal nanoparticles are also used in medical therapies, most commonly for the targeting of tumours through local heating [186]. A second light-responsive mechanism is photochromism, the reversible transformation of a molecular structure between two isomers occurs due to optical stimulation. This can be utilised to effect changes in properties of the bulk material such as conductivity, refractive index or morphology [427]. In particular, photochromic polymers have been widely adopted in the design of soft microrobots owing to their ability to reversibly deform as a response to incident light [23, 130, 284].

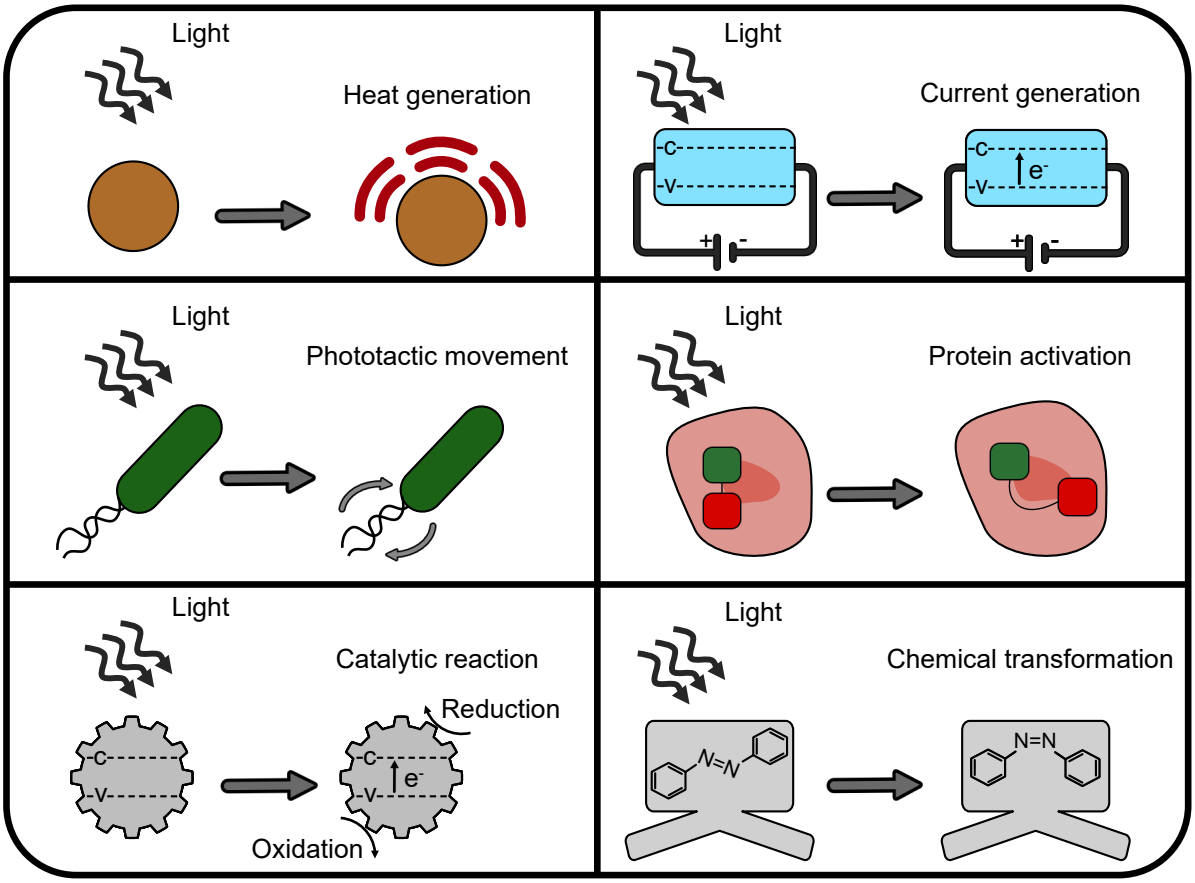

Figure 1.3: **Mechanisms for light conversion.** Non-exhaustive list of mechanisms by which light can be converted at small scales. Included here are heat generation, current generation, phototactic movement, protein activation, catalytic reaction and chemical transformation.

Another light reactive phenomenon is photoconductivity, in which the electrical conductivity of a material increases due to the absorption of light. Many crystalline semiconducting materials posses photoconductive properties and hence are commonly used in light-sensitive devices such as photodetectors and photoresistors [318]. In these materials, the absorption of photons causes electrons to be promoted across the energy gap, from valance to conduction band, where they are able to contribute to the overall conductivity. In the context of microagent manipulation, the primary application of this is for the construction of optoelectronic devices, which use light to locally enhance the conductivity of a photoconductive substrate. This allows for a hybrid control scheme in which light is used to induce dielectrophoresis, typically with a greater level of independence and spatial resolution than is possible with electric fields alone [61, 385]. Photocatalytic reactions operate in a somewhat similar way, with the absorption of light triggering the promotion of electrons to the conduction band, leaving behind holes in the valance band. In a photocatalyst, the electron-hole pairs then migrate to the surface to participate in redox reactions with the surrounding medium, which can be used as a microagent power source [417].

Phototaxis is a light-responsive biological process that can manifest in different ways across a variety of microorganisms. Broadly, the term describes the movement of a living agent in response to light illumination, usually directionally towards or away from the source [190]. This can be observed across many types of organisms, both prokaryotic and eukaryotic [154, 323], and thus there is no singular way in which to describe the phototactic process. Commonly however, phototaxis in flagelleated microorganisms occurs when a change in light intensity leads to some variation in the beat pattern of the flagella [101, 108, 128, 410]. Phototaxis is useful for microagent control not only in terms of direct manipulation of phototactic microorganisms [218, 351], but also through the use of these agents a source of power and actuation within bio-hybrid microsystems [32, 355, 366]. Another way to interact optically with cellular systems is through the use of photoactivatable proteins, including optogenetic techniques [163, 420]. This can facilitate precise, optically-mediated control over biological processes such as velocity regulation and cellular signalling [394, 428].

Given the numerous light-responses detailed here, optical interaction as a means for developing control strategies applicable to many microagent types is highly feasible. In addition to the many microagent types that are directly light-responsive, optical control can also by applied to non-responsive microsystems through secondary interaction means, such as the use of light reactive substrates.

1.5 Democratisation of optical control techniques

While the primary goal of this work is the development and demonstration of a device for the optical control of microscopic agents and collectives, a secondary driving motivation is widening accessibility to these control techniques. The development of hardware for closed-loop optical control is not trivial, requiring the integration of optical, electronic and computational components. Implementations of optical control schemes in literature often employ entirely custom built set-ups specific to a particular application [131, 302, 324, 366], and although a number of reproducible platforms have been proposed [53, 64, 218, 224, 340, 369] little exists in terms of truly open-source hardware. The extent to which localised, closed-loop optical control has been adopted is therefore currently limited by the expertise and resources required to develop or recreate the appropriate hardware. Widening the accessibility of these control techniques could have significant implications across fields such as optogenetics [121, 205], microrobotics [303, 417], synthetic biology [227, 237], and optoelectronics [385, 430], which frequently employ light as a controller, but rarely the type of closed-loop spatiotemporal control scheme described here.

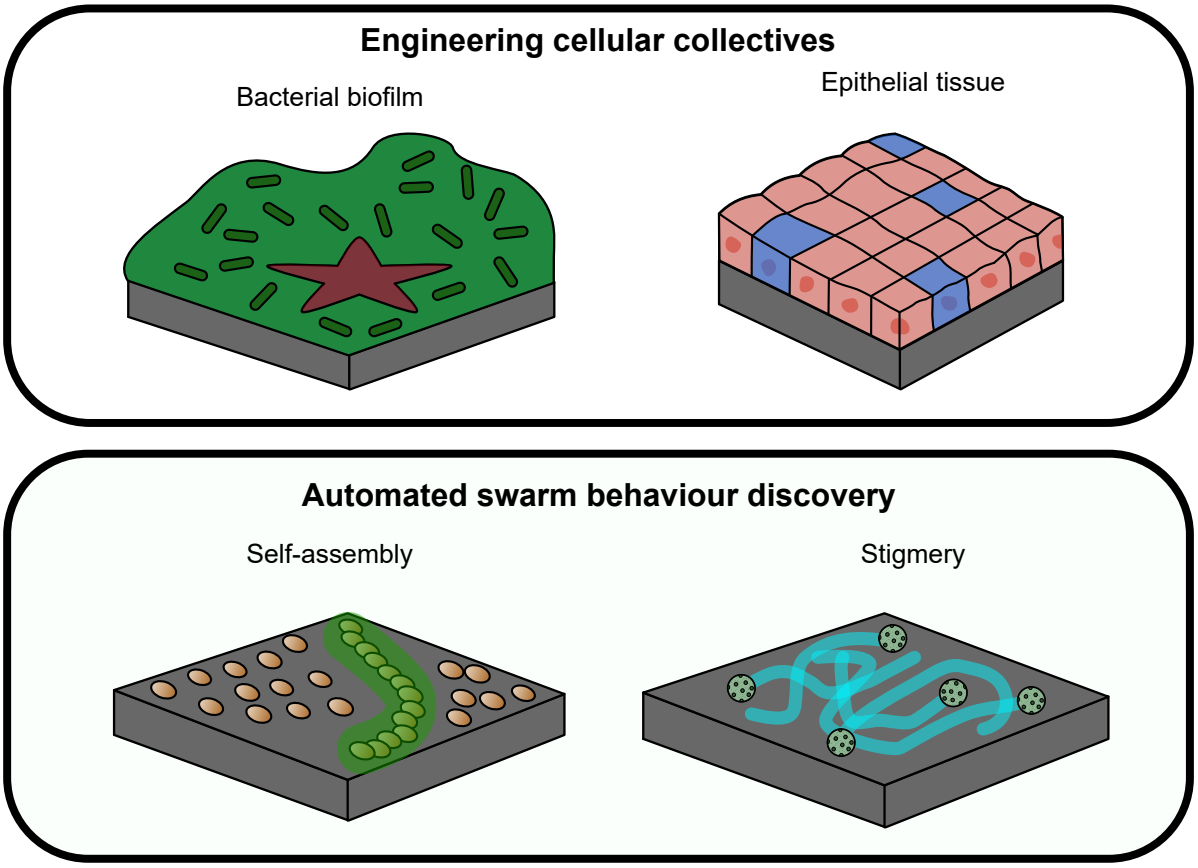

Figure 1.4: **Applications of closed-loop, localised optical control.** Two proposed applications; the engineering of cellular collectives such as biofilms and epithelial tissue, and the automated discovery of swarm behaviours such as self-assembly and sitgmergy in microagent systems.

1.6 Applications of collective control

To demonstrate the utility of a device capable of both individual and collective optical control, two potential applications are proposed in Figure 1.2. The first is the study and engineering of cellular systems which naturally act as collectives, such as biofilms [275], migrating epithelial tissue [335] and particular tumour environments [89, 133]. In systems such as these, local changes are capable of affecting the state of the system as a whole through various communication and competition channels. In order to fully understand these processes and the dynamics with which they may play out in real world environments, the ability to target individual cells is beneficial. Optical interaction is a widely employed technique for interacting with systems such as these through engineered optogenetic processes [46, 185, 271], or innate light responses [126, 146, 327]. However, in many instances this interaction is either not dynamic, spatially localised or parallelisable. Combining these optical interactions with a more sophisticated control scheme could allow for the collective dynamics of cellular systems to be better understood, and

reengineered.

The capability for closed-loop control also offers opportunities for automated study and engineering of microagent behaviour. In particular, this could be applicable to the engineering of swarm behaviours in microscale systems, an avenue of interest in fields such as drug delivery [161, 399] and microassembly [244, 361]. Swarm engineering takes inspiration from the collective behaviours that emerge in particular animal and insect groups through local interactions, and seeks to apply the same principles to artificial systems [138, 409]. In swarm robotics, agents are typically equipped with local sensing and communication capabilities that are facilitated by electronic components and computational control. When engineering swarm behaviour in a robotic collective with computational programmability, control parameters can be discovered and optimised through iterative algorithmic processes. The use of machine learning techniques further streamlines this process, removing the need for human intervention at every stage. In comparison, attempts to engineer similar behaviours in the types of microsystems discussed require careful iterative agent design and functionalisation owing to the limited capabilities and lack of straightforward programmability of agents. The significant human involvement and expenditure of consumable resources can make this process slow and resource intensive. As an alternative to this, the use of a closed-loop control system capable of interacting with individual agents could provide an external control framework for automated discovery of swarm behaviours in a microsystem. This could facilitate the exploration of parameters that lead to the emergence of swarm behaviours, providing a base of knowledge for the the design of new microswarm systems. Furthermore, a system for controlling microagent systems in a manner analogous to methods traditionally employed at the macroscale could allow for greater translatability of swarm engineering techniques across scales.

1.7 Thesis overview

A review of the literature is presented in Chapter 2 with specific focus on light based control of microagents and microagent collectives, as well as the state-of-the-art relating to optical control devices. Following this, Chapter 3 introduces the DOME, detailing fabrication, calibration and algorithmic control processes and presenting the results of characterisation tests. Chapter 4 then provides a discussion of swarm control across scales, and presents a number of building blocks towards collective behaviours at the microscale, implemented on the DOME using *Volvox* as a model microagent. Finally, Chapter 5 explores the potential of the DOME in future work, laying out some specific applications of the device.

Key contributions

- An overview of the state-of-the-art in light-based control of microagents and microscale collectives was completed.

- A new device called the Dynamic Optical Micro-Environment (DOME) was developed as an open-source platform for spatiotemporal control of microscopic collectives. The device provides 30×30μm resolution and can be built for under £700 using accessible fabrication techniques.
- Building blocks towards the engineering of swarm behaviour in microsystems were implemented on the DOME using *Volvox* colonies as model microagents.
- Discussion and preliminary work towards collective control of microagents using the DOME was carried out.
- Two papers were produced; "Augmented reality for the engineering of collective behaviours in microsystems" [92] and "An open platform for high resolution light-based control of microscopic collectives" [93].

CHAPTER 2

BACKGROUND

2.1 Introduction

At the microscale, light is capable of eliciting a vast array of responses, making it an incredibly versatile control mechanism. Many organic systems naturally exhibit light reactive tendencies, and many more hold the potential for synthetically engineered responsive behaviours. Inorganic systems may also react to light, for instance through the generation of current, local heating, or alterations to molecular alignment. This review will focus on the use of the light-responsive mechanisms discussed in Section 1.4 for the control of microagents. Examples of light-based control are spread across many disciplines, from robotics to synthetic biology and beyond. Consequently, reviews of optical control techniques and implementations are often limited to a particular subject area [303, 375, 402, 417]. Instead, this review aims to provide a broad overview of optical control across all disciplines. This will be limited to the use light-based interactions for microagent control, and will not include examples of alternative mechanisms such as magnetic manipulation or acoustic trapping. This review also does not set out to cover all possible interaction mechanisms with any given agent group, rather it is concerned specifically with spatiotemporal control and the potential this provides in engineering collective microsystems. Consequently, only examples of light-based control with spatial responses will be considered withing the scope. This could include movement in space or a spatially heterogeneous response but would exclude instances of a static system responding uniformly to light, such as light mediated expression of microbial fluorescence [199, 395], unless spatially selective [227]. Additionally, a review of the state-of-the-art for closed-loop optical control hardware is provided. This covers set-ups and devices that provide localised and dynamic interaction options, and that can allow independent control of multiple agents simultaneously.

To begin, light-based control of microagent types will be explored, followed by uses of optical

interaction in the context of engineering collective behaviour within microsystems. Finally, the experimental set-ups and devices which have been used to achieve localised light control over microagents systems will be detailed and compared.

2.2 Light-based microagent control

In this section, different techniques for light-based control of microagents will be discussed. This will consider the optical interaction mechanisms covered in Section 1.4 as applied to various agent types including bacteria, mammalian cells, polymer microrobots and micromotors. By focusing on control techniques rather than individual mechanisms or agent type, this section aims to explore the common threads that tie together work in light-based manipulation across many disciplines.

2.2.1 Phototatic microorganism control

The migration of an organism towards or away from a light source, known as phototaxis, is observed in both prokaryotes and eukaryotes [190, 323] and provides an in-built control mechanism for a variety of microorganisms. These organic microagents, driven by genetic circuits and biochemical interactions that have evolved over millions, or even billions of years typically demonstrate a higher level of complexity than their inorganic counterparts. Owing to this, as well as the capability of many microorganisms for autonomous movement, there is considerable interest in microorganisms as programmable microrobots [116]. As was touched upon in Section 1.4, among prokaryotes alone there are a wide variety of underlying biological processes that lead to phototactic behaviour [190, 408]. In many cases, prokaryotic phototaxis is the result of a biased random walk through the run and tumble motility mechanism that allows for gradient following [17, 289, 364]. This is not true of all phototactic bacteria, for example the non-flagellated cyanobacteria exhibit light reactive gliding motility and are even able to sense directionality as they act as spherical microlenses [56]. This directional light sensing was demonstrated by Schuergers et al. with the migration of *Synechocystis* cells towards an illumination source [351]. The light reactive motility of cyanobacteria is an example of naturally occurring phototaxis, however many commonly studied prokaryotes, such as *Escherichia coli* (*E. coli*), do not exhibit photoreactive behaviour. Nevertheless, advances in synthetic biology have made it possible to synthetically engineer light sensors in bacterial cells [237]. In one instance, a blue light-regulated genetic circuit was developed by Zhang et al. to control motility in *E. coli* [426], demonstrating the ability of the cells to perform aggregation and pattern formation based on synthetic negative phototaxis as seen in Figure 2.1A.

Phototactic responses are also found in eukaryotes, with mechanisms similarly varying between species. As with their prokaryotic counterparts, there are examples of light responses for both flagella [34] and gliding-based motility [286] which can be used to exert control over eukaryotic agents. In one such case, a gliding phototactic algae, *Porphyridium purpureum*, was

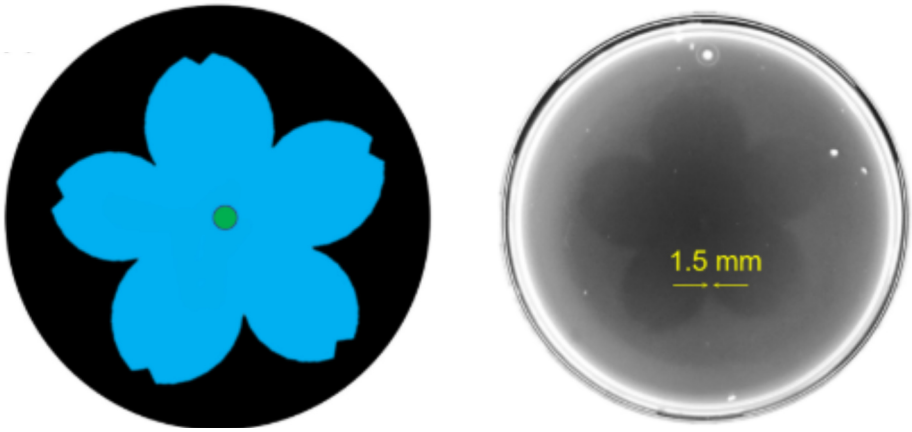

A

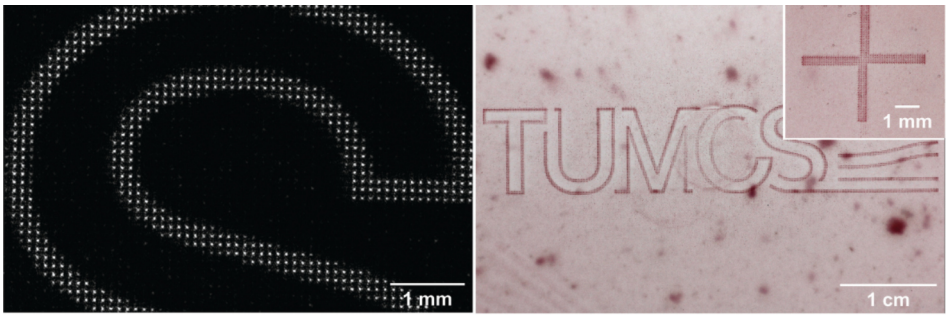

B

Figure 2.1: **Phototatic microorganism control. (A)** Sakura pattern formation by modified *E. coli* cells with a resolution of around 1.2 mm. Adapted with permission from [426] © 2020 Elsevier. **(B)** Partial image of the light pattern used for illumination (left) and the formation of the letters 'TUMCS' by *Porphyridium purpureum* after 8 days of illumination (right). Adapted with permission from [208] © 2020 Springer Nature.

used by Klotz et al. to produce patterned images using spatially structured light stimuli, shown in Figure 2.1B [208]. Spatiotemporal control over a phototactic flagellated algae, *Euglena gracilis*, was also demonstrated in work from Lam et al. that illustrated the viability of algae as a light-responsive active swarm microagent [218].

2.2.2 Biohybrid phototactic systems

The viability of motile light-responsive microorganisms as controllable agents has sparked interest in idea of biohybrid microrobotic systems [4]. Biohybrid microsystems can present in many forms, however the overarching principle is to harness the power of living microorganisms as a way to exert control over inorganic agents [31, 98]. One example of this, presented by Sentürk et el., is the use of *E. coli* as a cargo transport system [355]. Through surface functionalisation

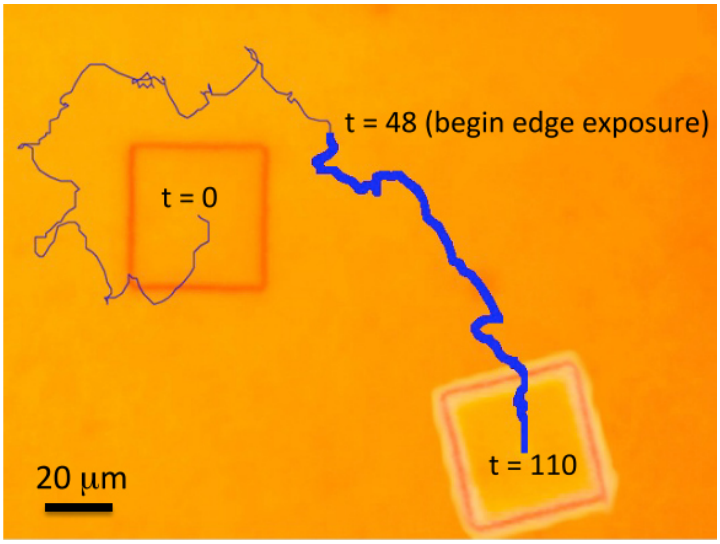

Figure 2.2: **Phototatic microorganism control.** A biohybrid microrobot powered by the phototactic response of *Serratia marcescens* cells is driven by edge exposure to light. Reproduced with permission from [366] © 2015 IEEE.

of the cells and cargo particles, the cells were able to bind to cargo under red light to form a microrobot agent, transport the cargo in space and release under near infared light. Spatial manipulation of a biohybrid microrobot was also demonstrated by Steager et al. using the light-responsive bacterium *Serratia marcescens* (*S. marcescens*) bound to an SU8 plate [366]. Selective illumination of subsections of the plate elicited a phototactic response in the illuminated bacteria, causing a non-uniform application of force across the microrobot that was used to achieve rotational and translational motion (Figure 2.2).

2.2.3 Optogenetics and photoactivatable proteins

In living systems such as bacteria and mammalian cells, it is possible to enact behavioural controlusing light to regulate biological activities and processes. This include optogenetics, the use of light to stimulate a genetic change within a biological system [163, 420, 428]. In contrast to classical genetic techniques, this approach allows precise spatiotemporal manipulation of cellular structures. In addition to optogenetic techniques, the use of photoactivatable proteins can also be used to achieve non-genetic changes, such as velocity modulation [394]. Both of these methods can be used to enact localised control over biological microagent systems to produce a wide array of behavioural outputs [5, 331].

One such example is spatial patterning, which can be achieved through the synthetic regulation of cellular fluorescence [340] and pigment production [227], or by using the cells themselves as patterning agents [193, 265]. In particular, Fernandez-Rodriguez et al. used a synthetically designed genetically encoded system to enable *E. coli* cells to sense and distinguish between red, blue and green wavelengths [123]. This facilitated the production of colour images on a bacterial

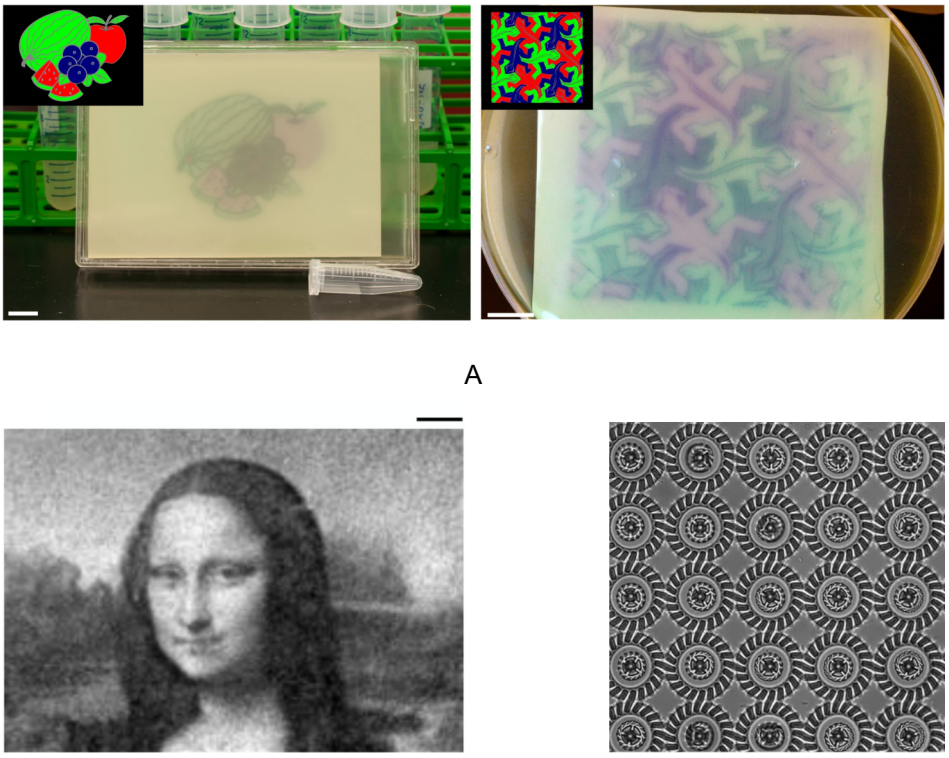

Figure 2.3: **Optogenetics and photoactivatable proteins. (A)** Pigmentation patterns produced by plates of *E. coli* cells by projecting the RGB images shown as insets. Reproduced with permission from [123] © 2017 Nature Publishing Group. **(B)** The Mona Lisa recreated by density patterning of modified *E. coli* cells controlled using projected light. Reproduced from [131] under CC BY–A 4.0. **(C)** Array of 36 rotating microscale motors powered by modified *E. coli* cells. Reproduced from [392] under CC BY–A 4.0.

plate in response to an RBG image projection, an example of which is given in Figure 2.3A. Spatial patterning has also been achieved through the engineering of cell motility, for example through bacterial density shaping demonstrated by Frangipane et al. [131]. In this case, genetically altered *E. coli* were used to recreate well known images such as the Mona Lisa in high resolution, as seen in Figure 2.3B. This was facilitated by the addition of a green-light driven proton pump proteorhodopsin [16, 394] into the cells, which allows light-based velocity control for a freely swimming bacterium. Similarly, *E. coli* cells engineered to express proteorhodopsin were also used by Vizsnyiczai et al. to apply torque to 3D microscale motors, causing them to rotate with speeds proportional to the intensity of incident light [392]. Through the the use of spatial light modulation, they were able to achieve individual control over each biohybrid motor in an array of 36 motors, as depicted in Figure 2.3C.

Light-activation of proteins has also been employed to control motility in mammalian cells by influencing cell migration dynamics [253, 398, 402, 415]. Additionally, in a 'skeletal muscle-

on-a-chip' designed by Sakar et al., a light-activated channel was encoded into skeletal muscle myoblasts [343], allowing for spatiotemporal control over the contraction of the muscle fibers. Optogenetic methods have additionally been used to facilitate programmed cell death, known as apoptosis, in mammalian cells through perforation by the translocation of light-activated proteins [180].

2.2.4 Optoelectronic agent control

The term optoelectronic in this context is used to refer to the control of electric fields using light, in particular for the purpose of microagent control. Most commonly this is achieved using an optoelectronic chip, also known as optoelectronic tweezers or an optoelectrokinetic device. The design of these devices typically consists of photoconductive layer, typically amorphous silicon (a-Hi:H), on an indium tin oxide (ITO)-coated glass substrate onto which the agent medium is placed [230]. A second piece of ITO glass is positioned atop, sandwiching the agents between two electrically conductive layers as shown in Figure 2.4. The ITO layers act as electrodes to which an AC bias potential can be applied, however in the absence of incident light the voltage drop occurs almost entirely across the a-Si:H layer. Upon light illumination, the photoconductivity of the silicon greatly increases, transferring the voltage to the liquid medium. If the light input is localised, this in turn creates a localised non-uniform electric field at the points of illumination. This photoinduced electric field has the effect of polarising microagents suspended within the chip, giving rise to useful phenomena in the context of agent control.

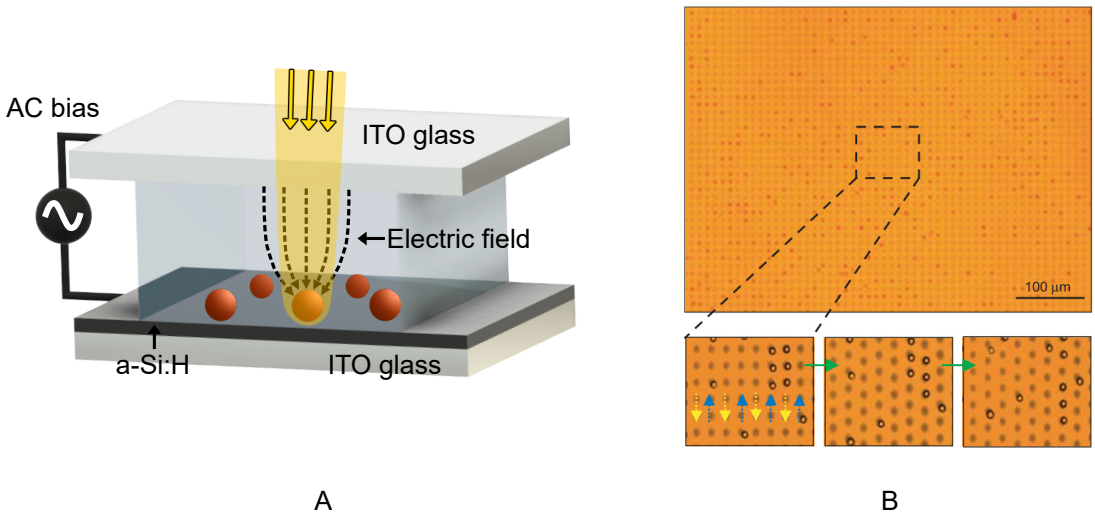

Figure 2.4: **Optoelectronic agent control. (A)** A chip for optoelectronic control in which microagents are suspended in a liquid medium are sandwiched between two ITO electrodes. An electric field can be induced within the medium by altering the photoconductivity of a silicon layer through local light illumination. **(B)** The creation of 15,000 particle traps with a 4.5µm diameter, each able to trap a single polystyrene bead using negative DEP forces. Reproduced with permission from [61] © 2005 Springer Nature.

The most commonly utilised phenomena is dielectrophoresis (DEP), a process by which the electric field interacts with a polarised agent to produce a force. This force may be attractive or repulsive depending on the dielectric properties of the agent [33, 385]. Optically-induced DEP (ODEP) can facilitate the manipulation of agents in space, with the advantage that this technique can be applied to many agent types without the need for an intrinsic light response. Additionally, the use of patterned light enables the parallel manipulation of many agents. This was initially demonstrated by Chiou et al. with the simultaneous trapping of 15,000 polystyrene beads using DEP force traps as seen in Figure 2.4, as well as the operation of a virtual optical conveyor belt to sort beads by size [61]. Furthermore, they were able to selectively sort live and dead human cells, owing to their differing dielectric properties. The relatively low light intensities required for ODEP in comparison to a technique like optical tweezers [258] makes it a particularly useful tool in relation to the manipulation of live cells. Studies have demonstrated optoelectronic control over live mammalian cells to achieve rotational [55] and translation motion, often used to achieve separation and sorting of cell groups with heterogeneous electric properties [231] or sizes [178]. In particular, an optoelectronic microfluidic device was used by Chiu et al. to isolate and harvest circulating tumour cell clusters through size-based selection [62]. Apart from mammalian cells, similar techniques have been employed with other microagent types. Notably, work by Lin et al. used ODEP forces to indirectly manipulate a single DNA molecule through interactions with beads bound to either end, indicating the potential for optoelectronics in single molecule studies [233]. Furthermore, the detection and isolation of bacterial cells with differing levels of antibiotic susceptibility was demonstrated by Wang et al. by viability-based sorting after ampicillin treatment [396].

In addition to spatial manipulation through DEP forces, there have been numerous investigations into optoelectronics as a tool for selective cell lysis. In this process, the non-uniform electric field is used to generate a transmembrane potential in the cell sufficient to disrupt the cell membrane through electroporation [258]. This allows individual cells to be selected for lysis without damage to surrounding cells, and without damage to the nucleus of the selected cell [234]. Using patterned light, this process of selection can be performed in parallel as demonstrated with a collection of HeLa cells by Valley et al. [386]. This technique can also provide a further layer of selectivity by discerning between cell types in a given area. Work by Kremer et al. showed that, given a mixed group of red and white blood cells, selective lysis of red blood cells could be achieved by detecting the ‘electrical shadow’ cast by the differently shaped cells [213].

The underlying DEP mechanism is the same in both selective cell lysis and spatial manipulation applications. The conditions for cells to undergo lysis relate to the voltage and frequency of the electric field and to the conductivity of the liquid medium, requiring higher values than for spatial manipulation. In general, optoelectronic spatial manipulation studies attempt to minimise the applied voltage to maximise cell viability [65].

2.2.5 Light reactive shape-changing polymers

Prevalent in fields such as soft robotics [284] and biomedical device design [207] are polymer-based materials that react to external stimulus, known as shape-changing polymers. Of these, polymeric materials that are responsive to light specifically are hydrogels, liquid crystalline polymers (LCPs) and shape-memory polymers [370]. In these materials, light-induced actuation is possible through both photothermal and photochromic mechanisms. In photothermal actuation, light is harvested by the polymer and converted to thermal energy that can be used for shape deformation. Photochromic actuation operates via changes to the chemical structure of a polymeric material that can be induced by the energy of incident photons. Such changes include isomerisation, bond forming and bond breaking [54]. A central application of light-responsive polymers has been in

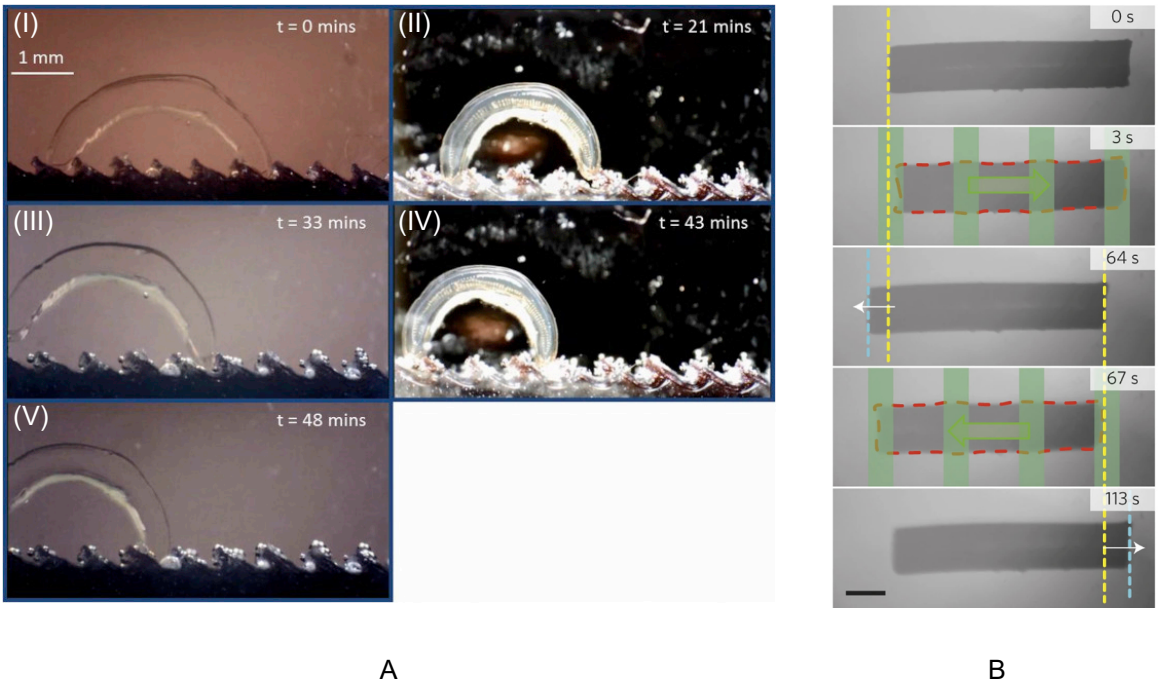

Figure 2.5: **Shape-changing polymers. (A)** Time series images showing a hydrogel microrobot walking across a ratcheted surface. The leg first contracts under illumination (I-II) then swells in the dark, causing the front leg to move over the ratchet (III). This is repeated in (IV-V), resulting in a walking motion by the microrobot. Reproduced with permission from [130] © 2017 Elsevier. **(B)** Travelling-wave motion of a cylindrical polymer microrobot generated by exposure to a periodic light pattern, represented by green overlays. Reproduced with permission from [302] © 2016 Springer Nature.

the design of small agents capable of locomotion. In one instance, an LCP caterpiller-inspired inching robot was created by Zeng et al. and shown to move across a variety of dry substrates [423]. For this robot, movement was achieved by an inching motion driven by a light-induced anisotropic thermal expansion. In an example of photochromically induced motion, Francis et al. developed a hydrogel bipedal walker capable of walking on a ratcheted surface, induced

by reversible shrinking and swelling [130]. This shrink and swell effect occurs as a result of chemical changes in the molecular structure of the hydrogel polymer when exposed to white light, producing a stepping motion (Figure 2.5A). For many shape-changing polymer agents, a combination of photoactive processes are used. This can be seen in work by Palagi et al., in which patterned light was used to generate a travelling-wave motion in an LCP microrobot, allowing the microrobot to achieve translational motion as shown in Figure 2.5B [302].

Locomotion is just one of the actuation types exhibited by shape-changing polymer systems. Another widely explored motion is that of gripping, a movement that is notoriously complex in both micro and macroscale robotics [37, 294]. In one example, Wani et al. developed a photochromically driven LCP artificial flytrap capable of executing a grasping motion [400]. Notably, the flytrap was able to function autonomously in response to the optical properties of nearby objects. Similarly, a light-driven microhand developed by Martella et al. was also shown to be capable of autonomous object recognition and gripping through an optical feedback mechanism, even demonstrating the ability to distinguish between different coloured particles [245]. A further application of light-responsive polymers was demonstrated by Zuo et al. with the fabrication of photothermally and photochromically active artificial flowers. These polymer flowers featured petals capable of furling and unfurling, as well as changing colour, when illuminated by various wavelengths of light [437].

2.2.6 Optothermally generated bubble actuation

It has been shown that surface bubbles can be formed and actuated by focusing a light beam onto an absorbent substrate [416, 429]. Through the actuation of these optothermally generated bubbles, indirect control over microagents can be achieved. In work by Zhao et al. a bubble was used to manipulate polystyrene beads by trapping the beads on its surface through surface tension and pressure forces [434]. When the position of the bubble generating laser beam was then moved with respect to the sample, the bubble was found to follow the laser trajectory, transporting the polystyrene cargo with it. Optothermally generated bubble have also been used by Hu et al. for the actuation of hydrogel microrobots, which were in turn used to assemble patterns of yeast cells. By employing an intermediate hydrogel control agent, they were able to circumvent the issue of shear stress on the cell membrane. This shear stress can result from direct contact between bubble and live cell, and has been utilised to achieve poration and lysis of cells [119, 120, 164]. Optothermal bubble-based control is typically achieved using a single focused laser beam, however in a number of instances spatial light modulation has been used to facilitate parallel manipulation of multiple bubble agents [174, 324]. In particular, Hu et al. used patterned light to generate and manipulate multiple bubbles for the assembly of microscale objects, as shown in Figure 2.6, and additionally demonstrated parallel independent control over three bubble agents [174].

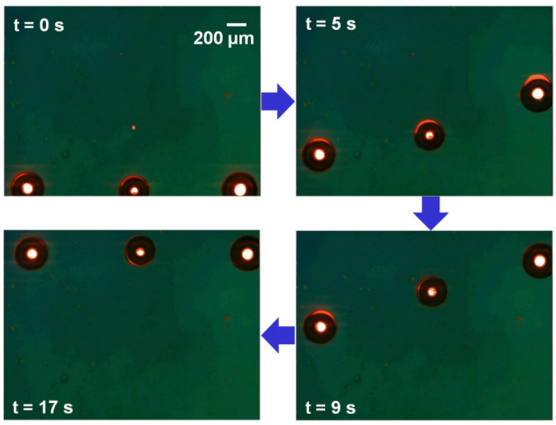

Figure 2.6: **Optothermally generated bubble actuation.** Independent parallel manipulation of three bubble microrobots. Reproduced with permission from [174] © 2011 AIP Publishing.

2.2.7 Light driven micromotors

The term micromotor is applied to microscale particles capable of self-propulsion. This propulsion can stem from external stimuli such as magnetic fields, temperature gradients or light [122]. Light driven micromotors can operate through a variety of photoactive mechanisms [390, 417], however two of the most commonly employed are photocatalytic and photothermal. Photocatalytically driven micromotors are typically fabricated using semiconducting materials, distinguished by well defined valance and conduction energy bands. In a semiconductor, these two energy bands are separated by a band gap that prevents the transfer of electrons that would be expected in a conductive metal. It is possible to promote an electron into the conduction band from the lower valance band given that it is supplied with energy equivalent to the band gap, something that can be achieved by light of the appropriate wavelength. Electron-hole pairs generated by incident light lead to redox reactions with the surrounding medium which, in photocatalytic micromotors, causes propulsion through self-electrophoresis, self-diffusiophoresis or bubble recoil from the resulting chemical gradient [212]. Photothermal micromotors on the other hand absorb light and convert the photonic energy to thermal energy, with movement then derived from self-thermophoresis as a result of the raised temperature in the surrounding medium [232].

Light-driven micromotors have applications in many fields including biomedicine, environmental remediation and cargo transport [196, 365, 417]. In an example from Wang et al., photocatalytic TiO_2 particles were used to remove suspended matter from environmental water samples [397]. These micromotors were able to operate both individually and collectively as assembled chains through phoretic interactions. Similarly, flocking catalytic TiO_2 micromotors were used by Mou et al. to demonstrate trajectory following, obstacle navigation and cargo transport in response to light, as seen in Figure 2.7A [267]. In both these examples the external light stimulus is in the UV range, as is common for photocatalytic materials owing to the high energy required to overcome the band gap. There is however much interest in the production of

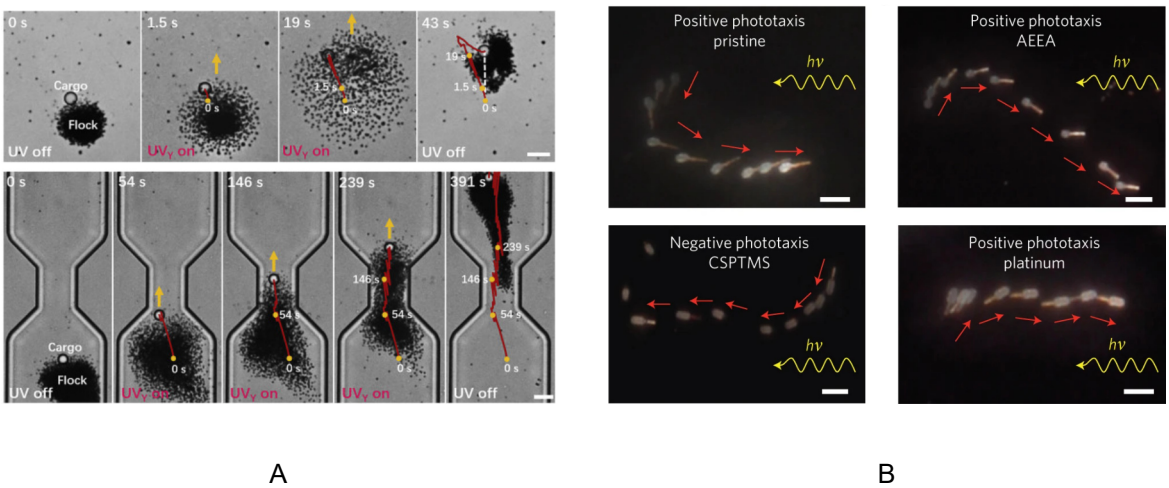

A B

Figure 2.7: **Light driven micromotors. (A)** A flock of micromotors performing collective cargo transport in open space (upper) and in an enclosed channel (lower). Reproduced from [267] under CC BY–NC–ND 4.0. **(B)** Superimposition of sequential frames showing that the Janus nanotrees exhibit either positive or negative phototaxis depending on the surface treatment of each. Reproduced with permission from [82] © 2016 Springer Nature.

visible light-driven micromotors [122], and in recent years some success has been found through the use of materials such as bismuth compounds [105, 389] and cadmium based quantum dots [298].

For photothermal micromotors, biomedical applications are of particular relevance due to the common use of near-infrared (IR) light, which is able to effectively penetrate living tissue [117]. One such example are the near-IR activated silica nanomotors used by Xuan et al. for active seeking of cancer cells and thermomechanical percolation of the cell membrane [418]. A near-IR photothermal effect has also been combined with a UV photocatalytic effect by Deng et al. using TiO2/Pt particles [91]. These micromotors were able to both move autonomously under UV illumination, and demonstrate a separate swarming behaviour under near-IR.

For all photoresponse types, the vast majority of self-propelling micromotors take the form of spherical particles. There are a number of exceptions however, including a nanotree structure designed by Dai et al. capable of mimicking phototactic behaviour. These nanotrees also have the ability to sense and steer towards the direction of a light source, exhibiting positive or negative phototaxis depending on the surface treatment applied (Figure 2.7B) [82].

2.2.8 Manipulation by optical forces

The final light-based control mechanism to be discussed is manipulation via the optical forces exerted on matter by light [21]. Optical force manipulation uses the momentum carried by photons to trap, transport, and control microagents [136]. Optical tweezers are a well known implementation of this, in which a high-numerical aperture objective is used to tightly focus

a laser beam to exert control over microagents. This technology, which gained popularity after its advent in 1986 by Ashkin et al. [22], provides the ability to trap and manipulate objects of microscopic size or smaller [259]. Although initially optical tweezers were largely only applicable to single agent manipulation, technical advances have since allowed this technique to be broadened for multi-agent manipulation [68]. In one case, a surface standing-wave light pattern was used by Čižmár et al. to create an optical conveyor belt for holding and sorting multiple particles in unison [69]. Additionally, parallel trapping and manipulation of many dielectric microbeads was demonstrated by Righini et al. using 2D surface plasmon based optical tweezers which utilise interface evanescent fields [333]. The use of holographic optical tweezers, which typically rely on some form of spatial light modulation, is another popular option for parallel agent manipulation [80, 299]. Outside of optical tweezers, optical forces have also been used as a fuel to drive autonomous microrobots. This was demonstrated by Búzás et al. with 'light sailboats', which owing to their angled wedge shape geometry were able to achieve translation motion in response to an incident laser light directed from above [47].

2.3 Light-mediated collective behaviour of microagent systems

The term collective behaviour broadly describes a wide array of phenomena including foraging, clustering and collective migration [147, 342, 388]. Generally, behaviour is considered collective if it arises, at least in part, due to the influence of local interactions between agents. These kinds of behaviours are observed in both natural and synthetic systems, and across scales. At the microscale, there are numerous ways in which light-based interactions can affect collective dynamics of a system [269]. In this section, three categories of light-mediated collective behaviour will be discussed. The first of these is optically influenced collective behaviour, in which naturally occurring collective behaviours in a microsystem are externally influenced using light. Following this will be an exploration of optically induced collective behaviours, in which light is used to generate collective behaviours in a system of microagents that would otherwise behave independently. Finally augmented collective behaviour will be discussed, in which optical interactions are used to engineer a collective response in a microsystem through augmented agent-agent interactions.

2.3.1 Optically influenced collective behaviour

In nature, there exist a number of microsystems which demonstrate collective behaviours without external input. One such example is the formation of bacterial biofilms. These are communities of densely packed cells embedded into an extracellular matrix of secreted polymeric material, which often show elevated antibiotic resistance when compared to individual cells [77, 276]. Given the prevalence of biofilms in everyday life, in both harmful and helpful capacities [419], there is much to be gained from the ability to control their formation and growth. One method by which

this has been achieved is the use of optogenetics for spatiotemporal control over biofilm growth dynamics. In work by Huang et al., optogenetic modules were incorporated in the chromosome of *Pseudomonas aeruginosa* that enabled control of a messenger molecule linked to regulation of biofilm formation [179]. Using focused projector images they were able to print and disperse custom biofilm shapes with 10 µm resolution, using 632 nm and 434 nm light to prompt cell attachment and detachment respectively. The same group also demonstrated that pDawn, a plasmid for light-regulated gene expression [293], could be used to inhibit biofilm formation of *Pseudomonas aeruginosa* in the presesnce of blue light [322]. Similarly, pDawn was used by Jin et al. to engineer blue-light regulated adhesion in *E. coli* cells [193]. They were thereby able to produce biofilms in a variety of patterns using static projected images, seen in Figure 2.8A, with a resolution of 25 µm. One potential application for synthetically engineered biofilms is the prevention of biofouling on water purification membranes. A major challenge in membrane based water purification is the unwanted growth of microorganisms into biofilms [125], a process that is mediated through quorum sensing. A route to tackling this is through the inclusion of quorum quenching bacteria, which inhibit quorum sensing in other cells [292]. Given this application, it is critical that the growth of quorum quenching biofilms on purification membranes is carefully controlled such that the constituent cells are immobilised, so as not to negatively affect the performance of the membrane itself. This was explored by Mukherjee et al. through the use of a dichromatic gene circuit that allowed the control of biofilm formation by *E. coli* [271]. They demonstrated the ability to promote growth and dispersal on a membrane using 632 nm and 465 nm light respectively. It was found that the quorum quenching *E. coli* biofilm inhibited the biofilm formation by *Pantoea stewartii*, a second bacteria species.

Biofilm patterning has also been achieved using light-based methods outside of optogenetics. In work by Chen et al., spatially controlled growth of *E. coli* biofilms was achieved by photopatterning of the adhesion surface [58]. A molecule known to be recognised by *E. coli* was linked to a nonadhesive surface using a photocleavable linker, so that when 365 nm UV light patterns were then projected onto the surface, the illuminated areas became nonadhesive and prohibited biofilm growth. Using this technique, indirect bacteria patterning was achieved with a resolution of 10 µm. The advantage of this method is that although the biofilm is initially created using optical interactions, continuous light illumination is not required after this point for the maintenance of the biofilm structure.

Besides the formation of biofilms, certain types of bacteria have been found to exhibit other types of collective behaviour such as bacterial swarming motility. This is characterised by elevated surfactant secretion and the growth of additional flagella by cells [188, 198]. These adaptations allow the cells to rapidly swarm over surfaces, and can also provide enhanced antibiotic resistance. As with biofilm formation, this collective behaviour is enacted only at a critical cell density and is therefore usually mediated through communicative signalling in the form of quorum sensing [85]. The dynamics of bacterial swarming are complex, and result from a combination of many biological

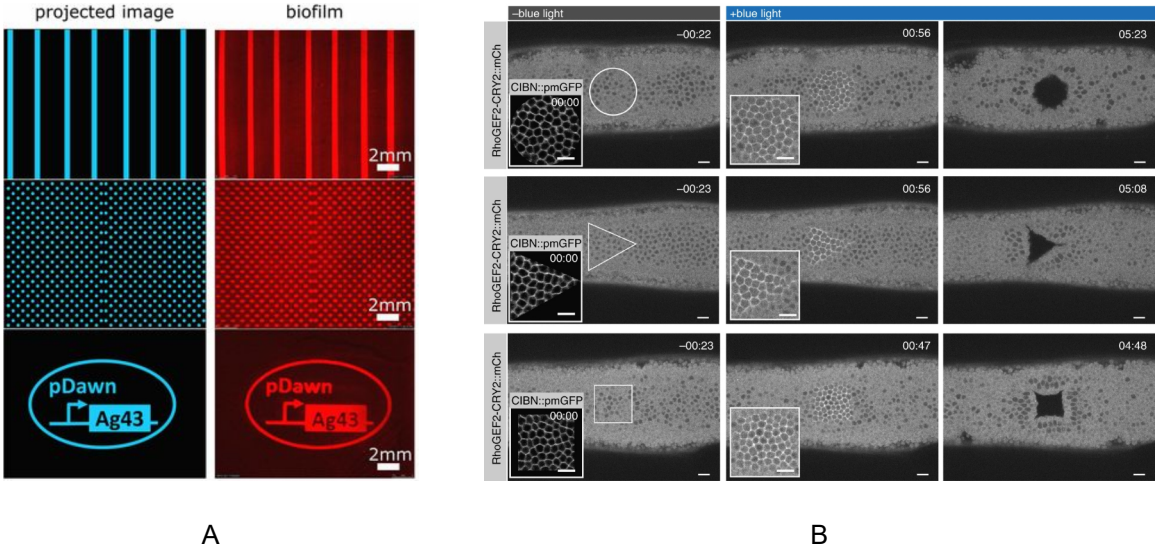

Figure 2.8: **Optically influenced collective behaviour. (A)** Patterning of an *E. coli* biofilm into stripes, polka dots and pictures using projected light images. Reproduced from [193] © 2018 AAAS. **(B)** Morphogenesis in early embryonic cells, optogenetically guided to form predetermined patterns of a circle (upper), triangle (middle) and square (lower). Adapted from [185] under CC BY–4.0.

processes. To better understand the collective motility, Patteson et al. used wide spectrum light with a significant UV components to perturb a swarming colony of *S. marcescens* [309]. It was found that light exposure induced immobilisation and quenching of the motile swarm, with the extent of these effects scaling positively with light intensity and exposure duration. Furthermore, in the illumination region for which quenching occurred, domains of immobilised cells were found to block the movement of cells into and out of the exposed region. This has two effects; firstly to localise photodamage only to the illuminated region, but also selection for UV resistance. The rational for this is that faster moving cells tended to escape the illuminated region, while slower moving cells that may be worse affected by the light were trapped by the outer immobilised cells. When the light source was removed a recovery of collective motility was observed, with swarming cells now able to access the quenched region and carry away those that had been immobilised.

There are also instances in which mammalian cells are found to exhibit collective behaviour. This occurs predominately through the collective cell migration that is seen during process such as wound healing, morphogenesis and tumour spread [132, 248, 335]. The underlying collective dynamics of these processes are complex, with influences from many distinct but interacting signalling and mechanical mechanisms [335]. A system of cells undergoing collective migration is intrinsically heterogeneous, largely due to edge effects at the migration frontier that result in leader and follower cells [336]. Owing to this, optogenetic techniques have proven valuable to probe these systems with precise spatiotemporal control [144, 158, 402]. In particular, a

photoactivatable form of the Rac protein, which modulates motility in epithelial cells [273], was developed by Wu et al. and shown to enable light-based control of actin protrusions for an individual cell [415]. This photoactivatable Rac protein has since been used by Wang et al. to direct collective migration in *Drosophila* ovary cells [398]. Using pulsed 485 nm laser illumination, they were able to redirect migration by choosing a new leader cell at the front of the cluster. Furthermore, they demonstrated that border cell migration could be reversed entirely such that the cluster moved in the opposite direction to their normal movement. As expected, it was found that increasing Rac activity through illumination of a cell caused protrusions to occur in that cell. Interestingly however, this was accompanied by the withdrawal of protrusions for cells on the side and back edges of the cluster which received no direct light stimulation. This highlights that Rac mediated collective cell migration is highly dependent on intercellular communication. An optogenetic approach was also employed by Izquierdo et al. to study the role of the Rho signalling pathway in the collective morphogenetic process of *Drosophila* embryogenesis [185]. Using a photoactivatable form of Rho, a protein that drives epithelial folding, they were able to recreate morphogenesis in early embryonic cells. Illumination of a monolayer of cells with 950 nm laser light in a variety shapes was seen to cause the photoactived cells to move out of the light region. This resulted in the reconfiguration of the cellular collective such that the monolayer contained a hollow region absent of cells, as shown in Figure 2.8B for circle, square and triangle shapes. Their results imply that Rho signalling alone is sufficient to drive this kind of tissue folding, and that the spatiotemporal dynamics of this signalling within the cell collective are fundamental to the folding process.

2.3.2 Optically induced emergent collective behaviour

Collective behaviour is by no means intrinsic to all microsystems. Many of the agent types that have been discussed in this chapter typically act as individuals, even when present in large numbers. In these systems, it is sometimes possible that collective behaviours can be induced through means such as chemical engineering or the application of external stimuli [86]. This section will consider the emergence of collective behaviours which in the absence of light would not be observed. One example that has been well established is the use of the photocatalytic processes present in certain microparticles to give rise to local agent-agent interactions [97]. In work by Ibele et al., schooling behaviour was generated in AgCl particles through UV light induced self-diffusiophoresis [182]. As these particles moved through the medium, ions secreted due to the diffusiophoretic process caused a schooling effect toward the areas of higher particle density. It was additionally found that a predator-prey dynamic occurred when photoinactive silica particles were added, with the silica particles surrounding the AgCl particles as a response to the ionic secretion. Similar behaviour has also been observed in other micromotor types, for example UV induced schooling and exclusion behaviours were demonstrated by Duan et al. with Ag_3PO_4 microparticles [109]. Photocatalytic agent-agent interactions have additionally been shown to facilitate the

formation of self-organised 'living cyrstals' in a collection of bimaterial colloids responsive to blue light [300]. Unlike the schooling behaviour discussed in the previous examples, the self-organisation of the microspheres was clearly ordered, forming a two-dimensional lattice structure. This arises owing to competition between osmotically driven self-propulsion and attractive phoertic forces, both of which can be optically activated. The emergent crystal structures are dynamic; observed to merge, break apart and explode under the presence of constant illumination. When illumination ceases, the living crystal structure rapidly begins to dissociate due to diffusion effects.

Photothermal effects have also been found to bring about collective behaviours in micromotor systems. In one instance, Deng et al. used photothermal convection currents induced by near-IR light to cause swarming behaviour in TiO_2/Pt particles that otherwise moved autonomously under UV light [91]. The particles were first formed into a swarm using 808 nm laser light, with collective migration then performed through movement of the near-IR spot. It was observed that due to the increased density of the swarm compared to dispersed particles, interactions between particles were stronger and more frequent. This led to an exclusion behaviour when UV light was pulsed on and off, and clustering behaviours when it was switched off, resulting from attractive electrostatic and repulsive diffusiophoretic interactions respectively. Notably, this swarming behaviour is independent of agent type as the photothermal process occurs in the liquid medium rather than the agent itself, and was demonstrated using other particle types as well as *E. coli* cells. Light-induced convection flows were similarly utilised by Hu et al. to bring about a swarming behaviour in composite microparticles formed by the in situ deposition of Fe_3O_4 nanoparticles onto polystyrene beads [176]. In contrast to the previous example however, convection flows were generated by the interaction of light with the particles themselves, specifically the Fe_3O_4 nanoparticle coating, rather than with the surrounding medium. Unusually, the photothermal effect was activated most strongly in the UV range, with blue and green wavelengths also giving rise to a swarm response.

One application of particular interest with regards to collective microparticle systems is microscale self-assembly, which can be difficult and time consuming to achieve through the control of individual agents. To this end, Schmidt et al. investigated how emergent collective phenomena could be engineered by creating building blocks of complexly interacting imotile microspheres [349]. The system was comprised of both light-absorbing and non-absorbing immotile silica microparticles, seen in Figure 2.9A. When illuminated by 532 nm light, heating occurred in the silica microspheres that were able to absorb light, causing a local temperature rise in the surrounding medium. Given the homogeneous composition of the particle, this local heating effect was isotropic and therefore did not give rise to thermally induced self-propulsion. Instead, various self-assembled configurations of the two particle species began to form through a combination of phoretic interactions and short range attractive forces. These assemblies were seen to exhibit configuration-dependent motile behaviours, arising due to the asymmetry of the newly formed

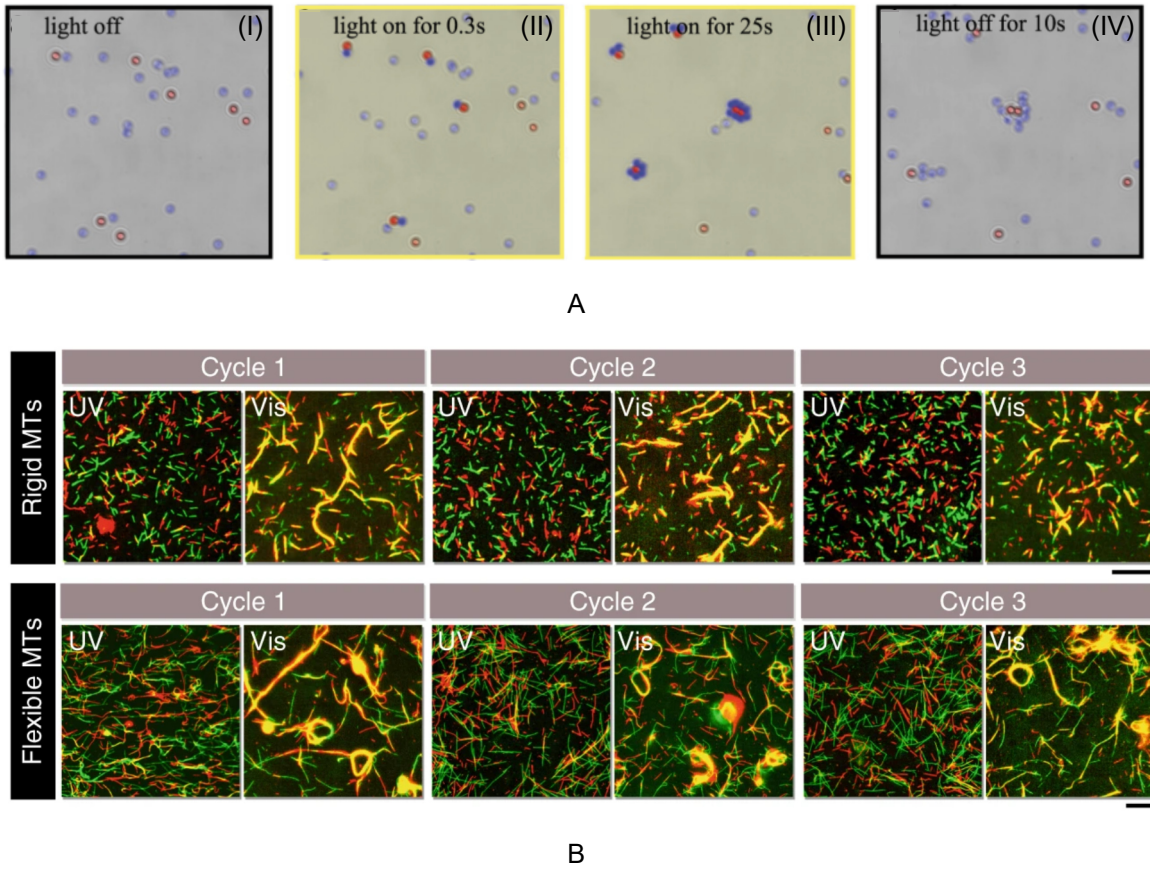

Figure 2.9: **Optically influenced collective behaviour. (A)** Light-absorbing (red) and non-absorbing (blue) colloid particles are initially non-interacting (I), but under illumination the absorbing particles begin to locally heat the surrounding medium. When the two species of particles meet under these conditions, they form dimers capable of self-propulsion (II), which over time grow to include other particles, forming more complex structures (III) that disassemble when illumination is switched off (IV). Reproduced with permission from [349] © 2019 AIP Publishing. **(B)** Photoresponsive microtubules are seen to to aggregate into swarms under visible light, and to dissociate into single strands under UV light. This is shown for both rigid (upper) and flexible (lower) microtubules, with swarms of flexible microtubules demonstrating a circular motion. Reproduced from [201] under CC BY–4.0.

structure. Through this scheme, they were able to transform immotile silica building blocks into active molecules such as migrators, spinners and rotators, laying the foundations for emergent collective phenomena driven microscale self-assembly.

Light has additionally been used to bring about collective behaviours in organic systems. In work by Keya et al. [201], the swarming of DNA-functionalised microtubules was demonstrated in which the tethered DNA acted as molecular computing modules for programming agent-agent interactions. In the first instance, swarming behaviour was induced by the introduction of linker DNA and thus independent of light illumination. Following this however, photoresponsive DNA strands were conjugated to the microtubules. The photoresponsive microtubules were shown to aggregate and swarm when irradiated with 480 nm visible light, and to dissociate and move independently under 365 nm UV light (Figure 2.9B). Swarming could therefore be switched on and off in a rapid, reversible and non-invasive manner via optical control.

2.3.3 Augmented collective behaviour

An as yet less explored idea is the use of light-based control to engineer collective behaviours in a microsystem that are not directly mediated by local agent interactions, referred to here as augmented collective behaviour. This type of control scheme utilises microagents that exhibit individual light responses, in conjunction with closed-loop computational methods, applied such that the microsystem behaves in a collective manner. An augmented control system is of particular interest in relation to the engineering of synthetic active particles, which unlike living organisms such as birds, fish or bacteria have no intrinsic means of sensing and feedback. An example of this is given by Bäuerle et al., in the implementation of quorum sensing rules by an external feedback-loop to effect self-organisation of light-activated particles [28]. In their control system, active silica particles are propelled using laser light, where the magnitude of propulsion is modulated by light intensity and direction is illumination independent. Using a real-time particle detection algorithm linked to laser beam position, quorum sensing inspired rules relating agent motility to local agent density were explored. Specifically, a rule was implemented that particles should move at a predefined velocity through light-based propulsion until the local concentration 'sensed' by a particle exceeded a given threshold. Once this was exceeded, illumination was set to zero, causing the particle to become non-motile apart from diffusive motion. Propulsion of particles in this system occurs due to an asymmetric chemical gradient around the particle induced by laser light heating. This quorum sensing based algorithm facilitated the organisation of an active particle suspension into clustered regions by endowing particles with augmented sensing capabilities. This work was later extended with the design of a similar motion-based feedback loop that, instead of quorum sensing rules, employed a sensing rule more akin to visual perception in social insects [221]. In this instance, agents were allowed to 'see' other agents within a restricted vision cone, where perception also decays with distance. By varying these parameters different emergent clustering dynamics were observed, providing insight into the

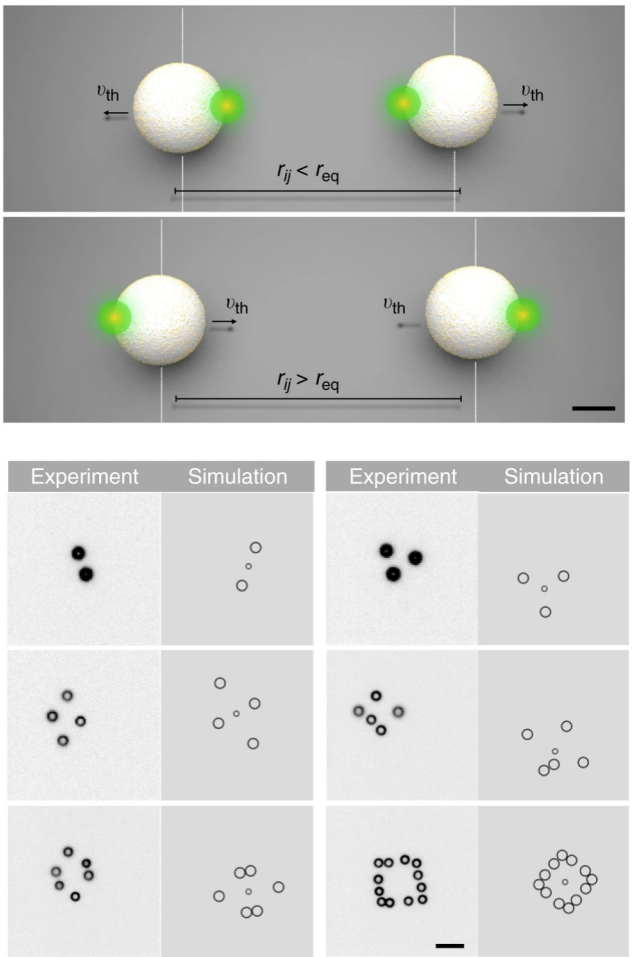

Figure 2.10: **Augmented collective behaviour.** Organisation of active particles using pair interaction rules, in which a laser is used to propel particles according to their separation distance in relation to their neighbours (upper). This results in the formation of various structures, the shape of which is determined by the defined separation distance and the number of particles in the system (lower). Adapted from [202] under CC BY–4.0.

effects and implications of anisotropic long-range sensing in both living and synthetic systems.

In a similar fashion, real-time tracking and feedback control was employed by Khadka et al. to facilitate information exchange between self-propelled laser-controlled active particles [202]. Despite the similar underlying control scheme, this implementation differs from the previous example in that propulsion occurs due to self-thermophoresis, and control is exerted over the direction of a particle rather than speed. Here, the laser beam is applied near the circumference of the particle, with the propulsion vector being given by the vector of this point to the particle center, as shown in Figure 2.10. The microsystem of functionalised melamine resin spheres was shown to undergo self-organisation when an augmented signalling channel was introduced by which positional information could be exchanged. Specifically, a pairwise control was established

in which the desired outcome was that a predefined separation distance was achieved and maintained. Where separation was found to be greater or lower than this value, particles would be directed towards or away from each other respectively. Through these simple interaction rules, self-organised structures were seen to emerge, with various arrangements being found at different population numbers, as depicted in Figure 2.10. Once these structures had been formed, the feedback control mechanisms continued to act to correct for the effects of Brownian motion.

In both of the systems described above, collective behaviours were able to emerge in the absence of intrinsic agent-agent interactions. The wider implication of this is that this approach could be broadened to other light-reactive agents, including living systems, with a plethora of possible rules that could be implemented. This could provide a general method to implement collective algorithms at the microscale, with applications in fields such as swarm robotics [29, 43] and active matter computing [113]. In particular, a closed-loop feedback set-up provides opportunity to incorporate artificial intelligence techniques for for the discovery and optimisation of collective behaviours in various microsystems [30, 67, 270, 320]. This kind of platform could also facilitate the rapid prototyping of collectively interacting microsystems. An example could be the use of optically augmented agent-agent interactions as a stand in for chemical interactions. This would allow conditions and dynamics required for emergent behaviours to be tested without requiring a new, time consuming round of synthesis and functionalisation for each parameter test.

2.3.4 Summary

In this section, and in Section 2.3, a wide variety of light-responsive agents have been discussed. Examples have been drawn from numerous different fields of research, however all are unified by the the utilisation of light-based phenomena to facilitate microscale control. To provide a summary of the work explored thus far, Table 2.1 presents a breakdown of each microagent system discussed, providing key characteristics including agent type, size and the mechanism of optical response. Details pertaining to the illumination scheme are also included, such as wavelength and hardware, as well as specifying whether a closed-loop control system was employed. Crucially, the response of the microagent system to the optical control scheme is also given, as well as an indication of whether any swarm-like collective behaviours were observed.

Agent type	Mechanism	Response	Illum. type	λ (nm)	Size (μm)	Closed	Swarm	Ref.
Micro-sailboats	Optical forces	Spatial manipulation	Laser	1070	9–12	N	N	[47]
Polystyrene MPs	Optical forces	Trapping, spatial manipulation	Laser	532	0.35–0.80	Y	N	[69]
Polystyrene MPs	Optical forces	Trapping, spatial manipulation	Laser	785	4.88	N	N	[333]
Silica MPs	Optical forces	Trapping, spatial manipulation	LCoS + laser	532	0.99	N	N	[80]
Mammalian cells	Optoelectronic	Lysis	DLP Projector	Visible	3–10	N	N	[213]
Mammalian cells, MPs	Optoelectronic	Spatial manipulation	LCD module	Visible	10–20	N	N	[142]
Mammalian cells	Optoelectronic	Spatial manipulation	DLP Projector	Visible	6–10	N	N	[55]
Mammalian cells	Optoelectronic	Spatial manipulation	LCD projector	Visible	3.5–8	N	N	[231]
Mammalian cells	Optoelectronic	Spatial manipulation	LCD projector	Visible	7–25	N	N	[62]
DNA molecules	Optoelectronic	Spatial manipulation	LED projector	Visible	1.5–10.1	N	N	[233]
Mammalian cells, polystyrene MPs	Optoelectronic	Spatial manipulation	DMD + LED	625	4.5-24	N	N	[61]
Mammalian cells	Optoelectronic	Spatial manipulation, electroporation	DLP Projector	Visible	20-40	N	N	[386]
Mammalian cells	Optoelectronic	Spatial manipulation, lysis	LCD projector	Visible	30*	N	N	[234]
E. coli bacteria	Optoelectronic	Spatial manipulation	LCD projector	Visible	0.5–2*	N	N	[396]
Saccharomyces cerevisiae yeast	Optogenetic	Patterning	DLP projector	450	5-10	Y	N	[340]
E. coli bacteria	Optogenetic	Patterning	Slide projector	650, 532, 470	0.5–2*	N	N	[123]
E. coli bacteria	Photoactivated proteins	Patterning	DLP projector	520	0.5–2*	Y	N	[131]
E. coli bacteria	Photoactivated proteins	Cargo transport	LEDs	630, 700–800	1–2	N	N	[355]

Table 2.1: **Light responsive microagents.** Continued on next page.

Agent type	Mechanism	Response	Illum. type	λ (nm)	Size (µm)	Closed	Swarm	Ref.
E. coli motors	Optogenetic	Patterning	Lamp	620–680	0.5–2*	N	N	[227]
E. coli bacteria	Photoactivated proteins	Rotational motion	DLP projector	565	7.6	Y	N	[392]
Mammalian cells	Optogenetic	Apoptosis	LED array	488	20–40*	N	N	[180]
Mammalian cells	Optogenetic	Cell migration	Unknown	Unknown	13–15*	N	Y	[12]
Macrophage cells	Optogenetic	Cell migration	Laser	445	10*	N	Y	[253]
Mammalian cells	Optogenetic	Morphogenesis	Laser	950	10*	N	Y	[185]
Mammalian cells	Optogenetic	Cell migration	Laser	458,473	20–40*	N	N	[415]
Mammalian cells	Optogenetic	Cell migration	Laser	485	20*	N	Y	[398]
E. coli biofilm	Optogenetic	Patterning	DLP projector	460	0.5–2*	N	Y	[193]
E. coli bacteria	Optogenetic	Patterning	LCD projector	530 & 660	0.5–2*	Y	N	[53]
E. coli biofilm	Optogenetic	Patterning	Unknown	660, 465	0.5–2*	N	Y	[271]
Pseudomonas aeruginosa biofilm	Optogenetic	Biofilm inhibition	Laser	488	0.5–3*	N	Y	[322]
Pseudomonas aeruginosa biofilm	Optogenetic	Patterning	DMD + LEDs	434, 632	0.5–3*	N	Y	[179]
Muscle-on-a-chip	Optogenetic	Shape actuation, stress control	LED, mercury lamp	473	144	N	N	[343]
Nanotree microswimmers	Photocatalytic	Translational motion	LEDs	365	2.6–11	N	Y	[82]
BiOI-Based Janus MMs	Photocatalytic	Translational motion	Mercury lamp and filters	520, 590	2–4	N	Y	[105]
Au@Ni@TiO2-based MMs	Photocatalytic	Translation motion, cargo transport	Lamp	385	0.7	N	N	[397]
BiVO4 MMs	Photocatalytic	Translation motion, cargo transport	LED	400	4–8	N	Y	[389]
Quantum dot MPs	Photocatalytic	Translation motion, cargo transport	LED	470–490	17	N	N	[298]

Table 2.1: **Light responsive microagents.** Continued on next page.

Agent type	Mechanism	Response	Illum. type	λ (nm)	Size (µm)	Closed	Swarm	Ref.
Polymer MPs	Photocatalytic	Self-organisation	Unknown	430-490	1-2*	N	Y	[300]
Polymeric walker	Photochemical	Shape actuation	LED lamp	Visible	1440–2810	N	N	[130]
Polymeric artificial flytrap	Photochemical	Shape actuation	Laser	488	1×10^4*	N	N	[400]
Polymer microrobot	Photochemical	Shape actuation, translation motion	Laser	488	1×10^4*	N	N	[423]
Ag3PO4 MPs	Photochemical	Schooling and exclusion	Unknown	320–380	2	N	Y	[109]
TiO2 MPs	Photochemical	Cargo transport	Lamps	365	1.2	N	Y	[267]
E. coli bacteria	Photocleavage	Biofilm patterning	Photomasked light	365nm	0.5–2*	N	Y	[58]
S. marcescens bacteria	Photodamage	Swarm quenching	Mercury lamp	Visible	0.5–2*	N	Y	[309]
AgCl MPs	Photodecomposition	Schooling, predator–prey	Unknown	320-–380	1–3*	N	Y	[182]
Euglena gracilis algae	Phototaxis	Translational motion	LED projector	Visible	50	Y	N	[218]
Synechocystis bacteria	Phototaxis	Group migration	LEDs	660, 535, 435	2000*	N	N	[56]
Synechocystis bacteria	Phototaxis	Individual migration	LED	625	2*	N	N	[351]
E. coli bacteria	Phototaxis	Migration, aggregation and patterning	Photomasked light	460	0.5–2*	N	Y	[426]
Bacteria-coated microplates	Phototaxis	Translational and rotation motion	DLP projector	<500	20–40	Y	N	[366]
Porphyridium purpureum aglae	Phototaxis	Translational manipulation	LCOS + laser	457	6–10	N	N	[208]

Table 2.1: **Light responsive microagents.** Continued on next page.

Agent type	Mechanism	Response	Illum. type	λ (nm)	Size (µm)	Closed	Swarm	Ref.
Polymer micro-hand	Photothermal	Shape actuation	Laser	532	100–300	N	N	[245]
Optothermally generated bubbles	Photothermal	Translational motion, cargo transport	Laser	980	171–244	N	N	[173]
Optothermally generated bubbles	Photothermal	Translational motion	LCoS + laser	1064	85	Y	N	[324]
Optothermally generated bubbles	Photothermal	Translational motion	DLP projector	Visible	125	N	N	[174]
Optothermally generated bubbles	Photothermal	Cell poration	Laser	980	10–15	N	N	[120]
Silica MPs	Photothermal	Translational motion, self-assembly	Laser	532	0.49	N	Y	[349]
Polystyrene MPs	Photothermal	Swarming	Unknown	320–550	5	N	Y	[176]
Silica MPs	Photothermal	Self-organisation	AOD + laser	532	4.4	Y	Y	[28]
Silica MPs	Photothermal	Clustering	AOD + laser	532	4.28	Y	Y	[221]
Melamine MP	Photothermal	Self-organisation	AOD + laser	532	1.09*	Y	Y	[202]
Silica nanomotors	Photothermal	Spatial manipulation, membrane perforation	Laser	808	0.08	N	Y	[418]
Polymeric artificial flower	Photothermal, photochemical	Colour changing and shape actuation	Unknown	365, 520, 808	2×10^4	N	N	[437]
Polymer micro-robot	Photothermal, photochemical	Shape actuation, translation motion	DMD + laser	532	50–1000	Y	N	[302]
TiO_2/Pt MPs	Photothermal, photocatalytic	Translation motion, collective migration	Laser, LED	808, 365	3	N	Y	[91]

Table 2.1: **Light responsive microagents.** Summary of the light-responsive microagents discussed throughout this chapter. For convenience, abbreviations have been made; MPs – microparticles, MMs– micromotors, λ – wavelength, illum. – illumination, closed – closed-loop control, swarm – any swarm-like collective behaviours demonstrated by the microagent system. Agent size refers to the size of single agents, even in cases where control was exerted over collective groups rather than individuals. Where agent size is not specified in text, the value was estimated from alternative literature, or inferred from figure and is marked with an asterisks (*).

2.4 Devices for the optical control of microagent systems

As has been laid out thus far in this chapter, applications of optical control at the microscale have been demonstrated in countless fields, and for a wide variety of microagents. The hardware set-ups used in these applications range in complexity, from open-loop, uniform illumination to highly localised, feedback-based light delivery. The latter type of system inherently allows for a significantly higher level of control in terms of spatiotemporal dynamics. This enhanced control enables the engineering of more complex microsystem behaviour, for example by independent interaction with multiple microagents in parallel [28, 64, 202, 218], or subsectional targeting of larger agents [302, 369]. For these applications, a custom-built optical set-up is often employed, requiring real time visualisation and image analysis coupled to a spatially localised light delivery system. The use of such control schemes is therefore limited by the expertise required for their construction, and may not be feasible in many instances. This is particularly true given the multi-disciplinary nature of the applications discussed, many of which are in fields such as microbiology, cell biology and surface chemistry. Despite an increasing trend towards interdisciplinarity in research [321], many research groups will not have the optical, electronic and computational experience required to build an entire optical control system from scratch. It is therefore sensible to examine implementations such systems that have been demonstrated thus far, and to consider not just the technical merits of each but also the accessibility and reproducibility. This section will detail the various experimental set-ups and devices from existing literature that have been used for optically engineering the behaviours of microscale systems. Specifically, those included must be capable of executing closed-loop feedback control over many microagents independently and in parallel.

2.4.1 Time-shared laser beams

One method for localised light delivery is the use of a laser beam, which can yield extremely high resolution when focused using a high-numerical aperture objective. This method can provide submicrometer resolution in some instances [149, 431], however by itself is limited to single agent control. Fortunately, technological innovations have made it possible to extend this type of system to the manipulation of multiple agents. One such innovation is the time-sharing of a single laser beam between a collective of spatially distributed agents. Given that microagents are almost always situated within a medium, diffusion dynamics are relatively slow. Thus, manipulation of multiple agents by a single beam is possible if the focal point of the laser is capable of rapid movement between positions. This concept was initially demonstrated by Sasaki et al. in the early 1990s with the use of 2 computer driven galvano mirrors to deflect a laser, allowing the spatial patterning of 1-2 µm polystyrene latex particles [345]. More recent implementations have favoured the use of acousto-optic deflectors (AOD) [391] or electro-optic deflectors (EOD) [384] for ultra precise beam deflection by acoustic waves and electric fields respectively. Many applications

of time-share laser-based manipulation operate on an open-loop basis, however a number of closed-loop implementations have been demonstrated. Notably, in Section 2.3.3, the work of Bauerle et al. [28] and Khadka et al. [202] were discussed. In both instances, a time-shared laser beam was utilised to facilitate collective behaviour through augmented particle communication. A simplified generic construction of such a system is shown in Figure 2.11, in which a laser beam is directed through a deflector (AOD, EOD or otherwise), the position of which is digitally controlled. Typically, the beam will then pass through relay optics before being reflected into a focusing objective by a dichroic mirror or a similar component, allowing for combination with a bright-field illumination light source. The focused laser and bright-field light passes through the objective to the sample, which is imaged using an objective and camera coupled to the control computer. To establish feedback control, the camera must be calibrated to the sample workspace such that the positions of agents can be used to inform the deflector positions. Additionally, real time image analysis of the camera images must be performed in order to transmit updated laser beam coordinates to the deflector as the microsystem evolves over time.

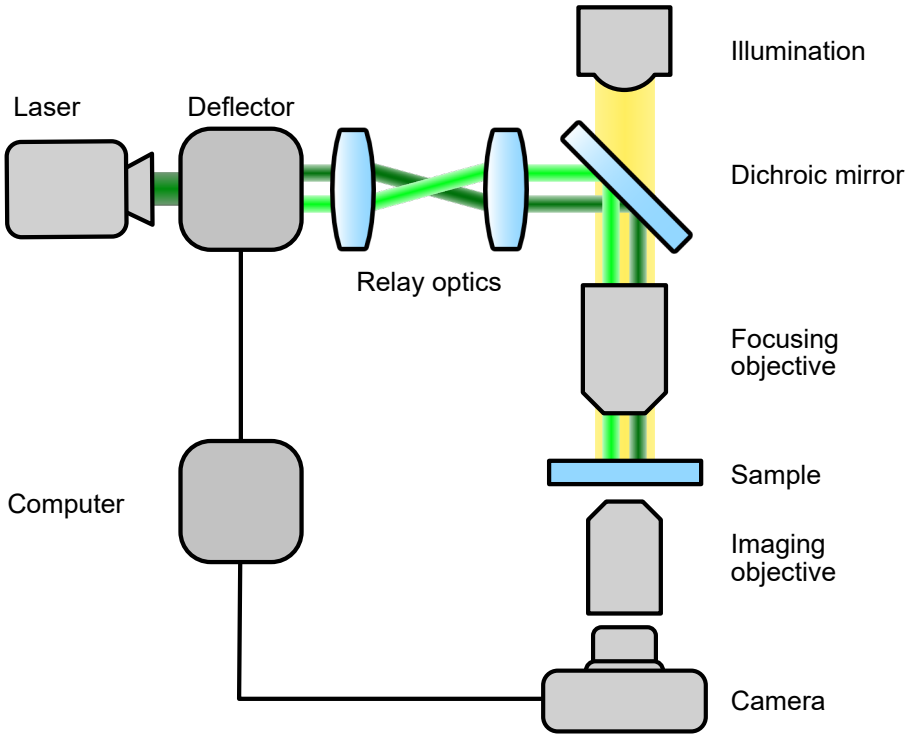

Figure 2.11: **Time-share laser beam.** Schematic representation of a time-share laser beam system, in which a single laser can be shared between multiple positions using a deflector such as an AOM or EOM.

A considerable advantage of the focused laser beam-based light delivery method is the high resolution attainable. The focusing of a single beam by a high-numerical aperture objective allows for accurate targeting of individual agents with microscale [28, 257, 345] or even submicroscale

[51, 384, 391] resolution. This has allowed the dual manipulation of DNA molecules to investigate protein organisation [83], as well as the implementation of active particle steering using subsectional targeting of ~1 µm particles [202]. The main drawback of a time-shared laser is that although technically allowing for multi-agent control, truly parallel manipulation is impossible. Although theoretically feasible to control 100s of particles simultaneously using this technique [28, 299], the overall time taken to complete a cycle of illumination must be small enough that significant diffusion does not occur in that period. Since the distance that a particle will diffuse in a given time period is inversely proportional to particle radius [69], this becomes less of an issue as agent size increases. However, even for larger, less diffusive microsystems there is a problem with scaling, as every additional agent results in a reduced illumination time per agent per cycle, since illumination is performed sequentially rather than in parallel. Even negating diffusive effects, this results in a significant slowing of the manipulation process. Another consequence of this is that highly motile agents such as flagellated bacteria would difficult to control with a time-share laser system. The high intensity provided by a focused single beam also presents a complication when dealing with living biological matter due to the risk of photodamage [39, 279, 325], although mitigation strategies are documented [256].

Time-shared laser beam systems provide an effective way to deliver a tightly localised, high intensity light to multiple microscale agents. While control is not strictly simultaneous, in most instances it can be considered as such, and employed for parallel optical control of multi-agent systems. This technique is well suited to the high speed manipulation of a small collection of agents with low diffusivity [14], but requires a relatively complex and precisely calibrated optical set-up. There is therefore a fairly high barrier in terms of costs and expertise associated that may make it inaccessible in many research settings.

2.4.2 Digitally controlled spatial light modulators

An alternative method for localised light delivery is to give spatial structure to the output of a light source, something that can be achieved using a spatial light modulator (SLM). At the most basic level, an SLM could simply be a static mask, however in practice it typically refers to a dynamic, digitally controlled output [346]. The most frequently used types of SLM are digital micromirror devices (DMDs) or liquid crystal (LC) based chips, both of which provide a controllable grid of pixels that can be used to dynamically pattern light. A DMD is a semiconductor based array of microscopic mirrors, depicted in Figure 2.12A. The mirrors are digitally switchable between a binary $+12\,^{\circ}$ and $-12\,^{\circ}$ tilt angle, representing 'on' and 'off' respectively. Incident light is thus spatially modulated through selective reflection.

For an LC material, the refractive index experienced by incident light is dependent on the molecular orientations of the individual liquid crystals within, as shown schematically in Figure 2.12B. Given that orientation can be controlled by an externally applied voltage, an electronically driven array of LC cells functions as a SLM.

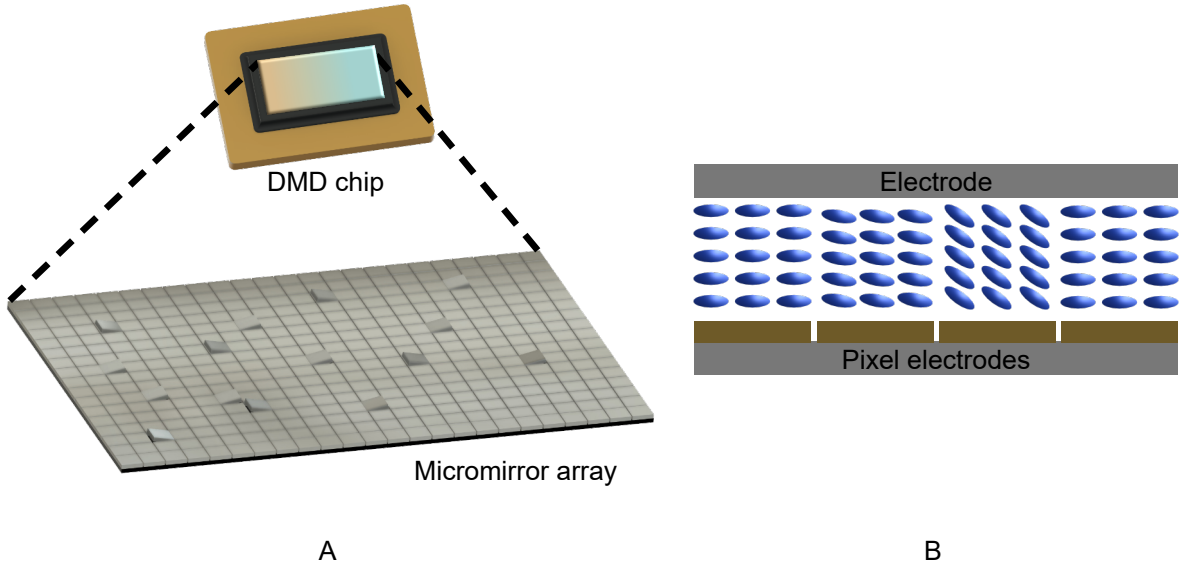

Figure 2.12: **SLM chips. (A)** A DMD device consists of an array of microscopic mirrors that can be angled between a binary 'on' and 'off' position. **(B)** An LC-based SLM contains an array of LC cells whose molecular orientations can be controlled using pixel electrodes.

The resolution attainable using DMD or LC-based devices equates to the number of microscopic mirrors, or number of LC cells contained in the full array. SLM technology has found widespread use both commercially and in highly precise optical applications including microscopy and holography [3, 110]. The choice between SLM types is highly dependent on application. LC-based SLMs are able to achieve significantly smaller pixel size, and are capable of modulating the intensity and phase of incident light where a DMD provides binary modulation [222]. DMDs however exhibit faster response times and superior beam-shaping fidelity [110]. In addition, the interaction of light with LC materials is highly wavelength dependent, prohibiting the use of short wavelengths in the UV range due to absorption. This makes LC-based SLMs unsuitable for use in UV-related processes such as lithography [222].

DMDs are commonly used in conjunction with a light source, optics and control electronics to create digital light processing (DLP) systems. The main example of this is the DLP projector, which can use a lamp, LED or laser light source. In a DLP projector, colour can be created either using a single DMD chip together with a colour wheel or pulsed LEDs, or alternatively by using three separate DMDs each relating to a single colour [197]. Liquid-crystal displays (LCDs) and liquid crystal on silicon (LCoS) displays are LC-based SLM devices used for display applications. In an LCD, the LC layer is sandwiched between conductive glass substrate layers that act as electrodes to shape the crystal alignment, in front of which is a polarising filter. An LCD may operate by transmission or reflection where illumination is delivered by a backlight or reflector respectively. Colour is usually generated by a filtering layer that can produce coloured subpixels. The backlight layer of an LCD makes them useful not only for light projection but also display

applications such as smart phones and televisions. On the other hand, an LCoS display can be thought of as combining principles of both LCD and DMD technology. An LC layer is used to shape incident light, and a reflectively-coated silicon layer is used to reflect this structured light back through the device. This results in less absorption than in an LCD, in which the layers of glass and polarizing filters have absorbing properties. Colour generation for an LCoS display works similarly to in a DLP system, with either a single or three chip arrangement.

In combination with microscopy techniques, SLM technology is powerful in the context of optical control of microagents [55, 61, 208, 233]. The digitally controlled nature of LC and DMD light delivery also allows a closed feedback loop to be realised, enabling complex microsystem control schemes. Such closed-loop optical control set-ups are typically less expensive and complex than comparable time-shared laser arrangements, however the integration of SLM technology with microscopy optics and a closed computational system is not trivial. At a base level, it must include an SLM based light delivery module, magnification optics and camera for agent visualisation, and a closed computational system. In this context, closed means that the computational system is capable of simultaneously performing image analysis of the camera feed, and outputting information to the projector. It should be noted that there are SLM-based, off-the-shelf light delivery systems designed to work with microscopic system available, namely the Polygon 400 (Mightex) and the Mosaic (Andor, Oxford Instruments). These systems, although powerful and high specification, are not here considered accessible, as they are priced in the £10,000s range and run on proprietary software that could make the implementation of custom control algorithms difficult. Furthermore, these devices do not constitute a full optical control system, rather they are an attachment for an existing microscope that provide localised light calibrated to the camera output. In contrast, this section will examine whole systems presented in literature that are capable of closed-loop, SLM-based optical control. Specifications such as minimal projection pixel size, total sample workspace and available illumination wavelengths will be highlighted. Also of interest is the accessibility demonstrated by each system, in particular the extent of openness and the provision of documentation, plans or protocols that would allow for the system to be easily reproduced.

2.4.2.1 Application specific set-ups

In the first instance, custom built set-ups that are presented as part of a methodology towards a specific application, as opposed to as an integrated platform will be considered. These systems are generally less well characterised and may have limited reproducibility, however offer an interesting point of comparison in regard to technical specifications.

In work from Rahman et al., closed-loop photothermal actuation of bubble microrobots was demonstrated using an LC-based SLM [324]. In this set-up, shown in Figure 2.13, a laser beam is directed through a beam expander and onto an LCoS chip (X10468- 07, Hamamatsu) to shape the beam. The structured light is then reflected from the SLM through a series of optical components,

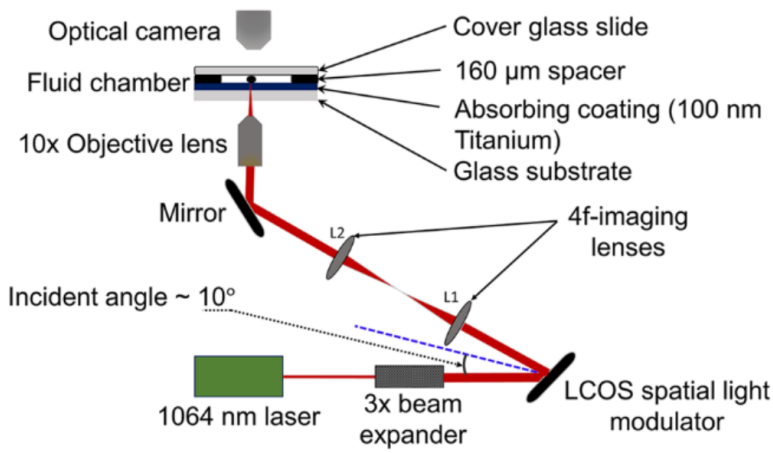

Figure 2.13: **Optical set-up for the photothermal actuation of bubble microrobots.** Reproduced from [324] under CC BY–4.0.

finishing by passing through a 10 ×objective lens to the sample, onto which a camera is aimed. An open-loop pattern generation algorithm developed in LabVIEW was combined with an image processing algorithm developed in MATLAB to facilitate a feedback-based control loop for the microrobots. Given that the total manipulation area is stated as 16 × 12 mm and the SLM chip used has a native resolution of 800 × 600 pixels, the minimum single pixel size can be estimated as 20 µm. A 1064 nm wavelength laser was used, however it would be possible to use other wavelengths with this set-up as there are no wavelength specific filters included.

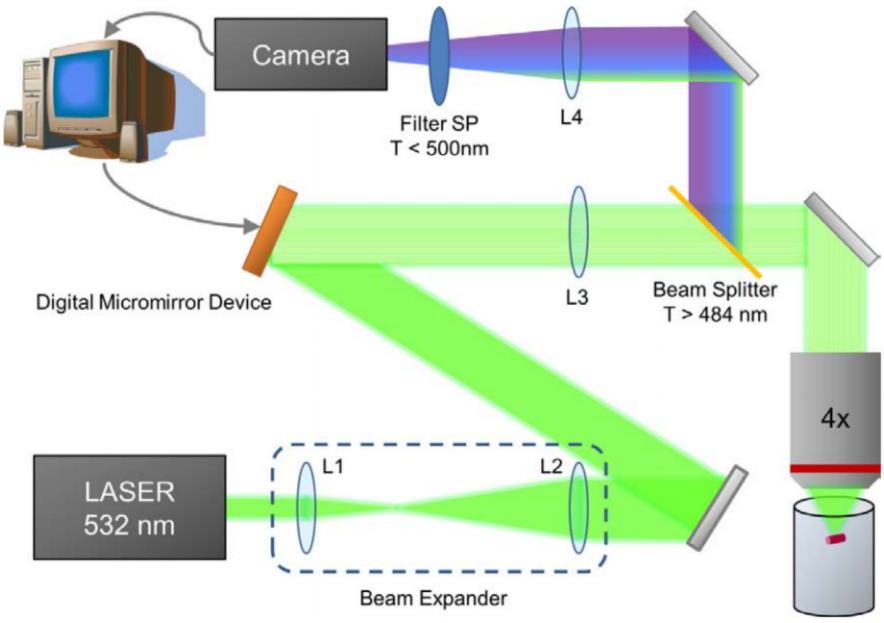

Figure 2.14: **Optical set-up for driving locomotion of a polymer microrobot.** Reproduced with permission from [302] © 2016 Springer Nature.

Figure 2.14 shows an optical set-up used by Palagi et al. for driving locomotion of a polymer microrobot [302]. Here, a 532 nm laser beam passes through a beam expander and is reflected by a mirror onto a DMD module (V-7000, ViaLUX). The patterned light is reflected onto a beam splitter and through a 4 ×objective and onto the sample. The beam splitter allows the sample to be imaged through the same objective, with light passed to a camera linked to the computer that drives the DMD module. The native resolution of the DMD used is 1024 × 768 pixels, however no specifications are given for the size of workspace or minimal pixel size. The beam splitter used here has a cut-off wavelength of 484 nm meaning that any light source with a wavelength longer than this could be used to supply light in place of the 532 nm laser. Due to the presence of the beam splitter, the light patterns incident on the sample are not visible in the collected images as only light under 484 nm is reflected to the camera.

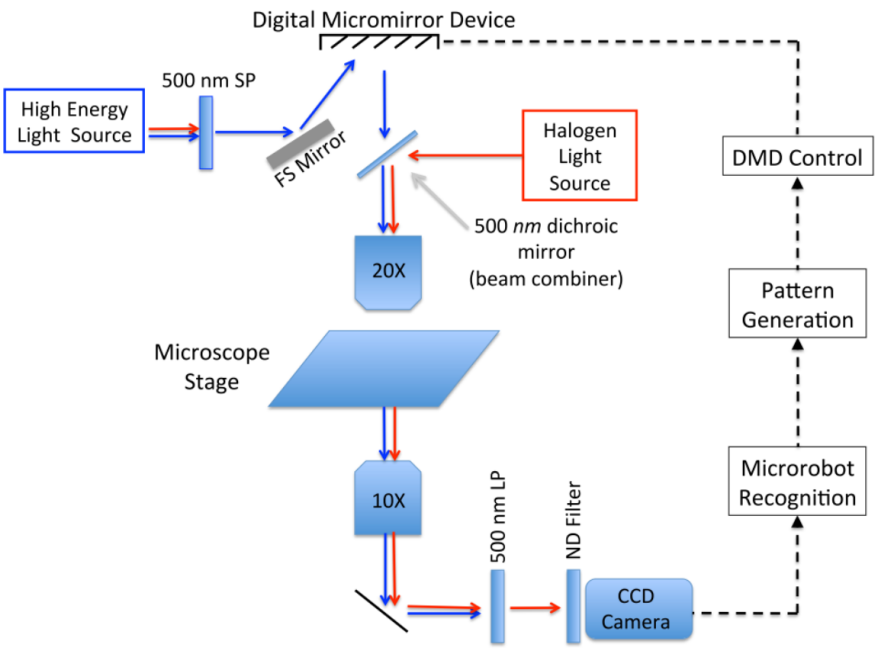

Figure 2.15: **Optical set-up for the manipulation of bio-hybrid microrobots.** Reproduced with permission from [366] © 2015 IEEE.

DMD technology was also utilised by Steager et al. for the manipulation of bio-hybrid microrobots through the phototactic control of bacteria cells [366]. This closed-loop system, shown in Figure 2.15, uses a DMD projector (Lightcrafter, Texas Instruments) modified by the replacement of the light engine by a high intensity blue and UV LED light source. Light from the projector is directed through a dichroic mirror, where it is combined with light from a halogen light source for bright-field imaging. The patterned blue light and background light is focused through a 20 × objective and onto the sample. A 10 × objective is used to image the sample, with light filtered through a longpass filter to remove the blue and UV light before reaching the camera. The minimum projector pixel size in the workspace is given as 1 µm, however the workspace size

as well as the projector model and resolution are unknown. Although in this set-up the projected light is filtered out of the camera images, this is stated to be for ease of microrobot tracking and could be included if desired.

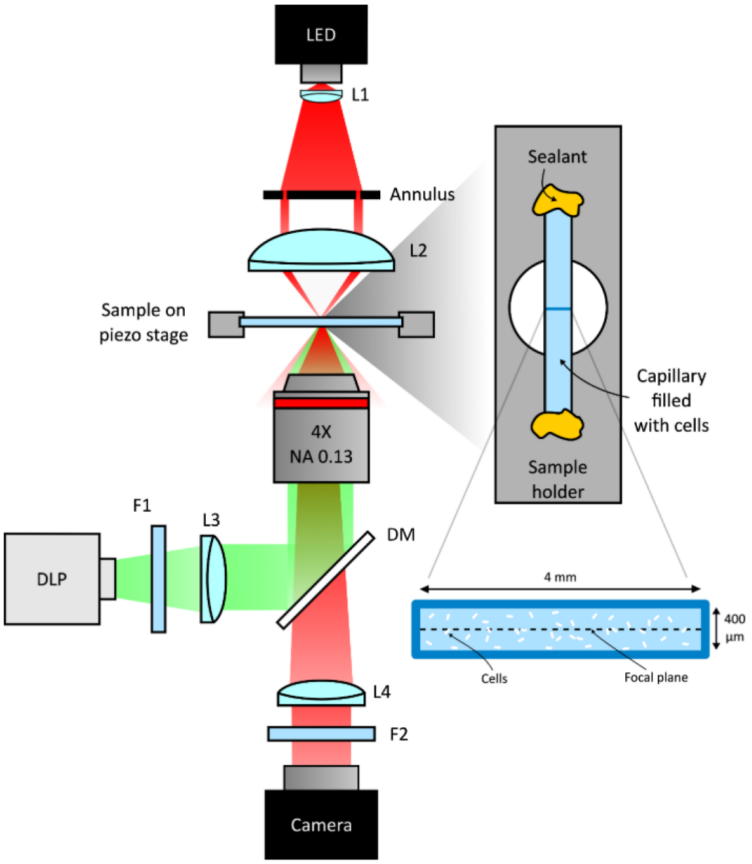

Figure 2.16: **Optical set-up for the density shaping of bacteria.** Reproduced from [131] under CC BY–4.0.

Shown in Figure 2.16 is an optical set-up employed by Frangipane et al. for the density shaping of bacteria into well known images through optogenetic motility control [131]. A DMD based projection module (DLP LightCrafter 4500, Texas Instruments) is directed through a 520 nm bandpass filter and reflected upwards by a dichroic mirror and through a 4× objective to the sample stage. The sample is imaged through the same objective, with red LED light passed through this lens and through the dichroic mirror to the camera. An automated feedback loop, running at 1 iteration every 20 seconds, was used to optimise the density control by comparing real time camera images to the target image. The minimal pixel resolution is stated to be 2 µm, giving an estimated workspace region of 1.82×2.28 mm based on the native 912×1140 resolution of the DMD module. The projection module is able to deliver light in 617, 520 and 465 nm wavelengths, however due to the dichroic mirror used to combine imaging and projection pathways only the latter two could be used with this set-up. The projected light is also not visible

in captured images, being first reflected away by the dichroic mirror and then further filtered out by a long pass filter before reaching the camera.

2.4.2.2 Open and reproducible optical control platforms

Where the previous section served to highlight some of the custom built optical systems employed for a particular control application, this section focuses on platforms presented for wider use for which a greater level of reproducibility should be expected. The availability of thorough documentation is an important factor in this, such as detailed schematics, parts lists and and availability of operational software.

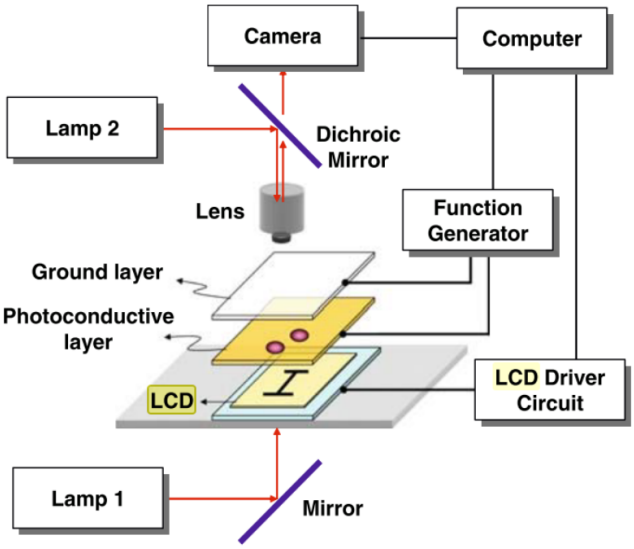

Figure 2.17: **'Lab-on-a-display' optical control device.** Reproduced with permission from [64] © 2006 Springer Nature.

A closed-loop optoelectronic manipulation device was designed by Choi et al., depicted in Figure 2.17, which they call a 'Lab-on-a-display' [64]. This device features a monochromatic LCD module that was removed from a commercial projector (EMP-5300, Epson). A photoconductive layer needed for optoelectronic control was placed directly on top of the LCD, however this is specific to the optoelectronic application. An upright, off-the-shelf microscope coupled with a digital camera was used for imaging. The microscope used features both downside and upside illumination, meaning that they were able to use the former for actuation and the latter for observation of the system. Although white light was delivered by the downside illumination source, only red light was able to permeate the photoconductive layer, likely due to wavelength-dependent absorption in the amorphous silicon. It should be noted however that these absorption effects would not be present in the absence of the photoconductive layer if a similar set-up was employed for applications outside optoelectronic control. It was also observed that 2 out of every 6 pixels failed to light up for reasons thought to originate in the LCD driver circuits. This meant

that the image patterns sent to the SLM chip were not reproduced in their entirety. Despite this, the system was demonstrated to be capable of assembling polystyrene beads into an I shape within 60 seconds. It is unclear whether a closed-loop algorithm was used in this instance, as the images were drawn using Microsoft PowerPoint. Given that the same computer is used to receive camera images and to drive the LCD however, this set-up does have the potential for closed-loop control. Since the sample workspace in this device is directly on top of the SLM chip, the minimal pixel size is simply equal to the pixel size of the chip. This is given as 33 µm, with a total workspace area of 26.4×19.6 mm.

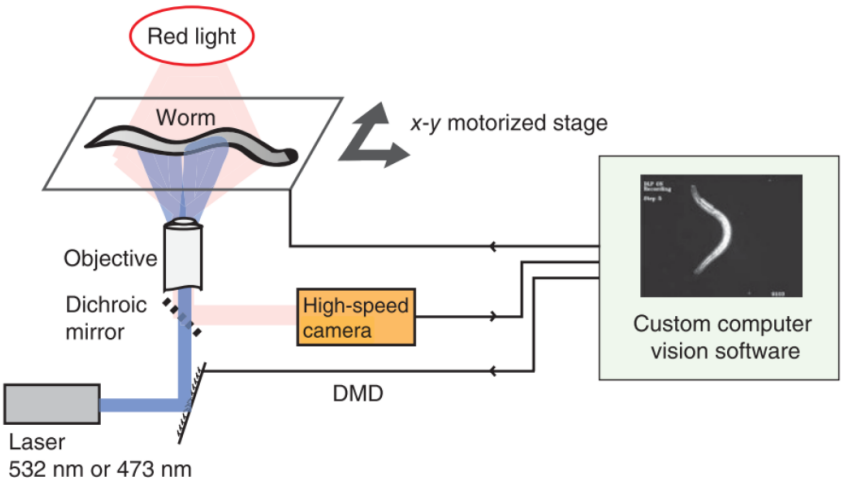

Figure 2.18: **Device for optogenetic illumination.** Reproduced with permission from [224] © Springer Nature 2011.

A device for optogenetic illumination based on a high speed feedback loop, proposed by Leifer et al. [224], is shown in Figure 2.18. The system was demonstrated to be capable of controlling the locomotion and behaviour of *Caenorhabditis elegans* through the optogenetic targeting of cells expressing light-responsive proteins. The system, known as Colbert, uses a fast patterning DMD module (Discovery 4000, Texas Instruments) to shape the light of a 532 nm or 473 nm laser beam. The structured light passes through a 580 nm dichroic mirror and through a 10× objective to the sample, which is situation on an x-y motorised stage. To avoid exciting the light sensitive proteins, red light is used for dark-field illumination of the sample, with light passing through the same objective and being reflected by the dichroic mirror to a high speed camera. Custom software written in C called MindControl was developed for real time image analysis and DMD pattern generation, all of which is available online. The minimum theoretical pixel size is given as 5 µm, though in practice the minimum spatial resolution demonstrated was 30 µm for a freely swimming worm with the system working at the maximum speed of around 50 frames per second. The size of the sample workspace is not given, however using the minimum pixel size of 5 µm and a native DMD resolution of 1024×786 pixels this can be estimated as a maximum of 5.12×3.93mm. Any wavelength of light under the 580 nm limit of the dichoric mirror should be

compatible with this system, however the light patterns are not visible to the camera due to the combined imaging pathway.

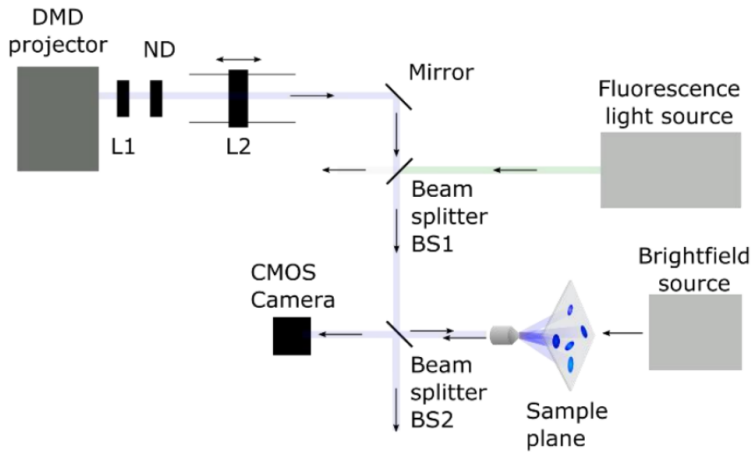

Figure 2.19: **Device for optogenetic illumination.** Reproduced by [340] under CC BY–NC–ND 4.0.

Another system for optogenetic illumination is presented in work by Rullan et al. (Figure 2.19), in this case used for the precise single-cell control of transcription in *Saccharomyces cerevisiae* [340]. This set-up uses a DMD based projector (DLP LightCrafter 4500, Texas Instruments) to pass light through focusing optics to an off-the-shelf inverted microscope. The microscope is equipped with both a fluorescence excitation light source and bright-field light source. Projector light is combined with fluorescence illumination using a 50/50 beam splitter, and passed to the sample plane by a second identical beam splitter. Light from the bright-field illumination source is directed to the sample plane and through the second beam splitter to a camera. The use of non-wavelength specific beam splitters means that projected light and fluorescence wavelengths are both visible to the camera in addition to bright-field imaging. Although only blue patterned light was used in the device demonstration, the light engine contained within this projection module is capable of delivering 617, 520 and 465 nm wavelengths, all of which could be delivered through the optics to the sample stage. The resolution and workspace size are unknown, however the components required to reproduce the set-up are provided as supplementary material, as well as an outline of the calibration process.

A platform for automated optogenetic illumination was also reported by Chait et al., and shown to be capable of of controlling optogenetic expression for hundreds of individual bacterial cells [53]. This plaform, shown in Figure 2.20, uses a LCD projector (PT-AT6000E, Panasonic) modified by the replacement of the original light source with 530 and 660 nm LED sources, and the removal of the projection lens. Light from the projector is carried by field and tubes lenses, then directed into an off-the-shelf inverted microscope by reflection from a 50/50 beamsplitter. The microscope also contains a fluorescence illumination light source, which is focused by the

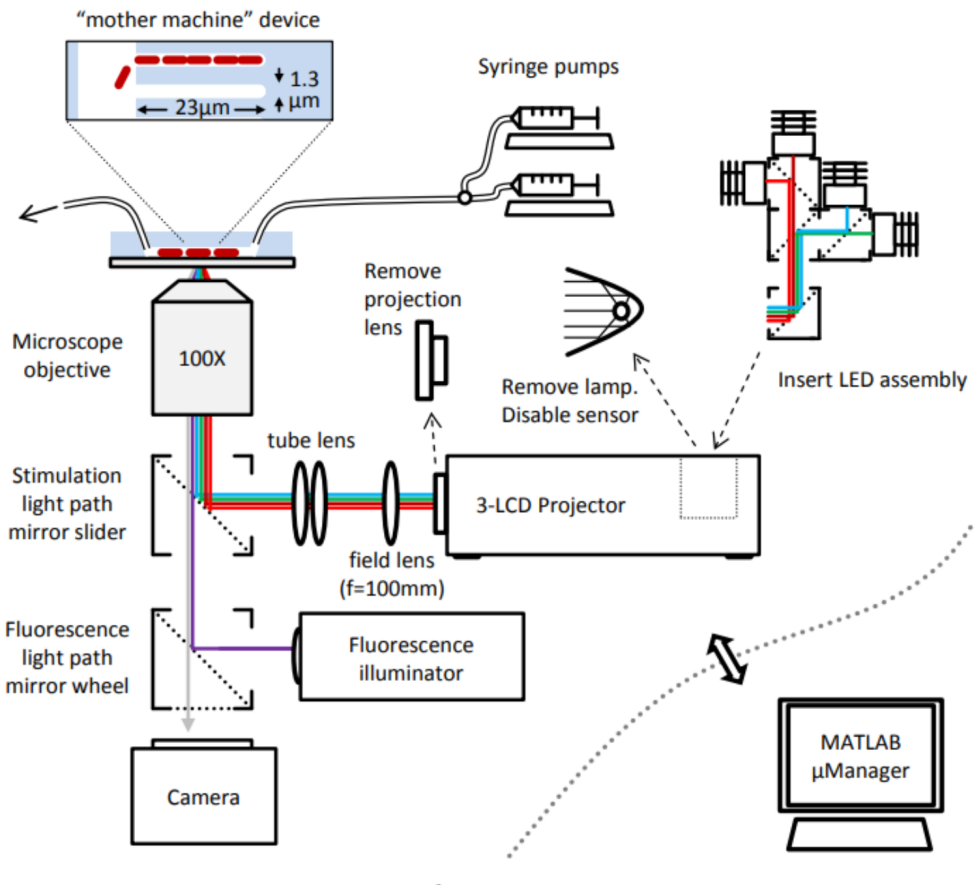

Figure 2.20: **Device for optogenetic illumination.** Reproduced by [53] under CC BY–A 4.0.

objective and used for sample imaging. Only fluorescence imaging is used in the set-up, with sample fluorescence imaged through the objective and delivered through the microscope to a high quantum efficiency camera. A pixel size as small as 0.24 µm is reported, although when lines were projected at this spacing they appear hard to resolve individually. The workspace size is not provided, however assuming that 0.24 µm is the minimal pixel size, the 1920×1080 native resolution of the projector would imply a maximum workspace of 0.46×0.26 mm. A feedback loop is operated using MATLAB, with the files needed for device control and data processing supplied as supplementary materials. Also provided are specifics of the optical set-up and components used, although details of the custom LED assembly used to replace the projector light source are not given.

A closed-loop optical set-up was developed by Lam. et al with the goal of providing a platform for the programming of swarm behaviours in microagent systems [218]. In this set-up, shown in Figure 2.21, a DLP projector (IVPJMP70, iVation) directs light through a 4× objective. The sample is then observed through 2 combined 4× objective lenses forming a relay lens, passing the image to a webcam linked to the control computer. This platform also includes an LED on each side of

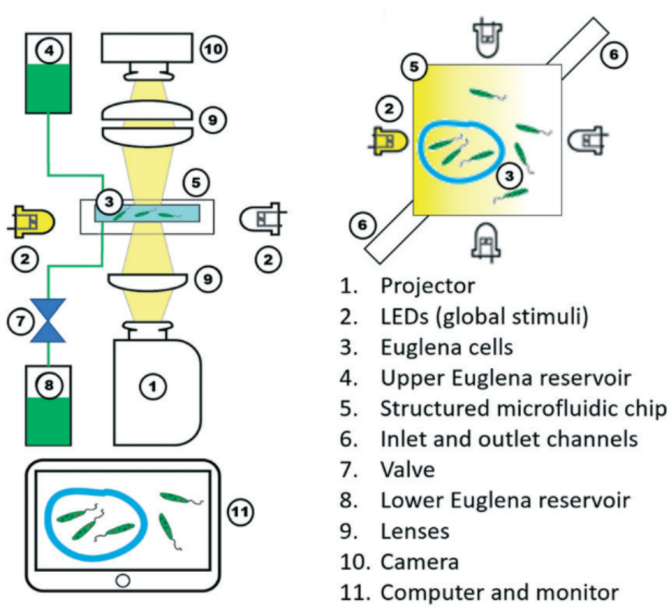

Figure 2.21: **An optical device for the programming of microswarms.** Reproduced from [218] under CC BY–NC 3.0 published by The Royal Society of Chemistry.

the sample stage (4 in total) to provide directional light stimuli in the sample plane. The device is demonstrated to be capable of directing a group of phototactic *Euglena gracilis* to complete tasks such as group migration and shape formation. The minimal pixel size is stated to be 20 µm with a 4.0×2.5 mm workspace. The projector uses a white light source, the emission spectra of which is not available. As no wavelength specific filters or mirrors are used, the full spectrum of light output by the projector is available to be used. All key components are detailed in text and the software developed for feedback control, written in Java, is provided as supplementary material. Detailed schematics are not available however, and although a construction cost of $750 is quoted, this excludes the optical breadboard and associated optomechanical that appear in the set-up.

In work by Stirman et al., a protocol for the construction of an illumination system for precise optical control of microscale structures was presented, depicted in Figure 2.22 [369]. Here, a LCD projector (CP-X605, Hitachi) is modified by the addition of bandpass filters to select for particular wavelengths contained within the native halide light source, and by the removal of the projection lens. The device requires a inverted microscope with epifluorescence port, as it is through this port that the projected light is passed using a tube lens or relay lens pair. Light is then directed upwards by reflection from a dichroic mirror to be focused onto the sample by an objective lens. The sample is imaged using the same objective lens, passing light through the dichroic mirror to a camera attached to the microscope. An example application is demonstrated in which the motility of *Caenorhabditis elegans* is optogenetically controlled. The minimal pixel resolution is dependent on the objective lens used, and is stated to be 14 or 5 µm for 4 or 25× lenses respectively. The manipulation area is not given, however using the native projector resolution of 1024×768 the

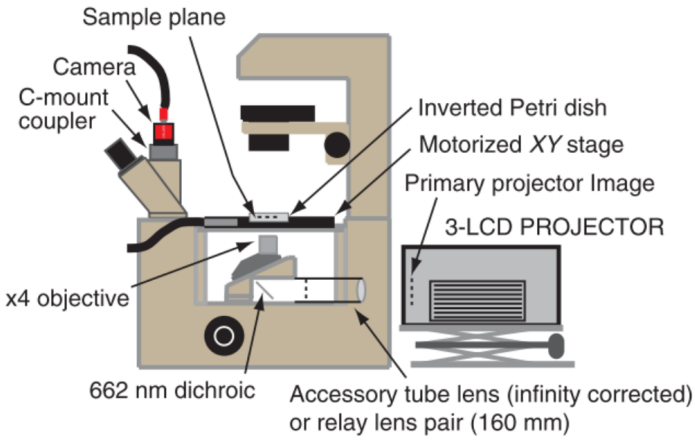

Figure 2.22: **Device for optogenetic illumination.** Reproduced with permision from [369] © Springer Nature 2012

maximum area can be estimated as 14.37×10.75 mm for the lower magnification a 4× lens. The wavelengths provided by the system are 430–475, 543–593 and 585–670 nm, however as these are dependent on the bandpass filters added to the projector this could be easily customised. Since the dichroic mirror used to combine imaging and projection pathways has a cut-off wavelength of 662 nm, projected patterns can be visualised by the camera. It is notable that of the systems described thus far, this is the only instance in which instructions for the replication of the full device are provided, with a detailed step-by-step procedure included alongside details of required components. In this sense, this is the only system thus far that could be considered as an open platform. Software is not provided but a high level description of the control scheme is given.

2.4.3 Devices summary and comparison

A summary of the technical specifications and available documentation for the devices discussed is shown in Table 2.2. Presented are a number of high-quality platforms that provide a more accessible path to closed-loop optical control than commercially available options. Alongside the devices that have been laid out thus far in this chapter, the final row in the table also gives specifications for the DOME platform that is the partial subject of this thesis, and which is presented in full in Chapter 3. In summary, the DOME is an open-source platform for the closed loop control of microagent systems which utilises DLP technology in combination with light microscopy to enact this control scheme. It is a fully integrated, stand alone device fabricated using 3D printing, with all printing files available online along with the relevant calibration code. As seen in Table 2.2, the DOME provides light patterning with 30×30 µm resolution to a sample area of 2.79×1.74 or 14.56×14.56, depending on the level of magnification. These specifications are competitive with the other devices included in the table, although at the slightly lower end of the resolution range. The DOME is one of the few devices to offer three different illumination

Ref.	SLM type	Minimal pixel size (µm)	Manipulation area (mm)	Illumination wavelengths (nm)	Wavelength limitations (nm)	Imaging modes	Open	Schematics & documentation
[324]	LC module	20	16×12	1064	None	Unknown	No	Partially
[302]	DMD module	Unknown	Unknown	532	>484	Unknown	No	Partially
[64]	LC module	33	26.4×19.6	Unknown	None	BF	No	No
[340]	DLP projector	Unknown	Unknown	617, 520, 465	None	BF, FL	No	Yes
[131]	DLP projector	2	2.3×1.8*	617, 520, 465	<520	BF	No	Yes
[53]	LCD projector	0.24	0.5×0.3	530, 660	None	FL	Partially	Partially
[366]	DLP projector	1	1.1×0.9*	<500	<500	BF	No	No
[218]	DLP projector	20	4.0×2.5	Full spectrum	None	BF	No	Partially
[369]	LCD projector	5,14	4.4×10.8*	430–475, 543–593, 585–670	<662	BF	Yes	Yes
[224]	DMD module	10, 30	10.2×7.7, 30.72×23.04*	532, 473	<580	BF	No	Yes
[93]	DLP projector	30	2.8×1.7, 14.56×14.56	460, 510, 640	None	BF, FL	Yes	Yes

Table 2.2: **Specifications for optical control systems.** Summary of the key specifications of the closed-loop optical control devices reviewed here. Some values, indicated by an asterisk (*), were calculated using inferences from the text and not directly stated by the authors. The abbreviations BF and FL here stand for bright-field and fluorescence.

wavelengths without any limitations imposed due to the use of filters in the optical pathway. Crucially however, the DOME is one of only two platforms that constitutes open hardware. The other open-source system is that presented by Stirman et al. [369], although unlike the DOME there are no design files to be made available online, rather a detailed protocol for the assembly of components using an off-the-shelf microscope and projector. The cost of constructing this platform is higher than for the DOME by a factor of 10, as can be seen in Table 2.3 A-F, in which the costs associated which each platform are broken down by major component. Specifically, the cost of this system is given in Table 2.3 F at £6860, compared to £685 for for the DOME. For all but one of the optical control systems detailed here, construction prices run into the thousands. The exception to this is the system proposed by Lam et al., with much lower estimated cost of just £524 (Table 2.2 E) [218]. However, this total does not include the optical breadboard used in the construction and alignment of the system, a cost that could not be calculated as these parts were not detailed in the text, but would likely be in the £100s at minimum. Of all these devices, only the DOME provides a fully integrated device, where all others require external computer connections, and in some cases specialised equipment such as optical breadboards. The technical specifications of the DOME are comparable to those offered by similar devices at a significantly lower price point.

2.5 Future perspective

This chapter has explored the use of a light as a control agent for both individually acting and collective microagent systems. This includes a vast array of agent types, including bacteria, polymer microrobots, microparticles and mammalian cells. By locally structuring the light delivered to these agents, more complex behaviours can be facilitated such as shaping collective cell migration [398], and biomimetic locomotion [302]. The further addition of closed-loop computation results in an automated feedback scheme that allows the rapid changes in the patterning and delivery of light based on the evolving dynamics of a microsystem. In certain fields, such as optogenetics, there is a notable presence of such systems, however in general the adoption of such systems is not yet widespread. Even in optoelectronic applications, which often use SLM technology for light patterning, there is little integration of closed-loop computation for automation of manipulation processes. Likewise for light-based micromotors, optical interaction is mostly limited to single, uniform light sources. This despite the probing of collective phenomena that could benefit greatly from a dynamic, locally structured light environment. In summary, there is significant potential for closed-loop optical control techniques in applications for which they are not currently commonplace. It is reasonable to assume that in some instances the cost and expertise associated with their construction is a prohibiting factor. Owing to this, the availability of accessible optical control platforms, such as the DOME, could impact wider research by bring spatiotemporal feedback-based light control into settings where it would otherwise have little chance of use.

Component	**Specifics**	**Cost (£)**
Microscope	Zeiss Axioskop	3000*
SLM type	Epson EMP-5300	50
Camera	Coolpix5400	85
Additional Optics	-	-
Light source	-	-
Other	Function generator	225
Total estimated costs	3360	

A

Component	**Specifics**	**Cost (£)**
Microscope	Nikon Eclipse TE2000-U	5000*
SLM type	DLP discovery 400	715
Camera	PhotonFocus MV2-D1280-640CL	1500*
Additional Optics	Filters and lenses	648*
Light source	Laser sources	508
Other	-	-
Total estimated costs	8371	

B

Component	**Specifics**	**Cost (£)**
Microscope	Nikon Ti-Eclipse	5000*
SLM type	DLP LightCrafter 4500	1345
Camera	ORCA-Flash4.0	1000
Additional Optics	Filters and lenses	721
Light source	-	-
Other	-	-
Total estimated costs	8066	

C

Component	**Specifics**	**Cost (£)**
Microscope	Olympus IX83	10,000*
SLM type	Panasonic PT-AT6000E	500*
Camera	ORCA-Flash4.0v2	1000*
Additional Optics	Filters and lenses	203*
Light source	LED sources	640
Other	-	-
Total estimated costs	12,343	

D

Component	**Specifics**	**Cost (£)**
Microscope	Custom	217
SLM type	iVation IVPJMP70	216
Camera	Logitech c905 webcam	71
Additional Optics	-	-
Light source	-	-
Other	Optical breadboard	Unknown
	Ardunio Uno	20
Total estimated costs	524	

E

Component	**Specifics**	**Cost (£)**
Microscope	Olympus IMT-2	4000*
SLM type	Hitachi CP-X605	1647
Camera	AVT Guppy F-033	676
Additional Optics	Filters and lenses	537
Light source	-	-
Other	-	-
Total estimated costs	6860	

F

Table 2.3: **Cost breakdown for various optical control devices.** Construction cost for optical control platforms proposed by **(A)** Choi et al. [64], **(B)** Leifer et al. [224], **(C)** Rullan et al. [340], **(D)** Chait et al. [53], **(E)** Lam et al. [218] and **(F)** Stirman et al. [369]. Components that are no longer available or not directly costable from a verifiable retailer for any other reason are marked with an asterisk (*). All prices are given to the nearest whole pound (£).

CHAPTER 3

THE DYNAMIC OPTICAL MICRO-ENVIRONMENT

Key Findings

This section relates to the fabrication methods and characterisation results of the DOME, a device for closed-loop optical control at the microscale, parts of which are also presented in [93] The DOME takes advantage of 3D printing and inexpensive electronics, ensuring that the device is low-cost and reproducible. The integration of imaging optics, DLP technology and a closed computational set-up facilitates multi-wavelength optical control, localised with 30μm resolution. The use of feedback control, based on real time image analysis makes the DOME an effective platform for closed-loop control of microagents systems.

3.1 Introduction

Light is a versatile and powerful tool for microagent control owing to the many photoresponsive mechanisms encountered at these small-scales. As discussed in Chapter 2, optical control has been demonstrated for a wide variety of different microagents and microsystems, with applications across many disciplines. Despite the widespread applicability of optical control methods, hardware options for the localised, dynamic control of microagents are limited. The few commercial options that exist are high-cost and rely on proprietary software, making customisation challenging. A number of non-commercial, reproducible set-ups have been proposed in literature [53, 64, 218, 224, 340, 369], as outlined in Section 2.4. Although these platforms demonstrate greater accessibility that commercial options, many still require expensive equipment such as off-the-shelf microscopes or optical breadboards. Furthermore, no platforms has yet fully integrated imaging optics, a light delivery system and closed computational infrastructure into a self-contained device. Here, the DOME is presented as an open-source, integrated device for closed-loop optical

control of microagent systems. The device is constructed using 3D printed parts, together with low-cost electronics and relatively simple optical components. All printing files and basic control scripts are provided online under a CC BY–4.0 licence [1]. Owing to this, the production process is straightforward and inexpensive in comparison to custom set-ups of comparable specifications. A modular design allows for switching between different magnification lenses and imaging modes, as well as the ability to adapt the set-up for different applications. By providing the DOME as an open-source device, it is hoped that the accessibility of light manipulation techniques can be broadened by largely removing the barriers of cost and expertise. This could facilitate the deeper exploration of optical control for agents such as micromotors, soft microrobots and phototactic organisms, all of which have been shown to be influenced by light-based interactions, but often in the absence of spatiotemporal control. The controllable pixel grid of light provided by the DOME is also well suited to working with collective systems, including biofilms or mammalian tissue, as the optical microenviornment can be shaped around many individual agents independently and in parallel.

This chapter will discuss the components and construction process of the DOME, and the integration of optical and computational components for effective closed loop control. The calibration process will also be outlined, as well as the image processing and control algorithms employed. Additionally, results of characterisation tests for important system parameters such as resolution and latency will be provided.

3.2 Background

The operation of the DOME is based around the closed-loop control of localised light delivery, coupled with microscopy imaging. While this kind of optical control has been demonstrated previously, the novelty of this device is it's self-contained design, open-source availability, and low-cost. In this background, the low-cost technology used to fabricate the DOME will be discussed, as well as the growing popularity and impact of the open-source movement.

3.2.1 The open-source movement

The term open-source is used to describe a project that is freely accessible for all to use, adapt and redistribute, encouraging a collaborative development process. It was originally coined in the late 1990s to refer primarily to open-source software. Open-source software rejects a rigid development structure in favour of a bottom up, decentralised process in which source code and documentation are readily available. Many open-source software projects are now popular in science and engineering applications, for example Python and Fiji [296, 348], as well as the more mainstream use of programs such as Mozilla Firefox and Linux [165, 288]. Around the time that

[1] STL files for 3D printing and custom PCB plans, along with calibration and control code for the DOME are all available at bitbucket.org/hauertlab/dome

the open-source software movement was formalised, the idea of open-source hardware also began to gain traction. This was driven in large part by growing availability of compact, cheap electronic tools and the advancement of DIY manufacturing processes such as 3D printing and laser cutting. Open-source hardware consists of physical products that are easily reproducible through freely accessible documentation such as schematics, PCB designs and CAD files. Although not a prerequisite, open-source hardware is typically inexpensive, costing around 1–10% the price of comparable commercial technology [326].

3.2.1.1 Open-source devices

Today, examples of open-source hardware products can be found in many areas. One of the best known examples is the Arduino, a microcontroller board which is not only itself open-source, but is futher utilised in numerous open-hardware projects [2, 8, 215, 319]. SparkFun Electronics also supply open microcontroller and breakout boards that, although designed with education in mind, are commonly utilised in more advanced hardware projects [10, 27, 281]. Open hardware design has additionally been brought to small-scale manufacturing. The RepRap project (short for replicating rapid prototyper) has created a number of open-source printers capable of producing some of their own parts, with the eventual goal of total self-replication [195]. Precious Plastics is another open-source project, based around a number of machines capable of recycling waste plastic into new products through a series of reconstitutive processes [100, 225]. Also notable is the Raspberry Pi range, a family of inexpensive single-board computers and related accessories. While the boards themselves are not open-source, they do run an open-source operating system and provide extensive documentation. This has resulted in the Raspberry Pi becoming a staple of the open-source movement [63, 228, 405, 407]. The examples given here give just a small glimpse into the wider world of open-source devices, with extensive lists available through the open-source Hardware Association, an organisation that advocates for and maintains certification of open hardware.

3.2.1.2 Open-source and DIY hardware in science and medicine

The influence of open-hardware is especially notable in the context of scientific and medical research, with the design and use of open-source labware, research equipment and medical devices becoming increasingly commonplace [84, 216, 283, 312]. Scientific equipment is traditionally expensive, in part due to the robust patent and copyright frameworks in which it is often developed, and can therefore be exclusionary to institutions working in low-income countries or with limited funding [52]. The development of affordable scientific hardware within an open-source framework is a challenge to this, elevating accessibility in these lower resource settings. Besides cost considerations, the open-hardware model for scientific equipment is also beneficial due to the enhanced speed at which innovation and distribution can occur, allowing for further community development. New scientific hardware can therefore be developed in a

rapid, decentralised manner in response to new discoveries and challenges. This was particularly apparent during the COVID-19 pandemic, with the widespread dissemination of open-source designs for personal protective equipment, ventilators and diagnostic technologies [240]. Moreover, cutting edge research often requires tools that simply do not yet exist, leading many to turn to technologies associated with open or DIY hardware. 3D printing has been especially popular in this regard, facilitating the rapid prototyping and fabrication of tailor-made parts [25, 70, 150], as well as the use of Arduinos and other microcontrollers for custom devices [111, 282]. Owing to the increasing prevalence of open hardware in the scientific community, journals have been established that focus specifically on this subject, most notably HardwareX and The Journal of Open Hardware [311].

Examples of open-source hardware can be found in many scientific fields, including the e-puck and Kilobot in robotics [261, 337], as well as numerous biotechnology innovations [211, 334, 367, 412]. Of particular relevance in the context of this work is the application of DIY techniques and open-source principles to the development of low-cost microscopes. One of the most prominent of these is the OpenFlexture microscope [72], a 3D-printed, automated microscope capable of laboratory grade imaging. The OpenFlexture microscope is highly modular, with customisable optics and filters providing a range of potential illumination and imaging modes. This highlights one of the key benefits of open-source hardware in general; different applications of a given device often require a different toolset, thus hardware that can be easily adapted is likely to be useful in a wider variety of settings than a closed-source commercial product. Another example is the FlyPi, a 3D printed microscope designed for monitoring the behaviour of small organisms such as *Drosophila*, and *Caenorhabditis elegans* using a Raspberry Pi with camera accessory [241]. The FlyPi is also capable of optogenetic stimulation, although the spatial localisation of this is limited to an 8×8 grid, dictated by the physical LED matrix used. A 3D printed microscope developed by Nuñez et al. was shown to be effective in the fluorescence imaging of multiple wavelength emissions, operating using a Raspberry Pi and 470nm excitation LEDs [287]. Aside from integrated microscope devices such as these, more modular microscopy toolboxes have also been investigated. One such toolbox is the UC2, a set of 3D printed modular cubes that can house various optical and electronic components, and can be connected in many different configurations for a custom imaging set-up [99].

The examples given here constitute just a slice of the open labware landscape, which is vast and ever growing. While much work remains to be done to standardise design principles, characterisation and documentation [290], the unprecedented level of accessibility afforded by the open hardware framework, together with the adaptability and community development it facilitates holds much promise for the future of scientific instrumentation.

3.2.2 Low-cost technology for closed-loop optical control

The development of closed-loop and localised optical control necessitates the integration of a number of different technologies, including light patterning, microscopy and closed-loop computation. Building a system that includes all of these elements while maintaining the accessibility and cost objectives can be challenging, as optical and electronic components have traditionally often been priced at hundreds, or even thousands of pounds individually. Increasingly however, low-cost alternatives are becoming available through new technological advances and a recognition by manufactures of the growing open-source hardware and hobbyist markets.

3.2.2.1 Localised light delivery

In Sections 2.4.1 and 2.4.2, the two main methods of delivering localised light were outlined, namely time-shared lasers and SLM devices. Time-shared laser beam systems, while an effective way to deliver highly localised light, require high level experience of optical systems to build, calibrate and operate. Furthermore, the high associated costs and issues with scaling for large agent numbers make this type of set-up unsuitable in this context. The alternative and most commonly used technology in optical control set-ups are DMD and LC-based SLM chips, either as stand alone modules or within DLP, LCD or LCoS projectors. Although a more accessible option, this technology has still traditionally been relatively expensive. The DLP LightCrafter 4500 (Texas Instruments) DMD module for instance, used in multiple devices discussed in Section 2.4, is priced at £1,345. Commercial projector systems vary dramatically in price, with some budget models such as that used in [218] retailing around just £210, up to the tens of thousands for higher-end devices. In regards to the specific application of building an open-source, closed-loop optical control device, off-the-shelf commercial projectors are problematic as they can be difficult to integrate and adapt. A solution that is both low-cost and designed with development in mind was launched by Texas Instruments in 2019, with the DMD-based DLP LightCrafter Display 2000 Evaluation Module. This module is priced around just £100, and can interface with single board computers for straightforward system integration. Thus far, this device has been used to build an open-source benchtop incubator with in built optogenetic capabilities [412], as well as facilitating light-based experimentation in educational contexts [305]. It is also the light delivery system employed in the DOME, providing rapid, digitally controllable RGB light projections while serving the low-cost aim.

3.2.2.2 Imaging and image processing

While light delivery is the bedrock of optical control, closing the loop necessitates the ability to visualise agents within a microsystem, and to process the images real time. Practically speaking, this requires a computer linked to a camera that is equipped with magnification optics. Conventionally, these pieces of equipment can be not only expensive but also bulky, and often use

proprietary software. For all of the closed-loop optical control devices Section 2.4, the computer was treated as external to the set-up, with the 'device' comprising the camera, microscopy optics and light delivery system. Conversely, the objective of designing the DOME is the realisation of a fully self-contained device that includes all projection, imaging and computational elements. The solution employed to achieve this while minimising the issues of size, cost and proprietary software is the use of a Raspberry Pi camera and computer board for image collection and analysis respectively. The first Raspberry Pi computer was launched in 2012 as a low-cost, compact single board computer capable operating as a classic PC as well as interfacing with other devices and integration into wider systems [242]. Today, there exist a range of Raspberry Pi computers, with prices ranging between ~ £10 – £75 for different models. Although the boards themselves are not open hardware, Raspberry Pi equipment is well suited for use in open-source projects owing to their 'hackability' and Debian-based open-source operating software. There also exist numerous accessories, including the camera used in the imaging set-up of the DOME. All the camera models are compact and low-cost, and interface neatly with the Raspberry Pi computer boards such that all camera settings and operation can be controlled by terminal commands or custom scripts. The use of Raspberry Pi technology to facilitate image capture and analysis in the DOME allows for a fully integrated, stand-alone device while keeping costs low. This also enables a level of portability that could be challenging for comparable non-integrated systems, including the potential to operate the device within an incubator. The open-source nature of the Raspberry Pi OS enables a great degree of control over the operation of the system, ensuring that the DOME can be adapted for different applications as needed.

3.2.2.3 3D printing

As briefly mentioned in Section 3.2.1, a major driving factor in the expansion of the open-source hardware movement has been the advancement of 3D printing. In 2018, the value of the global 3D printing market was estimated to be around $9.9 billion, with this number only set to increase [118]. 3D printers can now be accessed through almost all institutes of higher education and major research centers, as well as an ever growing ownership by private individuals. This is a revelation for open-source hardware such as the DOME, as it enables physical system designs to be uploaded and downloaded in the same manner as open-source software. It is through the use of 3D printed parts that the DOME avoids the need to incorporate expensive structural systems, such as optical breadboards or modified off-the-shelf microscopes.

The two main types of 3D printing, fused deposition modelling (FDM) and stereolithography (SLA), were established in the 1980s [150, 204, 280]. Both methods are additive, in that a product is formed by building up layers of printing material on top of one another based on a predefined pattern. SLA printing uses an laser beam to polymerise monomers within a resin to product a solidified structure, whereas FDM printing uses a continuous thermoplastic filament that is fed though a heated nozzle to deposit melted filament. SLA printers can achieve significantly

higher print resolution, as the limiting factor is laser spot size where FDM print resolution is limited by nozzle size, and the precision of x-y movement during printing. SLA printing also produces smoother prints, as layers are photochemically bonded together. Layer adhesion is much weaker in FDM prints and it relies on the new layer bonding to the previous by applying pressure and heat. The trade off for higher print quality is time and cost, as SLA prints are expensive and slow compared to FDM [70]. Additionally, SLA printed parts may require post-processing treatments such as washing, photo-curing or heating [280]. Owing to the faster printing time and lower financial burden, there is a much higher prevalence of FDM printers in the open-hardware movement and in the consumer market generally [70]. For these reasons, the DOME was designed with FDM printing in mind, allowing the greatest possible level of accessibility. By providing the system parts as open-source designs, potential users are also able to carry out modifications where necessary, enabling the flexibility to integrate alternative or new components.

3.3 Materials and methods

This work details the materials and methods that were involved in the fabrication and computational set-up of the DOME device. The DOME provides localised optical control over microagents such as bacteria, algae or mammalian cells by selective illumination of agents using a projection module, as demonstrated conceptually in Figure 3.1A. An imaging module observes changes in the micro-system such as agent density or position, and communicates these changes to the projection module via feedback control, causing the projected light to be restructured in line with the new state of the system.

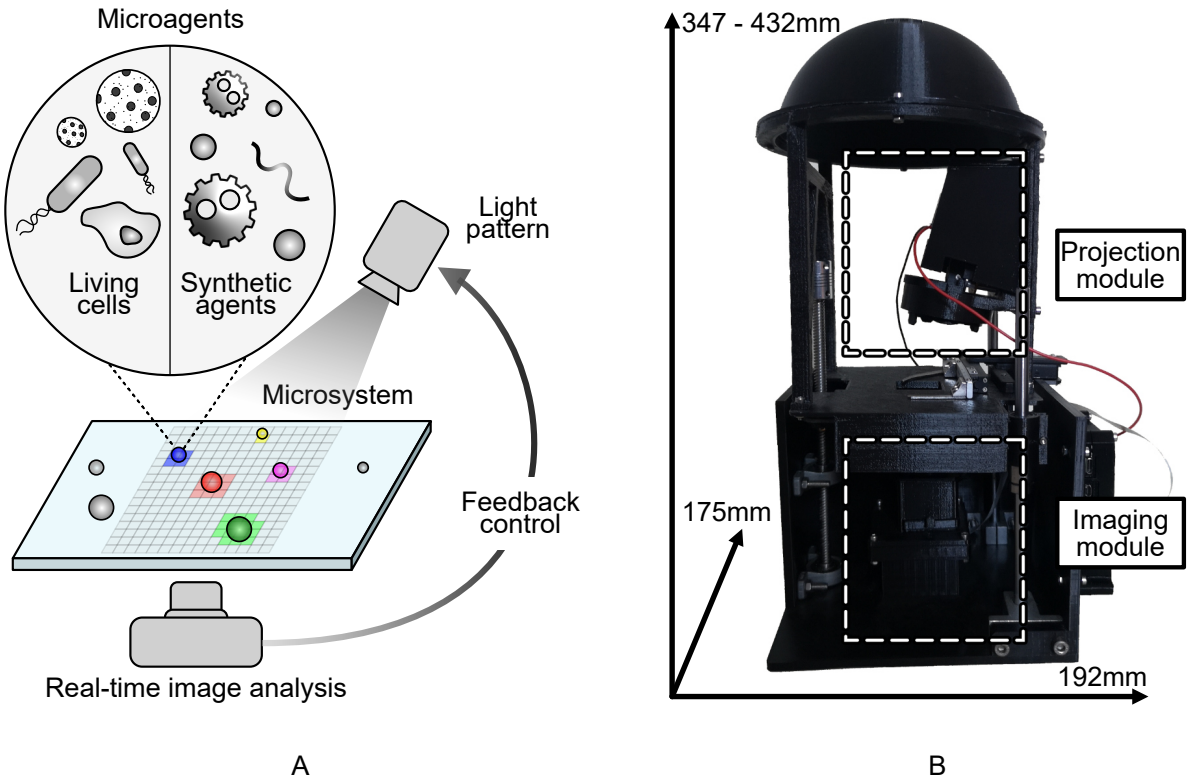

Figure 3.1: **The DOME. (A)** Conceptional diagram of the DOME in which a microagent system is illuminated by light patterns generated by a projection module. The microsystem is observed by an imaging module that connects via a feedback control node to the projection module. **(B)** A picture of the DOME with dashed boxes indicating the position of the projection and imaging modules.

The DOME, pictured in in Figure 3.1B, uses an inverted microscopy in combination with light projection technology to enable closed-loop control of microagents. A schematic representation of this closed-loop control scheme can be seen in Figure 3.2, with light projected down through a condenser lens onto a sample stage. Microagents within the sample are imaged using an inverted microscopy set-up consisting of magnification lenses, a Raspberry Pi camera and optional optical filters. Both camera and projector are controlled by Raspberry Pi computers that connect over

a local network to allow two way communication for closed-loop control. Both computers run Raspberry Pi OS, a Debian GNU/Linux based operating system, and control scripts are written in Python 3. The set-up measures 192×175 mm in width and depth, with height varying between 347 and 432 mm depending on magnification. Samples may be imaged using bright-field or fluorescence illumination, or using solely the projector.

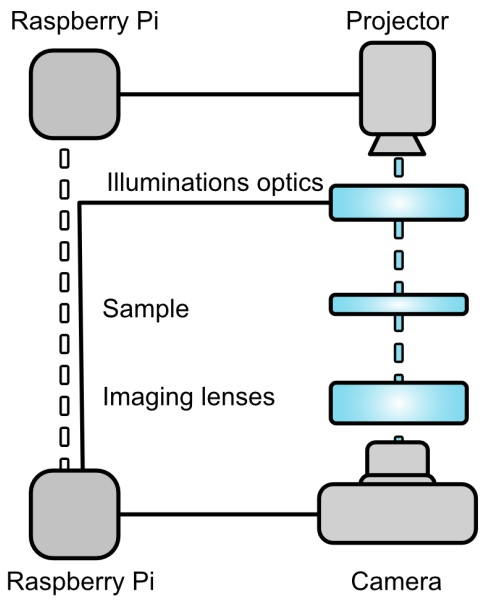

Figure 3.2: **Schematic of the DOME's closed-loop control.** Optical components are shown in blue and electrical components in grey. A solid line indicates a physical connection, such as between camera and Raspberry Pi, while a dashed line indicates intangible connections, namely a wireless network and light beam.

3.3.1 Projection module

Localised light delivery in the DOME is achieved using light projection technology, owing to its low cost and ease of use relative to alternative methods such as time-shared laser beams (see Section 2.4). The SLM-based optical projector outputs a digitally controllable pixel light grid that can be used to interact with a microsystem sample. A DLP projector was chosen to build the DOME due to lower light absorption rates compared to an LCD device, and superior contrast performance at a lower cost in comparison to an LCoS projector. Light absorption is a particularly important parameter, as some applications may require a change of light source to wavelengths at the edge of or beyond the visible light spectrum that are often absorbed at higher rates. The projection device used in the DOME is the DLP Lightcrafter Display 2000 EVM (Texas instruments), which is a complete projection module containing a DMD-based light engine and driver board. The device measures under 55×75 mm, facilitating straightforward integration into a self-contained device compared to a standard sized model. The projector, positioned at the top of the DOME as seen in Figure 3.3A, projects light directly onto the sample stage. The 0.2 inch

ultra compact DMD inside contains a 640×360 micromirror array, and an LED RGB light source based optical engine.

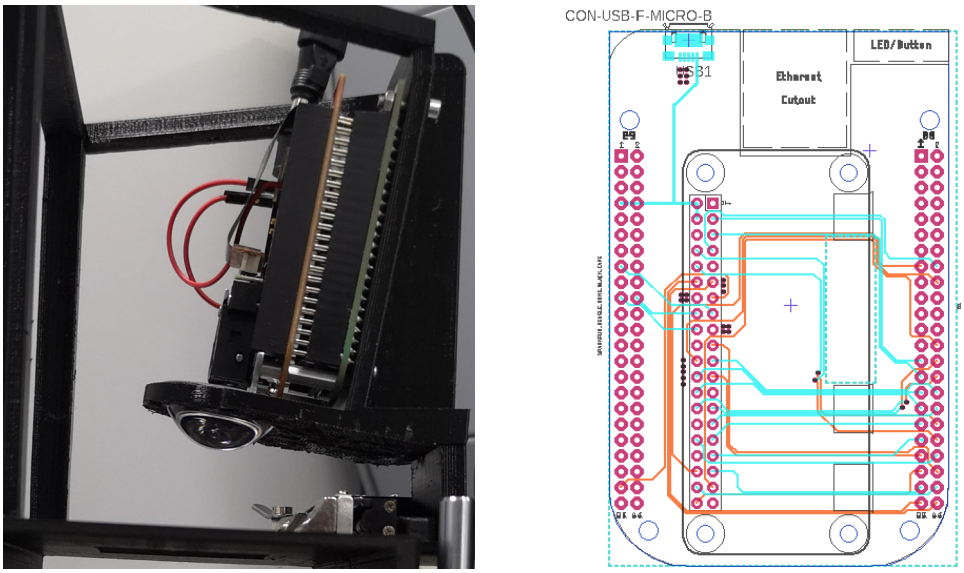

Figure 3.3: **Projection module. (A)** Plans for the custom PCB used to interface the DLP projection module with a Raspberry Pi Zero controller. **(B)** The full projection module shown installed on the DOME.

The DLP Lightcrafter module is designed to interface with a BeagleBone Black single-board computer (Texas Instruments) as a controller. In the DOME however, it was desired that all computational control instead be carried out using Raspberry Pi boards, for several reasons. Although the BeagleBone Black is a higher specification board than those offered by Raspberry Pi, offering more processing power and onboard storage, it also comes at a higher price, with just a single USB connection port and no HDMI connection. Furthermore, a major asset of the Raspberry Pi brand is its flexibility and easy of use, with a familiar desktop environment and support for widely used programming languages such as Python, Java and C++ [242].

Since the Raspberry Pi 4 that forms that basis of the imaging module is also the main user interaction interface, it was desirable that this board remain freely accessible, thus a Raspberry Pi Zero W was introduced as second computer to act as a controller for the DLP Lightcrafter module. While it could be possible to operate both projector and camera from the Raspberry Pi 4, the difficulties in interfacing with the projector are significant and would make the connection of peripherals such as HDMI and imaging LEDs difficult. Additionally, having a dedicated computer responsible for controlling light projection allows use of the imaging module computer as a user interface, minimising the possibility that actions taken by the user will cause a change or interruption to the light output of the system. To facilitate the use of a Raspberry Pi Zero as a controller, a custom PCB was designed in collaboration with technical support staff. This PCB,

the plans of which are shown in Figure 3.3A, enables the DLP Lightcrafter to interface directly with a Raspberry Pi Zero as seen in Figure 3.3B.

3.3.2 Imaging module

While general settings of the Raspberry Pi camera such as resolution and ISO will vary between applications, there is a fixed protocol to initialise the camera such that frames produced can be used within the DOME. Firstly, the camera frame must be cropped to eliminate dead space that occurs due to the series of circular lenses through which the camera images. This is done by collecting a raw camera frame, either while the white bright-field LED is turned on or the projector displays a uniform bright screen. The full camera frame will show a largely black rectangular image with a circular bright spot towards the centre, as seen in Figure 3.4. The perimeter points of the circle are found using contour detection, from which the width, height and center point can be computed by using the OpenCV `rotatedRect` function to find the enclosing rectangle. Once these parameters have been calculated the dimensions of the largest rectangle that may fit inside the circle are found using Equation 3.1 where a is the full, uncropped dimension and b is the new cropped dimension. These values can then be imported by all other scripts running on the DOME to keep cropping consistent.

$$b = \frac{a\sqrt{2}}{2} \tag{3.1}$$

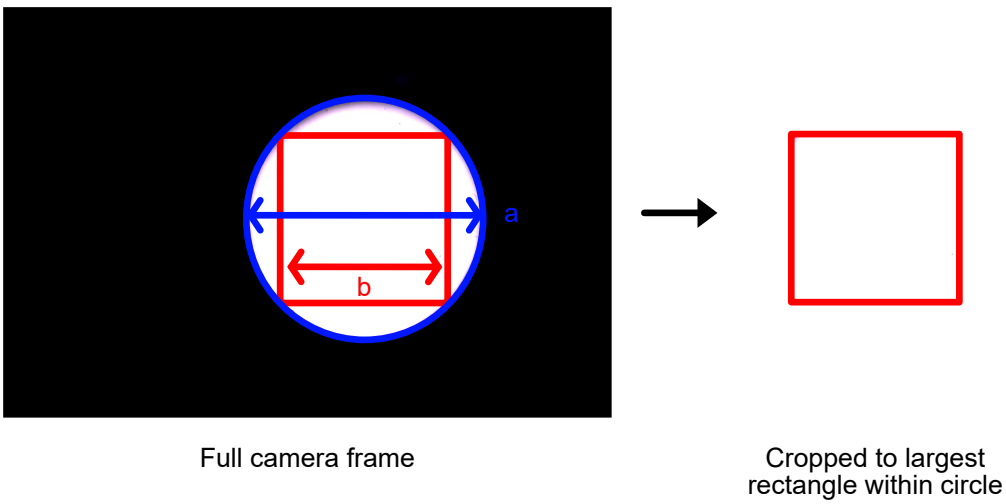

Figure 3.4: **Camera frame cropping process.** Within the full camera frame a circular area indicates the active imaging space. The diameter, a, of this area can be used to calculate the side length, b, of the largest rectangle that fits inside the circle.

Next, camera frames must be re-orientated to align with the orientation of the projected images to facilitate accurate calibration. This is done by projecting an irregular shape with

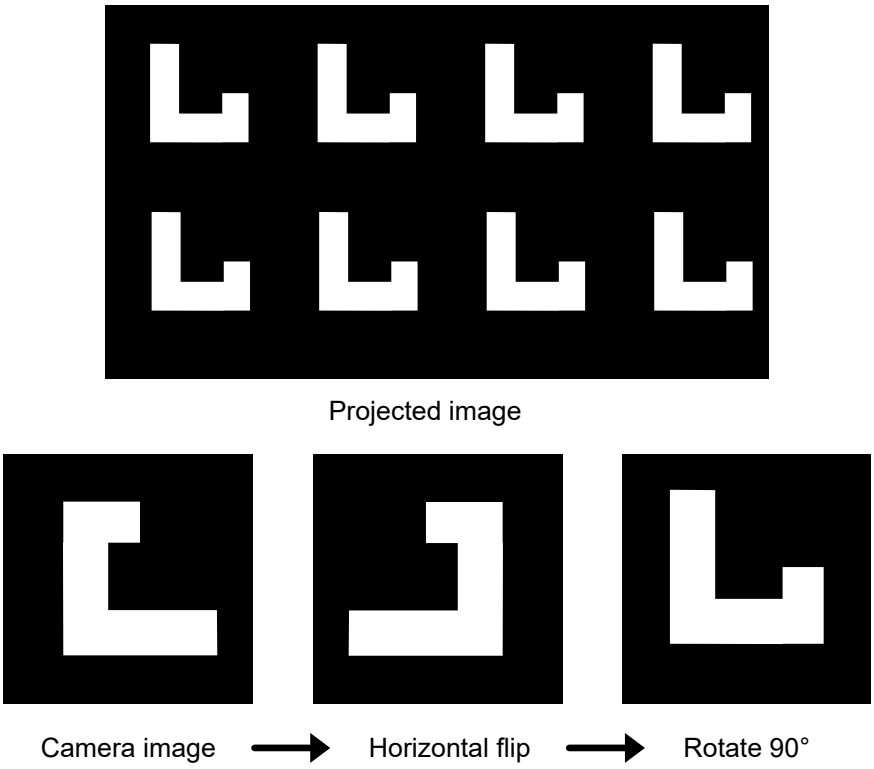

Figure 3.5: **Reorientation of the camera frame.** Projecting an irregular shape with no rotational symmetry allows the orientation of the camera frame to be adjusted to replicate the projection image.

no rotational symmetry, and finding the transformations necessary to display the same shape in the camera frame, as demonstrated in Figure 3.5. This process of cropping and orientation should only require repeating if a change to the physical set-up occurs, for example a change in magnification.

3.3.3 Device integration

A feature that sets the DOME apart from optical control systems that have been implemented thus far (see Section 2.4.2.2) is that it comprises a fully integrated, self-contained device. This means that the imaging and projection modules described above are physically combined into a 3D printed body, which also contains the mechanical components necessary to perform z plane focusing and adjust the sample in the x-y plane. The design of the integrated optical pathway and structural components are detailed in this section.

3.3.3.1 Optical path design

To enable closed-loop control, the DOME must have the ability visualise agents and target them with localised light. This necessitates combining together the optical pathways required for projection and light microscopy (Figure 3.6). The light projection pathway begins inside the

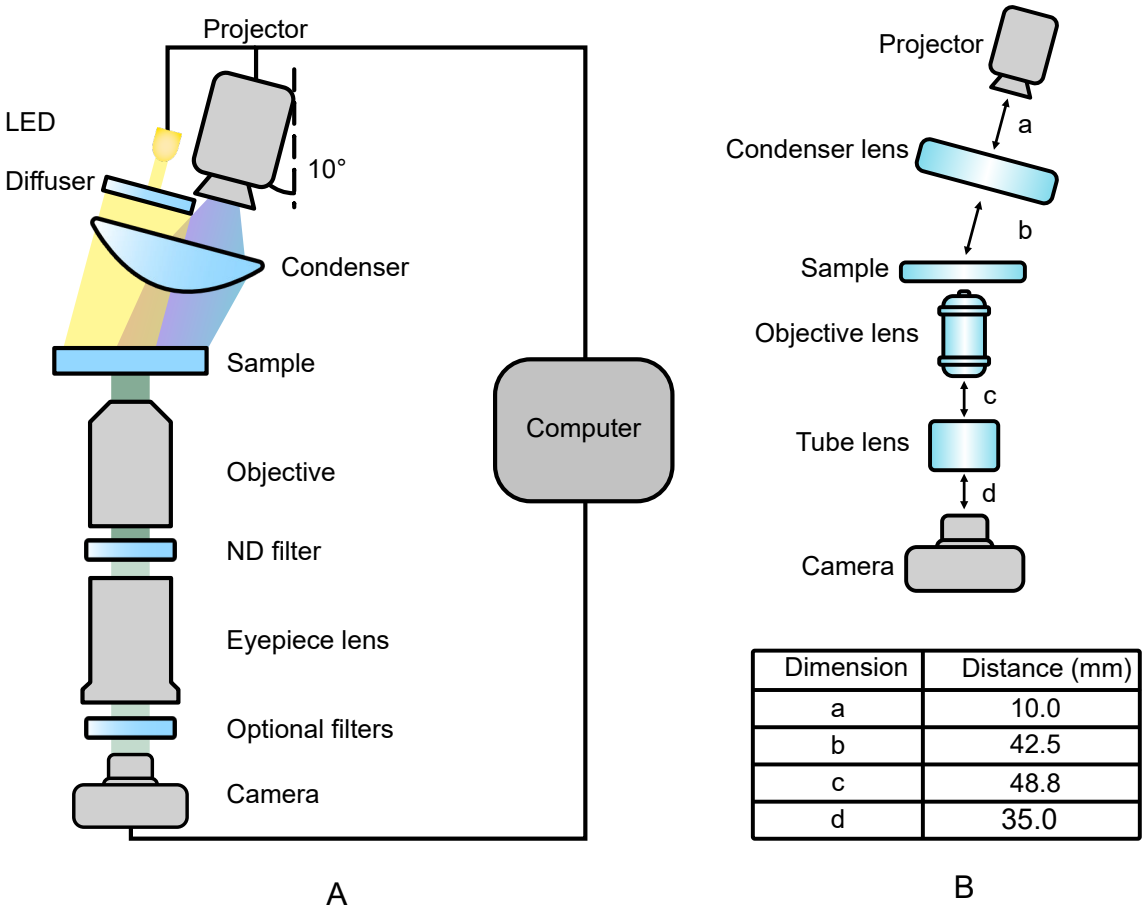

Dimension	Distance (mm)
a	10.0
b	42.5
c	48.8
d	35.0

Figure 3.6: **Optical path diagram for the DOME. (A)** Diagram shows all illumination and imaging components that may be used within the DOME. Simple single lens optical components are represented in blue, while compound lenses and optoelectronics are shown in grey. All computational components of the system are here simplified to a single computer element. **(B)** Specifications of optical path design, with distances between components.

projector where light is generated by RGB LEDs, shaped by reflection from the DMD and emitted as a structured divergent beam. A plano-convex condenser lens (50mm diameter, Edmund Optics) collects and condenses the beam of light to illuminate the sample stage. A white LED, positioned next to the projector, directs light onto a ground glass diffusor (DG10-1500, Thor Labs) to widen the field of illumination. This white light then passes through the condenser lens alongside the structured projector light to provide brightfield illumination for imaging the sample. The DOME uses an inverted microscope imaging set-up, meaning that the sample is imaged from

below through a series of lenses and filters. The specific configuration of the imaging pathway is customisable and depends on the magnification and illumination type used. For a higher magnification application, light from the sample is gathered and focused by a 10x finite conjugate microscope objective (semi-plan standard objective, Edmund Optics). The image is then magnified further by an eyepiece lens (9× eyepiece cell assembly, Edmund Optics) to produce a virtual image that is relayed to the camera (Raspberry Pi camera V2, The Pi Hut) which has an integrated fixed focus lens. A neutral density (ND) filter (NE10B-A, Thor Labs) of optical density 1 is placed atop the eyepiece lens to reduce overall intensity by 90%, minimising optical artifacts and avoiding over saturation of the camera sensor. Additional filters can be placed between the eyepiece and camera, for example wavelength cut off filters for fluorescent imaging. For lower magnification applications, the microscope objective can be removed and the 9× eyepiece lens used to image the sample directly. The challenge in combining the projection and imaging pathways is that projecting light into a camera can cause hotspotting, an extreme oversaturation caused when the camera is exposed to the light source inside the projector (Figure 3.7A). This is exacerbated by the condensing of light into a much smaller beam than would otherwise be produced by the projector, meaning that the size of the 'bright spot' is large compared to that of the projected pattern. To circumvent this problem in the DOME, the projector is placed at an angle θ relative to the sample and camera. By allowing off-axis projection, the camera is able to image the sample, including projected light, without facing directly into the projector bright spot as shown in Figure 3.7B. The choice of angle θ is a trade off between even image saturation, and the distortion of each projected pixel which increases with larger projection angle. The optimal θ is the minimal angle for which the image saturation is sufficiently even to obtain clear images which here was found to be 10°through iterative part design.

An alternative to this, used in several other projector-microscope set-ups [53, 131, 302, 340, 369], is to bypass the hotspot issue by using a beamsplitter to combine projection and imaging pathways perpendicular to each other (Figure 3.8). Beamsplitters are optical filters with both reflective and transmissive properties that can split a beam of light based either on a cut-off wavelength or simply by a given ratio. This property can also be used to combine perpendicular beams into a single path. This is an effective method of beam combination in light projection devices, as it enables light from the projector to be delivered through the objective to the sample stage, where it interacts with the sample in tandem with the standard illumination light source. The drawback to this design however is that it places limitations on the system. The use of a wavelength dependent beamsplitter requires that a cut-off wavelength be chosen, meaning that that only wavelengths on one side of the cut off can be used in projection, and these wavelengths will not be seen by the camera. In the example shown in Figure. 3.8, the reflective cut off wavelength is in the green visible light range, meaning that blue and green light from the projector can be reflected upwards towards the sample, but only red light is able to pass back through the beamsplitter to reach the camera. Therefore while this set-up is effective for

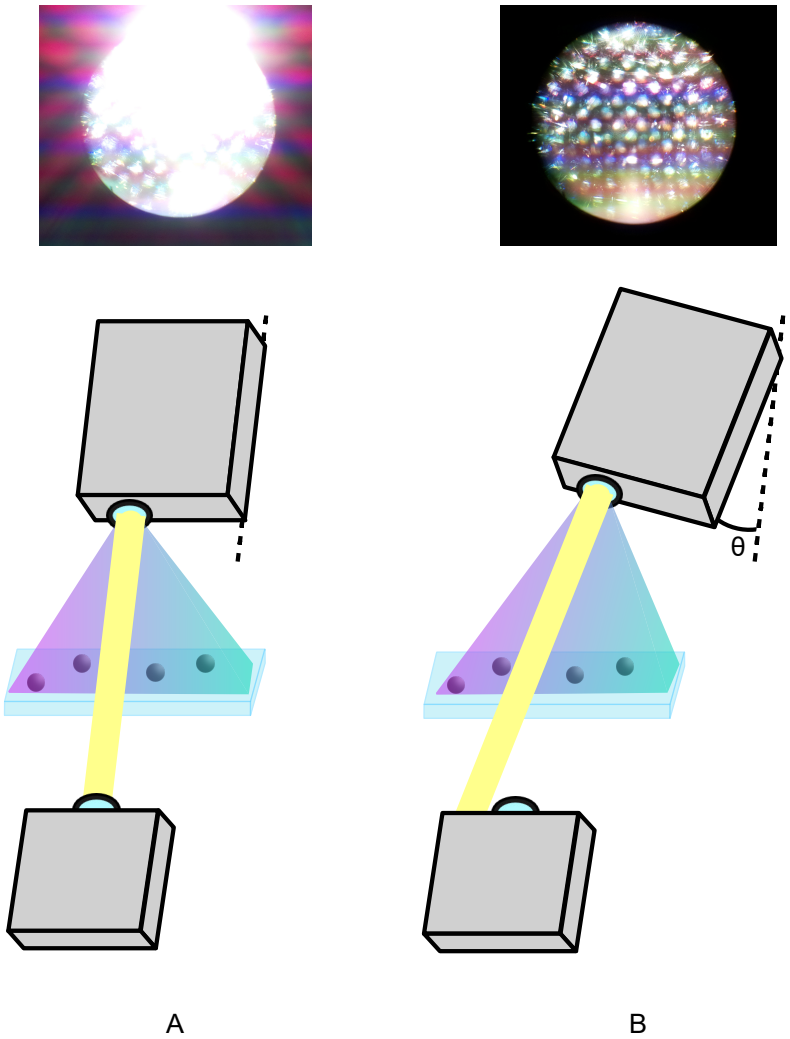

Figure 3.7: **Hotspotting in camera images. (A)** An oversaturated camera image (upper) caused by light projected directly into camera (lower). **(B)** Improved brightness balance (upper) due to off-axis projection at angle θ such that the internal light source of the projector is not visible to the camera (lower).

individual applications, it is less well suited for a device that aims to be modular and applicable to a wide variety of uses. Alternatively, a beamsplitter that operates by a transmission-reflection ratio could be used. This is arguably less limiting as all wavelengths remain available for both projection and imaging, however does lead to a drop in intensity in terms of the light delivered both to the microsystem and the camera.

3.3.3.2 Structural part fabrication

The main structure of the DOME consists primarily of 3D printed custom parts. These parts are modular, with the entire printed structure of the DOME formed of 12 pieces. Parts were

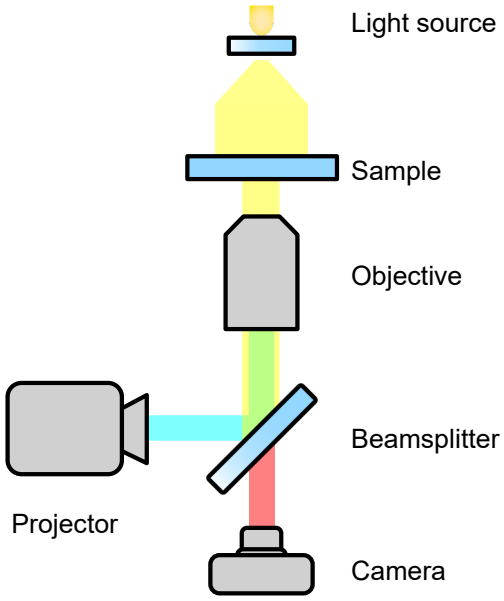

Figure 3.8: **Alternative optical pathway design.** Projection and imaging pathways combined using a beamsplitting filter with wavelength cut off in the green visible light range.

created using computer-aided design (CAD) software, specifically Inventor and Fusion 360 from Autodesk. These part designs are shown in Figure 3.9, broken down into main body components (Figure 3.9A-E), imaging column components (Figure 3.9F-I) and projection and illumination components (Figure 3.9J-N). Part A forms the top half of the DOME, onto which the light blocking lid (B) and projection components attach, fastening to the top of the sample stage (C). The sample stage, which has a square hole cut out in the middle through which the sample is imaged, attaches to the base of the DOME (D) by way of a linear guide rod set. In the center of the DOME base is a raised platform to which the imaging column components are connected. At the base of the imaging column is camera mount onto which a Raspberry Pi camera (E) can be fixed such that it faces upwards. Connected to the mount is a filter block (F), which features a hinged circular filter holder that can be opened and closed by the user in order to add filters to the system. This hinged component is an print-in-place part, a term describing 3D printed designs which have moving parts but can be printed as one piece. This effect is achieved by leaving a small gap, in this case 0.25mm, between moving parts so that the hinge may move freely. Onto the filter block is connected the lens array, which can be an objective and magnifying eyepiece (G) or simply the eyepiece for lower magnification applications (H). Both lenses are externally threaded, and so can be secured to parts H and I using printed complementary internal threads.

The DLP projector is mounted onto a base (I) that attaches to the upper half of the DOME (A). Incorporated into the projector mount is a circular holder into which the condenser lens can be fitted. The holder is internally threaded such that an externally threaded clamp (J) can

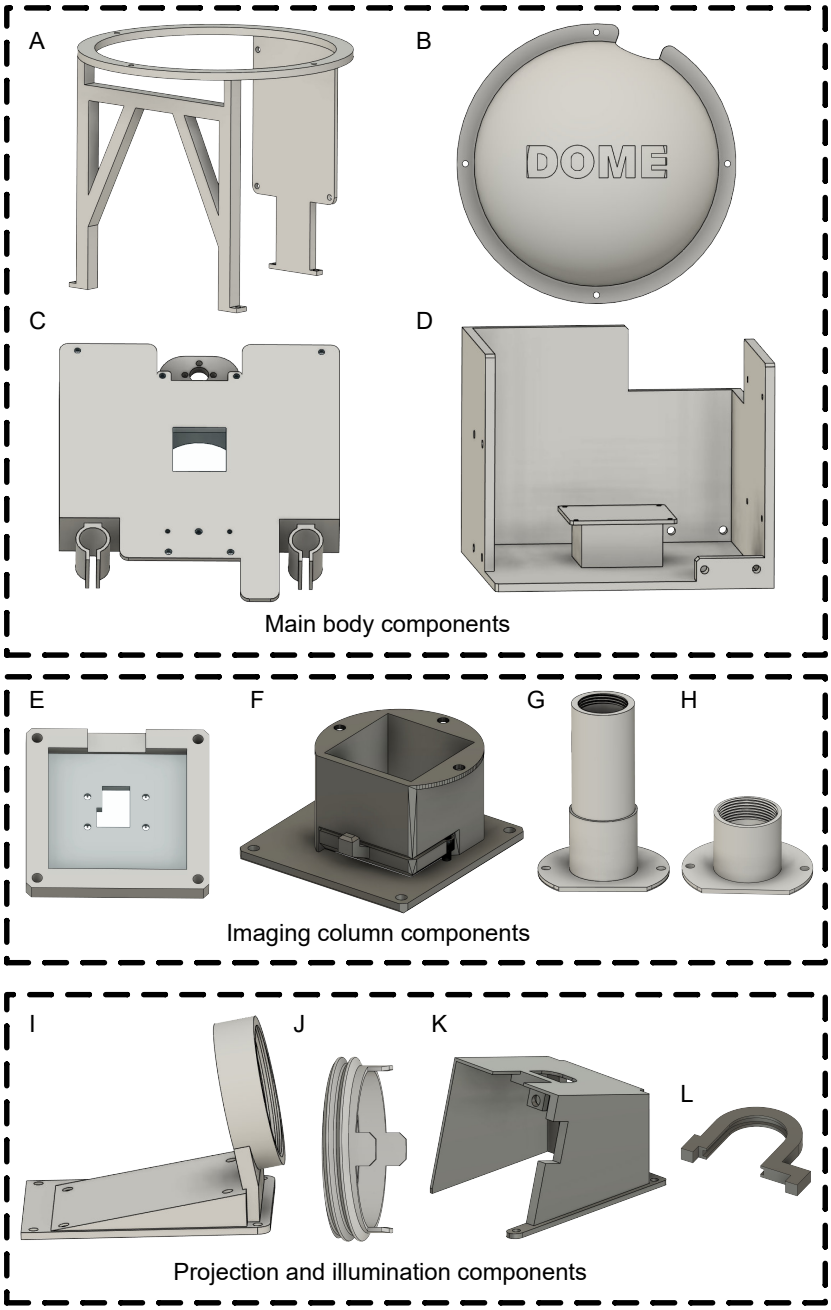

Figure 3.9: **CAD designs of all DOME components.** Parts are split into main body, imaging and projection and illumination components.

be screwed in to secure the condenser lens in place. The projector is enclosed by a cover piece (K) that shields the projector board from dust, and provides an attachment point for a white illumination LED that is used for bright-field imaging. Light from this LED is diffused by a ground glass diffuser, held in place by a clip (L) that fits above the condenser lens.

Parts are attached to one another using standard metric nuts and bolts, with the exception of

the sample stage which attaches to the base by linear guide rods, and the density filter clip which is slotted into place rather than mechanically fastened. All parts were printed using polylactic acid (PLA), with parts being initially printed using Ultimaker 2+ and later replicated using an lower budget model, the Anycubic i3 Mega. PLA is one of the most commonly used materials in 3D printing filament, being cheaply producible from renewable sources [24] and carrying less health risks than the more traditional acrylonitrile butadiene styrene (ABS) filament. The main drawback of PLA filament, it's propensity for deformation at temperatures above 50° [226], is not a relevant consideration in the fabrication of the DOME as it is unlikely that any application will require temperatures above this deformation point.

3.3.3.3 Mechanical components

To operate effectively as a microscope, the DOME must be able to adjust the position of the imaging focal point relative to the sample in the x, y and z directions. As precision moving parts can be difficult to produce by 3D printing, this is achieved using a linear rod guide set and x-y adjustable stage caliper. The x-y stage caliper, which attaches to the sample stage (Figure 3.10A), allows the sample to be moved in the x-y plane by the turning of two adjustment dials. The linear guide rod set connects the sample stage to the body of the DOME (Figure 3.10B). It is comprised of a shaft optical axis with support shaft bearing and linear motion ball bearing, and a lead screw with flexible shaft coupling, screw nut and bearing mounts. The sample stage moves up and down the optical axis shaft when the lead screw is turned to allow precision focusing.

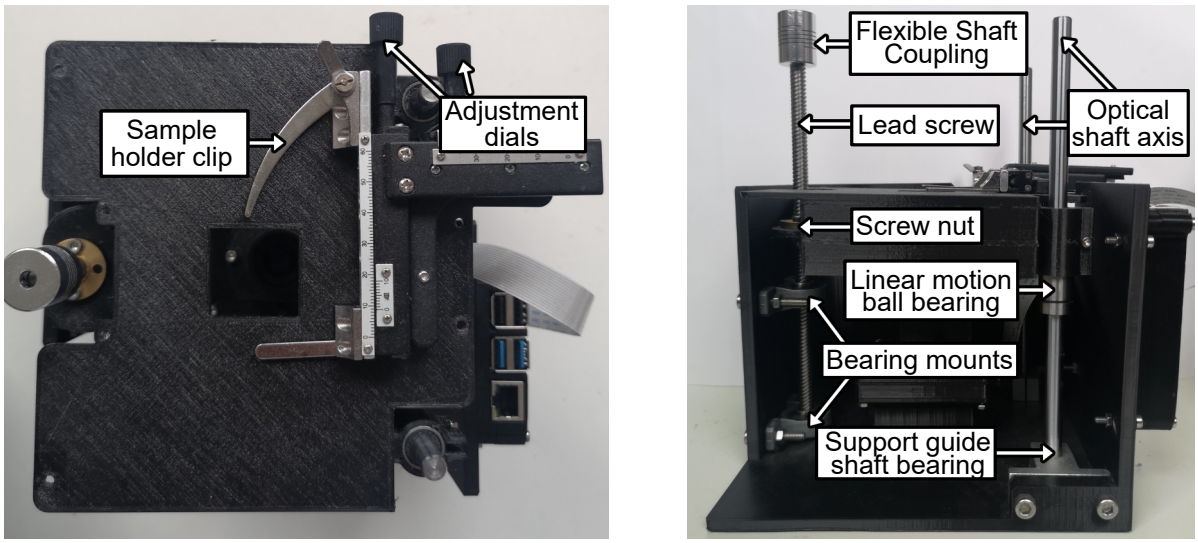

A B

Figure 3.10: **Mechanical components of the DOME. (A)** x-y adjustable stage caliper. **(B)** Linear guide rod set.

3.3.4 Closed-loop feedback control

For the execution of closed-loop control algorithms, it is necessary that the imaging and projection module are able to communicate in real time. Furthermore, to ensure accurately localised illumination of agents and their local environment, a protocol is required that enables a mapping between camera and projector space. This section lays out the computational set-up and calibration process used to achieve this in the DOME.

3.3.4.1 Computation and communication infrastructure

The light output of the DOME is constantly updated based on observed changed in the microsystem, as shown conceptually in Figure 3.1A, making it a closed-loop control system. The imaging module is comprised of a Raspberry Pi 4, Raspberry Pi camera and LEDs for bright-field and fluorescent illumination. This computer acts as the primary computing module and user interface, and can be connected via USB to a monitor, mouse and keyboard, or accessed remotely by secure shell (SSH) or virtual network computing (VNC). The projection module is comprised of the DLP projector interfaced with a Raspberry Pi Zero W through a custom PCB.

To close the loop between the imaging and projection modules, they must be set-up for two way communication. Due to the interface between the Raspberry Pi Zero and projector there are no ports available for a physical connection. Instead, both computers are configured as nodes in an ad-hoc wireless network. This has the additional benefit that, theoretically, more computers could be included in this control process as desired, for example as a means to remotely connect to the system or to facilitate additional functionalities such as temperature and humidity control. The network is established by editing the network interface files on both Raspberry Pis to include details of the required ad-hoc connection, as well as IP addresses for both nodes. Using the Python `socket` library, the imaging module operates as a server socket (`serversocket`) to which the projection module can connect as a client (`clientsocket`). Data can then be transmitted between the sockets in a UTF-8 encoded format using the JSON encode and decode functions `json.dumps()` and `json.loads()` from the `json` library. The networked configuration also allows the user to interface with the projection module from the imaging module interface via VNC connection by running VNC viewer on both devices.

3.3.4.2 Image capture and projection algorithm

Standard image capture in the imaging module of the DOME is performed using the `picamera` package, a Python interface for the Raspberry Pi camera module. With this package, camera settings can be defined and redefined within the code as needed, with key attributes being `camera.resolution`, `camera.shutter_speed` and `camera.exposure_mode`. These settings will vary between applications, however in general `camera.exposure_mode` is set to `spotlight` as this was found to provide the clearest images while minimising optical interference artifacts. The

camera is operated using the `capture_continuous` method, which capture frames continuously as an infinite iterator until either the loop is manually interrupted via keyboard input, or broken by the end of a control algorithm. The `PiRGBArray` class is specified as the output for this method, producing 3-dimensional RGB numpy arrays from these unencoded frame captures.

Image processing is performed using the `OpenCV` library, specifically the `cv2` interface. The most basic processing for a captured frame is conversion to grayscale using `cv2.cvtColor()` with the `COLOR_BGR2GRAY` colour space conversion code. After this, application specific processing stages such as thresholding, blurring and dilation can be performed using the OpenCV library to isolate relevant features in the camera frame.

In the projection module, a blank projection image is created through the creation of an empty `numpy` array of size (display height, display width, 3) for a `np.uint8` data type. The image can then be patterned by accessing array indices and assigning new RGB values, or by using drawing functions such as `cv2.circle` around particular indices. This image is displayed as a fullscreen image using `cv2.imshow()` with `cv2.WND_PROP_FULLSCREEN`.

3.3.4.3 Coordinate transformation calibration

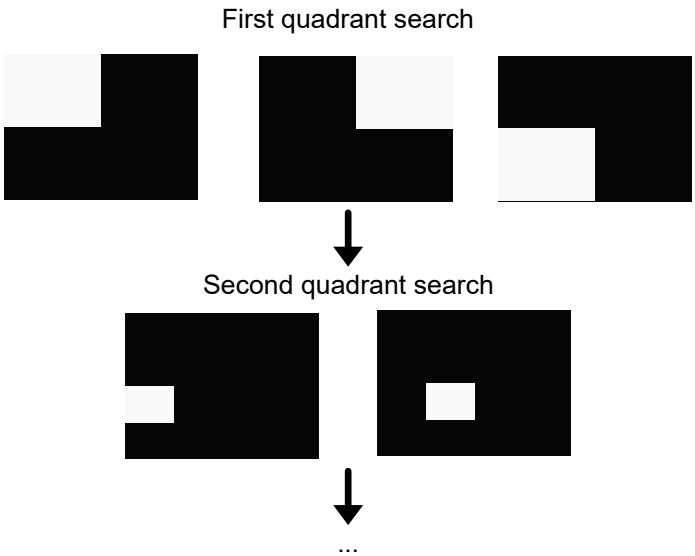

Figure 3.11: **Iterative quadrant search.** Total projection area is divided into quadrants which are illuminated successively until an approximate center location of the camera field of view is located. The number of iterations in this process depends on the current magnification of the system.

Critical to the closed-loop operation of the DOME is the calibration of the camera to the projector space. The first step in this process is finding the approximate point of the projector coordinate system onto which the camera field of view is focused. This step is required as the projected image will generally be larger than the camera field of view, particularly as

magnification increases. Thus to find the area in which the camera is focused, an iterative quadrant search is performed (Figure 3.11) in which each quadrant of the projection area is lit up until the camera field of view is illuminated. Once the correct quadrant has been chosen, a quadrant search of this subset area is performed, with iterative searches eventually locating an approximate central coordinate. The projector coordinate located need only be approximately centralised with respect to the camera field of view, as this process is just the first step in a more rigorous calibration process.

For accurately localised illumination, it must be possible to translate a point **m** in the camera image into a point **M** in projector space, such that light patterns can be projected with respect to features within a given camera frame. The projection mapping methodology used in the DOME is similar to camera calibration techniques employed in computer vision [433], however the quasi-2D nature of set-up allows for simplification. Unlike in most applications, the surface imaged by the camera and onto which light is projected is fixed and can be considered flat, given that variations in z height within a given microsystem will be small compared to the x and y dimensions.

A transformation between camera point **c** and projector point **p** can be treated as a two dimensional spatial transformation between coordinate systems, described by a transformation matrix **M** as shown by Equation 3.2.

$$\boldsymbol{p} = \boldsymbol{M}\boldsymbol{c} \tag{3.2}$$

In the scheme of the DOME as described above, points **p** and **c** are in a two dimensional plane. This transformation can therefore be written as in Equation 3.3.

$$\begin{pmatrix} x' \\ y' \\ 1 \end{pmatrix} = \boldsymbol{M} \begin{pmatrix} x \\ y \\ 1 \end{pmatrix} \tag{3.3}$$

The coordinate systems of the camera and projector are related by an overall transformation comprised of a translation, rotation and scaling. This is achieved by the application of a translation, **T**, rotation **R**, and scaling **S** matrices.

$$\boldsymbol{T} = \begin{pmatrix} 1 & 0 & t_x \\ 0 & 1 & t_y \\ 0 & 0 & 1 \end{pmatrix} \tag{3.4}$$

$$\boldsymbol{R} = \begin{pmatrix} \cos\theta & -\sin\theta & 0 \\ \sin\theta & \cos\theta & 0 \\ 0 & 0 & 1 \end{pmatrix} \tag{3.5}$$

$$\boldsymbol{S} = \begin{pmatrix} s_x & 0 & 0 \\ 0 & s_y & 0 \\ 0 & 0 & 1 \end{pmatrix} \tag{3.6}$$

The translation matrix, $\boldsymbol{T}$, (Equation 3.4) shifts points along the x and y axes by amounts t_x and t_y respectively. The rotation matrix, $\boldsymbol{R}$, (Equation 3.5) rotates points with respect to the x axis by angle θ and the scaling matrix, $\boldsymbol{S}$, alters the the distance between points along the x and y axes, effectively stretching or squeezing the coordinate system by s_x and s_y.

To apply the full transformation there are 5 parameters that must be calculated; t_x, t_y, θ, s_x and s_y. To obtain these parameters, a 4-point calibration grid is generated around the approximate center of the camera field of view generated by the iterative quadrant search and projected onto a plain surface. The projected grid, shown in Figure 3.12, is read as a a camera frame, and the centers of each point localised using contour detection. This gives 2 sets of points, one describing the grid as generated in the projector coordinate system, the other describing the grid as viewed in the camera coordinate system. Using OpenCV, a minimum area bounding rectangle is computed for both sets of points using `minAreaRect`, a function which returns the central coordinate of the rectangle as well as width, height and angle of clockwise rotation. These can be written as $(x_p, y_p), (w_p, h_p)$ and θ_p for the projector rectangle, and $(x_c, y_c), (w_c, h_c)$ and θ_c for the camera rectangle. The transformation parameters can be extracted by comparing the relative positions, rotations and sizes of the two shapes. Translational parameters are given by the amount by which the rectangles are shifted with respect to each other (Equations 3.7 and 3.8) while scaling parameters are found by taking the ratio of the widths and heights for both rectangles (Equations 3.9 and 3.10).

$$t_x = x_p - x_c \tag{3.7}$$

$$t_y = y_p - y_c \tag{3.8}$$

$$s_x = \frac{w_p}{w_c} \tag{3.9}$$

$$s_y = \frac{h_p}{h_c} \tag{3.10}$$

Stretching and rotation transformations are simplified if performed with respect to the origin. To this end, the translation transformation is split into two operations such that the first shifts

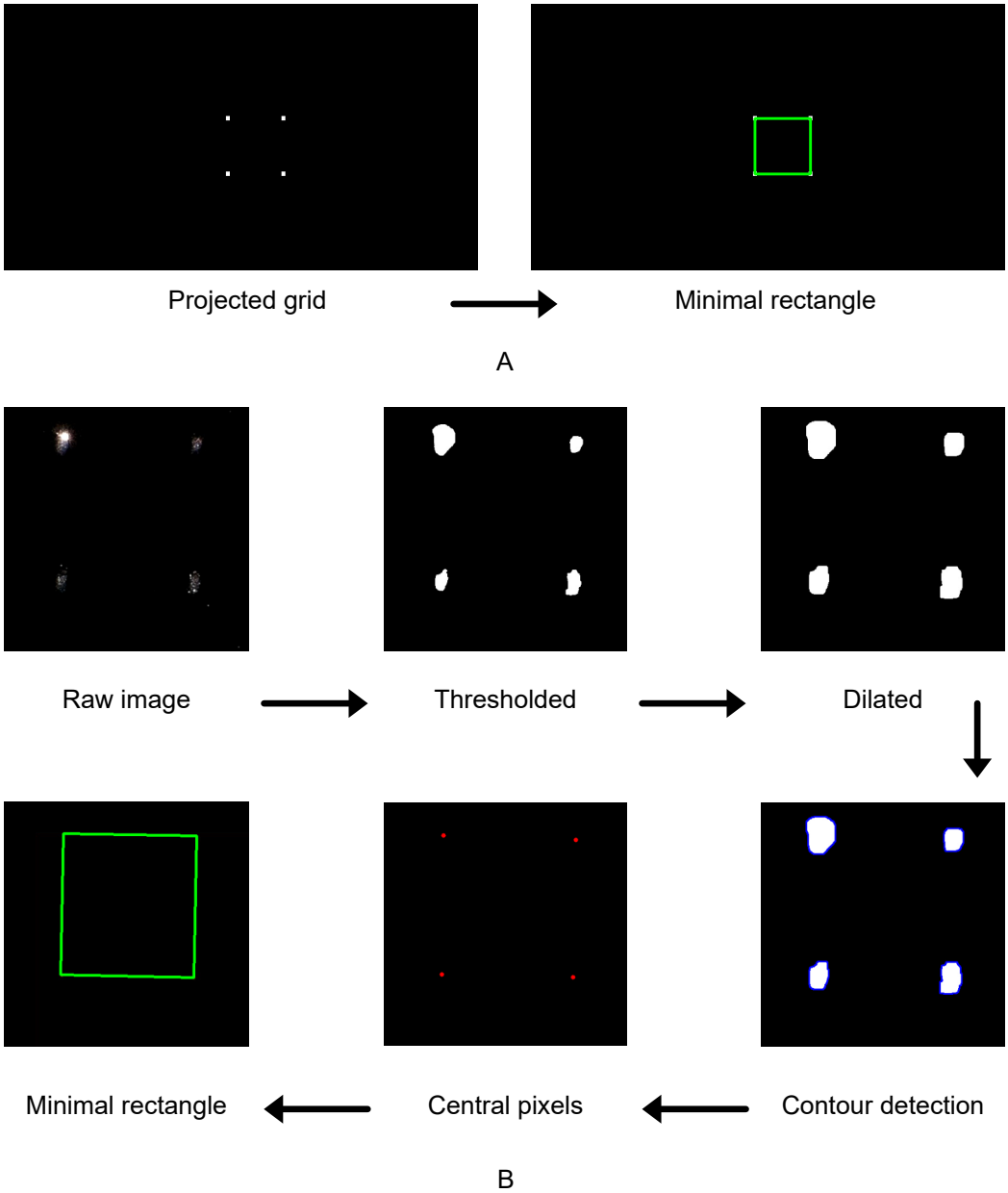

Figure 3.12: **Calibration process for the DOME.** A mapping of camera to projector coordinate system is performed through the image processing sequence shown, with a projected grid used to generate 2 sets of points. This enables a minimal area rectangle (green) to be drawn for both projector and camera coordinate system.

the points to the origin. The sequential order in which the transformation matrices are applied is therefore: translation, rotation scaling and translation (Equation 3.11).

$$\boldsymbol{p} = \boldsymbol{T_2 S R T_1 c} \tag{3.11}$$

$$\boldsymbol{T_1} = \begin{pmatrix} 1 & 0 & -x_c \\ 0 & 1 & -y_c \\ 0 & 0 & 1 \end{pmatrix} \tag{3.12}$$

$$\boldsymbol{T_2} = \begin{pmatrix} 1 & 0 & x_p \\ 0 & 1 & y_p \\ 0 & 0 & 1 \end{pmatrix} \tag{3.13}$$

$$\boldsymbol{S} = \begin{pmatrix} \left(\frac{w_p}{w_c}\right) & 0 & 0 \\ 0 & \left(\frac{h_p}{h_c}\right) & 0 \\ 0 & 0 & 1 \end{pmatrix} \tag{3.14}$$

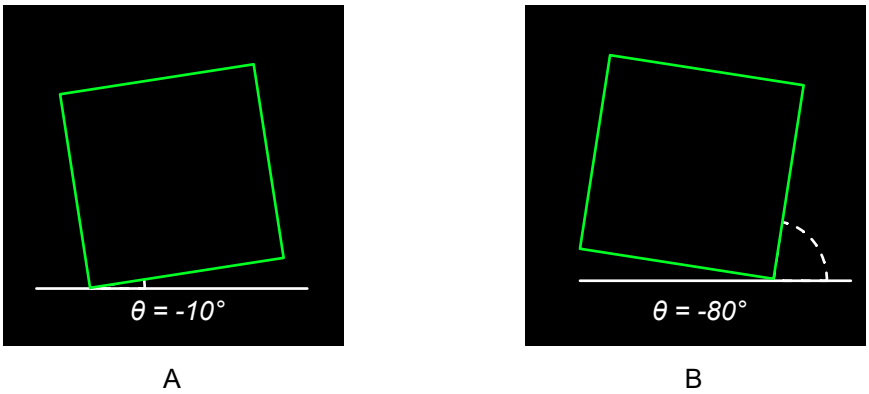

Figure 3.13: **Determination of rotation angle.** Calculation of rotation angle θ by OpenCV package `minAreaRect` is performed with respect to a horizontal line drawn at the lowest vertex of the rectangle, where θ is -90 for an non-rotated shape.

The rotational parameter θ describes the relative rotation of the two rectangles. The method by which `minAreaRect` calculates and returns the angle of rotation is to consider θ as the anticlockwise angle from a horizontal line drawn with respect to the lowest vertex, where $-90 \leq \theta < 0$ (Figure 3.13). In the case of the DOME calibration process, this effectively means that $\theta_p = -90$ in all cases, while θ_c will be closer to 0 for an anticlockwise rotation (Figure 3.13A), and closer to -90 for a clockwise rotation (Figure 3.13B). This assumes that camera frames have been appropriately rotated and flipped as described in Section 3.3.2. For the purpose of calculating a rotation parameter, it is more convenient that θ be negative in one rotational direction and positive in the other. To this end, a piecewise function is used to determine θ, as described in Equation 3.15.

$$\theta = \begin{cases} \theta_c & 0 < \theta_c \leq 45 \\ \theta_c + 90 & 90 \leq \theta_c < 45 \end{cases} \tag{3.15}$$

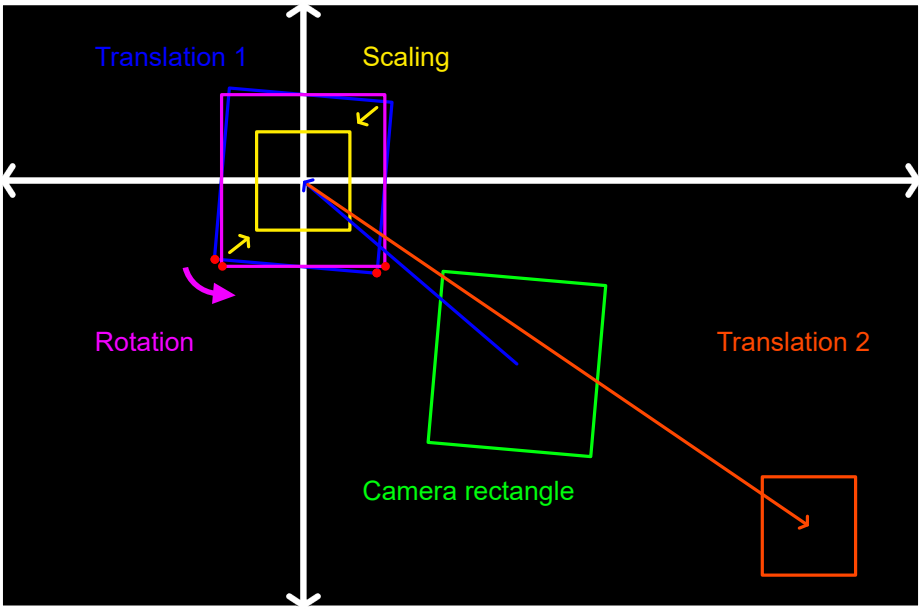

Figure 3.14: **Transformation mapping camera to projector space.** The original rectangle obtained from the 4 point grid as observed in the camera frame (green) is transformed by translation to the origin (blue), rotation about origin (purple), scaling about origin (yellow) and finally translation to projector space (orange).

Thus the transformation matrix is given by Equation 3.16, where θ is given by Equation 3.15. This represents the full transformation process that maps the rectangle produced by the 4 point projector grid to the resulting rectangle that appears in the camera field of view, demonstrated step by step in Figure 3.14. The transformation parameters are exported as a text file that can be imported by any DOME application, which can then use the matrix to map camera points into projector space.

$$\boldsymbol{T_2SRT_1} = \begin{pmatrix} \left(\frac{w_p}{w_c}\right)\cos\theta & \left(\frac{w_p}{w_c}\right)\sin\theta & \left(\frac{w_p}{w_c}\right)(x_c\cos\theta + y_c\sin\theta) + x_p \\ -\left(\frac{h_p}{h_c}\right)\sin\theta & \left(\frac{h_p}{h_c}\right)\cos\theta & \left(\frac{h_p}{h_c}\right)(y_c\cos\theta - x_c\sin\theta) + y_p \\ 0 & 0 & 1 \end{pmatrix} \tag{3.16}$$

This calibration process should be completed after the z plane and projector focus have been appropriately adjusted. Figure 3.15 demonstrates proper system focusing, in which both the projector and imaging systems are focused onto the microsystem plane, as well as improper system focusing, in which the who systems are focused on different points. The imaging system

should be the first to be focused on the sample, followed by focusing the projector onto the same plane by rotating in-built focusing screw until the image appears crisp and well defined. The surface onto which the calibration grid is projected should be similar to that of the relevant sample to account for different sample dimensions and compositions, for example that of a petri dish compared to a glass slide. Ideally, calibration is completed on the sample itself at a point that does not contain the light sensitive microsystem, for example at the edge of a glass slide.

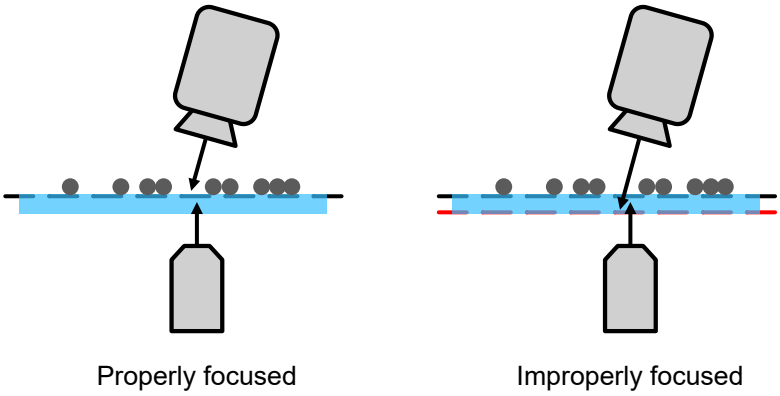

Figure 3.15: **Focusing of projector and imaging systems.** In a properly focused system (left) both image and projection systems have the same focal plane, which is that at which the sample is positioned. An improperly focused system (right) has the two systems focused at different planes, at least one of which is not sample plane.

3.3.5 Previous versions

The development process leading to the current DOME design as described above was an iterative process in which different approaches to the integration of projection, imaging and computational systems were evaluated and improved upon. Disregarding minor alterations, the design of the DOME underwent 3 major iterations, shown in Figure 3.16. The current DOME, (Figure 3.16C) is therefore DOMEv3, with predecessors v2 and v1 shown in Figures 3.16B and 3.16A respectively. While materials and fabrication methods used for each version of the DOME differed slightly, the core configuration (Figure 3.2) remained largely the same throughout the design process.

In the DOMEv1-2 light, was delivered using an off-the-shelf DLP projector (Mitsubishi XD221U) containing a DLP5500 0.55inch DMD chip with a 1024×768 micromirror array. The projector was adapted by removal of the original halogen lamp light source (Figure 3.17A) and RGB colour wheel. The light source was replaced by a LZ4-04UV00 4 UV LedEngin LED mounted to a star metal core PCB on an LED Star Heatsink (Figure 3.17B). This light source was selected as this original DOME design featured a UV wavelength output rather than RGB. A fail safe circuit in place to prevent operation of the projector in the absence of the lamp was bypassed by soldering together two PCB connections. and the magnification lens was removed (Figure 3.17C). Due to the large size of the projector, it was not possible in either DOMEv1 or v2

A B C

Figure 3.16: **Iterative timeline of the DOME design. (A)** v1. **(B)** v2. **(C)** v3

to integrate the projection module directly into this main body. Instead, the projector was placed directly behind the body, projecting light through the achromatic doublet lens and onto a dichroic mirror (ThorLabs, DMLP490R) positioned at 45° to reflect light toward the sample stage. The magnification lens was also removed (Figure 3.17C), to be replaced by an achromatic doublet lens (Thor Labs MAP104040-A) with magnification ratio 1:1 that would sit inside the main body of the DOME, extending the throw distance of the projector to 40mm from the focal plane of the previous magnification lens.

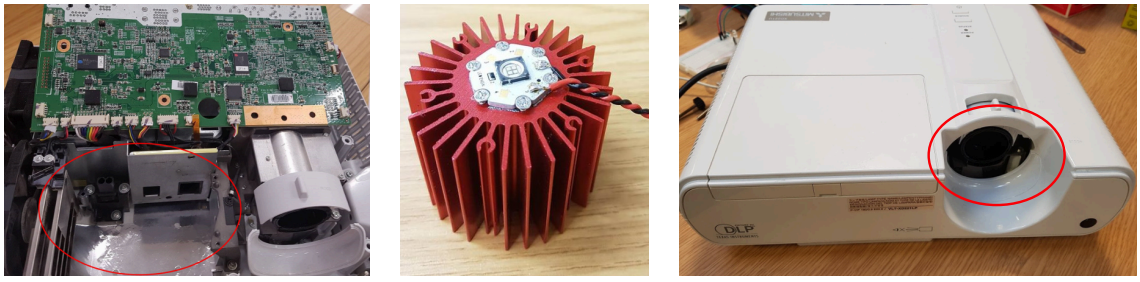

A B C

Figure 3.17: **Alterations to DLP projector used in DOME v1-v2. (A)** Removal of original halogen light source (red circle). **(B)** New UV LED light source attached to heat sink. **(C)** Removal of magnifying lens (red circle).

The DOMEv1, used a non-inverted imaging set-up and featured a small sample slot rather than a stage, meaning that only microscope slides could be imaged. This version was fabricated by assembling 3D printed and laser cut parts, as can be seen in Figure 3.16A. In v2, laser cut

parts were replaced by printed parts to simplify the fabrication process. The imaging set-up was also inverted to allow for the imaging of petri dish based samples.

The configuration of the closed-loop computational set-up was also altered between v1-2 and v3, as in these previous versions only one Raspberry Pi was used. A Raspberry Pi was used to control the camera used for imaging, as in v3, however the Mitsubishi projector was controlled via HDMI using an computer external to the DOME system. Two way communication was achieved using simple web server generated using the Flask package in Python, a method that was replaced by using sockets over an ad-hoc network in v3.

3.4 Characterisation results

A primary challenge in the effort to bring open-source and DIY hardware into mainstream scientific use is ensuring that results obtained using these devices are reliable and replicable [326]. A critical part of this is ensuring that open-source technology is well characterised and documented [272]. In the case of the DOME, it is important to characterise both the imaging and projection capabilities, as well as the efficiency of the closed loop control scheme.

3.4.1 Light emission spectrum

The optical response of microagents is often dependent on the illumination wavelength. Commonly, light response is seen only in a specific wavelength range [59, 227], however in some cases different responses may be induced by distinct wavelengths [5, 60, 177]. It is therefore crucial that any device for optical control has a well defined and characterised emission spectrum. The wavelength spectrum produced by the LED light source inside the DLP projector (Figure 3.18) shows three peaks at 455, 517 and 632 nm, produced by the blue, green and red LEDs with little overlap (< 2%) between each. Using the full width at half maximum, the spread of each peak can be quantified. The half maximum intensity spans the ranges of 445 – 465 nm, 497 – 577 nm and 621 – 639 nm for the blue, green and red peaks respectively. The spectrum was measured using a UV-visable light spectrometer (Ocean Optics, FLAME-S-UV-VIS-ES) by placing the optical fiber facing upwards at the plane of the sample stage. The blue, green and red measurements were taken by generating subsequent full screen uniform images with RBG pixel values `(0, 255, 0)`, `(0, 0, 255)` and `(255, 0, 0)` respectively.

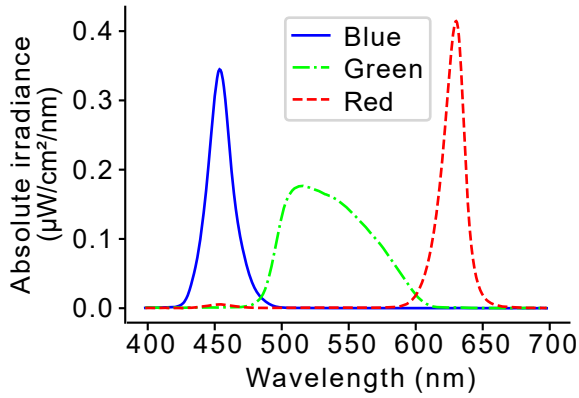

Figure 3.18: **Projector light spectrum.** Light emission spectrum measured from the DLP Lightcrafter module, measured separately for the blue, green and red LEDs contained in the optical engine.

3.4.2 Imaging modes

The DOME is capable of three different imaging modes that use fluorescent and off-axis illumination. In the bright-field mode, a white LED positioned next to the projector is used, with a direct optical path through a diffusion filter to the sample plane and into the imaging lens. This produces images such as that shown in Figure 3.19A, with agents appearing dark against a brightly lit white background. The fluorescence mode uses a UV LED positioned at an off axis angle towards the sample stage, with this light being used to activate fluorescent compounds such as green fluorescent protein (GFP). In this mode, a longpass or bandpass filter must be placed in the filter block to remove any UV and blue wavelengths, leaving only the green light emitted from the sample, as in Figure 3.19B. The final imaging mode requires no additional LEDs, instead using the projector light as an illumination source. The off-axis projection of this light results in agents appearing brightly coloured against a dark background, as demonstrated in Figure 3.19C, in which a low level of red light is uniformly projected across the sample.

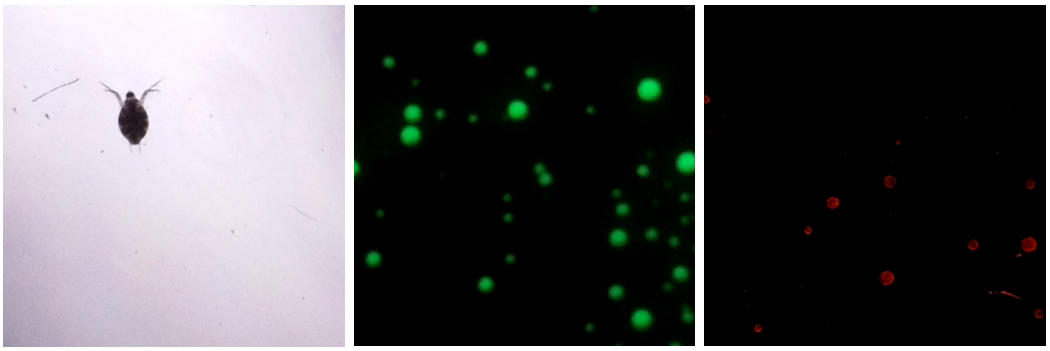

A B C

Figure 3.19: **Imaging modes of the DOME. (A)** bright-field imaging of a water mite using a white LED light source. **(B)** Fluorescence imaging of a GFP-expressing *E. Coli* colonies using a UV LED light source. **(C)** Off-axis illumination imaging of *Volvox* colonies using light from the DOME's projection module.

3.4.3 Imaging resolution

The imaging resolution describes the size in physical space at the sample plane that a single pixel in the camera image corresponds to. This dictates the minimal agent size that can be resolved by the DOME, as objects below this size will typically not register on the camera sensor, assuming a standard bright-field imaging set-up. The imaging resolution will vary based on camera resolution and level of magnification used. However, to get a baseline value characterisation was carried out at a standard operational resolution setting of 1920×1088 pixels for both 9× and 90× magnification. A camera image of a transparent measuring ruler placed onto the sample stage was collected at both magnifications, allowing a scale to be calculated using Fiji, an open-source

image processing software [348]. From this, the size of a single pixel in the camera frame can be translated into physical space, giving 12 µm at 9× and 3.75 µm at 90× magnification. Since the size of the projection area on the sample stage is fixed, the number of projected pixels that are visible to the camera changes depending on the field of view, which in turn depends on the magnification used. It was found that, after cropping of the camera image shown in Figure 3.4, 300×300 and 88×66 pixels were visible for the 9× and 90× magnifications respectively.

3.4.4 Projection resolution

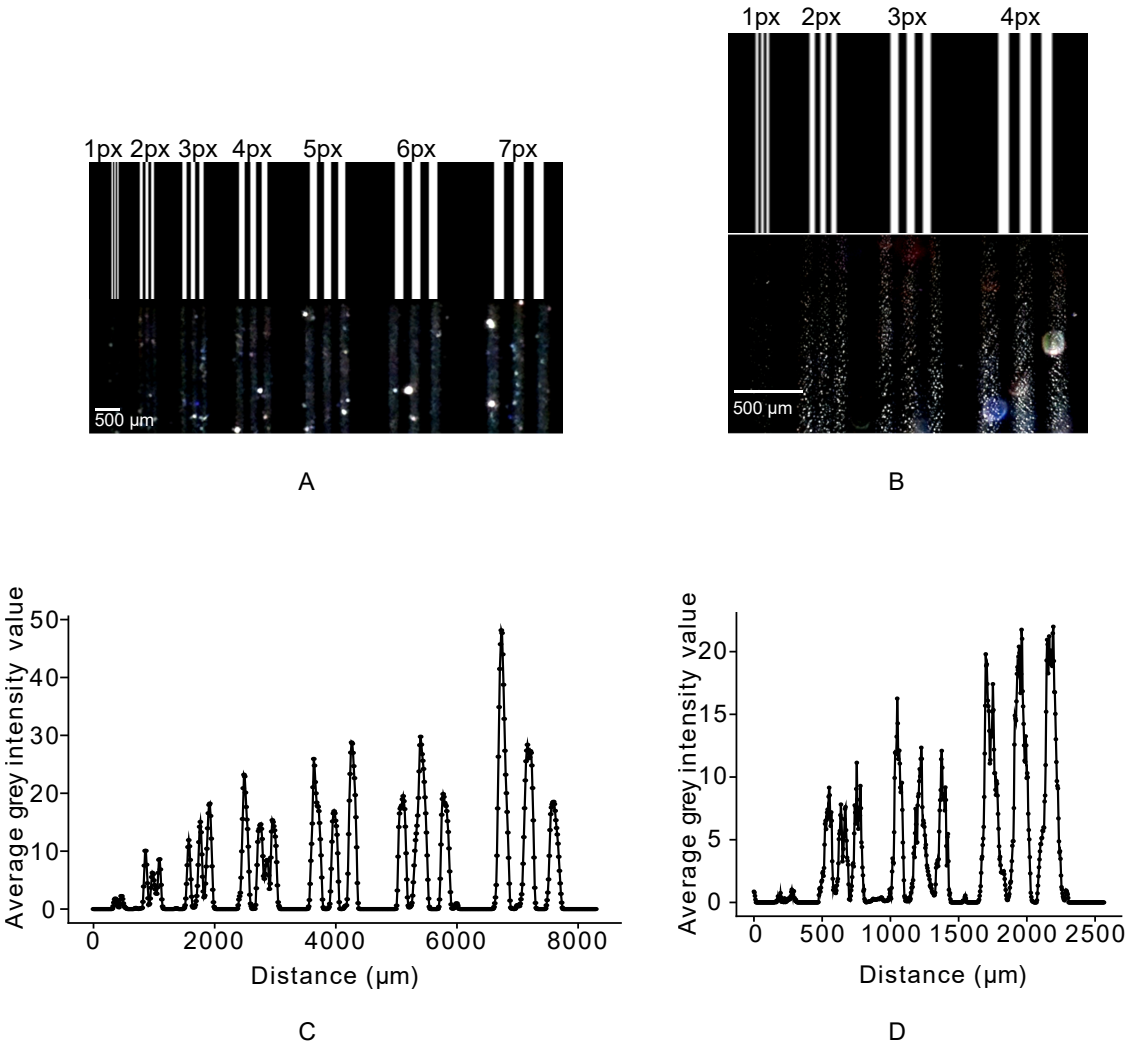

Figure 3.20: **Resolution of light projection in the DOME. (A)** Projection image of line triplets of increasing width up to 7 pixels for 9× magnification (upper) and corresponding camera image (lower). **(B)** Projection image of line triplets of increasing width up to 4 pixels for 90× magnification (upper) and corresponding camera image (lower). Intensity plot across camera frame for 9× magnification **(C)** and 90× magnification **(D)**, measured as the average grey-scale value for each pixel column in the image.

Where the imaging resolution dictates the size of microagents that may be observed using the DOME, the projection resolution refers to the smallest individual area that can be illuminated by the system. The projection resolution of the DOME is described by the area covered on the sample by 1 projected pixel. This can be calculated indirectly by considering the number of micromirrors on the DMD compared to the size of the full projected image area on the sample stage. The DMD contained within the DLP Lightcrafter module used in the DOME houses a 640×360 micromirror array, and the size of image projection at the sample stage is measured at 14.5×26 mm. This gives 30×30 µm as the theoretical resolution of projection, however in order to verify this in practice, resolution was also measured directly by projecting line triplets (Figure 3.20A-B) onto a neutral density filter with optical density equal to 1. Intensity plots across the resulting camera images were obtained using a Python script to average grey-scale value for each column, where a high resolution of projected patterns would be expected to result in clear differences in light intensity. The resulting intensity plots show distinct intensity peaks for lines of 2 pixel line width and separation for both 9× (Figure 3.20C) and 90× (Figure 3.20D) magnification, although with slightly less distinction for the 9× result. The intensity peaks for a 1 pixel line width and separation are visible, though less clearly distinguishable. This is in part due to the low overall intensity detected through the optical density filter, which also accounts for the variance seen between intensity peaks of the same line triplet. Measuring the peak separation for line triplets of width greater than 1 and dividing by the pixel separation gives an average measurement of a single pixel width of 30×30 µm± 5%, in agreement with the indirect calculation.

3.4.5 Control loop latency

In a closed-loop control system, minimising latency is key in delivering a timely feedback response. The feedback loop operated in the DOME (Figure 3.21A) takes an image captured by the imaging module and implements an analysis algorithm specific to the particular application. The resulting data points are then transmitted to the projection module, which generates and projects the corresponding light patterns. Upon projection of the new light patterns, confirmation is sent back to the imaging module, at which point the next image is captured and the loop continues. The control loop latency is therefore described by the time between capturing subsequent camera frames, as a new frame is captured only when confirmation of light pattern projection has been received by the imaging module from the projection module. As the captured image provides just a snapshot of the state of the microsystem at a given point in time, a greater latency can lead to a projection pattern that no longer relates accurately to the state of the system in the present moment.

Of the control loop steps laid out in Figure 3.21A, all remain relatively constant regardless of the specific control algorithm aside from the image analysis step. Therefore, to characterise the base latency a reduced feedback loop with no image analysis step, shown in Figure 3.21B, was operated. In this baseline loop, a signal was sent to the projection module after the capture

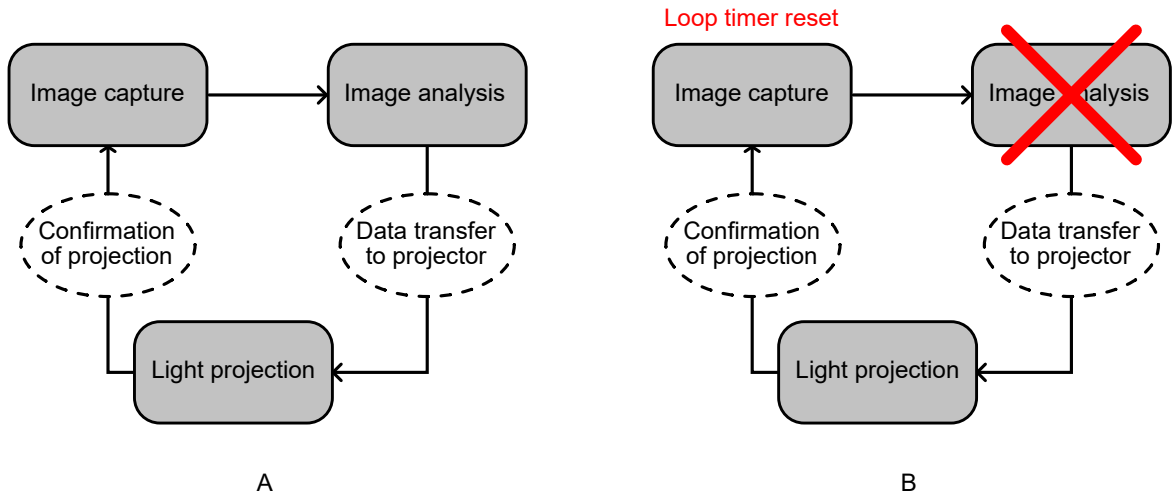

Figure 3.21: **Closed-loop control scheme. (A)** Full closed-loop scheme operated by the DOME during control algorithm. **(B)** Reduced closed-loop scheme used to test base latency in the DOME by removal of image analysis step.

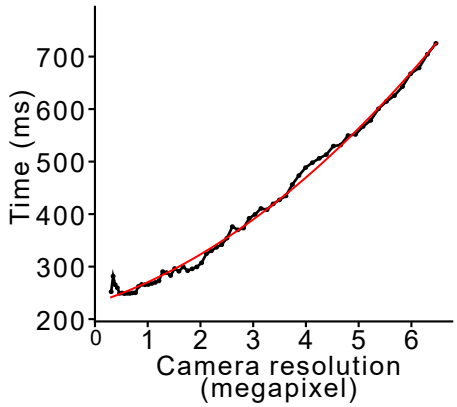

Figure 3.22: **Latency of DOME control loop.** Each of the 63 resolution point values (black) were averaged over 100 repeats. A second order polynomial fit of $y = 6.8x^2 + 32.6x + 231$ is shown in red.

of each camera frame, causing the projector to switch between and on (white) and off (black) state. A signal was then sent back to the imaging module, completing the loop and triggering the capture of the next camera frame. Image capture time varies with camera resolution, which for the Raspberry Pi camera goes from a minimum of 640×480 pixels to a maximum of 3280×2464 pixels, the number of pixels on the camera sensor. Base system latency was hence characterised by running the reduced feedback loop at 63 different camera resolution settings, starting with 640×480 pixels and increasing in increments of 32×32 pixels until maximum vertical camera resolution was reached at 2646×2464 pixels. At each resolution step, the feedback loop was run at a shutter speed of 100 ms and repeated 100 times to obtain an average latency. Plotting the

results, as in Figure 3.22, shows that system latency scales with the number of camera pixels to a second order polynomial fit. Time taken to complete the control loop was found to vary from 250 ms at 640×480 pixel resolution to 725 ms at 2646×2464 pixel resolution.

3.4.6 System cost

As discussed throughout this work, another important aspect of the DOME project is widening accessibility to optical control tools. The design process was therefore driven in part by the aim of producing a device that was not only open-source and user friendly, but also low-cost. This was achieved by the use of 3D printing to fabricate all structural elements, and the sourcing of inexpensive electrical and computational components such as the Raspberry Pi boards and DLP Lightcrafter Display module. A cost breakdown of the DOME by components in shown in Table 3.1, presenting a total cost of £685. The information included in this table represent prices quoted from UK manufacturers at time of writing, inclusive of VAT and rounded to the nearest pound.

Component	Cost (£)
Optical	
Projector (DLP Lightcrafter Display 2000 EV, Texas Instruments)	109
Condenser lens (50mm Diameter PCX , Edmund Optics)	37
Tube lens (9X Eyepiece Cell Assembly, Edmund Optics)	61
10X objective (Semi-Plan Standard Objective, Edmund Optics)	122
Glass diffuser (DG10-1500, Thor Labs)	15
Neutral density filter (NE10B-A, Thor Labs)	47
Longpass filter (FEL0500, Thor Labs)	60
Electrical	
Raspberry Pi (Raspberry Pi 4 Model 4GB, The Pi Hut)	54
Raspberry Pi (Raspberry Pi Zero W, The Pi Hut)	9
Camera (Raspberry Pi Camera V2, The Pi Hut)	24
2 × SD card (SanDisk Ultra 16GB microSDHC, Amazon)	14
Interface PCB (Pi Zero W DLP2000EVM adaptor board, Tindie)	3
Power supply (UK Raspberry Pi 4 Power Supply The Pi Hut)	8
Power supply (Raspberry Pi 3 Universal Power Supply)	8
Mechanical	
PLA filament (Black Premium PLA 1.75mm, FilaPrint)	28
Linear rail set (Glvanc 3D Printer Guide Rail Sets, Amazon)	21
x-y stage (Zetiling Microscope Moveable Stage, Amazon)	15
Linear Motion Ball Bearing (LM8LUU, Amazon)	7
Lighting and fastening sundries	41
Total cost	**685**

Table 3.1: **Breakdown of DOME component costs.** The cost of each component used to build the DOME as described in this chapter, where all prices are given to the nearest pound (£) and inclusive of 20% VAT.

3.5 Discussion

In this chapter, the DOME was introduced as a open-source device for the closed-loop spatiotemporal control of microagent systems. The fabrication process was detailed, along with the calibration steps necessary to map the camera to projector space to achieve effective closed loop control. Characterisation results were also presented for a number of important system parameters.

One such parameter was imaging resolution, describing the smallest feature sizes that can be resolved by the DOME's imaging module. It was found that for a standard 1920 × 1088 resolution, a single pixel in the camera field of view translated to 12 and 3.75 µm in physical space using the 9 × and 90 × magnification modes respectively. It therefore follows that the DOME is capable of imaging agents of sizes larger than 3.75 µm using the higher magnification, and 12 µm for the lower. Referring back to Table 2.1 in Chapter 2, this can be compared against the sizes of microagents that have been previously employed in optical control based experimentation. This comparison demonstrates that for all mammalian cells and polymer microrobots, this imaging resolution would be more than sufficient to resolve individual agents, likewise for algae and yeast cells. The sizes of micromotors and microparticles span a wide distribution that centers much smaller, meaning that some fall over and some under this resolution threshold. Individual bacteria also fall largely under this 3.75 µm limit [243], however in many instances included in this table it is bacterial collectives, rather than individual cells, that are the control targets. Despite this, there are doubtless many microsystems, including those mentioned here, that fall under the resolvable limit measured for this configuration of the DOME. In future work, there are a number of ways in which this could be further optimised. Firstly, the use of a higher camera resolution could go some way to addressing the issue, although this would have latency trade offs. A superior solution could be the use of a higher magnification imaging lens, a change that would be simple to implement given the modularity of the DOME. Finally, the DOME is also capable of fluorescence microscopy, which can facilitate the resolution of features smaller than the bright-field resolution limit.

While the imaging resolution describes the smallest features that the DOME can resolve, the projection resolution relates to to smallest individual area than can be illuminated by the light projector. This was found to be 30×30 µm, which can once again be compared to the sizes of various light-responsive microagents given in Table 2.1 to understand the degree of individual agent control offered. From these figures, it can be seen that for polymer microrobots, algae, optothermally generated bubbles and most mammalian cells, this resolution is sufficient to target individuals, or even subsections of single agents in some cases. For bacteria, micromotors and microparticles however this projection resolution would be insufficient for individual interaction. For applications that require this finer level of control, there are a number of steps that could be taken towards increasing resolution. One would be the use of stronger focusing optics, for example by using a microscope objective in place of the condenser lens, with the trade off of a smaller overall working area of projected light onto the sample. An alternative could be the use

Agent	**Speed** ($\mu m\,s^{-1}$)	**Reference**
TiO2 micromotors	66*	[397]
AgCl micromotors	100	[182]
Silica Janus particles	4*	[238]
Si/TiO2 nanotree microswimmer	5	[435]
Modified *E. Coli*	20	[98]
E. Coli biohybrid microrobot	8	[355]
Volvox barberi	600	[360]
Euglena gracilis	100*	[218]

Table 3.2: **Microagent speeds.** Speed of various light-responsive microagents rounded to the nearest whole number. Cases of multiple quoted speeds are denoted by an * symbol, with the number given representing the maximum of these speeds.

of a higher resolution projector, such as the recently released DLP LightCrafter Display 230NP (Texas Instruments) which uses a higher resolution DMD chip containing 960 × 540 micromirrors as opposed to the 640 × 350 offered by the current projector. The LightCrafter Display 230NP is priced at just over £300, meaning that if included in the DOME set-up it would be esily the most expensive component. Even with the addition of this higher resolution projector however, the total price would still fall significantly under the £1000 mark making this a feasible solution while maintaining the DOME as a low-cost device.

The primary source of latency was found to be the the time needed by the camera to capture an image, which is dependent on the resolution used. The algorithm was therefore run over a range of resolution settings, with results presented in Figure 3.22. These results showed that even for the highest resolutions, the loop was closed in under a second. For a single-agent projection area of a single pixel (30 × 30 µm), any agent moving < 41 $\mu m\,s^{-1}$ could therefore be imaged at the highest possible resolution (latency of 0.725 s) whilst maintaining accurate light projection in relation to their position. In the more typical case in which the DOME is operated at a resolution of 1920 × 1088 pixels, for which the latency is 0.25 s, agents moving at < 120 $\mu m\,s^{-1}$ could be accurately tracked and illuminated. For context, Table 3.2 presents the speeds of 7 distinct optically responsive microagents as quoted in various works. As can be seen from these numbers, in all but one cases agent speed falls below the 120 $\mu m\,s^{-1}$ threshold, with almost all also falling below the lower threshold of 41 $\mu m\,s^{-1}$. The 600 $\mu m\,s^{-1}$ speed quoted for *Volvox barberi* is significant as it represents the highest ever recorded speed for the Volvocine algae group to which it belongs. In comparison with the other algae type listed here, *Euglena gracilis*, *Volvox barberi* can be seen to be an extraordinarily motile microorganism. It should be noted that *Volvox barberi* are also signficiantly larger than many of the other agents listed in Table 3.2. The diameter of the colonies used to extract the figure of 600 $\mu m\,s^{-1}$ was 338 µm, meaning that a single agent would be over 10 times larger than the smallest projection area in the DOME. It is therefore likely that many pixels would be used in order to illuminate a single agent of this type,

rather than the 30 × 30 µm used in the above calculations. Furthermore, for agents of this size it would be effective to use a lower camera resolution to decrease latency if required. In general, most implementations of light-based microagent control are unlikely to require the tracking of highly motile agents while simultaneously requiring high spatial localisation, as faster moving agents tend to be of larger sizes.

At present, the light wavelengths offered by the DOME are limited by the use of the standard optical engine of the projector. The light emission of the optical engine was found to have peak wavelengths at 445, 517 and 632 nm, as seen in the light spectrum presented in Figure 3.4.1. The spread of each peak, quantified using the full width at half maximum, was found to be 445 – 465 nm, 497 – 577 nm and 621 – 639 nm for the blue, green and red LEDs respectively. From this, it can be seen that a significant amount of the visible light spectrum is covered by these LEDs at no less than half of their full intensity. In Table 2.1, the illumination wavelengths used to interact with various light-responsive microagents in literature were specified and can thus be contrasted with these results. For well over 60% of the agents listed, the wavelengths offered by the DOME align with the light sources used in the control experiments. Since all that is given in most literature is the light source used rather than the total spectral range for which the agents are responsive, the number of agents for which the DOME could constitute a suitable controller is likely to be much higher than this. The cases for which the control wavelength range deviates significantly from that provided by the DOME is where UV or IR light is used. This is particularly prevalent in micromotor-based applications, for which UV and IR wavelengths are generally used to induce photocatalytic and photothermal reactions respectively, although there is also growing interest in the design of visible light based motors [122]. Given the utility of non-visible light for applications such as these, it may be beneficial in future work to extend the capabilities of the DOME to allow for the inclusion of custom wavelengths. This would be achieved by replacing the optical engine of the Lightcrafter projection unit with a custom LED arrangement, as in a previous version of the DOME which operated in the UV range, discussed in Section 3.3.5.

The DOME is a low-cost device, totalling just £685 to build with the components listed in Table 3.1. To contextualise this figure, it can be contrasted with alternative optical control systems designed for a similar purpose, presented in Table 2.3A-F. In all but one case, the cost of building the proposed systems exceeds the £685 price of the DOME by around a factor of 10. The exception to this is the work presented by Lam et al., [218] for which the cost was calculated to be around £524 for the projection and imaging components. However, this set-up is built using an optical table and associated optomechanical parts to align and structure the optical components. These parts are not discussed in the text and thus it is impossible to obtain an accurate estimate of cost, however in general these types of assemblies are priced in the range of hundreds or thousands of pounds. This device is therefore best suited for users who already has access to optical equipment of this kind and the expertise to correctly perform alignment. In contrast with this, as well as the other open or reproducible optical control devices presented in Table 2.3A-F, the DOME is

entirely self-contained and not reliant on external equipment such as an optical breadboard or computer. Crucially, the files required to print and build the device are all publicly available on Bitbucket [2], meaning the platform is entirely open-source. Additionally, much of the alignment of optical components is handled by the printed body of the DOME, meaning that less physical calibration is required. As a result, the DOME meets the previously stated goal of providing an open-source, low-cost platform for spatiotemporal optical control with minimal barriers in terms of expertise in comparison with comparable devices.

3.6 Conclusion

In this chapter, the DOME was introduced as a low-cost, open-source device for the closed-loop control of microagent systems using light. Through the integration of accessible light projection technology with a custom microscopy set up, multi-wavelength closed-loop optical control with 30 µm resolution was achieved, for the construction price of just £685. All designs and protocols needed to build the DOME are freely available as an open-source project, ensuring maximum reproducibility. As a self-contained, open-source device capable of dynamic, high resolution control, the DOME offers novel opportunities for the engineering of microsystem collectives, and widens the accessibility of optical control techniques at the microscale.

[2] STL files for 3D printing and custom PCB plans, along with calibration and control code for the DOME are all available at bitbucket.org/hauertlab/dome

CHAPTER 4

BUILDING BLOCKS TOWARDS SWARM CONTROL AT THE MICROSCALE

Key Findings

This chapter presents building blocks towards swarm control across scales, and their implementation at the microscale using the DOME platform. In this work, *Volvox* colonies are used as a model microagent to demonstrate interagent communication, stigmergy, and motion control. Much of the content of this chapter is taken from [93].

4.1 Introduction

The ability to engineer the self-organisation of microscopic agents has implications from medicine [356] to material science [315]. The power of microswarms, whether robotic or natural, comes from the large numbers of agents driving robust collective phenomena such as coordinated motion [162] or trail formation [260]. Engineering swarms at the microscale is challenging in comparison to the macroscale, with limited capabilities of microagents and difficulty in programming their motion and local interactions. While the engineering of interactions has been achieved using chemical diffusion [374], energy [306], or environmental modifications [148, 393], achieving a desired collective behaviour typically requires extensive work to fine-tune the ability of microagents to react to each other or their local environment. An alternative approach to embedding complex behavioral rules within a microagent is providing control externally through environmental stimuli to ultimately lead to swarm outcomes.

This chapter presents a number of building blocks towards externally implemented swarm behaviour. The DOME is used to 'augment' [92] the capabilities of simple microagents, and to

implement microscale interactions using light. Specifically, living *Volvox* colonies are employed as a model microagent to explore light-based signalling, stigmergy and motion control. These three building blocks are often used as a basis for common collective behaviours at the heart of many robotic and natural swarm systems [43], and have significant potential for applications in microrobotcs, medicine, and synthetic biology if efficiently controlled at the microscale.

4.2 Background

The use of the DOME platform for the augmentation and closed-loop control of light-reactive microagents, together with the demonstration of various building blocks for the emergence of collective behaviours, presents a first step towards democratising swarm engineering at the microscale. This background will review collective behaviours commonly seen in natural and engineered swarms systems, from the macro to microscale. This does not aim to provide an exhaustive review of all swarm behaviours, but to highlight some of the parallels found across these length scales. From here, a number of key building blocks towards swarm control common throughout these collective behaviours will be extracted. The use of augmented reality to enhance microagent capabilities so as to enact these blocks will then be explored, and implemented in practice using the DOME.

4.2.1 Swarm control across scales

Swarm behaviour is a phenomena that is studied in natural systems, such as social insects, and implemented in artificial, typically robotic, systems. Owing to the interdisciplinary nature of swarm studies, definitions of a swarm vary. In this work, the word swarm is used to describe a system of agents that, through local interactions, are able to collectively perform actions that are beyond the capabilities of an individual. Swarm behaviour is observed throughout the natural world across many species. Many of the most widely studied natural collective phenomena are found in social insects, relatively simple individuals which at a colony level are capable of extraordinary feats, both physical and intelligence-based [9, 41, 94, 353]. Bees demonstrate the ability to make collective decisions about the optimum food source through communicative dance [353], and build colonies with consistent, well-organised patterns despite limited knowledge of this higher level organisation [48]. Similarly, ants have been found to deposit chemical trails for detection by other colony members in an indirect communication method known as stigmergy [378]. This is used to enable collective processes such as spatial exploration, foraging and route selection [95, 112]. Swarm behaviours are also found in many larger animals such as birds [295] and fish [217], which demonstrate abilities to move collectively in flocks and shoals as a protective measure against potential predators. Likewise, collective processes are also abundant at the microscale. Bacteria posses a motility mode that is known specifically as swarming [198], however outside of this there are many other bacterial collective behaviours that fit the definition

of swarming used here. The formation of biofilms for instance is a process by which many bacteria adhere to a surface, and each other, becoming embedded in an extracellular matrix comprised of substances secreted by the individual cells [76]. As a collective biofilm, bacteria often demonstrate a higher resistance to harmful conditions, such as the introduction of antibiotics [368] or high energy light [73], as well as the ability for enhanced signalling capabilities and division of labour between the group [189]. A number of collective processes are also found in eukaryotic cells, notable examples including morphogenesis and collective cell migration in embryonic and epithelial tissue [132, 246, 335, 381].

These naturally occurring behaviours have been a source of inspiration for the field of swarm engineering, which seeks to harness the principles of swarm intelligence for the purpose of systems design [40, 409]. The underlying principles that make swarm systems so powerful are robustness, scalability, and flexibility. Robust, in this context, means that the failure or loss of individual agents does not lead to a failure of the system as a whole, while scalability suggests that the system may operate across a range of group sizes, rather than requiring a particular agent number. Flexibility describes the ability of a system to adapt its behavioural output in the face of different tasks, problems or environments [277]. One field in which this is particularly attractive is robotics, which often seeks to address tasks that can be challenging for a single robot [43, 277]. These include the transportation of objects of varying size and shape [152, 214], which requires flexibility, large scale environmental mapping [341, 344], which is time consuming for an individual agent, and search and rescue functions in unstable environments [18, 262], for which robustness is beneficial due to the possibility of damage or destruction. A robotic swarm system can be differentiated from a more general multi-robot system by the following characteristics; autonomous environmental interaction, a large group size, mostly homogeneous agents, simplicity of individual agents, and the capacity for only local sensing and communication [342]. Although the field is still relatively young, already a number of robotic platforms exist that are frequently employed for the purpose of exploring swarm dynamics [11], including the Kilobot [337], e-puck [66], and swarm-bot [263].

Increasingly, there is also significant interest in the implementation of swarm principles in non-robotic scenarios, particularly at smaller scales, such as the design of smart nanomedicines [160, 161], self-organising microsystems [28, 91] and synthetically engineered collective cell processes [185, 271]. Despite obvious differences in the degree of programmability of these systems compared to traditional robotics, fundamentally similar collective behaviours can be seen to emerge across scales. A breakdown of some these behaviours is shown in Figure 4.1, grouped into three subcategories; spatial-organisation, navigation, and collective decision making [43]. Note that although the term swarm connotes some spatial or motility component in traditional usage, decision-making behaviours are included in swarm engineering. As will be highlighted here, implementations of these collective behaviours can be found in both robotic and microscopic systems, often with strikingly similar outcomes.

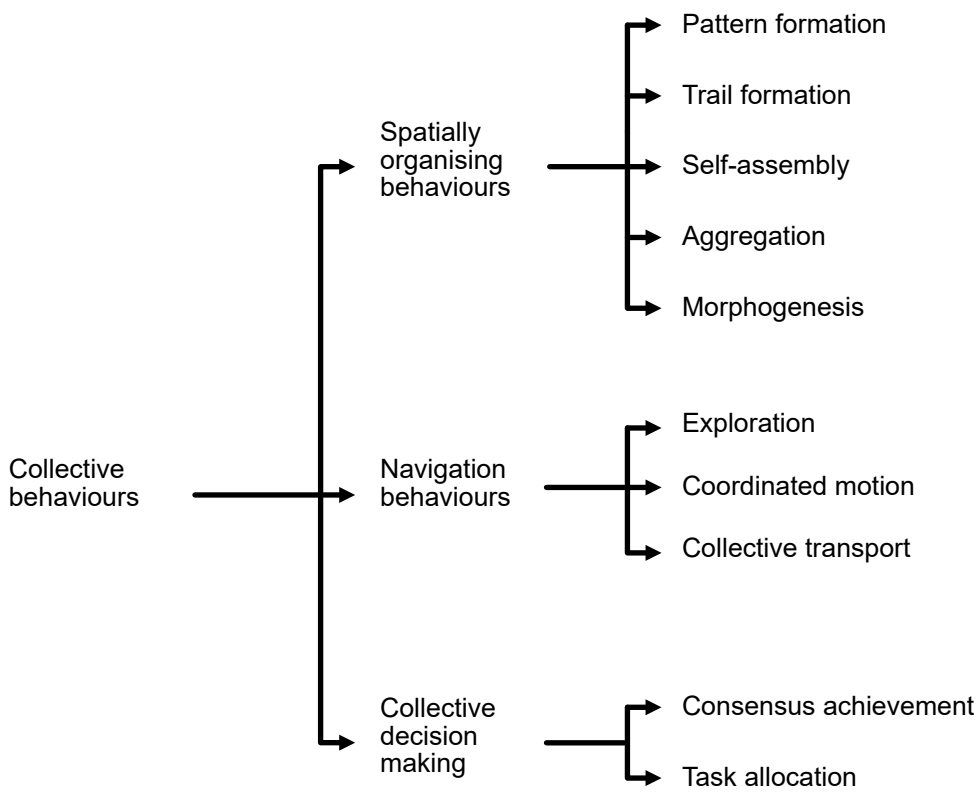

Figure 4.1: **Categorisation of collective behaviours.** A breakdown of collective behaviours that are observed in nature and implemented in swarm systems across scales. Adapted with permission from [43].

4.2.1.1 Spatially-organised behaviours

A collective behaviour can be considered spatially organised if the primary feature is the distribution of agents in space. In Figure 4.1 this can be seen to include aggregation, pattern formation, trail formation, self-assembly, and morphogenesis. These behaviours can overlap to some degree, but have slightly different implications. For example, trail formation could be seen as a subcategory of pattern formation in which a start or end point is defined.

Aggregation and self-assembly are fundamental examples of spatially-organised behaviours. Aggregation requires simply that agents gather into a somewhat localised area, something that is observed in nature by some animal [187, 308] and bacterial [114, 426] systems. Many implementations of this collective behaviour have been demonstrated using robotic collectives [20, 75, 274] and various synthetic microsystems [266, 414]. Self-assembly is here defined as the formation of local connections between agents, and does not require the generation of a particular spatial configuration, as would be the case for behaviours such as pattern formation. The engineering of self-assembling systems has been achieved from the micro [206, 235, 397, 425] to macroscale [151, 339, 401]. This is demonstrated in Figure 4.2, which shows the self-assembly of

a collection of s-bots [151] (Figure 4.2A) and a sample of polystyrene microbeads mixed with TiO_2 nanoparticles (Figure 4.2B) [397]. Both systems are initially dispersed and largely unconnected, but over time through local interactions begin to form interconnected groups. In the robotic system, the s-bots are equipped with a gripper that allows them to grasp onto the connection ring of neighbouring robots, and tracks and wheels that allow movement in space. Conversely, the assembly of polystyrene microbeads occurs by attractive phoretic interactions between TiO_2 nanoparticles, which are able to move through the solution due to photocatalytic propulsion. Despite these very different modes of mobility and interaction, the emergent behaviour is remarkably similar, although the robotic system has a much smaller population.

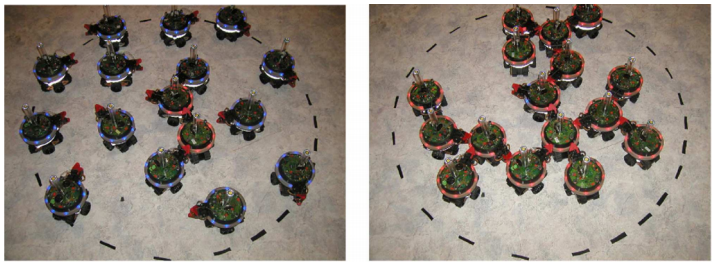

A

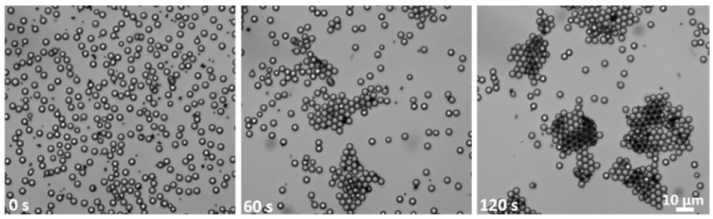

B

Figure 4.2: **Self-assembly in collective systems.** Self-assembly performed by **(A)** s-bots and **(B)** polystyrene microbeads mixed with TiO_2 nanoparticles. **(A)** Reproduced with permission from [151] © 2006 IEEE and **(B)** Reproduced with permission from [397] © 2019 American Chemical Society.

Morphogenesis is a collective behaviour by which a system self-organises into complex patterns. Often associated with embryonic development [168], morphogenesis has also received significant attention in robotics [194, 347]. Figure 4.3 shows two systems undergoing controlled morphogenetic processes, one of which is robotic the other organic. In Figure 4.3A, a 300 Kilobot swarm is seen to develop Turing spots, then to physically self-organise around these patterns to create emergent morphologies [358]. The Kilobots are able to communicate to others within a local radius through IR messaging to facilitate a reaction-diffusion process throughout the system. Virtual molecules stored in each robot are allowed to react with each other and diffuse between agents, with molecular concentrations indicated by a changing LED colour that enables Turing spots to form. Kilobots situated at the edge of the swarm then begin to migrate from

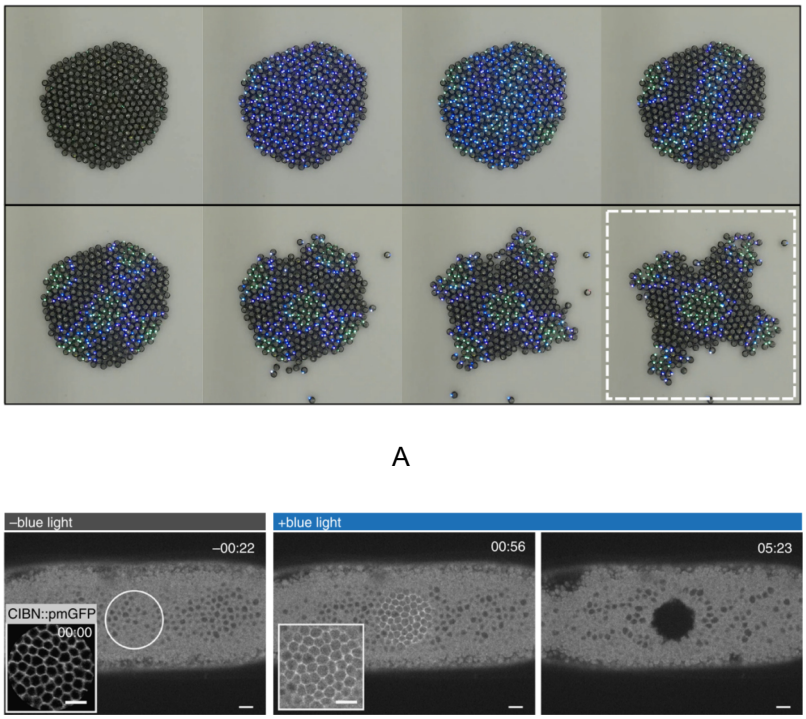

Figure 4.3: **Morphogenesis in collective systems.** Morphogenesis in **(A)** a swarm of Kilobots demonstrating emergent self-organisation through reaction-diffusion Turing patterns and **(B)** embryonic *Drosophila* tissue undergoing optogenetically directed epithelial folding. **(A)** Adapted from [358] © 2018 AAAS and **(B)** adapted from [185] under CC BY–A 4.0.

areas of low to high concentrations, resulting in the formation of limb-like protrusions around the spots. A loosely corresponding microsystem (Figure 4.3B) of embryonic *Drosophila* tissue can also be seen to undergo morphogenetic changes via optogenetically controlled epithelial folding, with the reorganisation of cells causing a circular hole to emerge in the collective tissue [185]. In this process, cells expressing a light-activated signalling pathway Rho that is capable of driving epithelial folding were targeted by a circular pattern of laser light to drive collective tissue reconfiguration. For both the robotic and cellular systems, morphogenisis occurs in response to collective dynamics of the agents interacting with various levels of the virtual molecule and Rho activity respectively. The similarity of these two processes is reflected in the comparable organic physical changes observed in the systems over time.

Pattern and trail formation involve the positioning of swarm agents in particular spatial locations. This differs slightly from self-assembling and morphogenetic behaviours, which are more associated with the reorganisation of agents relative to each other, and generally involve a more direct connection between agents. Trail formation on the other hand is concerned with the positioning of agents between two defined points, inspired by observations of ant foraging [90]. Although implementations of this at the microscale are limited, this behaviour has been the

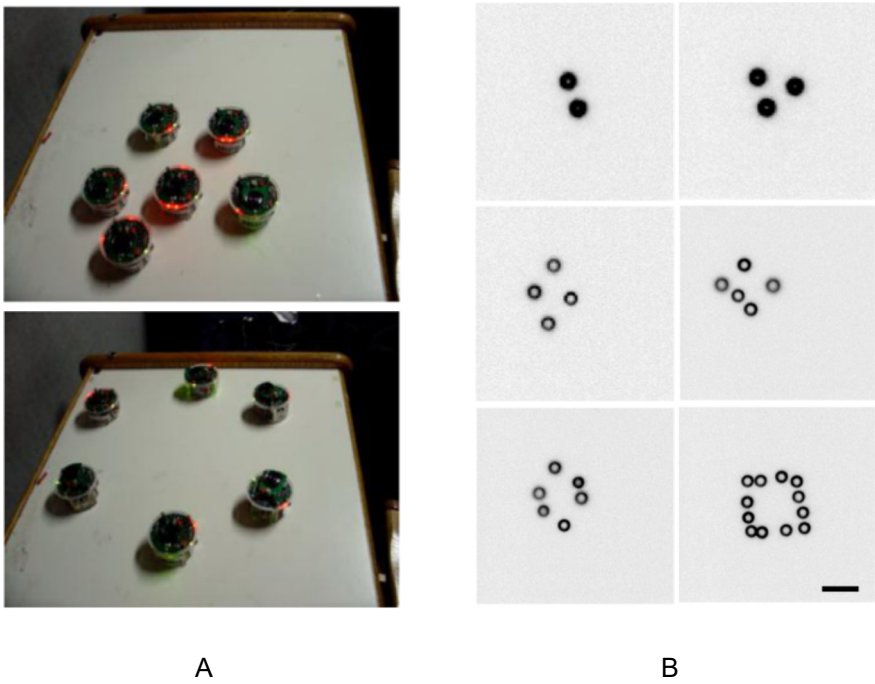

Figure 4.4: **Pattern formation by collective systems.** Formation of **(A)** a circular pattern by a swarm of e-pucks through IR sensing, and **(B)** various shapes by melamine microparticles through a light-based augmented signalling channel. **(A)** Adapted with permission from [251] © 2013 Elsevier and **(B)** adapted from [202] under CC BY–A 4.0.

inspiration of swarm intelligence algorithms [106], and has been replicated in robotic collectives [260, 285]. The final spatially-organised behaviour, pattern formation, has various discipline specific definitions, but broadly refers to the organisation of a system into an orderly structure. It is observed in natural biological and physical processes, including crystal growth [219] and animal coat patterning [209]. In swarm robotics, pattern formation is executed by the repositioning of a group of robots into a regular, repetitive pattern that is either pre-defined or emergent under particular rules [43, 183, 291]. Similarly, several examples of pattern formation algorithms at the microscales have been demonstrated. Examples of both a robotic and microparticle-based system executing pattern formation is shown in Figure 4.4. In Figure 4.4A, a system of e-puck robots is shown before and after assembling into a circular pattern [251]. The melamine microparticles shown in Figure 4.4B are also be seen to assemble into various shapes depending on the number of agents present in the system [202]. For the microparticles, a time-shared laser beam is used to establish an external augmented signalling channel for the exchange of positional information. Based on this information, repositioning of microagents occurs as a function of local separation distances. In the robotic system on the other hand, agents are equipped with IR proximity sensors and wheels such that they can move and reorganise with respect to each other. In both implementations, local positional information is used to facilitate the formation of patterns by the agent collectives.

4.2.1.2 Navigation behaviours

Navigational behaviours differ from spatially-organised behaviours in that the key property is the collective manner in which agents move through space, rather than the specific configuration or organisation of the agents. The three examples included in the Figure 4.1 breakdown are exploration, coordinated motion and collective transport.

Collective exploration loosely describes the movement of an agent group around an environment, often to aid in the discovery of food sources or for mapping purposes. This behaviour is observed in various biological systems such as some species of ant [49, 95, 129] and fish [217], and the same principles are commonly applied in swarm robotics tasks that require the mapping or monitoring of an area [43, 191]. In one example, shown in Figure 4.6A, a swarm of Kilobots were deployed to explore the local environment in which two areas of interest had been placed, with the goal of forming a trail between these areas and the original release point [260]. A similar kind of environmental exploration can also be seen in the slime mould *Physarum polycephalum*. In a well-known experiment, *Physarum* was able to largely recreate the structure of Tokyo's rail system when surrounded with food sources, which were positioned so as to represent neighbouring major cities (Figure 4.6B) [376].

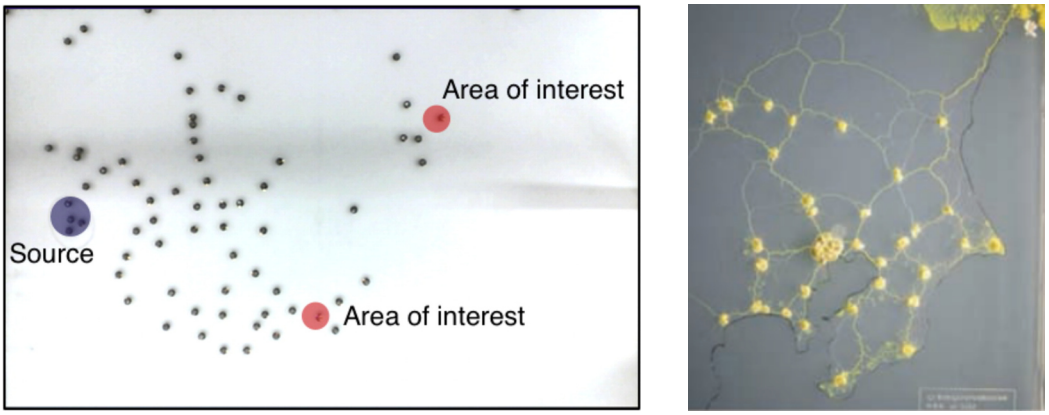

A B

Figure 4.5: **Exploration by collective systems. (A)** A Kilobot swarm performing trail formation between a release point (source) and two areas of interest. Reproduced with permission from [260] © 2019 Taylor & Francis. **(B)** *Physarum polycephalum* placed amongst an arrangement of food sources to represent Tokyo and major surrounding cities. Adapted from [376] © 2010 AAAS.

Coordinated motion is another navigational behaviour that is found in natural systems such as birds and fish, often referred to as flocking or schooling respectively when demonstrated by these animals [162, 295, 388]. This behaviour has been widely adopted in the field of swarm robotics [29], typically using the basic rules of collision avoidance, velocity matching and flock centering proposed by Reynolds et al. [332]. An implementation of this using a swarm of Kobots equipped with short range IR sensors for distance sensing is shown in Figure 4.6A [382]. Similar

behaviour has also been achieved at the microscale, in one instance with TiO_2/Pt micromotors that were found to be capable of collective migration under near-IR light (Figure 4.6B) [91]. In the robotic system, self-organised flocking was carried out using on-board sensing and communication capabilities to avoid collisions, modulate velocity and perform necessary realignments as the group moved through space. In comparison, the collective migration seen in the TiO_2/Pt microsystem occurs due to the light-induced convection flow, which causes the agents to gather into a concentrated area, at which point local interparticle interactions are brought strongly into play. Somewhat connected to collective motion is collective transport, a swarm behaviour by which an agent group acts cooperative to move an object in space. This has been commonly observed in ant populations [214, 371], as well as with kinesin motors [135]. Collective transport is an important task in swarm robotics [152, 338], with algorithms typically employing decentralised control through local force, position and orientation sensing [104]. More recently, there has been significant interest in the design of micro and nanosystems capable of collective cargo transportation, with a primary application being environmental remediation [91, 397, 414].

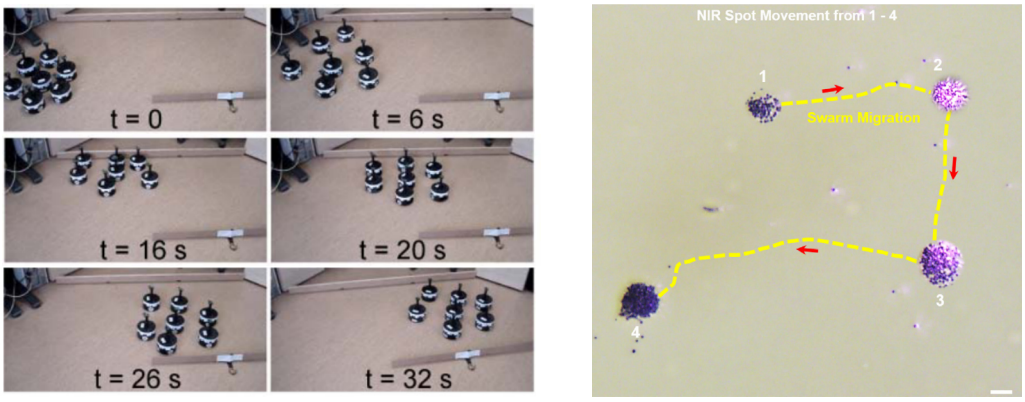

A B

Figure 4.6: **Coordinated motion of collective systems.** Coordinated motion performed by **(A)** s-bots through local infared sensing, and **(B)** locally interacting TiO_2/Pt micromotors under the guidance of infared light. **(A)** Adapted with permission from [382] © 2012 SAGE Publications, and **(B)** reproduced with permission from [91], © 2013 Elsevier.

4.2.1.3 Collective decision-making

Collective decision-making is the process by which a multi-agent system makes a collective choice from a number of options, and is employed in functions such as consensus achievement and task allocation. Unlike the previous categories of collective behaviour, decision-making does not have an intrinsic spatial component, as it can theoretically be achieved solely through agent communication. In the case of most social insects including bees [353], ants [94] and cockroaches [9, 156, 354] however, spatially-organised behaviours like aggregation do play a role. For robotic systems, a consensus can be reached either through direct communication between

agents [79, 307], or indirectly through signifiers such as positional change [43, 88, 137, 200]. The former behaviour is similar to the way that decision-making occurs in a human social group, while the latter is closer to the interaction of social insects. Another example of collective decision making is task allocation, in which agents are able to decide amongst themselves which task should be performed by which agent. It is through this process that many social insects are able to divide necessary labour between a large population [379, 380]. Task allocation is important in swarm robotics due to limited communication and decentralised control within the collective systems [36, 192, 236].

At the microscale, there exist several examples of naturally occurring decision making processes. These include an ability for phages to use molecular communication to decide whether to lay dormant or to replicate and kill their host bacteria [115], cellular decisions present in the wound healing process [406], and foraging decisions undertaken by organism such as *Physarum polycephalum* [31]. In terms of the engineering of synthetic or hybrid microswarm systems however, implementations of collective decision making algorithms remain limited. An obvious reason for this is that this behaviour type typically requires a more traditional form of computing capability than many of the other behaviours discussed previously. It seems reasonable therefore, given the continuing development of increasingly complex methods of programming and control at the microscale, that the ability to engineer collective decision-making behaviours in synthetic microswarm systems may be on the horizon.

4.2.2 Building blocks of swarm control

Although swarm engineering can generate a wide range of behavioural outputs, there are a number of common building blocks for agent control that facilitate these behaviours. This is true for many types of swarming systems across scales, both natural and synthetic. Here, the 3 building blocks that will be discussed are agent-agent signalling, stigmergy and motion control, although these by no means constitute the totality of swarm control elements.

4.2.2.1 Control mechanisms for collective outcomes

Signalling in this context is used to refer to a direct form of communication between agents, such as the dance performed by honey bees [352] or the transmission of information between robotic agents through channels like Wi-Fi, Bluetooth and IR [277]. This is in contrast to stigmergy, which is a method of indirect communication, often implemented through the environmental deposition of real or virtual pheromones in both natural and robotic systems [50, 134, 181, 274, 330]. Motion control is distinct from these two as it not communication-based, but plays a crucial role in both spatially organised and navigational behaviours. A clear example of this is collective motion or transport, in which the velocity and orientation of swarm agents must be regularly adjusted based on information from the environment and local neighbours [332]. To see how these building blocks play into the collective behaviours explored in Section 4.2.1, Table 4.1 gives a breakdown

Collective behaviour(s)	Signalling	Stigmergy	Motion control	Ref.
Aggregation Consensus achievement		×	×	[200]
Aggregation Consensus achievement	×	×	×	[252]
Self-assembly	×		×	[151]
Collective transport Coordinated motion	×		×	[338]
Collective transport Collective exploration		×	×	[134]
Aggregation Collective exploration Pattern formation	×		×	[35]
Morphogenesis Pattern formation	×		×	[358]
Morphogenesis Pattern formation	×		×	[251]
Aggregation Morphogenesis Task allocation	×		×	[362]
Pattern formation Self-assembly	×		×	[339]
Coordinated motion	×		×	[162]
Consensus achievement	×		×	[79]
Aggregation Consensus achievement	×		×	[137]
Coordinated motion	×		×	[382]
Consensus achievement		×	×	[156]
Collective exploration	×		×	[181]

Table 4.1: **Swarm control building blocks towards collective behaviours.** The use of signalling, stigmergy and motion control in various collective behaviours demonstrated by swarm robotics systems in literature.

of the use of these control blocks to achieve various collective behaviours, as presented in swarm robotics literature. In general, though not as a rule, these behaviours are achieved through the use of either a signalling or stigmergic communication channel, combined with with controlled motion that can respond dynamically based on these communicative processes.

4.2.2.2 Augmented agent capabilities for control of microswarms

The three building blocks laid out here are commonly observed in the natural world and have been demonstrated in many swarm robotics implementations. Application at the microscale is significantly less straightforward however. Where animals may communicate via sound or

movement patterns and robots may transmit transmit data, there is not such a clear pathway to implement interagent signalling for most microagents. Even for microagents with established means of communication such as bacteria, these pathways are often deeply complex, even disputed [328, 403]. It can therefore be difficult to hijack and repurpose these pathways, although advances in synthetic biology have made this type of engineering increasingly more feasible and accessible. Motion control can also be a significant challenge when moving from programmable robotic agents equipped with wheels, legs and other components for directed movement to microscopic agents. Although self-propulsion of many types of microagents has been demonstrated through chemical and thermal reactions, or by beating flagella in organic systems, their motility is not programmable in the same way as for robots. Due to these issues of limited programmability and simple agent design, it can be challenging to build robust swarm control methods at the microscale that are generally applicable and not strictly dependent on agent-specific mechanisms such as quorum sensing or phoretic interactions.

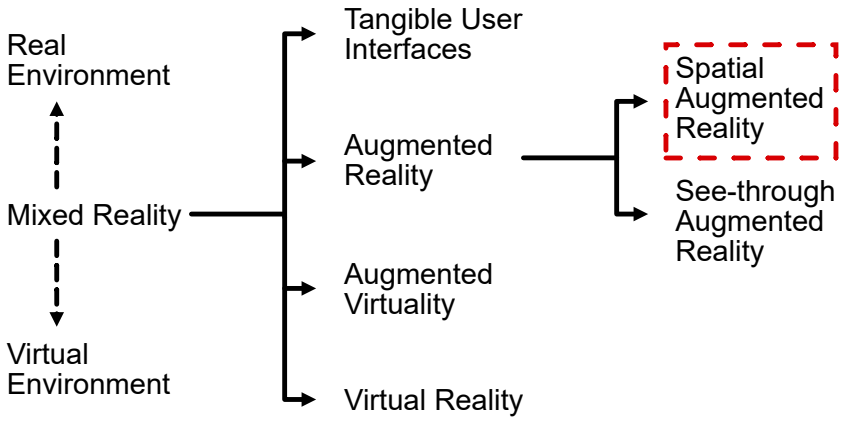

Figure 4.7: **The reality–virtuality continuum.** The landscape of mixed realities, in which 'real environment' and 'virtual environment' constitute the two extremes, with a dashed box indicating the location of SAR. Originally proposed by Milgram et al. [254].

For light-responsive microsystems in particular, one way to tackle these limitations is to enhance agents with augmented capabilities. The addition of an externally applied 'augmented reality layer' [92] onto a microsystem could help to facilitate the emergence of collective dynamics without relying exclusively on intrinsic systems properties. This could serve as a stepping stone to determine key functionalities needed before finally engineering the capabilities in the microagents directly. Augmented reality as a broader term refers to the augmentation or enhancement of a real world environment by computer generated information, and can be placed the wider context of mixed reality. Figure 4.7 depicts the reality–virtuality continuum, originally proposed by Milgram et al. [254], which places various augmented and virtual reality technologies on a spectrum between real and virtual environment. The category of augmented reality can be further broken down into see-through augmented reality, which typically uses head-mounted displays or glasses, and spatially augmented reality (SAR). In SAR, an augmented layer in overlaid onto a

real system, typically using a camera and light projector set-up as seen in Figure 4.8 [38].

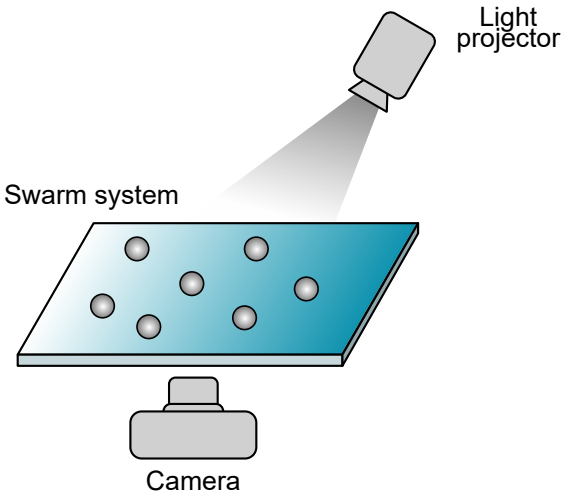

Figure 4.8: **Generic SAR setup.** A system consisting of swarm agents, augmented by the projection of a light gradient while simultaneously imaged using a camera.

The enhancement of microagents via augmentation as proposed here would be categorised as SAR, as in this scheme patterned light is projected onto a real system to create an augmented reality layer. For a microsystem consisting of light-responsive agents, this projection constitutes a tangible control layer with which they are able to interact, meaning that the dynamics of the real word system can be enhanced through SAR. While traditional SAR doesn't necessarily feature this feedback loop of light reactivity, there are examples in which it has been used in this way. Specifically in the context of facilitating swarm behaviours, a number of implementations of SAR-type systems can be found, although often not self-described as augmented reality setups. In swarm robotics, projected light has been used to enhance the capabilities of robotic agents towards collective behaviours such as morphogenesis [362], aggregation [252], exploration [181, 372] and consensus achievement [139] as well as in swarm user interfaces [223, 373] and human-swarm interaction [7]. In particular, an aggregation-based strategy for collective perception and decision making was implemented by Mermoud et al. [252] by projecting green and red spots to indicate 'good' and 'bad' sites in an environment. In this augmented system, shown in Figure 4.9A, aggregation is used as an implicit communication mechanism, as groups of more than one robot are able to trigger the 'destruction' of a spot that they collectively judge to be bad. Similarly in work by Garnier et al. [139], projected light is used to endow robots with the ability to deposit a virtual pheromone that can be detected by other swarm members, with increased pheromone intensity indicated by an increase in the gray level of the light. With this set-up, robotic agents can follow pheromone trails laid by the rest of the swarm, as seen in Figure 4.9B, and thus were able to reach an ant colony-like consensus between two identical paths linking their nest to a food source.

Although there are numerous examples of light projection systems employed at the microscale,

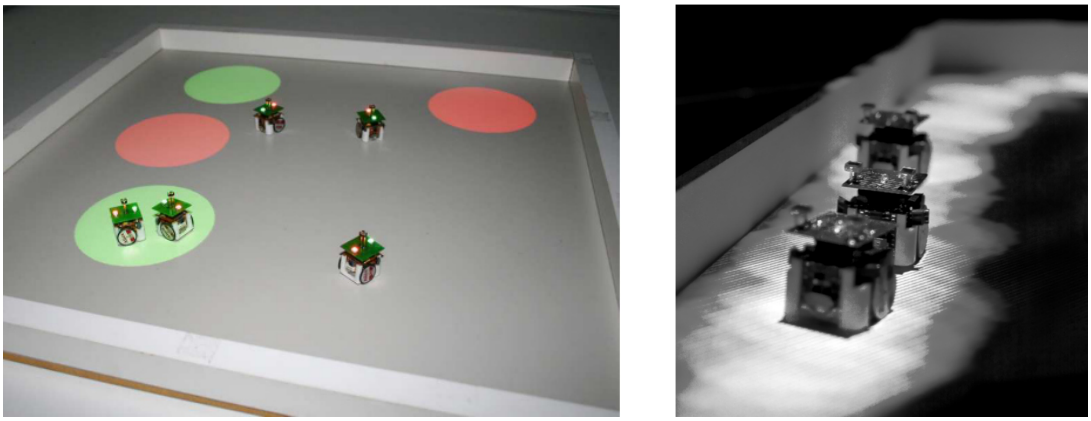

A B

Figure 4.9: **Swarm behaviours facilitated by SAR. (A)** Aggregation-mediated collective perception and decision making by a group of robots facilitated by the projection of green and red spots to indicate 'good' and 'bad' sites. **(B)** Pheromone trail deposition and following by autonomous robots facilitated by the projection of light. **(A)** Reproduced from [252] © 2010 IFAAMAS and **(B)** reproduced with permission from [139] © 2007 IEEE

as laid out in Section 2.4, most of these cannot be said to facilitate swarm behaviour as there is neither direct (signalling) nor indirect (deposition) interaction between agents. Exceptions can be found in the works of Khadka et al. [202], Bauerle et al. [28] and Lavergne et al. [221], although in these cases light was delivered by a time-shared laser beam rather than light projection in the strict sense. In these setups, discussed in detail in Section 2.3.3, augmented signalling channels between agents were established by tying the light delivered to individual microagents to local information such as density or positioning. In the case of Lavergne et al., agents were given the ability to sense neighbours within a restricted vision cone and move with respect to this information through the implementation of a laser-based external feedback loop, shown in Figure 4.10. Through this control scheme, self-organising collective behaviours were found to emerge with various clustering dynamics observed for different perception parameters.

The introduction of an augmented layer on top of a real system, or in this case a microsystem, allows building blocks for control to be designed in a more generic way that allows for a higher degree of transferability between different agent types. In the examples discussed above, any light-propelled microagent could be substituted into the setup without significant changes to the control scheme. The augmented layer also lends additional complexity, meaning that swarm robotics algorithms that rely on the emission and sensing of light [35, 251, 382] or of virtual molecules that can be simulated with light [151, 358] could be reproduced at the microscale. Further, collective decision making behaviours that are currently challenging to implement at these scales could be explored using the enhanced capabilities of augmented microagents.

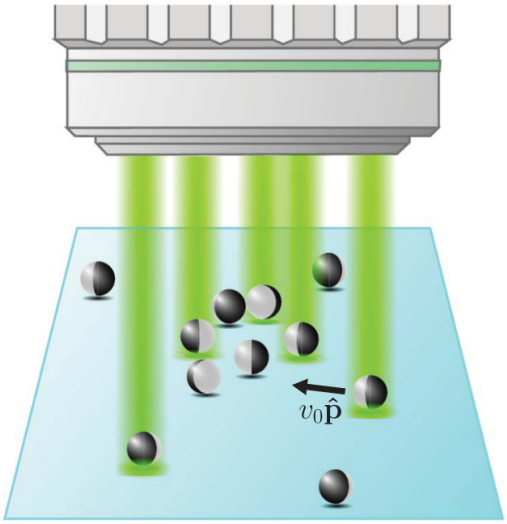

Figure 4.10: **Swarm behaviour facilitated by SAR at the microscale.** An external feedback loop to endow light-responsive microagents with the ability to perceive agents in their local environment. Agents are able to move with respect to this information with velocity $v_0\hat{p}$ where the $\hat{p}$ is an orientation based on this environmental perception. Reproduced from [221] © 2019 AAAS.

4.3 Materials and methods

Having laid out above three basic building blocks towards swarm control at the microscale, this section sets out to detail their implementation in a real world system. This is carried out using the DOME platform to provide an augmented reality layer to enhance the capabilities of simple light-responsive microagents.

4.3.1 *Volvox* as model microagents

The aim of developing building blocks towards microscale swarm control as described in this chapter is to construct generic control blocks that could be generalised many light-responsive systems. The specific type of microagent used in these proof-of-concept demonstrations is therefore less important in this context than the behavioural building blocks themselves. Given this, *Volvox* were chosen as a model microagent as they are easy to visualise, safe to work with, and naturally responsive to light.*Volvox* is an algae found in freshwater ponds across the world that assembles into spherical colonies, as seen in Figure 4.11, with flagellated somatic cells at the surface for swimming through a liquid environment [247, 313]. A light response has been established in many species of *Volvox*, with the activity of *Volvox carteri* and *Volvox aureus* flagella in particular found to be noticeably responsive to intermittent light stimulation [108, 157].

All algae in the volvocine group are flagellates that display phototactic behaviour in order to reorientate into areas of higher light intensity for photosynthesis [155]. This movement is

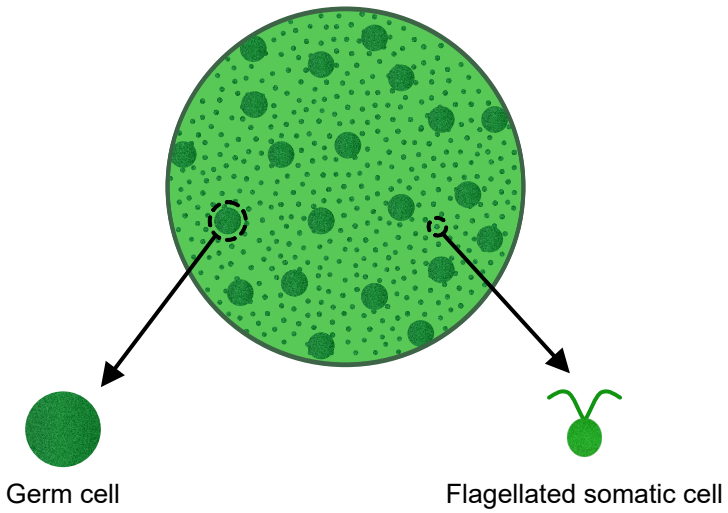

Figure 4.11: **Diagram of a *Volvox* colony**. Spherical *Volvox* colonies are made up of thousands of individual cells and two distinct cells types. Germ cells are larger and reproductive, while the smaller somatic cells are flagellated, facilitating motility.

brought about by the two flagella found on each somatic cell of the algae, which also each possess a light-perceiving eyespot. Forward swimming is only possible in *Volvox* because the cellular anterior-posterior axis differs from the anterior-posterior axis of the organism as a whole [171]. If this were not the case, the surface layer of identically acting cells would simply exert an opposing force on each side of the body and no locomotion would be achieved. The strokes of the flagella have the effect of pushing the algae towards the posterior-anterior direction, however as the net effective propulsion generated is not precisely parallel to this axis a rotational effect also occurs during forward swimming [170].

Interestingly, it has been found that no direct communication occurs between cells during phototactic reorientation in *Volvox*. This is demonstrated most clearly in species such as *Volvox carteri* which posses no intercellular connections, and yet are able to coordinate the same locomotive responses as other species in response to changing light conditions [172]. Although the phototactic mechanism is still not fully understood, a study by Ueki et al. [383] has found that in the species *Volvox* rousseletii both the beat frequency in the anterior hemisphere, and the beat direction of the flagella change in response to alterations in light intensity. The group observed a rapid response to changes in light conditions when the algae was subjected to pulsed illumination. This photatactic response is utilised in the work described here, with *Volvox* treated as light-controllable agents.

The size of a *Volvox* colony varies over its life cycle and so is difficult to quantify precisely. For the sample used here the diameters of visible colonies were found to fall largely between the range of 100-300 µm. The sample, obtained from Blades Biological UK, were originally collected from UK ponds and are believed to be of the species *Volvox aureus*. To allow the free movement of *Volvox* during imaging in the DOME, a sample area with a depth multiple times their diameter

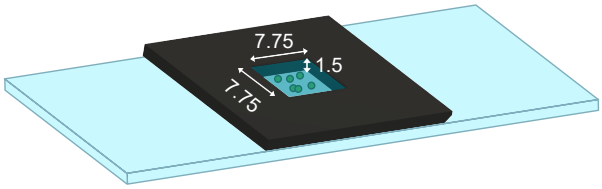

Figure 4.12: **Sample arena.** A 3D printed chip attached to a microscope slide forming a sample arena for *Volvox* colonies to move freely. Dimensions shown in units of mm.

was used. This arena, shown in Figure 4.12, consists of a 3D printed PLA chip with a square well of dimensions 7.75 × 7.75 × 1.5 mm at the center. Before use, the chip was attached to a standard glass microscope slide by using a superglue adhesive and left to dry overnight. For these swarm control demonstrations, 75 µl of a *Volvox* suspension, maintained at room temperature, was added to the sample arena.

4.3.2 Augmenting real world microsystems using the DOME

Central to the work presented here is the DOME platform, the development and characterisation of which was the subject of Chapter 3. In brief, the DOME is an open-source platform capable of producing dynamic, finely tuned coloured light patterns by combining light projection technology with microscopy imaging and on-board computation. It is capable of multi-wavelength illumination at 460, 510 and 640 nm, delivered by the DLP projector contained within it. The DOME can be understood as consisting of an imaging and a projection module, linked together by a local network.

4.3.2.1 Imaging microagents in the DOME

For image collection, the DOME camera was operated at at 9× magnification. Camera resolution was set to 1920 × 1088, with exposure mode 'spotlight' and a shutter speed of 200 ms. The camera was operated using the capture continuous method, which captures images in an infinite loop, iterating over frames. Due to this method of image capture, the frame rate is dictated by the length of time required to capture each frame and then perform the relevant analysis and control functions for a given algorithm. For the algorithms implemented here, the frame rate was found to be between 3 and 4 fps depending on the control algorithm. A neutral density filter of optical density 1 was also placed in the filter holder to minimise optical interference artifacts and avoid camera saturation.

Volvox samples were uniformly illuminated with low-level red light using a dark red background projection image. This image was generated using a NumPy array of size (360 × 630 × 3), where 640×360 is the projector resolution and 3 refers to the RGB colour channels. All points in the array were set to RGB pixels of `(50,0,0)`, giving the dark red illumination required. Due to the off-axis projection, this produced images in which *Volvox* agents appear red against a

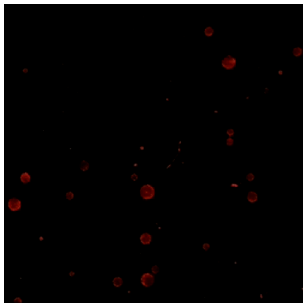

Figure 4.13: ***Volvox* imaging.** A projection of low level red light is used for imaging to minimise the effect on the light-responsive *Volvox*.

dark background. By keeping background light levels low, and using red light for illumination, the effect of background light on agents was minimised, as red wavelengths are known to be phototactically neutral to *Volvox aureus* [157].

4.3.2.2 Closed-loop control algorithms in the DOME

Although different algorithms are used for the three building blocks demonstrated here, a sizable chunk of the algorithmic control process is common to all and can be discussed in general terms. Python 3 scripts run in parallel on the imaging and projection modules of the DOME were used to facilitate image capture and processing, and the generation of new projection images based on this information. This closed-loop control process is represented diagrammatically in Figure 4.14, which shows the steps followed on both the imaging and projection module to complete a single iteration.

The control loop begins with the capturing of a camera frame as detailed above. Agents are located within the frame using the `cv2.findContours` contour detection function from the OpenCV library, which is employed for all image analysis performed here. Contours are filtered for size and shape based on the observed parameters of typical *Volvox* agents to exclude any unwanted matter present in the suspension. A simple ID-based tracking system is implemented by matching the locations of contours in a given frame to those in the previous frame. The closest match is assumed to be the same agent, provided that the distance between the two locations is less than 35 pixels. This distance relates in real world terms to 420 µm, and so given the 3 fps frame rate of the DOME, a *Volvox* agent would require a speed of 1260 μms^{-1} to move out of its possible match area. As the highest recorded speed for any species of *Volvox* is ~600 μms^{-1} for *Volvox barberi* [360], it can be assumed that this will not occur. This ID-matching allows useful parameters such as agent velocity or signalling status to be stored over time, with this history being accessible in all subsequent frames and written as a file after the control algorithm is terminated.

Once agents in the current frame have been ID-matched, agent tracking information for the current frame and all previous frames can be used to generate projection images. The specific

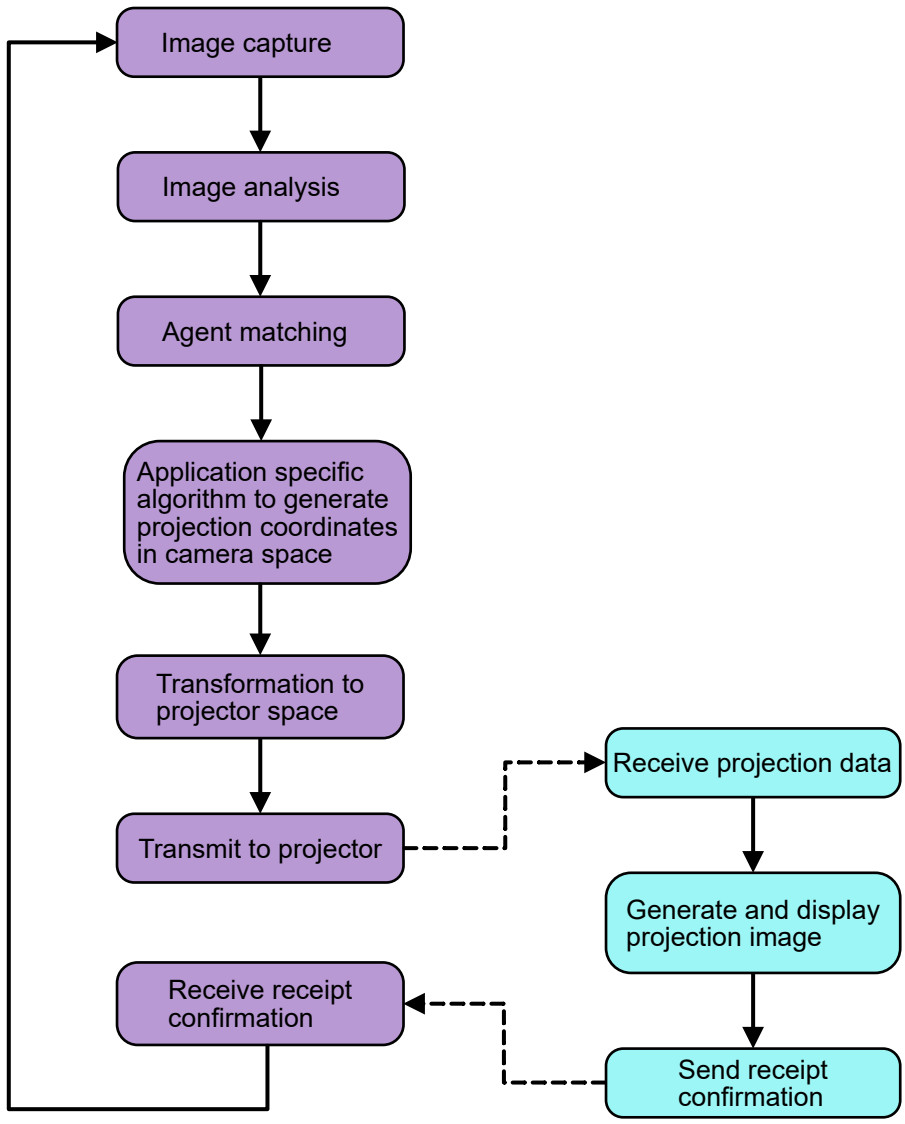

Figure 4.14: **Flow diagram of control algorithm enacted in the DOME**. Each iteration of the control loop algorithm begins with the capturing of a frame, the analysis of which provides data points to generate an updated projection image. The purple and blue colour codes indicate parts of the algorithm that are run on the imaging and projection modules respectively. A solid line indicates the flow of the control process within the same module, while a dashed line indicates the transmission of information between modules via local network.

implementation of this is application dependent, and thus will be detailed further in subsequent sections. The general process however is to algorithmically decide which coordinates in the current camera frame should be part of the patterned light projected onto the system for the subsequent frame. These coordinates are then transformed to the projector space through a matrix transformation established during the DOME calibration process, more details of which can be found in Section 3.3.5. These translated coordinates are then transmitted as a JSON list

to the projection module over the DOME's internal Wi-Fi network.

Upon receipt of this data by the projection module, a projection image is generated by adding high intensity coloured patterns centered on the coordinates in this data set to the otherwise plain dark red background image. This is achieved either by accessing and altering the RGB values of a particular block of pixels in the NumPy array representing the projection image, or by using the drawing function `cv2.circle`. The projection image, and thereby the augmented reality layer, is then updated by displaying the new image using `cv2.imshow`. Upon completion, a confirmation of receipt and projection is transmitted back to the imaging module and and loop begins again with the capture of a new frame.

4.4 Results

In this work, augmented signalling and stigmergy as well as light-based motion control were implemented in a population of *Volvox* colonies. For this, the open-source DOME platform was used to create an augmented reality layer consisting of projected light patterns.

4.4.1 Augmented signalling

Signalling is used here to describe direct communication between agents, as opposed to indirect methods of communication such as stigmergy. In this signalling system, *Volvox* agents are augmented with a projected light halo with a tuneable range and colour that can be transmitted to others if they are within range. As a demonstration of this signalling system, the propagation of light-based 'messages' through a population of agents was implemented. Initially, a seed *Volvox* was chosen at random to begin with an active signal, encoded as a projected halo of light centered on the agent. This light signal could then be transmitted to other agents that moved within the communication range r of the signalling agent. This was implemented for a variety of ranges, and with both single and multiple signalling channels at play. Note that in this system, agents are able to move out of the region of interest entirely and thus it is possible for the signal to 'die out' if propagation events occur at a low rate compared to the average length of time a given agent stays in view. It is important to emphasise that this signalling is entirely virtual, occurring as an augmented reality layer on top of the natural movement of the *Volvox*. Although it is likely that there is some effect on this movement due to the presence of light, as *Volvox* is a phototactic organism, this is not considered or quantified here. Moreover, it is likely that this effect is small since the phototactic response of is adaptive [108], and thus reacts primarily to intermittent changes in light intensity, rather than a continuous illumination.

4.4.1.1 Single channel signalling

Initially, a single signalling channel was used, meaning only one colour of light was used in in the projected layer. In the first control loop iteration a seed agent was chosen at random, and its

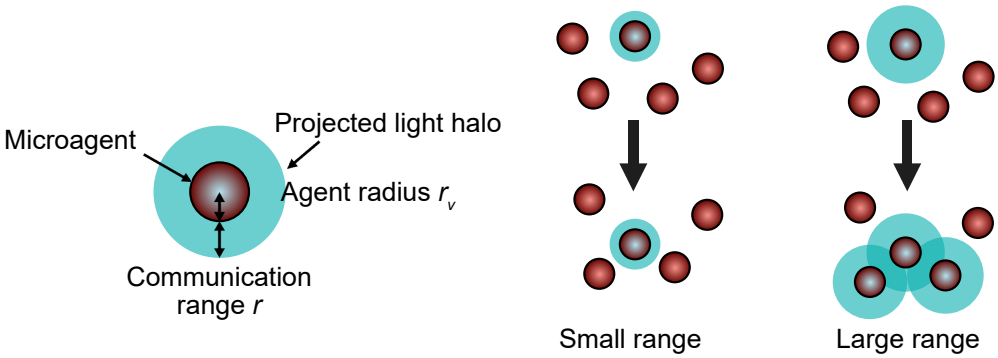

Figure 4.15: **Schematic of augmented single channel signalling.** Microagents are enhanced with augmented signalling capabilities that allow for the propagation of a signal, here a projected light halo, to other agents within the communication range r. A smaller communication range leads to fewer propagation events, with a larger radius causing the signal to propagate faster through a local population.

agent ID added to a list of signalling agents. When passed to the projector module, a projection image was generated with circles centered on the coordinates of signalling agents. These circles, which constitute the signal in the augmented reality layer, were drawn using `cv2.circle`, with a radius equal to $r + r_v$ where r_v is the radius of the *Volvox* agent. In each subsequent frame the locations of all non-signalling agents were checked to ascertain if any fell within range of a signalling agent. If so, a signal propagation event would occur, meaning that the ID of the newly propagating agent was added to the signalling list. For this single channel implementation, the signal colour used was cyan, coded as RGB pixel values `(0,255,255)` on the projector. Each time new data was set received by the projector, the projection image was reset back to the plain red background image and patterned with the new data. This resulted in only current agent locations being included in the augmented layer.

Three different r values were tested to explore the effect of communication range on the propagation dynamics. As can been seen in Figure 4.15, this range is defined from the edge of the agent outwards, and quantified in terms of pixel distances in the camera field of view. It would be expected that fewer propagation events should occur for a small range, causing the signal to spread slower through the population than for a larger range. Indeed, this was found to be the case when the signalling algorithm was implemented for communication ranges of 10, 20 and 30 pixels, equating to real world distances of 120, 240 and 360 µm respectively. This can be seen in Figure 4.16, which shows snapshot images from the DOME of signals propagating through a *Volvox* system at each communication range over 200 seconds.

For the smallest communication range of 120 µm, the signal can be seen to propagate slowly, and only to the closest of neighbours. At the final time point no actively signalling agents remain, as all have moved out of view before a propagation event was able to occur. Looking to the next largest range, 240 µm, signal propagation can be seen to occur much more effectively, with a

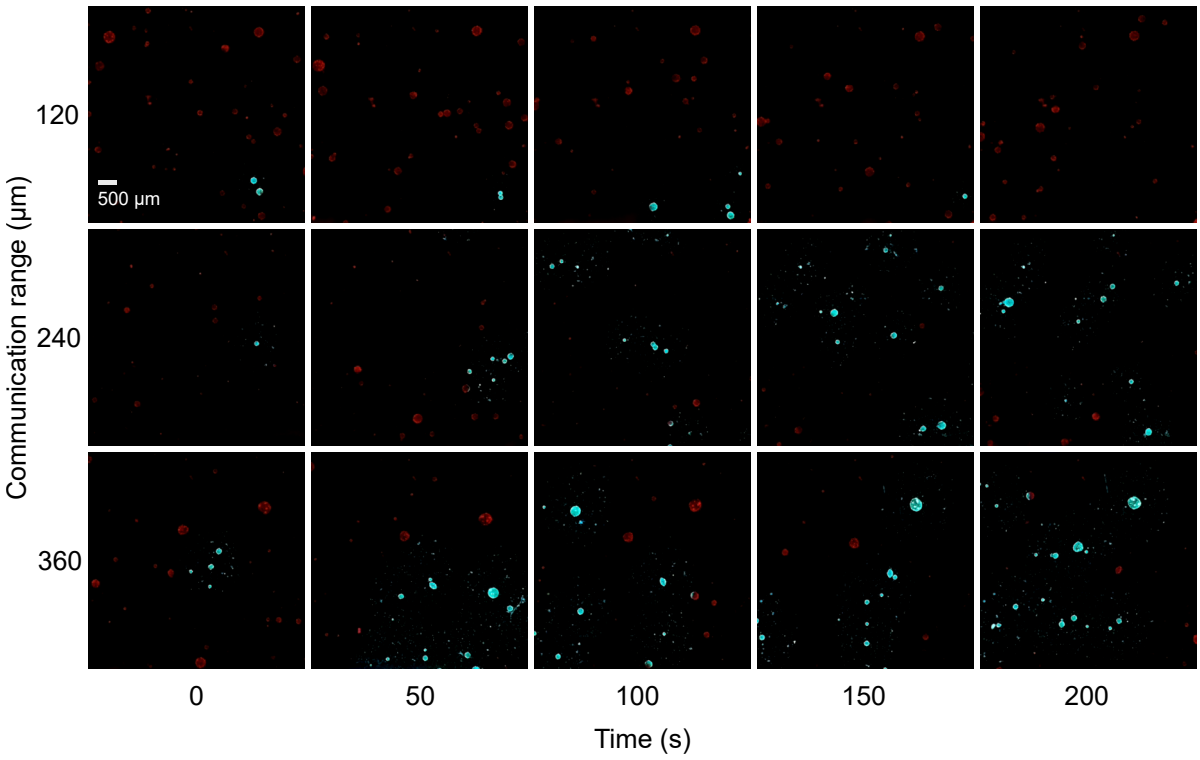

Figure 4.16: **Augmented single channel signalling in a *Volvox* system.** For three different communication ranges of 120, 240 and 360 µm a active signalling agent is randomly seeded, with this able to propagate to other agents that enter the communication range of a signalling agent. Here, non-signalling are red, while signalling agents are cyan.

initial local spread visible after 50 seconds, increasing over time to more distant agents. For the the maximum tested range of 360 µm, propagation occurs rapidly through the population, with the majority of agents seen to be in a signalling state after 50 seconds. After this, the ratio of signalling to non-signalling agents remains fairly consistent. This can be seen quantitatively in Figure 4.17, in which the number of signalling agents is plotted over time.

It follows from this that the choice of communication radius when implementing this type of signalling must be application dependant. The density of agents within the microsystem is an important parameter, since if the *Volvox* in Figure 4.16 were more densely packed, a 120 µm range may have found more success in propagating. The desired behaviour is another important factor to consider, as the dynamics of signal propagation could alter system-wide outcomes significantly. An example of this is trail formation, which in robotics systems has been found to produce less well defined trails when communication ranges between agents are large [260]. On the other hand, for a more general behaviour such as aggregation in which agents need only be located in a loosely-defined area, a faster propagation could be beneficial.

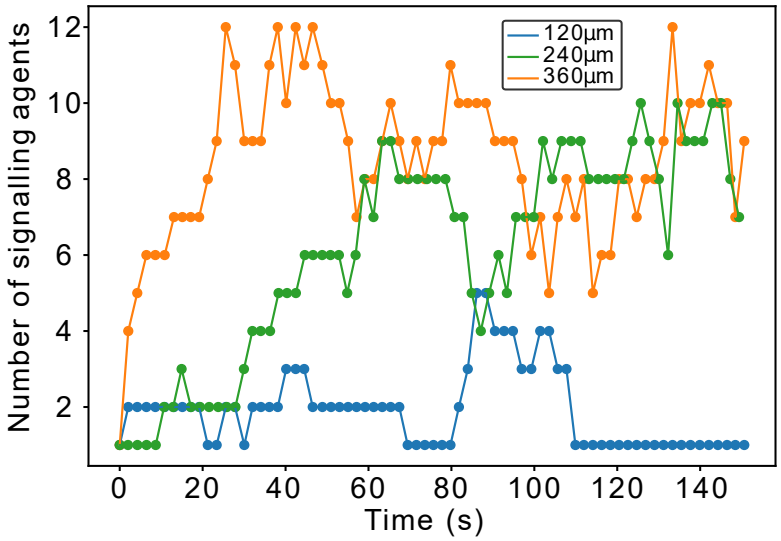

Figure 4.17: **Augmented single channel signalling in a *Volvox* system.** For three different communication ranges of 120, 240 and 360 µm, the rate of propagation is shown by plotting the number of signalling agents over time for each range.

4.4.1.2 Multichannel signalling

In addition to the use of variable communication rages for augmented signalling, multichannel signalling was also implemented to allow the parallel propagation of signals, indicated by different colour projections. A fixed communication radius of 240 µm was used for this, as this was judged to allow sufficient propagation events for efficient signal spreed, but avoided the rapid spread seen at a larger range.

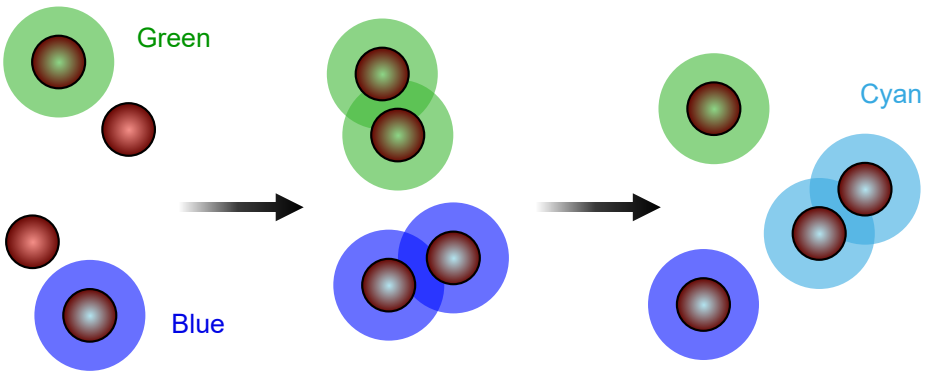

Figure 4.18: **Schematic of augmented multichannel signalling.** Microagents are enhanced with augmented signalling capabilities that allow for the simultaneous propagation of multiple signals. Two signalling states, blue and green, are initially seeded, however a third mixed state, cyan, is entered when signalling agents of different states interact.

The control algorithm used was the same as that described above for single channel signalling, however in this case two signalling channels were initially seeded, coded as blue and green.

A third signalling state, cyan, was also available, occurring when signalling agents came into contact with a colour other than their own (Figure 4.18). To distinguish between colour channels, agents were assigned a parameter, which took on values of 1, 2 or 3 to represent blue, green and cyan respectively. This information was passed to the projector alongside location data, allowing the correct colour signals to be assigned to each agent. Since both signalling and non-signalling

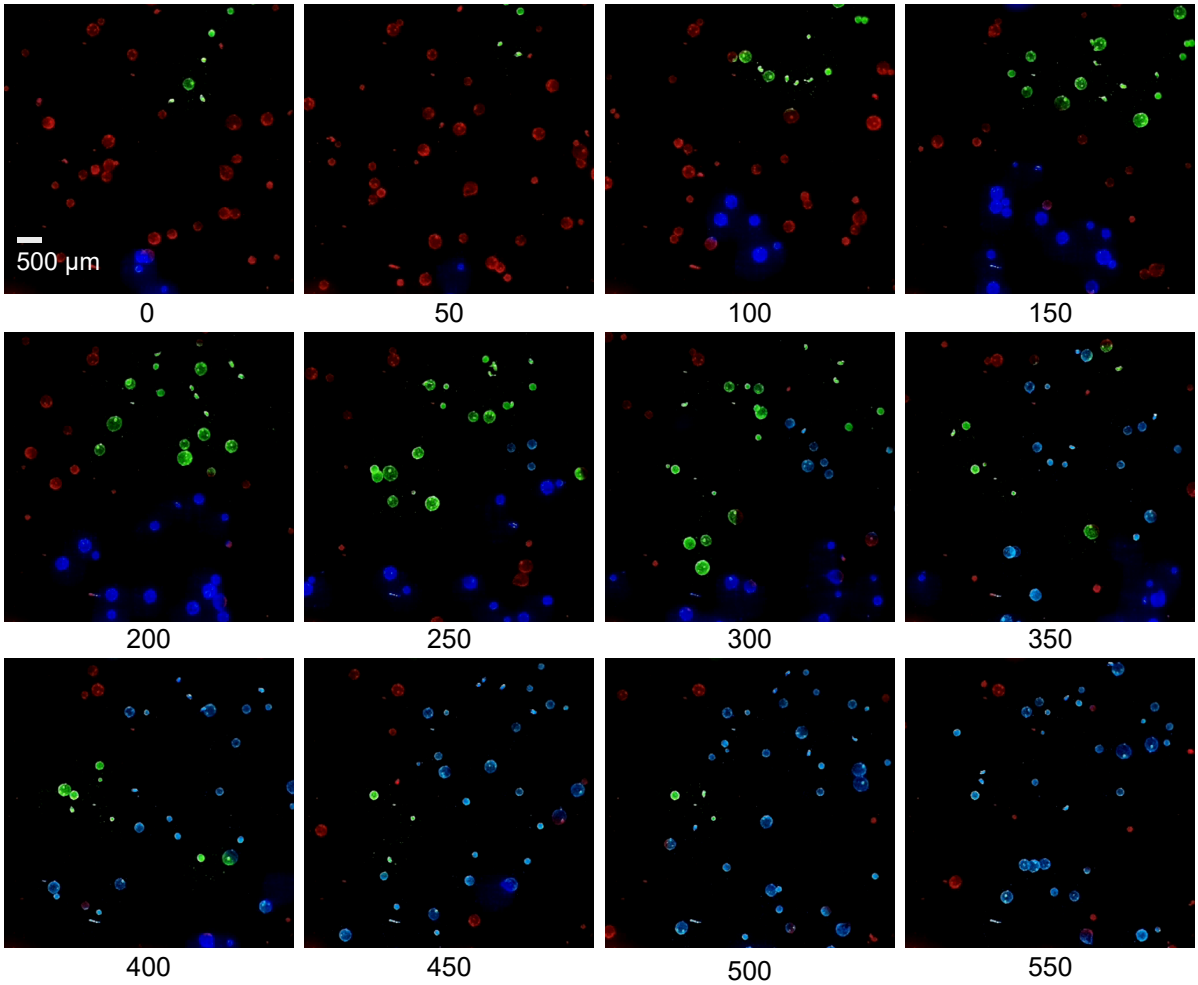

Figure 4.19: **Augmented multichannel signalling in a *Volvox* system.** Two signalling channels, blue and green, are initially seeded at opposite sides of the environment. Upon the interaction of blue and green signalling agent, a mixed state designated as cyan is reached. Time is given in units of s.

agents also enter the mixed cyan state upon contact with a mixed state agent, the system should be expected to tend towards cyan as time goes on. This can be seen to play out in time series images from an implementation of this multichannel signalling algorithm (Figure 4.19) that shows the evolution of the system over a total of 550 seconds. The two signals are seeded at opposite sides of the environment, and can be seen to propagate through the population separately until the first mixed state agents appear at 250 seconds. As the established blue and green groups

interact further, the number of mixed state agents grows until only this channel remains at the final time point.

Although these signalling channels are augmented and the *Volvox* themselves are unaware of the transmission mechanism, their spatiotemporal dynamics and interactions play a direct role in the spread of signals, and could offer an essential building block for collective decision making behaviours, as well as lending insight into phenomena such as disease propagation or the spread of information through a social collective.

4.4.2 Augmented stigmergy

Stigmergy is a form of indirect communication in which some trace is deposited into the environment by a swarm agent such that it may be detected by other agent, or itself [167]. Collective behaviours, including exploration and trail formation, are often facilitated by some form of stigmergy as for swarm systems such as social insects this is a primary means of communication.

In this implementation of augmented stigmergy, *Volvox* microagents are enhanced with the ability to 'deposit' trails of light onto their environment as seen in Figure 4.20, in a manner similar to pheromone deposition in ant collectives [107]. This was achieved by sending agent locations in each frame to the projector, which unlike in the signalling algorithm was not instructed to reset the projection image between iterations. The result of this was that the entire path of the agent for all from time point zero onwards was included in the trail patterning, which was performed using cyan light.

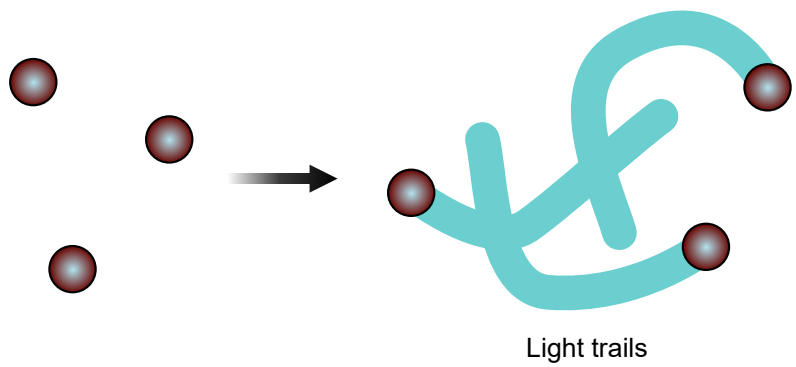

Figure 4.20: **Schematic of augmented stigmergy.** Microagents are enhanced with augmented capabilities for stigmergy that allow for the environmental deposition of light trails.

A time series of the *Volvox* system over 45 seconds can be seen in Figure 4.21, with projected light trails deposited as the agents move around the environment. This has the effect of producing a real time tracking and coverage map that builds over time.

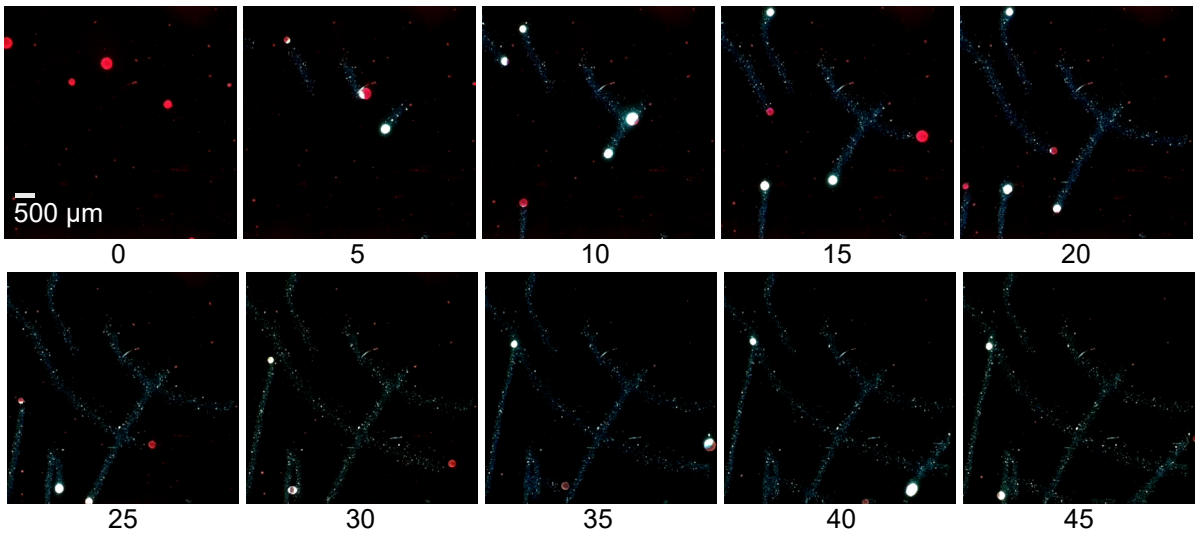

Figure 4.21: **Augmented stigmergy by a *Volvox* system.** As *Volvox* agents move around the environment, trails of cyan light are deposited. Time is given in s.

4.4.3 Motion control

The ability for the motion of agents to be fine tuned based on the local environment, or local agent interactions, is key to swarm engineering. Spatially organised behaviours such as trail formation [260] and coordinated motion [332] rely heavily on this capability, as do navigational behaviours. As outlined in Section 4.3.1, *Volvox aureus* are known to posses an innate light-response [157]. Using the localised light environment created by the DOME, it should therefore be possible to regulate the motion of many individual *Volvox* in parallel as a building block for swarm control.

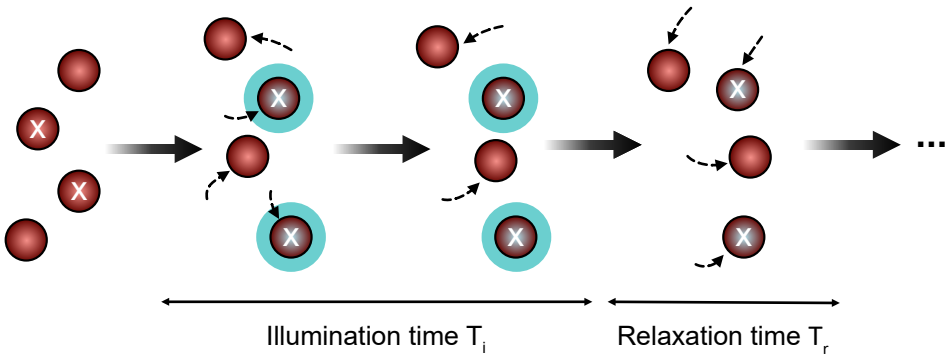

Figure 4.22: **Schematic of light-based motion control.** The velocity of microagents is regulated by pulsing cyan light on and off, localised to half the total population for the purposes of comparison. Light is pulsed on for an illumination time T_i, then switched off for a relaxation time T_r, causing agents to slow periodically.

This was implemented by illuminating half the population of *Volvox* in the frame for illumination time T_i, followed by a period of no illumination for a relaxation time T_r, as seem in

Figure 4.22. The use of pulsed light rather than constant illumination is designed to minimise the adaptive property of the *Volvox* light response, with T_i aiming to line up with the length of time before this adaptive process begins. *Volvox* are known be responsive to blue light of wavelength 430 nm and non-responsive to red wavelengths [157], however a thorough characterisation of light response across wavelengths was not found in the literature. Given this, an equal mixture of blue and green patterning was used, meaning that cyan light constituting 460 nm and 510 nm wavelengths was delivered by the DOME. The control algorithm used here was largely similar to that used for signalling, the difference being that data was sent the the projector for illumination only for the frames that fell within the illumination period. Agent IDs were used to decide which agents would be in the illuminated group, split by even and odd numbers. Time series images displayed in Figure 4.23 demonstrate how this was carried out in the DOME, with illumination being applied for $T_i = 0.5\ s$, followed by a period of no illumination for $T_r = 2.5\ s$, taking up 2 and 9 camera frames respectively.

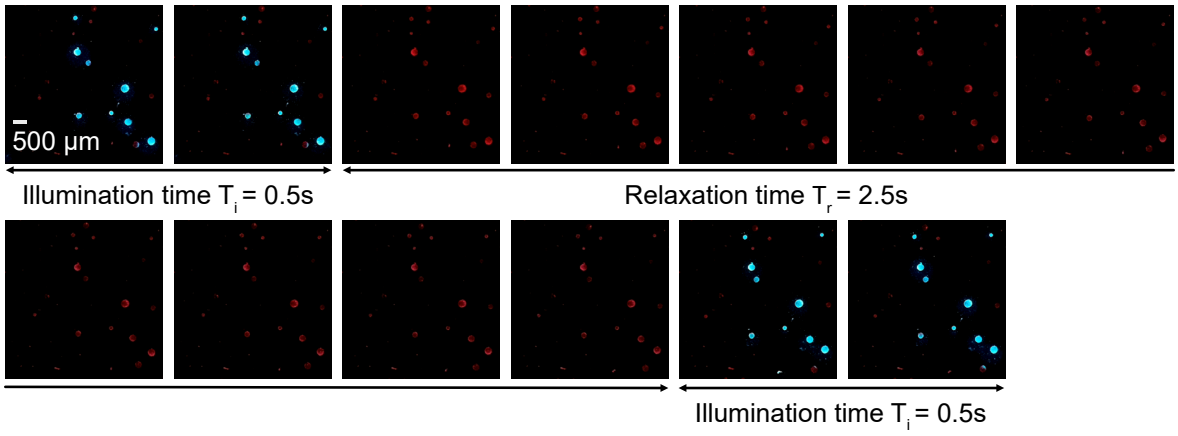

Figure 4.23: **Motion control of a *Volvox* system.** Pulses of cyan light lasting for time T_i are used to regulate the velocity of motile *Volvox* agents, interspersed with a relaxation period of length T_r in which no illumination is delivered.

In video of this experiment, it was observed that this illumination caused the *Volvox* to slow periodically, in line with the illumination cycle. To obtain some quantification for the effect of this intermittent illumination on the *Volvox* system, individual velocities were calculated and stored during 9 experimental repeats. Velocity data for individual agents was then aggregated across these repeats and grouped into those with and without illumination, to produce velocity heat maps for both groups, shown in Figure 4.24. For the group subjected to intermittent illumination, a periodicity in velocity can be seen for many agents, aligning with the illumination period. This is not the case for the non-illuminated group, which demonstrates relatively constant velocities with some random noise variation. Furthermore, it is found that agents moving with higher velocity tend to exhibit a stronger light-response. This heterogeneity could be down to factors such as colony size or differing points in life cycle, and is to be expected in biological systems.

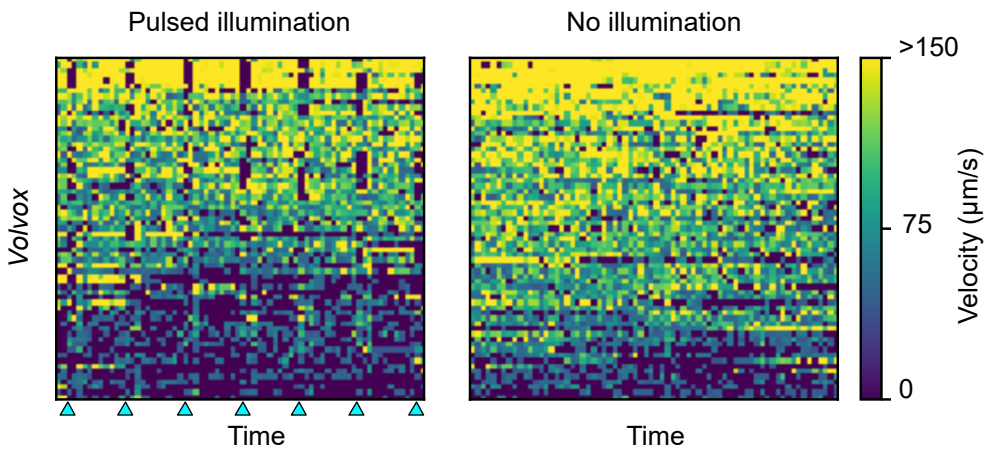

Figure 4.24: ***Volvox* velocities with and without motion control.** Heat map of each Volvox agent's velocity over a 17.5 second time period split by (left) those exposed to 0.5 second pulses of cyan light, and (right) those without illumination. Triangles denote the start of illumination time periods T_i.

To demonstrate the statistical significance of the velocity differences between the illuminated and non-illuminated groups, Kruskal-Wallis analysis of variance was performed on the velocity data sets. An average velocity was calculated for both groups at each time step, the results of which are shown in Figure 4.25, and the Kruskal-Wallis H-test run on these data sets using the `scipy.stats.kruskal`. The result of this was a H statistic of 55.4, and a p-value of $p \leq 0.001$, indicating that there is a significant difference between the average velocity of the two agent groups based on illumination.

In the images shown in Figure 4.23 it can be seen that more than half the population of agents in view are illuminated during the illumination period. This is due to the fact that this time series subset is taken after 14 seconds has already elapsed, meaning that this is the fifth illumination cycle. Given that illuminated agents tend to be slowed, or even stopped, by the light pulses, they are more likely to stay in frame for longer than their non-illuminated counterparts. Since the decision as to whether an agent is illuminated or not is dependent on whether their fixed agent ID is even or odd, new agents entering the frame will be distributed evenly between the two states. Over time, the result of this is an aggregation of illuminated agents. To demonstrate this, Figure 4.26 shows the state of the system for both the first and fifth illumination cycle. For the first cycle, there is an even split of illuminated and non-illuminated agents, with 7 in each group. By fifth cycle, the population of these groups has shifted to 9 and 6 respectively, suggested that the delivery of pulsed illumination has the effect of holding agents in place for longer than would be otherwise expected.

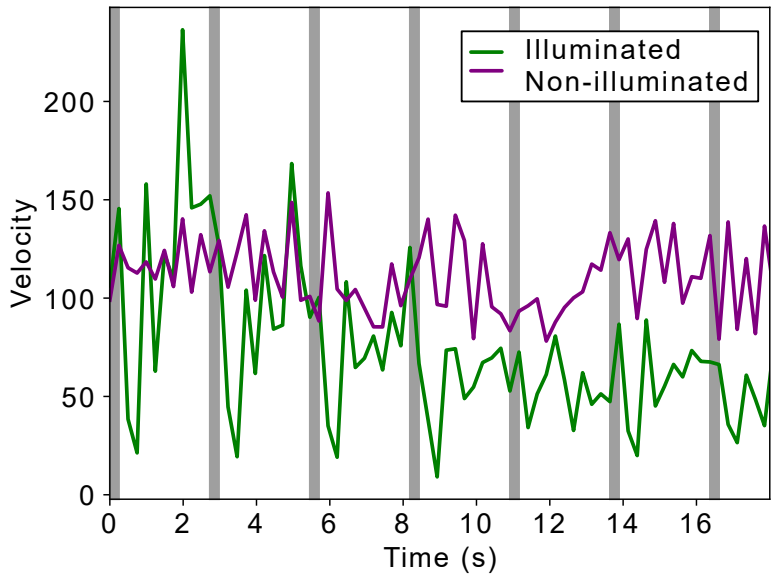

Figure 4.25: **Average *Volvox* velocities with and without motion control.** Average velocities of the illuminated and non-illuminated groups of *Volvox* over time. Gray shaded lines indicate when illumination pulses were applied.

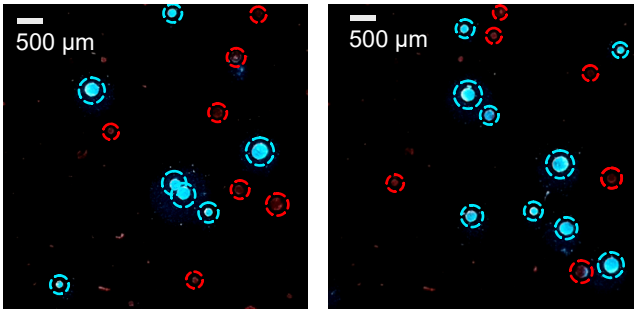

Illumination cycle	1	5
Illuminated agents	7	9
Non-illuminated agents	7	6

Figure 4.26: **Motion control of a *Volvox* system.** Frames taken during the first (left) and fifth (right) illumination cycle show that the number of illuminated agents in frame increases over time relative to the number of non-illuminated agents.

4.5 Discussion

In this work, the viability of this augmented system for enacting swarm control building blocks has been demonstrated. The next step is therefore to consider how these building blocks may be used to explore the collective behaviours discussed in Section 4.2.1. As can be seen in Table 4.1, all spatially organised and navigation based behaviour types require the combination of motion

control with signalling or stigmergy. Given this, it is expected that by combining the control blocks implemented here, collective behaviour may emerge. A simple example of this would be the direct integration of the motion control and signalling blocks to allow agents to 'self-regulate' their velocity based on local communication. If signal propagation were to proceed as before but with a pulsed rather than constant signal, the velocity of propagating agents should slow periodically while all other are unaffected. By tweaking r, T_i and T_r, it may be possible to enact a morphogenesis-type self assembly. A proposed schematic of this is shown in Figure 4.27, with limb like protrusions growing outwards from the original seed agent, as newly propagating agents remain relatively fixed in position due to their own signal. Navigational behaviours could also be explored by enacting a stigmergy scheme in which deposited trails decay, as would be the case for a real world pheromone based system. For any agent exhibiting a light-response, whether positive or negative, this could lead to interesting emergent behaviours such as exploration or aggregation. The signalling and stigmergy blocks implemented here are intentionally generic, and could thus be translated to agent types other than *Volvox*. Many examples of light-responsive microagents can be found in Chapter 2 including micromotors, polymer microrobots, bacteria and mammalian cells. The control scheme laid out here could easily be adapted to work with any of these systems, with only the motion control algorithm requiring agent specific modifications.

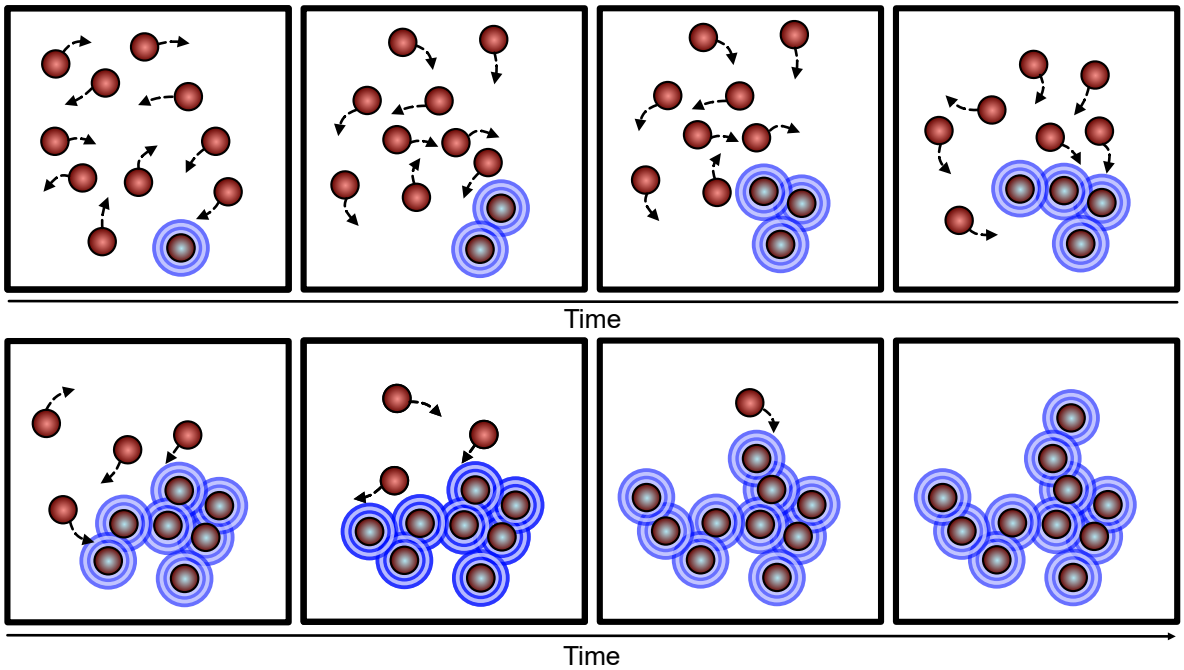

Figure 4.27: **Schematic of morphogensis by light-responsive microagents.** In this proposed scheme, a pulsed signal is propagated through the microsystem, leading to mophogenetic self-assembly due to the slowing of propagating agents.

Unlike many traditional forms of augmented reality, the augmented layer enacted here has been demonstrated to have tangible effects on the dynamics of the real world system. This was

observed to some degree in the implementation of all three control blocks, but was specifically quantified in the motion control experiments. This work provided a verification that the velocity of *Volvox* agents can be regulated through an automated optical control algorithm. Furthermore, the comparison of frames given in Figure 4.26 indicates that this has the potential to be used to enact some spatial organisation, since it is possible to hold agents in a location to some degree. The next stage in extending this motion control in future work would be to explore illumination parameters to find the optimum control conditions. Variable parameters here are illumination and relaxation time, T_i and T_r, as well as the intensity and wavelength of projection light. As is demonstrated by the results in Figure 4.24, a large degree of heterogeneity exists in the light-responses of agents within the same population. This is true not only for *Volvox*, but for most biological systems. It is likely the case therefore that individually tuned parameters would be most effective for precise control. This individualised scheme could be realised by enacting machine learning algorithms on the DOME to automatically discover optimal control parameters. A comparable control scheme was enacted by Muiños-Landin et al., with the use of reinforcement learning on self-thermophoretic microswimmers for the purposes of navigating a grid like environment [268]. The further development of these techniques could help to pave the way for direct translation of swarm robotics principles to swarm engineering at the microscale.

A limitation of this work is the simplicity of the agent tracking and ID-matching system. This system was found to be largely effective in locating and matching agents in the work presented here, and was more than sufficient to aid in the development and demonstration of swarm control blocks. It was found however that the algorithm had difficulty distinguishing agents where multiple came into contact, and was liable to confuse agent IDs when this occurred. To avoid results being skewed by these events, particularly the motion control data, the tracking algorithm was instructed to assign new IDs to the agents once separated. This was effective in this work, particularly given the low density of *Volvox* used, however moving forward a more rigorous approach should be pursued. The tracking system could be improved upon by the inclusion of more advanced image segmentation techniques, including those with basis in machine learning. In particular, future work will explore the use of the Cheetah platform, a neural network based image segmentation tool for integrating real-time image analysis with cellular control algorithms [314].

4.6 Conclusion

The engineering of swarm behaviours at the microscale has significant potential impact across many fields [315, 356], but is often constrained by the simple design and limited programmability of agents. This work sought to address these challenges through the development of building blocks towards swarm control that act to enhance the capabilities of these agents. The building blocks implemented here, signalling, stigmergy and motion control, form the basis for many

collective behaviours commonly employed in more tradition swarm engineering practices. Demonstration of these building blocks was achieved by using the DOME to overlay an augmented layer onto a system of light-responsive microagents. The use of the DOME as a low-cost, open-source platform for this purpose provides a step towards the development of more complex collective behaviours, and the democratisation of swarm engineering at the microscale.

CHAPTER 5

POTENTIAL APPLICATIONS

5.1 Introduction

Having introduced the DOME and demonstrated its functionality as a platform for the control of microscale collectives in Chapters 3 and 4, this chapter will explore potential future applications of the device. The broad applications covered here will be parallel experimentation, de novo swarm behaviour discovery and control of cellular collectives, as well as art, entertainment and outreach. While this list is not exhaustive, it aims to demonstrate some of the ways in which the DOME has begun to be used thus far, as well as some of the versatile real world applications it could be used for moving forward.

5.2 Art, entertainment and outreach

While the primary applications of the DOME are in areas of scientific instrumentation and research, the DOME also presents avenues for engaging in art, entertainment and outreach projects. Images produced by the DOME have a striking appearance, with detailed multi-coloured patterns against a black background, and agents appearing bright and colourful. This leaves room for the use of the DOME as a tool for the creation of art that is inspired by science and technology. This artistic aspect was explored to some degree with the 'Game of Light', an art piece that was presented at the ALIFE 2020 conference gallery session. This piece utilised an algorithm for Conway's Game of Life, with the DOME used to extend the traditional version to interact with a real system of living *Volvox*.

Conway's Game of Life is a well known cellular automaton in which each cell in a discrete grid is either dead or alive, and subsequent generations are formed based on the population of their neighbouring cells. The system is originally seeded with a pattern, random or otherwise,

from which point onward each generation is produced by applying the same set of rules to all cells. These rules may be summarised as:

1. If a cell is alive, it remains so providing it has two or three live neighbours.

2. If a cell is dead, it becomes alive only when it has exactly three live neighbours.

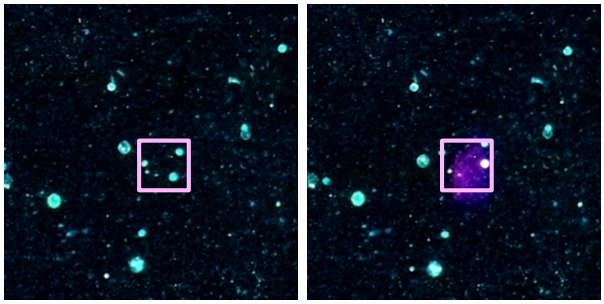

Figure 5.1: **Seeding the Game of Light.** Three *Volvox* agents move within close proximity of each other, indicated by the boxed region, triggering life in a neighbouring artificial cell.

The traditional Game of Life is therefore deterministic, with each generation a direct function of that which proceeded it. An adapted version of this game was implemented on the DOME using an augmented realty layer interacting with a real system of *Volvox* colonies. In this version, called the Game of Light, *Volvox* agents move and interact with augmented 'cells' comprised of projected light. Using real time image analysis on the DOME, the position of *Volvox* agents in relation to augmented cells is fed into the algorithm, meaning that a 'neighbour' could be comprised of either a real or augmented agent. The evolving system is therefore no longer deterministic, as it is influenced by the spatial dynamics of the motile *Volvox* agents.

Traditional implementations of the Game of Life typically use a randomly generated initial pattern to seed subsequent generations. In comparison, the Game of Light is configured such that all artificial cells must be seeded from real life. In this process, three *Volvox* agents must move into close proximity to each other to trigger artificial life in a fourth neighbouring cell, as shown in Figure 5.1. This means that the automated cell population typically begins in 1 highly localised spot before spreading gradually throughout the space, as seen in Figure 5.2.

An interesting way in which the Game of Light builds on the original automaton is in the dynamics of stable pattern formation. There are a vast array patterns that can be formed by evolving system which, assuming the surrounding cells remain unpopulated, will remain eternally stable. Some examples of these patterns are shown in Figure 5.3, which shows the end result of a fully evolved Game of Life simulation that has reached a system wide steady state. A number of basic stable patterns can be seen here, namely the beehive, block and loaf shapes. Also depicted is a repeating pattern that is in a steady state of oscillation between two configurations, in this case between a vertically and horizontally orientation three cell line. In this traditional version,

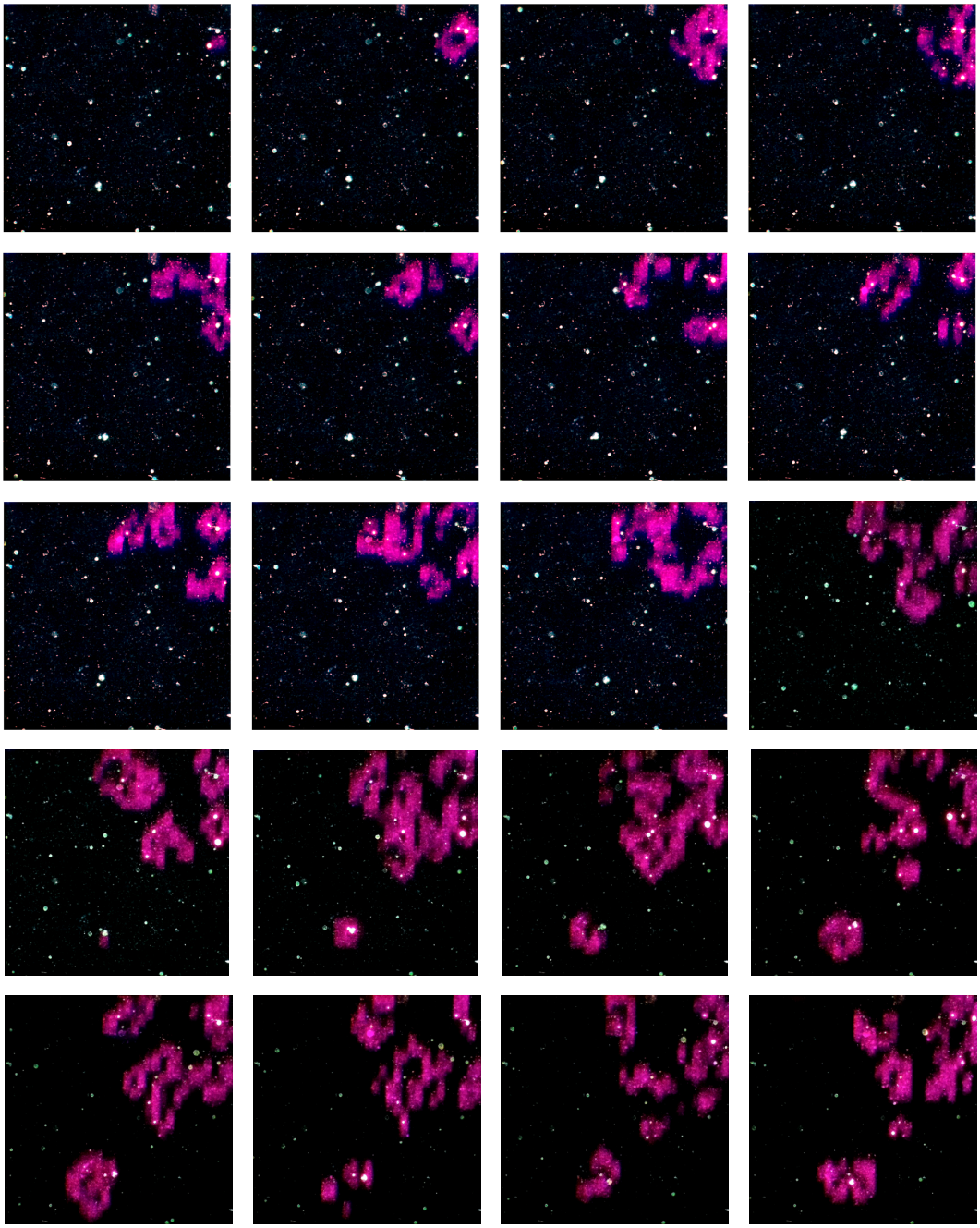

Figure 5.2: **Game of light.** Time series images from an implementation of the Game of Light, with *Volvox* agents and augmented cells appearing as cyan and pink respectively.

the system as a whole will either reach a state of steady patterns such as this or alternatively die out out entirely due to underpopulation.

The Game of Light differs from this, as a steady state cannot be reached due to the movement of the *Volvox* agents which have the ability to interrupt stable patterns. This is demonstrated in Figure 5.4, in which a stable block of 4 augmented cells becomes unstable after interaction

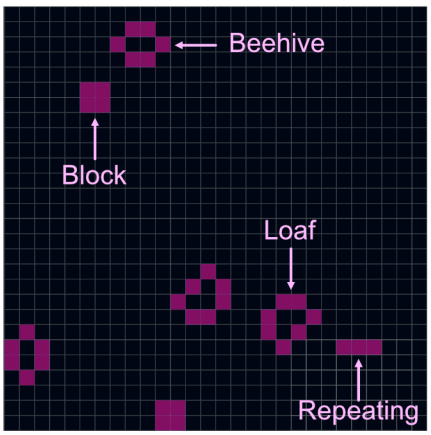

Figure 5.3: **Stable pattern formation in simulation.** A fully evolved Game of Light computer simulation having reached a steady state in which all patterns are either still or repeating.

with a *Volvox* agent, causing the pattern to evolve into a beehive shape. The Game of Light demonstrates a way in which artificial life can be layered with real life to create hybrid systems. This constitutes just one example of how the DOME may be used for the purpose of art and entertainment.

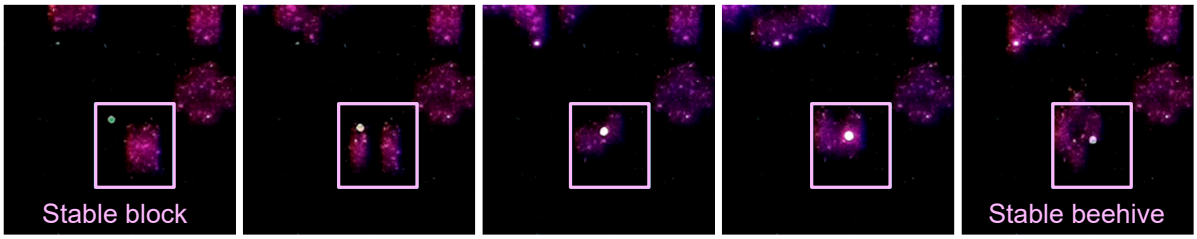

Figure 5.4: **Stable pattern formation in the DOME.** A stable block pattern is perturbed by interaction with a motile *Volvox* agent, eventually morphing into a stable beehive pattern.

The design of the DOME is highly modular, meaning that interchanging and adding new components is straightforward. This leaves room for adaptations that allow for greater interactivity with the DOME, particularly useful in an educational or outreach setting. As an example, Figure 5.6 shows an earlier version of the DOME, which featured a touchscreen interface (Raspberry Pi 7" Display) that allowed the user to manually draw light patterns onto a sample. Although this interface was not used in the work described in this thesis, it would be trivial to reincorporate, simply by plugging directly into the Raspberry Pi found in the imaging module. This type of configuration could be useful in outreach and education settings, as it would allow for direct engagement with the system, enabling the selection of particular illumination areas and even the guiding of light-responsive microagents.

In general, the DOME is also well suited to outreach work due to the low barriers in terms of cost and expertise associated with both the fabrication and operation of the device. 3D printing

technology is increasingly used in educational contexts [127], as are the Raspberry Pi boards on which the DOME operates [26]. While a number of microscopes focused on education and outreach exist at present [72, 81], the closed-loop optical control of the DOME presents teaching opportunities related to image processing and algorithmic control. Additionally, the ability to deliver light to samples could allow for insight into the importance of light for biological organisms, such as those easily sourced from local pond water. As an example of this, Figure 5.5 shows a water mite in the DOME that was collected from a local pond in Bristol. It was observed that when a blue circle was projected as shown, the mite tended to follow the shape of the light circle, demonstrating a basic way in which the DOME could be used to convey information about the ability for microscale organisms to sense and react to light.

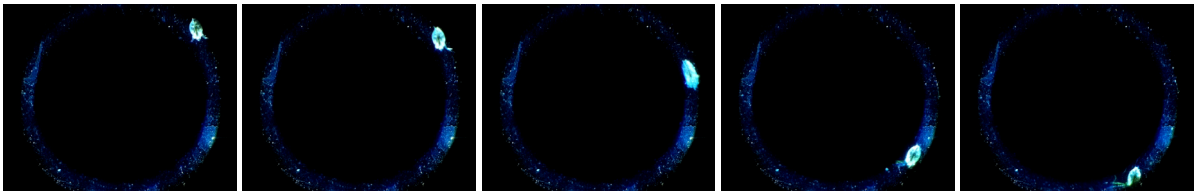

Figure 5.5: **Water mite in the DOME.** A water mite collected from local pond water was found to preferentially swim in the illuminated circle rather than the darker regions.

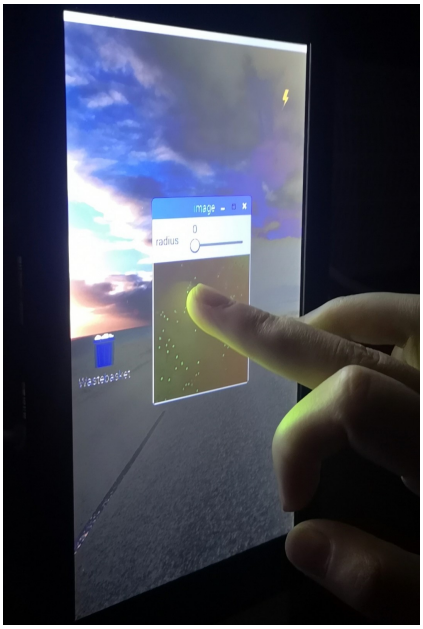

Figure 5.6: **Touchscreen DOME interface.** A touchscreen interface on a previous version of the DOME, here used to manually draw light patterns onto a collection of cells.

5.3 Parallel experimentation

The DOME is capable of delivering multi-wavelength illumination to many agents simultaneously and independently. Taken together with the automated optical control loop, this provides the capacity for the parallelisation of experiments. The use of automation and parallel experimentation techniques is increasingly prevalent in chemistry and the biological sciences [44, 159, 404]. A notable example is high-throughput screening, which takes a chemical or compound library and applies a particular assay method in an automated manner through the combination of robotics and data analysis [166]. This allows for massively parallelised testing to identify chemical or biological components of interest, and has been especially instrumental in the drug discovery process in the past decades [249, 250].

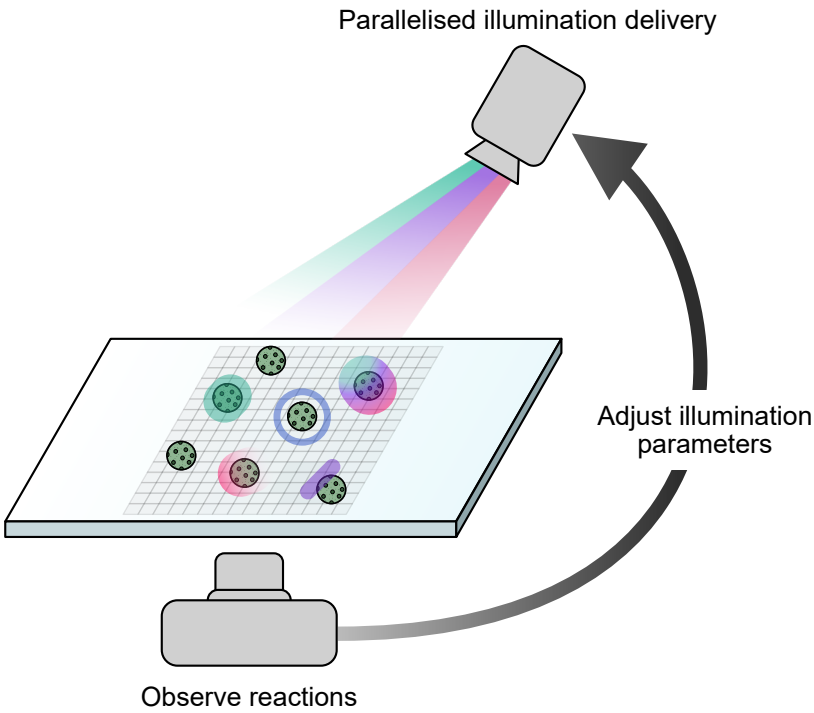

Figure 5.7: **Parallel experimentation.** A schematic of a proposed parallel experimentation scheme in the DOME, in which agents can be subjected to varying optical stimuli simultaneously.

Platforms for parallelised experimentation typically use a liquid handling system to dispense small volumes of liquid into spatially distinct locations to induce some chemically or biologically reactive processes [169, 210]. The DOME provides the opportunity to enact a similar process using optical stimulation as an inducer. One application of this would be to test the light-responsive tendencies of agents within a given microsystem. This could prove particularly informative for biological agents, as light responses in these systems are rarely straightforward and typically manifest as a function of many factors such as wavelength and intensity. Using the DOME, these parameters could be varied across a large population of responsive agents such as bacteria, algae

or mammalian cells, enabling parallel testing under identical conditions as depicted in Figure 5.7.

Machine learning techniques have also proved invaluable for parallelised experimentation, enabling rapid and autonomous discovery processes [159]. The integration of machine learning in the context of the DOME could facilitate the characterisation of more complex light-response schemes, for instance the adaptive phototactic behaviour observed is some species of bacteria [19] and algae [87, 108]. The use of machine learning here would allow for the exploration of illumination parameters, such as wavelength and time scales, that result in the optimum response in line with the adaptive process. The ability to perform this in parallel not only enables a faster exploration process, but also allows for the possibility of some variability across the population.

5.4 De novo swarm behaviour discovery

In Chapter 4, a number of building blocks towards swarm control were demonstrated using the DOME, presenting a first step towards the engineering of microscale collective behaviours. Looking forward, this work could be extended to facilitate the discovery of swarm behaviours and control algorithms in microscale systems.

In many ways, microagents often intrinsically posses many of the characteristics used to define a swarm agent in that they do not rely on a centralised command, typically occur in very high numbers, are largely homogeneous, and are relatively incapable as individuals [342]. The question of local sensing and communication, which is crucial in swarm engineering, is less straightforward however. Many organic microagents posses intrinsic abilities to process their environment and even to communicate amongst themselves, with quorum sensing in bacteria being a prime example [255]. The repurposing of these communication pathways for a specific aim is a key issue addressed by synthetic biology and, although increasingly attainable as the field continues to advance, remains deeply complex. The engineering of sensing and communication capabilities in inorganic or synthetic microagents is also incredibly challenging. In the absence of biological processes to commandeer, thoughtful design and functionalisation is required in order to achievement environmental sensing [301, 363, 432]. Communication between agents is an even harder problem, requiring intricate development of interaction pathways reliant on various chemical and physical phenomena [124, 363, 421].

For all types of microsystem, whether organic or inorganic, this limited capacity for interaction with the local environment and other agents presents a significant barrier to microswarm engineering. Although the implementation of new behaviours is possible through careful agent design and functionlisation, this process can be incredibly intensive in terms of time and resources, relying on an extended optimization process to perfect the chemical or genetic process. To reduce this burden, the DOME could be used to facilitate augmented local sensing and interactions between agents for the the discovery of de novo swarm behaviours, allowing the exploration of

parameters such as communication radius or decay time of stigmergy trails.

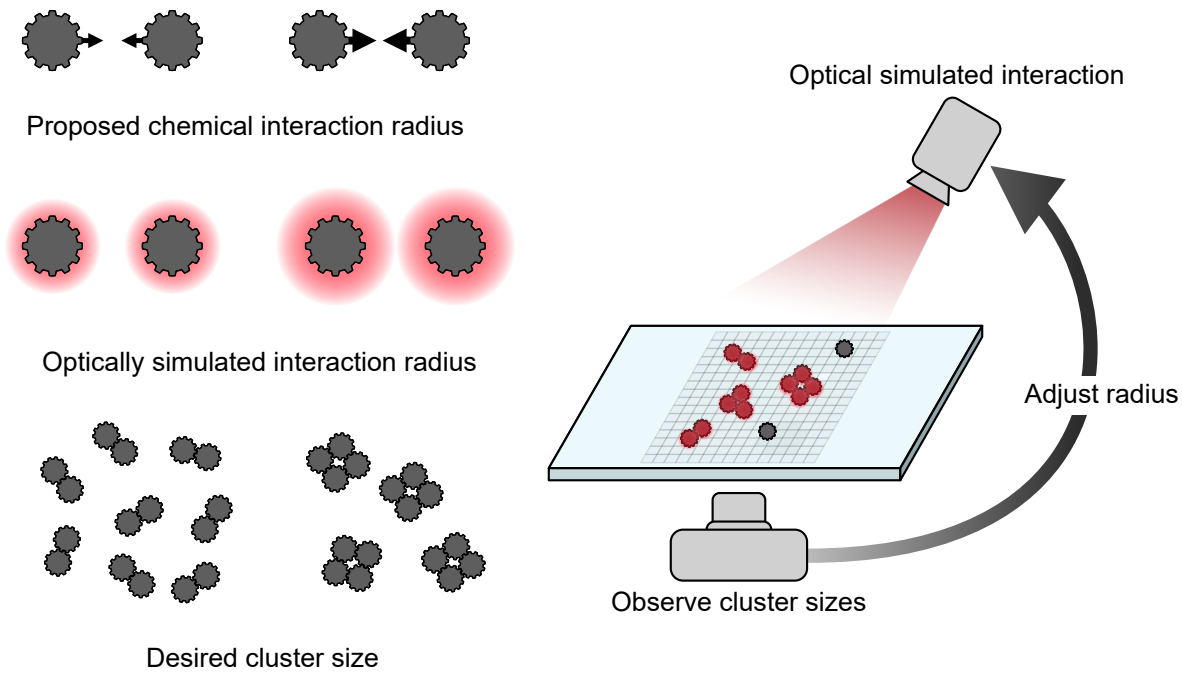

Figure 5.8: **De novo swarm behaviour discovery.** Schematic of a proposed scheme for the discovery of swarm behaviour using the DOME platform. Here, parameters for the interaction radius required to achieve various clustering dynamics are explored by using the DOME to provide agents with augmented light-based interaction capabilities.

To increase the efficiency of this process, machine learning techniques such as reinforcement learning could also be employed to perform parameter optimisation towards a desired swarm behaviour. Implementations of reinforcement learning in macroscale robotics systems have been used to achieve swarm behaviours such as schooling [141, 387] and collective phototaxis [304]. In recent years, there has been significant interest in the application of these same learning processes to small-scale systems, particularly to aid in navigation and steering for active microagents [67, 71, 350]. Especially relevant in the context of the DOME is the work of Muiños-Landin et al., in which optically responsive self-thermophoretic microparticles were controlled using a closed loop laser beam and microscopy set up. Using this system, a reinforcement learning algorithm was implemented with the goal of navigating a grid-like real world environment. This was demonstrated for a single agent as well as for two cooperatively interacting agents.

The closed-loop, localised optical control scheme offered by the DOME makes it an especially suitable platform for the discovery and implementation of rules for swarm behaviour in microsystems. This would be powerful in applications such as environmental remediation and functional materials development, in which direct control over light-responsive agents can be realised. More generally however, this would also provide a testbed to explore properties and parameters that

lead to the emergence of swarm behaviours in a generic microsystem, informing the design of new swarm microagents. An example of this pipeline is proposed in Figure 5.8 with the design of a swarming micromotor. In this scheme the desired behavioural output is clustering, here mediated by chemical interactions between agents that decay with a given radius. Using the DOME, an established light-responsive micromotor [303, 417] could be used to test the effect on cluster dynamic of varying the interaction radius by optically simulating this interaction radius. A similar process could also be used to explore alternative behaviours such as pattern formation. This could be performed either using the type of learning algorithms discussed above, or with more traditional optimisation algorithms, essentially acting as a real world simulator.

5.5 Control of cellular collectives

Examples of collective cellular systems can be found throughout nature with biofilms, tumours and epithelial tissue being just a few examples. As was discussed in Section 2.3.1, there are various mechanisms by which optical stimulation can be used to interact with these microsystems to influence their collective dynamics. The capacity of the DOME to provide optical control at both an individual and collective level positions it as a potential tool with with to address these cellular systems. As the device can be operated remotely through accessing the local network, it would be feasible to operate the DOME from inside an off-the-shelf incubator of sufficient size, or to integrate custom hardware for temperature control in an insulated enclosure. This set up would facilitate the live imaging of cells that demonstrate a temperature sensitivity while performing localised optical targeting.

A specific example of a potential application for the DOME in working with cellular collectives is depicted in Figure 5.10, with the localised targeting of epithelial tissue undergoing a wound healing process. During wound healing, epithelial cells undergo a collective migration in which cells move as an interconnected group, often demonstrating leader-follower dynamics [335]. It has been found that optical stimulation can, through various innate biological mechanisms, be applied to a wound to accelerate the healing process [1, 57]. Given this, the DOME could be a suitable platform with which to explore the effect of spatially localised optical illumination of the dynamics of would healing, with possible applications in wearable healthcare technology. In addition to activation of these innate mechanisms, optogenetic processes could also be used to probe the dynamics of collectively migrating cell tissue to understand how local changes can affect the whole system. The protein RhoA for example has been used to influence the emergence of leader cells in would healing [229], something that could be extended optogenetically, as demonstrated by the use of a photoactivatable form of the protein in the study of embryogenesis [185].

Similar applications include the light-based engineering of biofilms [146, 193, 271] and optogenetic targeting of developing embryonic tissue [175, 185], both collectively interacting

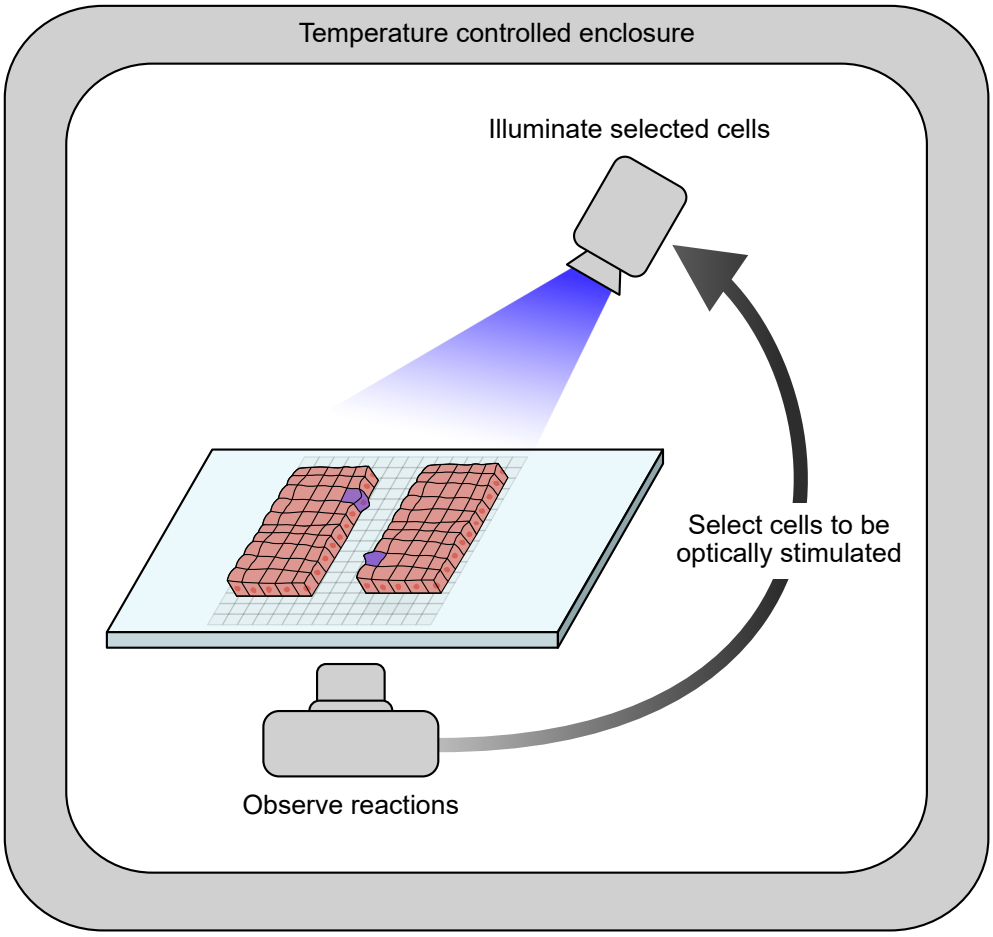

Figure 5.9: **Control of cellular collectives.** Schematic of a proposed scheme for the control of cellular collectives using the DOME, in which a temperature controlled environment and localised optical targeting is used to interact with epithelial tissue undergoing collective migration during the wound healing process.

cellular systems in which spatiotemporal dynamics play a crucial role.

5.6 Discussion

A number of current and potential applications of the DOME have been explored in this chapter.

5.7 Conclusion

The applications presented here are by no means a comprehensive list, rather they serve to highlight some interesting potential work that has been considered thus far, some of which is currently being explored as part of wider collaborations. Not mentioned here are possibilities such as the shaping of bacterial populations [131], localised polymer actuation [302] and the

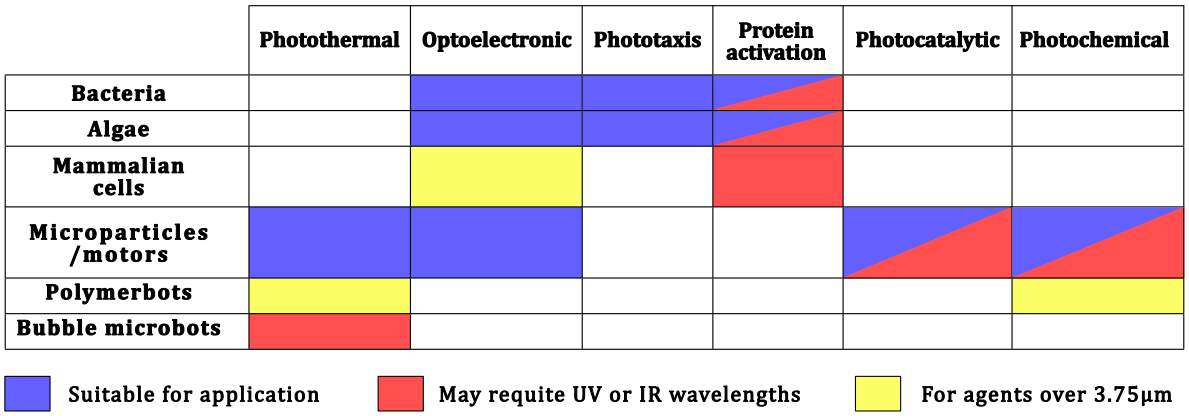

Figure 5.10: **Control of cellular collectives.** Schematic of a proposed scheme for the control of cellular collectives using the DOME, in which a temperature controlled environment and localised optical targeting is used to interact with epithelial tissue undergoing collective migration during the wound healing process.

implementation of closed-loop optoelectronic systems [413]. The modular design of the DOME allows for a wide scope in terms of potential future uses, as the device can be adapted with relative ease. This modularity could be extended even further in the future by the design of an interchangeable projector light engine, which at present is limited to 3 off-the-shelf LED wavelengths. Furthermore, the incorporation of more automated elements such as directional stage adjustment would open up additional avenues in long term agent tracking and live cell imaging. Even in the absence of any of these changes however, the current capabilities of the DOME allow for its use in the applications discussed here, and more.

CHAPTER 6

CONCLUSION

The power to control microagent behaviour is pivotal in applications such as drug delivery [239, 306, 365], environmental remediation [212, 271], development of biomedical therapies [89, 278, 356] and the design of new functional materials [15, 184]. A light-based control scheme is advantageous as it offers the potential for dynamic, high resolution control that may be applied to many agents independently and in parallel. At the microscale, light has the power to affect many biological, chemical and physical processes, including the generation of local heating and currents, alterations to molecular structure and phototactic behaviour in some microorganisms. Owing to this versatility, there are a vast number of ways in which optical control is implemented across a range of disciplines. Devices that make use of light-based control have been explored in the past, often very effectively, but typically lack reproducibility, have prohibitively high construction costs expensive or assume access to significant resources and expertise. Furthermore, none provide a fully integrated device not reliant on external optical, structural or computational components.

With this in mind, the construction of the DOME was motivated by the desire to provide a platform for closed-loop, spatiotemporal control over microagent systems, with the goal of widening accessibility to these kinds of optical control techniques. As was laid out in Chapter 3, the DOME integrates DLP technology with a custom microscopy set-up to achieve a closed-loop control optical scheme. In its current configuration, the DOME is able to deliver patterned illumination with 30×30 μm resolution at peak wavelengths of 445, 517 and 632 nm. Even at the highest possible imaging resolutions, the control loop is closed in well under a second, and for the standard 1920×1088 pixel imaging resolution used in this work the control loop latency was found to be 0.25 s. The use of inexpensive electronics and computational components, together with the use of 3D printing to fabricate the chassis and structural components, allows the device to be built

for just £685. This makes the DOME significantly cheaper than other proposed platforms, which often make use of expensive off-the-shelf microscopes or other high-end equipment such as optical breadboards. The DOME is also the only platform that can be described as an integrated device, rather than simply a hardware set-up, as once assembled it forms an entirely self-contained apparatus that does not require connection to an external computer. The open-sourcing of the DOME design and code, together with the use of highly accessible Raspberry Pi computers, makes the device straightforward to replicate and operate. Additionally, its modular design means it can be adapted with ease to suit a given application, for instance by altering magnification by interchanging lenses, using higher specification computers and cameras, or adding capabilities such as temperature control and automatic focusing. Taken together, the modular and open-source nature of the DOME leaves room for the device to be further developed by a future user base, such that it may continue to evolve multidirectionally to suit specific applications.

The ability of the DOME to interact with microagents in a localised and dynamic way was demonstrated through its application in building towards swarm control at the microscale. Given the large numbers in which microscale agents such as bacteria, mamallian cells and micro or nanoparticles typically work, there is interest in the engineering of collective microsystems for purposes including swarming nanomedicine [160, 161] and control of collective cellular processes [74, 89, 229]. The engineering of swarm behaviours, such as coordinated motion or trail formation, is a greater challenge at these small scales than in traditional macroscale engineering owing to the limited interaction capabilities of most microagents and lack of programmability. One way to tackle this challenge is to use external control or augmentation to enhance microagent capabilities to achieve swarm outcomes. Using the DOME, three building blocks towards swarm control were implemented through the light-based augmentation of *Volvox* colonies, employed here as a model microagent. Specifically, *Volvox* agents were enhanced with the abilities to signal to one another through light-based message propagation, and to perform stigmergy through the environmental deposition of light trails. Additionally, pulsed light was used to exert motion control over *Volvox* agents by causing them to slow and in some cases stop, owing to their natural light-responsive properties. These three building blocks of signalling, stigmergy and motion control are fundamental to swarm systems, underpinning many of the collective behaviours engineered across scales. The ability to enact swarm control building blocks using the augmentation provided by the DOME could allow for the engineering of microswarms in a manner more analogous to traditional macroscale methods that rely on programmability. This kind of control scheme also paves the way for the discovery of rules and system parameters that lead to the emergence of new collective behaviours. In particular, the potential for integration of machine learning techniques such reinforcement learning would allow exploration of the conditions required to achieve desired swarm outcomes.

More generally, the DOME is significant in the context of widening the accessibility of optical control techniques. While implementations of closed-loop optical control schemes are fairly

commonplace in some fields such as optogenetics [53, 224, 340, 369], in others they are rarely seen despite the use of light-responsive microagents. The development of a low-cost, open-source platform that is accessible to users without extensive optical or computation expertise helps to address this, by removing the need for high-end equipment or custom set-ups built from scratch. Potential applications of the DOME for collective control of microagents which have begun to be explored include; the discovery and implementation of microscale swarm algorithms in light-responsive systems such as algae and micromotors, the engineering of collective processes in bacterial and mammalian cells, and use in art, outreach and educational settings. The ability to influence collective dynamics in mammalian cells has particular significance in biomedical contexts, since many medically relevant processes, including wound healing and tumour growth, operate through collective means. The ability to probe these systems at the individual cell level could thus provide a much greater understanding of these processes, and aid in the development of more efficient treatment strategies. Overall it is hoped that the open-source DOME, together with the demonstration of programmability of microagent capabilities through light-based augmentation, as well as an outline of how such control could be used across applications from medicine to entertainment, presents first steps towards the democratisation of light-control of collectives at the microscale.

BIBLIOGRAPHY

[1] N. ADAMSKAYA, P. DUNGEL, R. MITTERMAYR, J. HARTINGER, G. FEICHTINGER, K. WASSERMANN, H. REDL, AND M. VAN GRIENSVEN, *Light therapy by blue led improves wound healing in an excision model in rats*, Injury, 42 (2011), pp. 917–921.

[2] N. AGRAWAL AND S. SINGHAL, *Smart drip irrigation system using raspberry pi and arduino*, in International Conference on Computing, Communication & Automation, IEEE, 2015, pp. 928–932.

[3] S. AHDEROM, M. RAISI, K. LO, K. E. ALAMEH, AND R. MAVADDAT, *Applications of liquid crystal spatial light modulators in optical communications*, in 5th IEEE International Conference on High Speed Networks and Multimedia Communication (Cat. No. 02EX612), IEEE, 2002, pp. 239–242.

[4] Y. ALAPAN, O. YASA, B. YIGIT, I. C. YASA, P. ERKOC, AND M. SITTI, *Microrobotics and microorganisms: Biohybrid autonomous cellular robots*, Annual Review of Control, Robotics, and Autonomous Systems, 2 (2019), pp. 205–230.

[5] L. ALBERT AND O. VÁZQUEZ, *Photoswitchable peptides for spatiotemporal control of biological functions*, Chemical Communications, 55 (2019), pp. 10192–10213.

[6] C. ALEXIOU, D. DIEHL, P. HENNINGER, H. IRO, R. ROCKELEIN, W. SCHMIDT, AND H. WEBER, *A high field gradient magnet for magnetic drug targeting*, IEEE Transactions on applied superconductivity, 16 (2006), pp. 1527–1530.

[7] M. ALHAFNAWI, S. HAUERT, AND P. O'DOWD, *Robotic canvas: Interactive painting onto robot swarms*, in Artificial Life Conference Proceedings, MIT Press, 2020, pp. 163–170.

[8] A. S. ALI, Z. ZANZINGER, D. DEBOSE, AND B. STEPHENS, *Open source building science sensors (osbss): A low-cost arduino-based platform for long-term indoor environmental data collection*, Building and Environment, 100 (2016), pp. 114–126.

[9] J.-M. AMÉ, J. HALLOY, C. RIVAULT, C. DETRAIN, AND J. L. DENEUBOURG, *Collegial decision making based on social amplification leads to optimal group formation*, Proceedings of the National Academy of Sciences, 103 (2006), pp. 5835–5840.

[10] S. V. ANGUS, S. CHO, D. K. HARSHMAN, J.-Y. SONG, AND J.-Y. YOON, *A portable, shock-proof, surface-heated droplet pcr system for escherichia coli detection*, Biosensors and Bioelectronics, 74 (2015), pp. 360–368.

[11] A. ANOOP AND P. KANAKASABAPATHY, *Review on swarm robotics platforms*, in 2017 International Conference on Technological Advancements in Power and Energy (TAP Energy), IEEE, 2017, pp. 1–6.

[12] K. AOKI, Y. KONDO, H. NAOKI, T. HIRATSUKA, R. E. ITOH, AND M. MATSUDA, *Propagating wave of erk activation orients collective cell migration*, Developmental cell, 43 (2017), pp. 305–317.

[13] R. W. APPLEGATE, D. W. MARR, J. SQUIER, AND S. W. GRAVES, *Particle size limits when using optical trapping and deflection of particles for sorting using diode laser bars*, Optics express, 17 (2009), pp. 16731–16738.

[14] F. ARAI, K. ONDA, R. IITSUKA, AND H. MARUYAMA, *Multi-beam laser micromanipulation of microtool by integrated optical tweezers*, in 2009 IEEE International Conference on Robotics and Automation, IEEE, 2009, pp. 1832–1837.

[15] K. ARIGA, J. P. HILL, M. V. LEE, A. VINU, R. CHARVET, AND S. ACHARYA, *Challenges and breakthroughs in recent research on self-assembly*, Science and technology of advanced materials, (2008).

[16] J. ARLT, V. A. MARTINEZ, A. DAWSON, T. PILIZOTA, AND W. C. POON, *Painting with light-powered bacteria*, Nature communications, 9 (2018), pp. 1–7.

[17] J. P. ARMITAGE AND K. J. HELLINGWERF, *Light-induced behavioral responses ('phototaxis') in prokaryotes*, Discoveries in Photosynthesis, (2005), pp. 985–995.

[18] R. D. ARNOLD, H. YAMAGUCHI, AND T. TANAKA, *Search and rescue with autonomous flying robots through behavior-based cooperative intelligence*, Journal of International Humanitarian Action, 3 (2018), pp. 1–18.

[19] J. ARRIETA, A. BARREIRA, M. CHIOCCIOLI, M. POLIN, AND I. TUVAL, *Phototaxis beyond turning: persistent accumulation and response acclimation of the microalga chlamydomonas reinhardtii*, Scientific reports, 7 (2017), pp. 1–7.

[20] F. ARVIN, J. C. MURRAY, L. SHI, C. ZHANG, AND S. YUE, *Development of an autonomous micro robot for swarm robotics*, in 2014 IEEE International Conference on Mechatronics and Automation, IEEE, 2014, pp. 635–640.

[21] A. ASHKIN, *Acceleration and trapping of particles by radiation pressure*, Physical review letters, 24 (1970), p. 156.

[22] A. ASHKIN, J. M. DZIEDZIC, J. E. BJORKHOLM, AND S. CHU, *Observation of a single-beam gradient force optical trap for dielectric particles*, Optics letters, 11 (1986), pp. 288–290.

[23] A. ATHANASSIOU, M. KALYVA, K. LAKIOTAKI, S. GEORGIOU, AND C. FOTAKIS, *All-optical reversible actuation of photochromic-polymer microsystems*, Advanced Materials, 17 (2005), pp. 988–992.

[24] O. AVINC AND A. KHODDAMI, *Overview of poly (lactic acid)(pla) fibre*, Fibre Chemistry, 41 (2009), pp. 391–401.

[25] T. BADEN, A. M. CHAGAS, G. GAGE, T. MARZULLO, L. L. PRIETO-GODINO, AND T. EULER, *Open labware: 3-d printing your own lab equipment*, PLoS biology, 13 (2015), p. e1002086.

[26] B. BALON AND M. SIMIĆ, *Using raspberry pi computers in education*, in 2019 42nd International Convention on Information and Communication Technology, Electronics and Microelectronics (MIPRO), IEEE, 2019, pp. 671–676.

[27] E. BARKALLAH, J. FREULARD, M. J.-D. OTIS, S. NGOMO, J. C. AYENA, AND C. DESROSIERS, *Wearable devices for classification of inadequate posture at work using neural networks*, Sensors, 17 (2017), p. 2003.

[28] T. BÄUERLE, A. FISCHER, T. SPECK, AND C. BECHINGER, *Self-organization of active particles by quorum sensing rules*, Nature communications, 9 (2018), pp. 1–8.

[29] L. BAYINDIR, *A review of swarm robotics tasks*, Neurocomputing, 172 (2016), pp. 292–321.

[30] C. BECHINGER, *Active suspensions with programmable interactions*, Journal of Physics: Condensed Matter, 32 (2020).

[31] M. BEEKMAN AND T. LATTY, *Brainless but multi-headed: decision making by the acellular slime mould physarum polycephalum*, Journal of molecular biology, 427 (2015), pp. 3734–3743.

[32] B. BEHKAM AND M. SITTI, *Bacterial flagella-based propulsion and on/off motion control of microscale objects*, Applied Physics Letters, 90 (2007), p. 023902.

[33] P. BENHAL, J. G. CHASE, P. GAYNOR, B. OBACK, AND W. WANG, *Ac electric field induced dipole-based on-chip 3d cell rotation*, Lab on a Chip, 14 (2014), pp. 2717–2727.

[34] R. R. BENNETT AND R. GOLESTANIAN, *A steering mechanism for phototaxis in chlamydomonas*, Journal of the Royal Society Interface, 12 (2015), p. 20141164.

[35] F. BERLINGER, M. GAUCI, AND R. NAGPAL, *Implicit coordination for 3d underwater collective behaviors in a fish-inspired robot swarm*, Science Robotics, 6 (2021).

[36] S. BERMAN, A. HALÁSZ, M. A. HSIEH, AND V. KUMAR, *Optimized stochastic policies for task allocation in swarms of robots*, IEEE transactions on robotics, 25 (2009), pp. 927–937.

[37] A. BICCHI AND V. KUMAR, *Robotic grasping and contact: A review*, in Proceedings 2000 ICRA. Millennium Conference. IEEE International Conference on Robotics and Automation. Symposia Proceedings (Cat. No. 00CH37065), vol. 1, IEEE, 2000, pp. 348–353.

[38] O. BIMBER AND R. RASKAR, *Modern approaches to augmented reality*, in ACM SIGGRAPH 2006 Courses, 2006, pp. 1–es.

[39] A. BLÁZQUEZ-CASTRO, *Optical tweezers: phototoxicity and thermal stress in cells and biomolecules*, Micromachines, 10 (2019), p. 507.

[40] E. BONABEAU, D. D. R. D. F. MARCO, M. DORIGO, G. THÉRAULAZ, G. THERAULAZ, ET AL., *Swarm intelligence: from natural to artificial systems*, no. 1, Oxford university press, 1999.

[41] E. BONABEAU, G. THERAULAZ, J.-L. DENEUBOURG, S. ARON, AND S. CAMAZINE, *Self-organization in social insects*, Trends in ecology & evolution, 12 (1997), pp. 188–193.

[42] J. BOOTE AND S. EVANS, *Dielectrophoretic manipulation and electrical characterization of gold nanowires*, Nanotechnology, 16 (2005), p. 1500.

[43] M. BRAMBILLA, E. FERRANTE, M. BIRATTARI, AND M. DORIGO, *Swarm robotics: a review from the swarm engineering perspective*, Swarm Intelligence, 7 (2013), pp. 1–41.

[44] C. BRÄNDLI, P. MAIWALD, AND J. SCHRÖER, *Automated equipment for high-throughput experimentation*, CHIMIA International Journal for Chemistry, 57 (2003), pp. 284–289.

[45] O. BRZOBOHATÝ, M. ŠILER, J. TROJEK, L. CHVÁTAL, V. KARÁSEK, AND P. ZEMÁNEK, *Non-spherical gold nanoparticles trapped in optical tweezers: shape matters*, Optics express, 23 (2015), pp. 8179–8189.

[46] L. J. BUGAJ, G. P. O'DONOGHUE, AND W. A. LIM, *Interrogating cellular perception and decision making with optogenetic tools*, Journal of Cell Biology, 216 (2017), pp. 25–28.

[47] A. BÚZÁS, L. KELEMEN, A. MATHESZ, L. OROSZI, G. VIZSNYICZAI, T. VICSEK, AND P. ORMOS, *Light sailboats: Laser driven autonomous microrobots*, Applied Physics Letters, 101 (2012), p. 041111.

[48] S. CAMAZINE, *Self-organizing pattern formation on the combs of honey bee colonies*, Behavioral ecology and sociobiology, 28 (1991), pp. 61–76.

[49] S. CAMAZINE, J.-L. DENEUBOURG, N. R. FRANKS, J. SNEYD, E. BONABEAU, AND G. THERAULA, *Self-organization in biological systems*, Princeton university press, 2003.

[50] S. CAMAZINE, J.-L. DENEUBOURG, N. R. FRANKS, J. SNEYD, G. THERAULA, AND E. BONABEAU, *Self-organization in biological systems*, Princeton university press, 2020.

[51] M. CAPITANIO, R. CICCHI, AND F. S. PAVONE, *Continuous and time-shared multiple optical tweezers for the study of single motor proteins*, Optics and Lasers in Engineering, 45 (2007), pp. 450–457.

[52] A. M. CHAGAS, *Haves and have nots must find a better way: The case for open scientific hardware*, PLoS biology, 16 (2018), p. e3000014.

[53] R. CHAIT, J. RUESS, T. BERGMILLER, G. TKAČIK, AND C. C. GUET, *Shaping bacterial population behavior through computer-interfaced control of individual cells*, Nature communications, 8 (2017), pp. 1–11.

[54] S. CHATANI, C. J. KLOXIN, AND C. N. BOWMAN, *The power of light in polymer science: photochemical processes to manipulate polymer formation, structure, and properties*, Polymer Chemistry, 5 (2014), pp. 2187–2201.

[55] L.-H. CHAU, W. LIANG, F. W. K. CHEUNG, W. K. LIU, W. J. LI, S.-C. CHEN, AND G.-B. LEE, *Self-rotation of cells in an irrotational ac e-field in an opto-electrokinetics chip*, PloS one, 8 (2013), p. e51577.

[56] R. M. W. CHAU, D. BHAYA, AND K. C. HUANG, *Emergent phototactic responses of cyanobacteria under complex light regimes*, MBio, 8 (2017).

[57] M. E. D. A. CHAVES, A. R. D. ARAÚJO, A. C. C. PIANCASTELLI, AND M. PINOTTI, *Effects of low-power light therapy on wound healing: Laser x led*, Anais brasileiros de dermatologia, 89 (2014), pp. 616–623.

[58] F. CHEN, J. RICKEN, D. XU, AND S. V. WEGNER, *Bacterial photolithography: patterning escherichia coli biofilms with high spatial control using photocleavable adhesion molecules*, Advanced Biosystems, 3 (2019), p. 1800269.

[59] F. CHEN AND S. V. WEGNER, *Blue light switchable bacterial adhesion as a key step toward the design of biofilms*, ACS synthetic biology, 6 (2017), pp. 2170–2174.

[60] Y. CHEN, Z. WANG, Y. HE, Y. J. YOON, J. JUNG, G. ZHANG, AND Z. LIN, *Light-enabled reversible self-assembly and tunable optical properties of stable hairy nanoparticles*, Proceedings of the National Academy of Sciences, 115 (2018), pp. E1391–E1400.

[61] P. Y. CHIOU, A. T. OHTA, AND M. C. WU, *Massively parallel manipulation of single cells and microparticles using optical images*, Nature, 436 (2005), pp. 370–372.

[62] T.-K. CHIU, A.-C. CHAO, W.-P. CHOU, C.-J. LIAO, H.-M. WANG, J.-H. CHANG, P.-H. CHEN, AND M.-H. WU, *Optically-induced-dielectrophoresis (odep)-based cell manipulation in a microfluidic system for high-purity isolation of integral circulating tumor cell (ctc) clusters based on their size characteristics*, Sensors and Actuators B: Chemical, 258 (2018), pp. 1161–1173.

[63] H. CHOI, M. GEEVES, B. ALSALAM, AND F. GONZALEZ, *Open source computer-vision based guidance system for uavs on-board decision making*, in 2016 IEEE Aerospace Conference, IEEE, 2016, pp. 1–5.

[64] W. CHOI, S.-H. KIM, J. JANG, AND J.-K. PARK, *Lab-on-a-display: a new microparticle manipulation platform using a liquid crystal display (lcd)*, Microfluidics and Nanofluidics, 3 (2007), pp. 217–225.

[65] P.-Y. CHU, C.-H. HSIEH, C.-R. LIN, AND M.-H. WU, *The effect of optically induced dielectrophoresis (odep)-based cell manipulation in a microfluidic system on the properties of biological cells*, Biosensors, 10 (2020), p. 65.

[66] C. M. CIANCI, X. RAEMY, J. PUGH, AND A. MARTINOLI, *Communication in a swarm of miniature robots: The e-puck as an educational tool for swarm robotics*, in International Workshop on Swarm Robotics, Springer, 2006, pp. 103–115.

[67] F. CICHOS, K. GUSTAVSSON, B. MEHLIG, AND G. VOLPE, *Machine learning for active matter*, Nature Machine Intelligence, 2 (2020), pp. 94–103.

[68] T. ČIŽMÁR, L. D. ROMERO, K. DHOLAKIA, AND D. ANDREWS, *Multiple optical trapping and binding: new routes to self-assembly*, Journal of Physics B: Atomic, Molecular and Optical Physics, 43 (2010), p. 102001.

[69] T. ČIŽMÁR, M. ŠILER, M. ŠERÝ, P. ZEMÁNEK, V. GARCÉS-CHÁVEZ, AND K. DHOLAKIA, *Optical sorting and detection of submicrometer objects in a motional standing wave*, Physical Review B, 74 (2006), p. 035105.

[70] M. COAKLEY AND D. E. HURT, *3d printing in the laboratory: Maximize time and funds with customized and open-source labware*, Journal of laboratory automation, 21 (2016), pp. 489–495.

[71] S. COLABRESE, K. GUSTAVSSON, A. CELANI, AND L. BIFERALE, *Flow navigation by smart microswimmers via reinforcement learning*, Physical review letters, 118 (2017), p. 158004.

[72] J. T. COLLINS, J. KNAPPER, J. STIRLING, J. MDUDA, C. MKINDI, V. MAYAGAYA, G. A. MWAKAJINGA, P. T. NYAKYI, V. L. SANGA, D. CARBERY, ET AL., *Robotic microscopy for everyone: the openflexure microscope*, Biomedical Optics Express, 11 (2020), pp. 2447–2460.

[73] I. M. CÓRDOVA-ALCÁNTARA, D. L. VENEGAS-CORTÉS, M. Á. MARTÍNEZ-RIVERA, N. O. PÉREZ, AND A. V. RODRIGUEZ-TOVAR, *Biofilm characterization of fusarium solani keratitis isolate: increased resistance to antifungals and uv light*, Journal of Microbiology, 57 (2019), pp. 485–497.

[74] D. M. CORNFORTH AND K. R. FOSTER, *Competition sensing: the social side of bacterial stress responses*, Nature Reviews Microbiology, 11 (2013), pp. 285–293.

[75] N. CORRELL AND A. MARTINOLI, *Modeling and designing self-organized aggregation in a swarm of miniature robots*, The International Journal of Robotics Research, 30 (2011), pp. 615–626.

[76] J. W. COSTERTON, *Introduction to biofilm*, International journal of antimicrobial agents, 11 (1999), pp. 217–221.

[77] J. W. COSTERTON, Z. LEWANDOWSKI, D. E. CALDWELL, D. R. KORBER, AND H. M. LAPPIN-SCOTT, *Microbial biofilms*, Annual review of microbiology, 49 (1995), pp. 711–745.

[78] C. R. COURTNEY, C.-K. ONG, B. DRINKWATER, A. BERNASSAU, P. WILCOX, AND D. CUMMING, *Manipulation of particles in two dimensions using phase controllable ultrasonic standing waves*, Proceedings of the Royal Society A: Mathematical, Physical and Engineering Sciences, 468 (2012), pp. 337–360.

[79] M. CROSSCOMBE, J. LAWRY, S. HAUERT, AND M. HOMER, *Robust distributed decision-making in robot swarms: Exploiting a third truth state*, in 2017 IEEE/RSJ International Conference on Intelligent Robots and Systems (IROS), IEEE, 2017, pp. 4326–4332.

[80] J. E. CURTIS, B. A. KOSS, AND D. G. GRIER, *Dynamic holographic optical tweezers*, Optics communications, 207 (2002), pp. 169–175.

[81] J. S. CYBULSKI, J. CLEMENTS, AND M. PRAKASH, *Foldscope: origami-based paper microscope*, PloS one, 9 (2014), p. e98781.

[82] B. DAI, J. WANG, Z. XIONG, X. ZHAN, W. DAI, C.-C. LI, S.-P. FENG, AND J. TANG, *Programmable artificial phototactic microswimmer*, Nature nanotechnology, 11 (2016), pp. 1087–1092.

[83] R. T. DAME, M. C. NOOM, AND G. J. WUITE, *Bacterial chromatin organization by h-ns protein unravelled using dual dna manipulation*, Nature, 444 (2006), pp. 387–390.

[84] F. DANIEL K AND G. PETER J, *Open-source hardware is a low-cost alternative for scientific instrumentation and research*, Modern instrumentation, 2012 (2012).

[85] R. DANIELS, J. VANDERLEYDEN, AND J. MICHIELS, *Quorum sensing and swarming migration in bacteria*, FEMS microbiology reviews, 28 (2004), pp. 261–289.

[86] D. DATTLER, G. FUKS, J. HEISER, E. MOULIN, A. PERROT, X. YAO, AND N. GIUSEPPONE, *Design of collective motions from synthetic molecular switches, rotors, and motors*, Chemical reviews, 120 (2019), pp. 310–433.

[87] H. DE MALEPRADE, F. MOISY, T. ISHIKAWA, AND R. E. GOLDSTEIN, *Motility and phototaxis of gonium, the simplest differentiated colonial alga*, Physical Review E, 101 (2020), p. 022416.

[88] M. A. M. DE OCA, E. FERRANTE, A. SCHEIDLER, C. PINCIROLI, M. BIRATTARI, AND M. DORIGO, *Majority-rule opinion dynamics with differential latency: a mechanism for self-organized collective decision-making*, Swarm Intelligence, 5 (2011), pp. 305–327.

[89] T. S. DEISBOECK AND I. D. COUZIN, *Collective behavior in cancer cell populations*, BioEssays, 31 (2009), pp. 190–197.

[90] J.-L. DENEUBOURG, S. ARON, S. GOSS, AND J. M. PASTEELS, *The self-organizing exploratory pattern of the argentine ant*, Journal of insect behavior, 3 (1990), pp. 159–168.

[91] Z. DENG, F. MOU, S. TANG, L. XU, M. LUO, AND J. GUAN, *Swarming and collective migration of micromotors under near infrared light*, Applied Materials Today, 13 (2018), pp. 45–53.

[92] A. M. R. DENNISS, T. E. GOROCHOWSKI, AND S. HAUERT, *Augmented reality for the engineering of collective behaviours in microsystems*, in 2019 International Conference on Manipulation, Automation and Robotics at Small Scales (MARSS), IEEE, 2019, pp. 1–6.

[93] A. R. DENNISS, T. E. GOROCHOWSKI, AND S. HAUERT, *An open platform for high-resolution light-based control of microscopic collectives*, bioRxiv, (2020).

[94] C. DETRAIN AND J.-L. DENEUBOURG, *Scavenging by pheidole pallidulaa key for understanding decision-making systems in ants*, Animal behaviour, 53 (1997), pp. 537–547.

[95] C. DEVIGNE AND C. DETRAIN, *Collective exploration and area marking in the ant lasius niger*, Insectes sociaux, 49 (2002), pp. 357–362.

[96] K. DHOLAKIA AND T. ČIŽMÁR, *Shaping the future of manipulation*, Nature photonics, 5 (2011), pp. 335–342.

[97] R. DI LEONARDO, *Controlled collective motions*, Nature materials, 15 (2016), pp. 1057–1058.

[98] R. DI LEONARDO, L. ANGELANI, D. DELL'ARCIPRETE, G. RUOCCO, V. IEBBA, S. SCHIPPA, M. P. CONTE, F. MECARINI, F. DE ANGELIS, AND E. DI FABRIZIO, *Bacterial ratchet motors*, Proceedings of the National Academy of Sciences, 107 (2010), pp. 9541–9545.

[99] B. DIEDERICH, R. LACHMANN, S. CARLSTEDT, B. MARSIKOVA, H. WANG, X. UWURUKUNDO, A. S. MOSIG, AND R. HEINTZMANN, *A versatile and customizable low-cost 3d-printed open standard for microscopic imaging*, Nature communications, 11 (2020), pp. 1–9.

[100] J.-C. DIEHL, M. STROOBER, P. MAJUMDAR, AND A. MINK, *Do-it-yourself (diy) workspaces run by local entrepreneurs that transform plastic waste into valuable water and sanitation products*, in 2018 IEEE Global Humanitarian Technology Conference (GHTC), IEEE, 2018, pp. 1–8.

[101] B. DIEHN, *Phototaxis and sensory transduction in euglena*, Science, 181 (1973), pp. 1009–1015.

[102] E. DILLER, J. GILTINAN, AND M. SITTI, *Independent control of multiple magnetic microrobots in three dimensions*, The International Journal of Robotics Research, 32 (2013), pp. 614–631.

[103] X. DING, S.-C. S. LIN, B. KIRALY, H. YUE, S. LI, I.-K. CHIANG, J. SHI, S. J. BENKOVIC, AND T. J. HUANG, *On-chip manipulation of single microparticles, cells, and organisms using surface acoustic waves*, Proceedings of the National Academy of Sciences, 109 (2012), pp. 11105–11109.

[104] B. R. DONALD, J. JENNINGS, AND D. RUS, *Information invariants for distributed manipulation*, The International Journal of Robotics Research, 16 (1997), pp. 673–702.

[105] R. DONG, Y. HU, Y. WU, W. GAO, B. REN, Q. WANG, AND Y. CAI, *Visible-light-driven bioi-based janus micromotor in pure water*, Journal of the American Chemical Society, 139 (2017), pp. 1722–1725.

[106] M. DORIGO, M. BIRATTARI, AND T. STUTZLE, *Ant colony optimization*, IEEE computational intelligence magazine, 1 (2006), pp. 28–39.

[107] M. DORIGO, E. BONABEAU, AND G. THERAULAZ, *Ant algorithms and stigmergy*, Future Generation Computer Systems, 16 (2000), pp. 851–871.

[108] K. DRESCHER, R. E. GOLDSTEIN, AND I. TUVAL, *Fidelity of adaptive phototaxis*, Proceedings of the National Academy of Sciences, 107 (2010), pp. 11171–11176.

[109] W. DUAN, R. LIU, AND A. SEN, *Transition between collective behaviors of micromotors in response to different stimuli*, Journal of the American Chemical Society, 135 (2013), pp. 1280–1283.

[110] D. DUDLEY, W. M. DUNCAN, AND J. SLAUGHTER, *Emerging digital micromirror device (dmd) applications*, in MOEMS display and imaging systems, vol. 4985, International Society for Optics and Photonics, 2003, pp. 14–25.

[111] A. D'AUSILIO, *Arduino: A low-cost multipurpose lab equipment*, Behavior research methods, 44 (2012), pp. 305–313.

[112] L. EDELSTEIN-KESHET, J. WATMOUGH, AND G. B. ERMENTROUT, *Trail following in ants: individual properties determine population behaviour*, Behavioral Ecology and Sociobiology, 36 (1995), pp. 119–133.

[113] J. ELGETI, R. G. WINKLER, AND G. GOMPPER, *Physics of microswimmers—single particle motion and collective behavior: a review*, Reports on progress in physics, 78 (2015), p. 056601.

[114] R. ERBAN AND H. G. OTHMER, *From individual to collective behavior in bacterial chemotaxis*, SIAM Journal on Applied Mathematics, 65 (2004), pp. 361–391.

[115] Z. EREZ, I. STEINBERGER-LEVY, M. SHAMIR, S. DORON, A. STOKAR-AVIHAIL, Y. PELEG, S. MELAMED, A. LEAVITT, A. SAVIDOR, S. ALBECK, ET AL., *Communication between viruses guides lysis–lysogeny decisions*, Nature, 541 (2017), pp. 488–493.

[116] P. ERKOC, I. C. YASA, H. CEYLAN, O. YASA, Y. ALAPAN, AND M. SITTI, *Mobile microrobots for active therapeutic delivery*, Advanced Therapeutics, 2 (2019), p. 1800064.

[117] H. ESKANDARLOO, A. KIERULF, AND A. ABBASPOURRAD, *Light-harvesting synthetic nano-and micromotors: a review*, Nanoscale, 9 (2017), pp. 12218–12230.

[118] D. FAN, Y. LI, X. WANG, T. ZHU, Q. WANG, H. CAI, W. LI, Y. TIAN, AND Z. LIU, *Progressive 3d printing technology and its application in medical materials*, Frontiers in pharmacology, 11 (2020).

[119] Q. FAN, W. HU, AND A. T. OHTA, *Laser-induced microbubble poration of localized single cells*, Lab on a Chip, 14 (2014), pp. 1572–1578.

[120] ——, *Efficient single-cell poration by microsecond laser pulses*, Lab on a Chip, 15 (2015), pp. 581–588.

[121] L. FENNO, O. YIZHAR, AND K. DEISSEROTH, *The development and application of optogenetics*, Annual review of neuroscience, 34 (2011).

[122] M. FERNÁNDEZ-MEDINA, M. A. RAMOS-DOCAMPO, O. HOVORKA, V. SALGUEIRIÑO, AND B. STÄDLER, *Recent advances in nano-and micromotors*, Advanced Functional Materials, 30 (2020), p. 1908283.

[123] J. FERNANDEZ-RODRIGUEZ, F. MOSER, M. SONG, AND C. A. VOIGT, *Engineering rgb color vision into escherichia coli*, Nature chemical biology, 13 (2017), pp. 706–708.

[124] A. FISCHER, F. SCHMID, AND T. SPECK, *Quorum-sensing active particles with discontinuous motility*, Physical Review E, 101 (2020), p. 012601.

[125] H.-C. FLEMMING, G. SCHAULE, T. GRIEBE, J. SCHMITT, AND A. TAMACHKIAROWA, *Biofouling—the achilles heel of membrane processes*, Desalination, 113 (1997), pp. 215–225.

[126] C. R. FONTANA, X. SONG, A. POLYMERI, J. M. GOODSON, X. WANG, AND N. S. SOUKOS, *The effect of blue light on periodontal biofilm growth in vitro*, Lasers in medical science, 30 (2015), pp. 2077–2086.

[127] S. FORD AND T. MINSHALL, *Invited review article: Where and how 3d printing is used in teaching and education*, Additive Manufacturing, 25 (2019), pp. 131–150.

[128] K. FOSTER AND R. SMYTH, *Light antennas in phototactic algae.*, Microbiological reviews, 44 (1980), p. 572.

[129] V. FOURCASSIE AND J.-L. DENEUBOURG, *The dynamics of collective exploration and trail-formation in monomorium pharaonis: experiments and model*, Physiological Entomology, 19 (1994), pp. 291–300.

[130] W. FRANCIS, A. DUNNE, C. DELANEY, L. FLOREA, AND D. DIAMOND, *Spiropyran based hydrogels actuators—walking in the light*, Sensors and Actuators B: Chemical, 250 (2017), pp. 608–616.

[131] G. FRANGIPANE, D. DELL'ARCIPRETE, S. PETRACCHINI, C. MAGGI, F. SAGLIMBENI, S. BIANCHI, G. VIZSNYICZAI, M. L. BERNARDINI, AND R. DI LEONARDO, *Dynamic density shaping of photokinetic e. coli*, Elife, 7 (2018), p. e36608.

[132] P. FRIEDL AND D. GILMOUR, *Collective cell migration in morphogenesis, regeneration and cancer*, Nature reviews Molecular cell biology, 10 (2009), pp. 445–457.

[133] P. FRIEDL, J. LOCKER, E. SAHAI, AND J. E. SEGALL, *Classifying collective cancer cell invasion*, Nature cell biology, 14 (2012), pp. 777–783.

[134] R. FUJISAWA, S. DOBATA, K. SUGAWARA, AND F. MATSUNO, *Designing pheromone communication in swarm robotics: Group foraging behavior mediated by chemical substance*, Swarm Intelligence, 8 (2014), pp. 227–246.

[135] K. FURUTA, A. FURUTA, Y. Y. TOYOSHIMA, M. AMINO, K. OIWA, AND H. KOJIMA, *Measuring collective transport by defined numbers of processive and nonprocessive kinesin motors*, Proceedings of the National Academy of Sciences, 110 (2013), pp. 501–506.

[136] D. GAO, W. DING, M. NIETO-VESPERINAS, X. DING, M. RAHMAN, T. ZHANG, C. LIM, AND C.-W. QIU, *Optical manipulation from the microscale to the nanoscale: fundamentals, advances and prospects*, Light: Science & Applications, 6 (2017), pp. e17039–e17039.

[137] S. GARNIER, J. GAUTRAIS, M. ASADPOUR, C. JOST, AND G. THERAULAZ, *Self-organized aggregation triggers collective decision making in a group of cockroach-like robots*, Adaptive Behavior, 17 (2009), pp. 109–133.

[138] S. GARNIER, J. GAUTRAIS, AND G. THERAULAZ, *The biological principles of swarm intelligence*, Swarm intelligence, 1 (2007), pp. 3–31.

[139] S. GARNIER, F. TACHE, M. COMBE, A. GRIMAL, AND G. THERAULAZ, *Alice in pheromone land: An experimental setup for the study of ant-like robots*, in 2007 IEEE swarm intelligence symposium, IEEE, 2007, pp. 37–44.

[140] P. R. GASCOYNE AND J. VYKOUKAL, *Particle separation by dielectrophoresis*, Electrophoresis, 23 (2002), p. 1973.

[141] M. GAZZOLA, A. A. TCHIEU, D. ALEXEEV, A. DE BRAUER, AND P. KOUMOUTSAKOS, *Learning to school in the presence of hydrodynamic interactions*, Journal of Fluid Mechanics, 789 (2016), pp. 726–749.

[142] H. J. GI, D. HAN, AND J.-K. PARK, *Optoelectrofluidic printing system for fabricating hydrogel sheets with on-demand patterned cells and microparticles*, Biofabrication, 9 (2017), p. 015011.

[143] G. GILLIES, R. RITTER, W. BROADDUS, M. GRADY, M. HOWARD III, AND R. MCNEIL, *Magnetic manipulation instrumentation for medical physics research*, Review of Scientific Instruments, 65 (1994), pp. 533–562.

[144] A. G. GOGLIA AND J. E. TOETTCHER, *A bright future: optogenetics to dissect the spatiotemporal control of cell behavior*, Current opinion in chemical biology, 48 (2019), pp. 106–113.

[145] C. F. GONZALEZ AND V. T. REMCHO, *Harnessing dielectric forces for separations of cells, fine particles and macromolecules*, Journal of Chromatography A, 1079 (2005), pp. 59–68.

[146] S. L. GORA, K. D. RAUCH, C. C. ONTIVEROS, A. K. STODDART, AND G. A. GAGNON, *Inactivation of biofilm-bound pseudomonas aeruginosa bacteria using uvc light emitting diodes (uvc leds)*, Water research, 151 (2019), pp. 193–202.

[147] D. M. GORDON, *The evolution of the algorithms for collective behavior*, Cell systems, 3 (2016), pp. 514–520.

[148] T. E. GOROCHOWSKI AND T. O. RICHARDSON, *How behaviour and the environment influence transmission in mobile groups*, in Temporal Network Epidemiology, Springer, 2017, pp. 17–42.

[149] D. G. GRIER, *A revolution in optical manipulation*, nature, 424 (2003), pp. 810–816.

[150] B. C. GROSS, J. L. ERKAL, S. Y. LOCKWOOD, C. CHEN, AND D. M. SPENCE, *Evaluation of 3d printing and its potential impact on biotechnology and the chemical sciences*, 2014.

[151] R. GROSS, M. BONANI, F. MONDADA, AND M. DORIGO, *Autonomous self-assembly in swarm-bots*, IEEE transactions on robotics, 22 (2006), pp. 1115–1130.

[152] R. GROSS AND M. DORIGO, *Towards group transport by swarms of robots*, International Journal of Bio-Inspired Computation, 1 (2009), pp. 1–13.

[153] F. GUO, Z. MAO, Y. CHEN, Z. XIE, J. P. LATA, P. LI, L. REN, J. LIU, J. YANG, M. DAO, ET AL., *Three-dimensional manipulation of single cells using surface acoustic waves*, Proceedings of the National Academy of Sciences, 113 (2016), pp. 1522–1527.

[154] D.-P. HÄDER AND M. LEBERT, *Photomovement*, Elsevier, 2001.

[155] D.-P. HÄDER AND M. LEBERT, *Photoorientation in photosynthetic flagellates*, Chemotaxis, (2009), pp. 51–65.

[156] J. HALLOY, G. SEMPO, G. CAPRARI, C. RIVAULT, M. ASADPOUR, F. TÂCHE, I. SAÏD, V. DURIER, S. CANONGE, J. M. AMÉ, ET AL., *Social integration of robots into groups of cockroaches to control self-organized choices*, Science, 318 (2007), pp. 1155–1158.

[157] W. G. HAND AND W. HAUPT, *Flagellar activity of the colony members of volvox aureus ehrbg. during light stimulation*, The Journal of Protozoology, 18 (1971), pp. 361–364.

[158] J. HARTMANN, D. KRUEGER, AND S. DE RENZIS, *Using optogenetics to tackle systems-level questions of multicellular morphogenesis*, Current opinion in cell biology, 66 (2020), pp. 19–27.

[159] F. HÄSE, L. M. ROCH, AND A. ASPURU-GUZIK, *Next-generation experimentation with self-driving laboratories*, Trends in Chemistry, 1 (2019), pp. 282–291.

[160] S. HAUERT, *Swarm engineering across scales: From robots to nanomedicine*, in Artificial Life Conference Proceedings 14, MIT Press, 2017, pp. 11–12.

[161] S. HAUERT AND S. N. BHATIA, *Mechanisms of cooperation in cancer nanomedicine: towards systems nanotechnology*, Trends in biotechnology, 32 (2014), pp. 448–455.

[162] S. HAUERT, S. LEVEN, M. VARGA, F. RUINI, A. CANGELOSI, J.-C. ZUFFEREY, AND D. FLOREANO, *Reynolds flocking in reality with fixed-wing robots: communication range vs. maximum turning rate*, in 2011 IEEE/RSJ International Conference on Intelligent Robots and Systems, IEEE, pp. 5015–5020.

[163] P. HEGEMANN AND G. NAGEL, *From channelrhodopsins to optogenetics*, EMBO molecular medicine, 5 (2013), pp. 173–176.

[164] A. N. HELLMAN, K. R. RAU, H. H. YOON, AND V. VENUGOPALAN, *Biophysical response to pulsed laser microbeam-induced cell lysis and molecular delivery*, Journal of biophotonics, 1 (2008), pp. 24–35.

[165] G. HERTEL, S. NIEDNER, AND S. HERRMANN, *Motivation of software developers in open source projects: an internet-based survey of contributors to the linux kernel*, Research policy, 32 (2003), pp. 1159–1177.

[166] R. P. HERTZBERG AND A. J. POPE, *High-throughput screening: new technology for the 21st century*, Current opinion in chemical biology, 4 (2000), pp. 445–451.

[167] F. HEYLIGHEN, *Stigmergy as a universal coordination mechanism i: Definition and components*, Cognitive Systems Research, 38 (2016), pp. 4–13.

[168] B. L. HOGAN, *Morphogenesis*, Cell, 96 (1999), pp. 225–233.

[169] J. HONG, J. B. EDEL, AND A. J. DEMELLO, *Micro-and nanofluidic systems for high-throughput biological screening*, Drug discovery today, 14 (2009), pp. 134–146.

[170] H. HOOPS, *Motility in the colonial and multicellular volvocales: structure, function, and evolution*, Protoplasma, 199 (1997), pp. 99–112.

[171] H. J. HOOPS, *Flagellar, cellular and organismal polarity in volvox carteri*, Journal of Cell Science, 104 (1993), pp. 105–117.

[172] H. J. HOOPS, I. NISHII, AND D. L. KIRK, *Cytoplasmic bridges in volvox and its relatives*, in Cell-cell channels, Springer, 2006, pp. 65–84.

[173] W. HU, K. S. ISHII, Q. FAN, AND A. T. OHTA, *Hydrogel microrobots actuated by optically generated vapour bubbles*, Lab on a Chip, 12 (2012), pp. 3821–3826.

[174] W. HU, K. S. ISHII, AND A. T. OHTA, *Micro-assembly using optically controlled bubble microrobots*, Applied Physics Letters, 99 (2011), p. 094103.

[175] W. HU, Q. LI, B. LI, K. MA, C. ZHANG, AND X. FU, *Optogenetics sheds new light on tissue engineering and regenerative medicine*, Biomaterials, 227 (2020), p. 119546.

[176] Y. HU, W. LIU, AND Y. SUN, *Multiwavelength phototactic micromotor with controllable swarming motion for "chemistry-on-the-fly"*, ACS Applied Materials & Interfaces, 12 (2020), pp. 41495–41505.

[177] C. HUANG, J.-A. LV, X. TIAN, Y. WANG, Y. YU, AND J. LIU, *Miniaturized swimming soft robot with complex movement actuated and controlled by remote light signals*, Scientific reports, 5 (2015), pp. 1–8.

[178] S.-B. HUANG, M.-H. WU, Y.-H. LIN, C.-H. HSIEH, C.-L. YANG, H.-C. LIN, C.-P. TSENG, AND G.-B. LEE, *High-purity and label-free isolation of circulating tumor cells (ctcs) in a microfluidic platform by using optically-induced-dielectrophoretic (odep) force*, Lab on a Chip, 13 (2013), pp. 1371–1383.

[179] Y. HUANG, A. XIA, G. YANG, AND F. JIN, *Bioprinting living biofilms through optogenetic manipulation*, ACS synthetic biology, 7 (2018), pp. 1195–1200.

[180] R. M. HUGHES, D. J. FREEMAN, K. N. LAMB, R. M. POLLET, W. J. SMITH, AND D. S. LAWRENCE, *Optogenetic apoptosis: Light-triggered cell death*, Angewandte Chemie, 127 (2015), pp. 12232–12236.

[181] E. R. HUNT, S. JONES, AND S. HAUERT, *Testing the limits of pheromone stigmergy in high-density robot swarms*, Royal Society open science, 6 (2019), p. 190225.

[182] M. IBELE, T. E. MALLOUK, AND A. SEN, *Schooling behavior of light-powered autonomous micromotors in water*, Angewandte Chemie, 121 (2009), pp. 3358–3362.

[183] Y. IKEMOTO, Y. HASEGAWA, T. FUKUDA, AND K. MATSUDA, *Gradual spatial pattern formation of homogeneous robot group*, Information Sciences, 171 (2005), pp. 431–445.

[184] O. IKKALA AND G. TEN BRINKE, *Functional materials based on self-assembly of polymeric supramolecules*, science, 295 (2002), pp. 2407–2409.

[185] E. IZQUIERDO, T. QUINKLER, AND S. DE RENZIS, *Guided morphogenesis through optogenetic activation of rho signalling during early drosophila embryogenesis*, Nature communications, 9 (2018), pp. 1–13.

[186] D. JAQUE, L. M. MAESTRO, B. DEL ROSAL, P. HARO-GONZALEZ, A. BENAYAS, J. PLAZA, E. M. RODRIGUEZ, AND J. G. SOLE, *Nanoparticles for photothermal therapies*, nanoscale, 6 (2014), pp. 9494–9530.

[187] R. JEANSON, C. RIVAULT, J.-L. DENEUBOURG, S. BLANCO, R. FOURNIER, C. JOST, AND G. THERAULAZ, *Self-organized aggregation in cockroaches*, Animal behaviour, 69 (2005), pp. 169–180.

[188] H. JECKEL, E. JELLI, R. HARTMANN, P. K. SINGH, R. MOK, J. F. TOTZ, L. VIDAKOVIC, B. ECKHARDT, J. DUNKEL, AND K. DRESCHER, *Learning the space-time phase diagram of bacterial swarm expansion*, Proceedings of the National Academy of Sciences, 116 (2019), pp. 1489–1494.

[189] K. K. JEFFERSON, *What drives bacteria to produce a biofilm?*, FEMS microbiology letters, 236 (2004), pp. 163–173.

[190] G. JÉKELY, *Evolution of phototaxis*, Philosophical Transactions of the Royal Society B: Biological Sciences, 364 (2009), pp. 2795–2808.

[191] A. JEVTIĆ AND D. ANDINA DE LA FUENTE, *Swarm intelligence and its applications in swarm robotics*, (2007).

[192] A. JEVTIC, A. GUTIÉRREZ, D. ANDINA, AND M. JAMSHIDI, *Distributed bees algorithm for task allocation in swarm of robots*, IEEE Systems Journal, 6 (2011), pp. 296–304.

[193] X. JIN AND I. H. RIEDEL-KRUSE, *Biofilm lithography enables high-resolution cell patterning via optogenetic adhesin expression*, Proceedings of the National Academy of Sciences, 115 (2018), pp. 3698–3703.

[194] Y. JIN AND Y. MENG, *Morphogenetic robotics: An emerging new field in developmental robotics*, IEEE Transactions on Systems, Man, and Cybernetics, Part C (Applications and Reviews), 41 (2010), pp. 145–160.

[195] R. JONES, P. HAUFE, E. SELLS, P. IRAVANI, V. OLLIVER, C. PALMER, AND A. BOWYER, *Reprap–the replicating rapid prototyper*, Robotica, 29 (2011), pp. 177–191.

[196] B. JURADO-SÁNCHEZ AND J. WANG, *Micromotors for environmental applications: a review*, Environmental Science: Nano, 5 (2018), pp. 1530–1544.

[197] G. KATAL, N. TYAGI, AND A. JOSHI, *Digital light processing and its future applications*, International journal of scientific and research publications, 3 (2013), pp. 1997–2004.

[198] D. B. KEARNS, *A field guide to bacterial swarming motility*, Nature Reviews Microbiology, 8 (2010), pp. 634–644.

[199] D. M. KEHOE AND A. GUTU, *Responding to color: the regulation of complementary chromatic adaptation*, Annu. Rev. Plant Biol., 57 (2006), pp. 127–150.

[200] S. KERNBACH, D. HÄBE, O. KERNBACH, R. THENIUS, G. RADSPIELER, T. KIMURA, AND T. SCHMICKL, *Adaptive collective decision-making in limited robot swarms without communication*, The International Journal of Robotics Research, 32 (2013), pp. 35–55.

[201] J. J. KEYA, R. SUZUKI, A. M. R. KABIR, D. INOUE, H. ASANUMA, K. SADA, H. HESS, A. KUZUYA, AND A. KAKUGO, *Dna-assisted swarm control in a biomolecular motor system*, Nature communications, 9 (2018), pp. 1–8.

[202] U. KHADKA, V. HOLUBEC, H. YANG, AND F. CICHOS, *Active particles bound by information flows*, Nature communications, 9 (2018), pp. 1–9.

[203] K. KHOSHMANESH, C. ZHANG, F. J. TOVAR-LOPEZ, S. NAHAVANDI, S. BARATCHI, K. KALANTAR-ZADEH, AND A. MITCHELL, *Dielectrophoretic manipulation and separation of microparticles using curved microelectrodes*, Electrophoresis, 30 (2009), pp. 3707–3717.

[204] J. KIETZMANN, L. PITT, AND P. BERTHON, *Disruptions, decisions, and destinations: Enter the age of 3-d printing and additive manufacturing*, Business Horizons, 58 (2015), pp. 209–215.

[205] C. K. KIM, A. ADHIKARI, AND K. DEISSEROTH, *Integration of optogenetics with complementary methodologies in systems neuroscience*, Nature Reviews Neuroscience, 18 (2017), pp. 222–235.

[206] Y. KIM, A. A. SHAH, AND M. J. SOLOMON, *Spatially and temporally reconfigurable assembly of colloidal crystals*, Nature communications, 5 (2014), pp. 1–8.

[207] A. KIRILLOVA AND L. IONOV, *Shape-changing polymers for biomedical applications*, Journal of Materials Chemistry B, 7 (2019), pp. 1597–1624.

[208] M. KLOTZ, S. DEUERLING, S. KUGLER, C. ZOLLFRANK, AND D. VAN OPDENBOSCH, *Light-diffractive patterning of porphyridium purpureum*, Photochemical & Photobiological Sciences, 19 (2020), pp. 515–523.

[209] A. KOCH AND H. MEINHARDT, *Biological pattern formation: from basic mechanisms to complex structures*, Reviews of modern physics, 66 (1994), p. 1481.

[210] J. P. KOLLENDER, A. I. MARDARE, AND A. W. HASSEL, *Multi-scanning droplet cell microscopy (multi-sdcm) for truly parallel high throughput electrochemical experimentation*, Electrochimica Acta, 179 (2015), pp. 32–37.

[211] D. S. KONG, T. A. THORSEN, J. BABB, S. T. WICK, J. J. GAM, R. WEISS, AND P. A. CARR, *Open-source, community-driven microfluidics with metafluidics*, Nature biotechnology, 35 (2017), p. 523.

[212] L. KONG, C. C. MAYORGA-MARTINEZ, J. GUAN, AND M. PUMERA, *Photocatalytic micromotors activated by uv to visible light for environmental remediation, micropumps, reversible assembly, transportation, and biomimicry*, Small, 16 (2020), p. 1903179.

[213] C. KREMER, C. WITTE, S. L. NEALE, J. REBOUD, M. P. BARRETT, AND J. M. COOPER, *Shape-dependent optoelectronic cell lysis*, Angewandte Chemie, 126 (2014), pp. 861–865.

[214] C. R. KUBE AND E. BONABEAU, *Cooperative transport by ants and robots*, Robotics and autonomous systems, 30 (2000), pp. 85–101.

[215] V. W.-A. KUMBOL, E. K. AMPOFO, AND M. A. TWUMASI, *Actifield, an automated open source actimeter for rodents*, HardwareX, 4 (2018), p. e00047.

[216] S. KUZNETSOV, C. DOONAN, N. WILSON, S. MOHAN, S. E. HUDSON, AND E. PAULOS, *Diybio things: open source biology tools as platforms for hybrid knowledge production and scientific participation*, in Proceedings of the 33rd Annual ACM Conference on Human Factors in Computing Systems, 2015, pp. 4065–4068.

[217] K. N. LALAND AND S. M. READER, *Foraging innovation in the guppy*, Animal Behaviour, 57 (1999), pp. 331–340.

[218] A. T. LAM, K. G. SAMUEL-GAMA, J. GRIFFIN, M. LOEUN, L. C. GERBER, Z. HOSSAIN, N. J. CIRA, S. A. LEE, AND I. H. RIEDEL-KRUSE, *Device and programming abstractions for spatiotemporal control of active micro-particle swarms*, Lab on a Chip, 17 (2017), pp. 1442–1451.

[219] J. S. LANGER, *Instabilities and pattern formation in crystal growth*, Reviews of modern physics, 52 (1980), p. 1.

[220] T. LAURELL, F. PETERSSON, AND A. NILSSON, *Chip integrated strategies for acoustic separation and manipulation of cells and particles*, Chemical Society Reviews, 36 (2007), pp. 492–506.

[221] F. A. LAVERGNE, H. WENDEHENNE, T. BÄUERLE, AND C. BECHINGER, *Group formation and cohesion of active particles with visual perception–dependent motility*, Science, 364 (2019), pp. 70–74.

[222] G. LAZAREV, A. HERMERSCHMIDT, S. KRÜGER, AND S. OSTEN, *Lcos spatial light modulators: trends and applications*, Optical Imaging and Metrology: Advanced Technologies, (2012), pp. 1–29.

[223] M. Le Goc, L. H. Kim, A. Parsaei, J.-D. Fekete, P. Dragicevic, and S. Follmer, *Zooids: Building blocks for swarm user interfaces*, in Proceedings of the 29th Annual Symposium on User Interface Software and Technology, 2016, pp. 97–109.

[224] A. M. Leifer, C. Fang-Yen, M. Gershow, M. J. Alkema, and A. D. Samuel, *Optogenetic manipulation of neural activity in freely moving caenorhabditis elegans*, Nature methods, 8 (2011), pp. 147–152.

[225] D. Lenton, *Photo essay: Plastic recycling workspace*, Engineering & Technology, 14 (2019), pp. 40–41.

[226] T. Letcher and M. Waytashek, *Material property testing of 3d-printed specimen in pla on an entry-level 3d printer*, in ASME International Mechanical Engineering Congress and Exposition, vol. 46438, American Society of Mechanical Engineers, 2014, p. V02AT02A014.

[227] A. Levskaya, A. A. Chevalier, J. J. Tabor, Z. B. Simpson, L. A. Lavery, M. Levy, E. A. Davidson, A. Scouras, A. D. Ellington, E. M. Marcotte, et al., *Engineering escherichia coli to see light*, Nature, 438 (2005), pp. 441–442.

[228] A. J. Lewis, M. Campbell, and P. Stavroulakis, *Performance evaluation of a cheap, open source, digital environmental monitor based on the raspberry pi*, Measurement, 87 (2016), pp. 228–235.

[229] L. Li, Y. He, M. Zhao, and J. Jiang, *Collective cell migration: Implications for wound healing and cancer invasion*, Burns & trauma, 1 (2013), pp. 2321–3868.

[230] W. Liang, L. Liu, H. Zhang, Y. Wang, and W. J. Li, *Optoelectrokinetics-based microfluidic platform for bioapplications: A review of recent advances*, Biomicrofluidics, 13 (2019), p. 051502.

[231] W. Liang, Y. Zhao, L. Liu, Y. Wang, Z. Dong, W. J. Li, G.-B. Lee, X. Xiao, and W. Zhang, *Rapid and label-free separation of burkitt's lymphoma cells from red blood cells by optically-induced electrokinetics*, PLoS One, 9 (2014), p. e90827.

[232] X. Lin, T. Si, Z. Wu, and Q. He, *Self-thermophoretic motion of controlled assembled micro-/nanomotors*, Physical Chemistry Chemical Physics, 19 (2017), pp. 23606–23613.

[233] Y.-H. Lin, C.-M. Chang, and G.-B. Lee, *Manipulation of single dna molecules by using optically projected images*, Optics Express, 17 (2009), pp. 15318–15329.

[234] Y.-H. Lin and G.-B. Lee, *An optically induced cell lysis device using dielectrophoresis*, Applied Physics Letters, 94 (2009), p. 033901.

[235] C. LIU, T. XU, L.-P. XU, AND X. ZHANG, *Controllable swarming and assembly of micro/nanomachines*, Micromachines, 9 (2018), p. 10.

[236] W. LIU, A. F. WINFIELD, J. SA, J. CHEN, AND L. DOU, *Towards energy optimization: Emergent task allocation in a swarm of foraging robots*, Adaptive behavior, 15 (2007), pp. 289–305.

[237] Z. LIU, J. ZHANG, J. JIN, Z. GENG, Q. QI, AND Q. LIANG, *Programming bacteria with light—sensors and applications in synthetic biology*, Frontiers in microbiology, 9 (2018), p. 2692.

[238] C. LOZANO, B. TEN HAGEN, H. LÖWEN, AND C. BECHINGER, *Phototaxis of synthetic microswimmers in optical landscapes*, Nature communications, 7 (2016), pp. 1–10.

[239] M. LUO, Y. FENG, T. WANG, AND J. GUAN, *Micro-/nanorobots at work in active drug delivery*, Advanced Functional Materials, 28 (2018), p. 1706100.

[240] A. MAIA CHAGAS, J. C. MOLLOY, L. L. PRIETO-GODINO, AND T. BADEN, *Leveraging open hardware to alleviate the burden of covid-19 on global health systems*, PLoS biology, 18 (2020), p. e3000730.

[241] A. MAIA CHAGAS, L. L. PRIETO-GODINO, A. B. ARRENBERG, AND T. BADEN, *The€ 100 lab: A 3d-printable open-source platform for fluorescence microscopy, optogenetics, and accurate temperature control during behaviour of zebrafish, drosophila, and caenorhabditis elegans*, PLoS biology, 15 (2017), p. e2002702.

[242] M. MAKSIMOVIĆ, V. VUJOVIĆ, N. DAVIDOVIĆ, V. MILOŠEVIĆ, AND B. PERIŠIĆ, *Raspberry pi as internet of things hardware: performances and constraints*, design issues, 3 (2014).

[243] W. F. MARSHALL, K. D. YOUNG, M. SWAFFER, E. WOOD, P. NURSE, A. KIMURA, J. FRANKEL, J. WALLINGFORD, V. WALBOT, X. QU, ET AL., *What determines cell size?*, BMC biology, 10 (2012), pp. 1–22.

[244] S. MARTEL AND M. MOHAMMADI, *Using a swarm of self-propelled natural microrobots in the form of flagellated bacteria to perform complex micro-assembly tasks*, in 2010 IEEE International Conference on Robotics and Automation, IEEE, 2010, pp. 500–505.

[245] D. MARTELLA, S. NOCENTINI, D. NUZHDIN, C. PARMEGGIANI, AND D. S. WIERSMA, *Photonic microhand with autonomous action*, Advanced Materials, 29 (2017), p. 1704047.

[246] P. MARTIN AND S. M. PARKHURST, *Parallels between tissue repair and embryo morphogenesis*, Development, 131 (2004), pp. 3021–3034.

[247] G. MATT AND J. UMEN, *Volvox: A simple algal model for embryogenesis, morphogenesis and cellular differentiation*, Developmental biology, 419 (2016), pp. 99–113.

[248] R. MAYOR AND S. ETIENNE-MANNEVILLE, *The front and rear of collective cell migration*, Nature reviews Molecular cell biology, 17 (2016), p. 97.

[249] L. M. MAYR AND D. BOJANIC, *Novel trends in high-throughput screening*, Current opinion in pharmacology, 9 (2009), pp. 580–588.

[250] L. M. MAYR AND P. FUERST, *The future of high-throughput screening*, Journal of biomolecular screening, 13 (2008), pp. 443–448.

[251] Y. MENG, H. GUO, AND Y. JIN, *A morphogenetic approach to flexible and robust shape formation for swarm robotic systems*, Robotics and Autonomous Systems, 61 (2013), pp. 25–38.

[252] G. MERMOUD, L. MATTHEY, W. C. EVANS, AND A. MARTINOLI, *Aggregation-mediated collective perception and action in a group of miniature robots*, in Proceedings of the 9th International Conference on Autonomous Agents and Multiagent Systems (AAMAS-2010), no. CONF, 2010, pp. 599–606.

[253] X. MESHIK, P. R. O'NEILL, AND N. GAUTAM, *Physical plasma membrane perturbation using subcellular optogenetics drives integrin-activated cell migration*, ACS synthetic biology, 8 (2019), pp. 498–510.

[254] P. MILGRAM AND F. KISHINO, *A taxonomy of mixed reality visual displays*, IEICE TRANSACTIONS on Information and Systems, 77 (1994), pp. 1321–1329.

[255] M. B. MILLER AND B. L. BASSLER, *Quorum sensing in bacteria*, Annual Reviews in Microbiology, 55 (2001), pp. 165–199.

[256] T. L. MIN, P. J. MEARS, L. M. CHUBIZ, C. V. RAO, I. GOLDING, AND Y. R. CHEMLA, *High-resolution, long-term characterization of bacterial motility using optical tweezers*, Nature methods, 6 (2009), pp. 831–835.

[257] C. MIO, T. GONG, A. TERRAY, AND D. MARR, *Design of a scanning laser optical trap for multiparticle manipulation*, Review of Scientific Instruments, 71 (2000), pp. 2196–2200.

[258] A. MISHRA, J.-S. KWON, R. THAKUR, AND S. WERELEY, *Optoelectrical microfluidics as a promising tool in biology*, Trends in biotechnology, 32 (2014), pp. 414–421.

[259] J. R. MOFFITT, Y. R. CHEMLA, S. B. SMITH, AND C. BUSTAMANTE, *Recent advances in optical tweezers*, Annu. Rev. Biochem., 77 (2008), pp. 205–228.

[260] P. MOLINS, N. STILLMAN, AND S. HAUERT, *Trail formation using large swarms of minimal robots*, Cybernetics and Systems, 50 (2019), pp. 693–710.

[261] F. MONDADA, M. BONANI, X. RAEMY, J. PUGH, C. CIANCI, A. KLAPTOCZ, S. MAGNENAT, J.-C. ZUFFEREY, D. FLOREANO, AND A. MARTINOLI, *The e-puck, a robot designed for education in engineering*, in Proceedings of the 9th conference on autonomous robot systems and competitions, vol. 1, IPCB: Instituto Politécnico de Castelo Branco, 2009, pp. 59–65.

[262] F. MONDADA, D. FLOREANO, A. GUIGNARD, J.-L. DENEUBOURG, L. GAMBARDELLA, S. NOLFI, AND M. DORIGO, *Search for rescue: an application for the swarm-bot self-assembling robot concept*, Technical report, LSA2-I2S-STI, (2002).

[263] F. MONDADA, G. C. PETTINARO, A. GUIGNARD, I. W. KWEE, D. FLOREANO, J.-L. DENEUBOURG, S. NOLFI, L. M. GAMBARDELLA, AND M. DORIGO, *Swarm-bot: A new distributed robotic concept*, Autonomous robots, 17 (2004), pp. 193–221.

[264] H. MORGAN AND N. G. GREEN, *Dielectrophoretic manipulation of rod-shaped viral particles*, Journal of Electrostatics, 42 (1997), pp. 279–293.

[265] F. MOSER, E. THAM, L. M. GONZÁLEZ, T. K. LU, AND C. A. VOIGT, *Light-controlled, high-resolution patterning of living engineered bacteria onto textiles, ceramics, and plastic*, Advanced Functional Materials, 29 (2019), p. 1901788.

[266] F. MOU, L. KONG, C. CHEN, Z. CHEN, L. XU, AND J. GUAN, *Light-controlled propulsion, aggregation and separation of water-fuelled tio 2 / pt janus submicromotors and their "on-the-fly" photocatalytic activities*, Nanoscale, 8 (2016), pp. 4976–4983.

[267] F. MOU, J. ZHANG, Z. WU, S. DU, Z. ZHANG, L. XU, AND J. GUAN, *Phototactic flocking of photochemical micromotors*, Iscience, 19 (2019), pp. 415–424.

[268] S. MUIÑOS-LANDIN, A. FISCHER, V. HOLUBEC, AND F. CICHOS, *Reinforcement learning with artificial microswimmers*, Science Robotics, 6 (2021).

[269] S. MUIÑOS-LANDIN, A. FISCHER, N. A. SÖKER, AND F. CICHOS, *Emergent collective phenomena through active particle control by light*, Journal of Physics: Condensed Matter, 32 (2020).

[270] S. MUIÑOS-LANDIN, K. GHAZI-ZAHEDI, AND F. CICHOS, *Reinforcement learning of artificial microswimmers*, arXiv preprint arXiv:1803.06425, (2018).

[271] M. MUKHERJEE, Y. HU, C. H. TAN, S. A. RICE, AND B. CAO, *Engineering a light-responsive, quorum quenching biofilm to mitigate biofouling on water purification membranes*, Science advances, 4 (2018), p. eaau1459.

[272] L. F. R. MURILLO AND T. WENZEL, *Welcome to the journal of open hardware*, (2017).

[273] A. M. MURPHY AND D. J. MONTELL, *Cell type-specific roles for cdc42, rac, and rhol in drosophila oogenesis.*, The Journal of cell biology, 133 (1996), pp. 617–630.

[274] S. NA, Y. QIU, A. E. TURGUT, J. ULRICH, T. KRAJNÍK, S. YUE, B. LENNOX, AND F. ARVIN, *Bio-inspired artificial pheromone system for swarm robotics applications*, Adaptive Behavior, (2020), p. 1059712320918936.

[275] C. D. NADELL, K. DRESCHER, AND K. R. FOSTER, *Spatial structure, cooperation and competition in biofilms*, Nature Reviews Microbiology, 14 (2016), pp. 589–600.

[276] C. D. NADELL, J. B. XAVIER, AND K. R. FOSTER, *The sociobiology of biofilms*, FEMS microbiology reviews, 33 (2008), pp. 206–224.

[277] I. NAVARRO AND F. MATÍA, *An introduction to swarm robotics*, International Scholarly Research Notices, 2013 (2013).

[278] B. J. NELSON, I. K. KALIAKATSOS, AND J. J. ABBOTT, *Microrobots for minimally invasive medicine*, Annual review of biomedical engineering, 12 (2010), pp. 55–85.

[279] K. C. NEUMAN, E. H. CHADD, G. F. LIOU, K. BERGMAN, AND S. M. BLOCK, *Characterization of photodamage to escherichia coli in optical traps*, Biophysical journal, 77 (1999), pp. 2856–2863.

[280] T. D. NGO, A. KASHANI, G. IMBALZANO, K. T. NGUYEN, AND D. HUI, *Additive manufacturing (3d printing): A review of materials, methods, applications and challenges*, Composites Part B: Engineering, 143 (2018), pp. 172–196.

[281] K. P. NGUYEN, T. J. O'NEAL, O. A. BOLONDURO, E. WHITE, AND A. V. KRAVITZ, *Feeding experimentation device (fed): A flexible open-source device for measuring feeding behavior*, Journal of neuroscience methods, 267 (2016), pp. 108–114.

[282] T. NGUYEN, S. ZOËGA ANDREASEN, A. WOLFF, AND D. DUONG BANG, *From lab on a chip to point of care devices: The role of open source microcontrollers*, Micromachines, 9 (2018), p. 403.

[283] G. NIEZEN, P. ESLAMBOLCHILAR, AND H. THIMBLEBY, *Open-source hardware for medical devices*, BMJ innovations, 2 (2016).

[284] S. NOCENTINI, C. PARMEGGIANI, D. MARTELLA, AND D. S. WIERSMA, *Optically driven soft micro robotics*, Advanced Optical Materials, 6 (2018), p. 1800207.

[285] S. NOUYAN, A. CAMPO, AND M. DORIGO, *Path formation in a robot swarm*, Swarm Intelligence, 2 (2008), pp. 1–23.

[286] W. NULTSCH AND H. SCHUCHART, *Photomovement of the red alga porphyridium cruentum (ag.) naegeli*, Archives of Microbiology, 125 (1980), pp. 181–188.

[287] I. NUÑEZ, T. MATUTE, R. HERRERA, J. KEYMER, T. MARZULLO, T. RUDGE, AND F. FEDERICI, *Low cost and open source multi-fluorescence imaging system for teaching and research in biology and bioengineering*, PloS one, 12 (2017), p. e0187163.

[288] M. NUROLAHZADE, S. M. NASEHI, S. H. KHANDKAR, AND S. RAWAL, *The role of patch review in software evolution: an analysis of the mozilla firefox*, in Proceedings of the joint international and annual ERCIM workshops on Principles of software evolution (IWPSE) and software evolution (Evol) workshops, 2009, pp. 9–18.

[289] T. NUTSCH, W. MARWAN, D. OESTERHELT, AND E. D. GILLES, *Signal processing and flagellar motor switching during phototaxis of halobacterium salinarum*, Genome research, 13 (2003), pp. 2406–2412.

[290] S. OBERLOIER AND J. M. PEARCE, *General design procedure for free and open-source hardware for scientific equipment*, Designs, 2 (2018), p. 2.

[291] H. OH, A. R. SHIRAZI, C. SUN, AND Y. JIN, *Bio-inspired self-organising multi-robot pattern formation: A review*, Robotics and Autonomous Systems, 91 (2017), pp. 83–100.

[292] H.-S. OH, K.-M. YEON, C.-S. YANG, S.-R. KIM, C.-H. LEE, S. Y. PARK, J. Y. HAN, AND J.-K. LEE, *Control of membrane biofouling in mbr for wastewater treatment by quorum quenching bacteria encapsulated in microporous membrane*, Environmental science & technology, 46 (2012), pp. 4877–4884.

[293] R. OHLENDORF, R. R. VIDAVSKI, A. ELDAR, K. MOFFAT, AND A. MÖGLICH, *From dusk till dawn: one-plasmid systems for light-regulated gene expression*, Journal of molecular biology, 416 (2012), pp. 534–542.

[294] A. M. OKAMURA, N. SMABY, AND M. R. CUTKOSKY, *An overview of dexterous manipulation*, in Proceedings 2000 ICRA. Millennium Conference. IEEE International Conference on Robotics and Automation. Symposia Proceedings (Cat. No. 00CH37065), vol. 1, IEEE, 2000, pp. 255–262.

[295] A. OKUBO, *Dynamical aspects of animal grouping: swarms, schools, flocks, and herds*, Advances in biophysics, 22 (1986), pp. 1–94.

[296] T. E. OLIPHANT, *Python for scientific computing*, Computing in Science & Engineering, 9 (2007), pp. 10–20.

[297] C. E. OWENS, C. W. SHIELDS, D. F. CRUZ, P. CHARBONNEAU, AND G. P. LÓPEZ, *Highly parallel acoustic assembly of microparticles into well-ordered colloidal crystallites*, Soft Matter, 12 (2016), pp. 717–728.

[298] M. PACHECO, B. JURADO-SÁNCHEZ, AND A. ESCARPA, *Visible-light-driven janus microvehicles in biological media*, Angewandte Chemie International Edition, 58 (2019), pp. 18017–18024.

[299] M. PADGETT AND R. DI LEONARDO, *Holographic optical tweezers and their relevance to lab on chip devices*, Lab on a Chip, 11 (2011), pp. 1196–1205.

[300] J. PALACCI, S. SACANNA, A. P. STEINBERG, D. J. PINE, AND P. M. CHAIKIN, *Living crystals of light-activated colloidal surfers*, Science, 339 (2013), pp. 936–940.

[301] S. PALAGI AND P. FISCHER, *Bioinspired microrobots*, Nature Reviews Materials, 3 (2018), pp. 113–124.

[302] S. PALAGI, A. G. MARK, S. Y. REIGH, K. MELDE, T. QIU, H. ZENG, C. PARMEGGIANI, D. MARTELLA, A. SANCHEZ-CASTILLO, N. KAPERNAUM, ET AL., *Structured light enables biomimetic swimming and versatile locomotion of photoresponsive soft microrobots*, Nature materials, 15 (2016), pp. 647–653.

[303] S. PALAGI, D. P. SINGH, AND P. FISCHER, *Light-controlled micromotors and soft microrobots*, Advanced Optical Materials, 7 (2019), p. 1900370.

[304] G. PALMER AND S. YAIDA, *Optimizing collective fieldtaxis of swarming agents through reinforcement learning*, arXiv preprint arXiv:1709.02379, (2017).

[305] S. PANARIN, J. MÜLLER, S. PRABHAKAR, AND R. FICKLER, *Spatial structuring of light for undergraduate laboratories*, American Journal of Physics, 89 (2021), pp. 210–219.

[306] J.-H. PARK, G. VON MALTZAHN, L. L. ONG, A. CENTRONE, T. A. HATTON, E. RUOSLAHTI, S. N. BHATIA, AND M. J. SAILOR, *Cooperative nanoparticles for tumor detection and photothermally triggered drug delivery*, Advanced Materials, 22 (2010), pp. 880–885.

[307] C. A. PARKER AND H. ZHANG, *Biologically inspired collective comparisons by robotic swarms*, The International Journal of Robotics Research, 30 (2011), pp. 524–535.

[308] J. K. PARRISH, S. V. VISCIDO, AND D. GRUNBAUM, *Self-organized fish schools: an examination of emergent properties*, The biological bulletin, 202 (2002), pp. 296–305.

[309] A. E. PATTESON, J. YANG, P. E. ARRATIA, AND A. GOPINATH, *Quenching an active swarm: Effects of light exposure on collective motility in swarming serratia marcescens colonies*, bioRxiv, (2018), p. 331801.

[310] C. PAWASHE, S. FLOYD, AND M. SITTI, *Multiple magnetic microrobot control using electrostatic anchoring*, Applied Physics Letters, 94 (2009), p. 164108.

[311] J. PEARCE, *Impacts of open source hardware in science and engineering*, The Bridge, (2017).

[312] J. M. PEARCE, *Building research equipment with free, open-source hardware*, Science, 337 (2012), pp. 1303–1304.

[313] T. J. PEDLEY, D. R. BRUMLEY, AND R. E. GOLDSTEIN, *Squirmers with swirl: a model for volvox swimming*, Journal of fluid mechanics, 798 (2016), pp. 165–186.

[314] E. PEDONE, I. DE CESARE, C. ZAMORA, D. HAENER, L. POSTIGLIONE, B. SHANNON, N. SAVERY, C. S. GRIERSON, M. DI BARNARDO, T. E. GOROCHOWSKI, ET AL., *Cheetah: a computational toolkit for cybergenetic control*, bioRxiv, (2020).

[315] K. H. PETERSEN, N. NAPP, R. STUART-SMITH, D. RUS, AND M. KOVAC, *A review of collective robotic construction*, Science Robotics, 4 (2019).

[316] R. PETHIG, *Dielectrophoresis: Status of the theory, technology, and applications*, Biomicrofluidics, 4 (2010), p. 022811.

[317] R. PETHIG AND G. H. MARKX, *Applications of dielectrophoresis in biotechnology*, Trends in biotechnology, 15 (1997), pp. 426–432.

[318] R. L. PETRITZ, *Theory of photoconductivity in semiconductor films*, Physical Review, 104 (1956), p. 1508.

[319] O. PINEÑO, *Arduipod box: A low-cost and open-source skinner box using an ipod touch and an arduino microcontroller*, Behavior research methods, 46 (2014), pp. 196–205.

[320] L. J. POINTS, J. W. TAYLOR, J. GRIZOU, K. DONKERS, AND L. CRONIN, *Artificial intelligence exploration of unstable protocells leads to predictable properties and discovery of collective behavior*, Proceedings of the National Academy of Sciences, 115 (2018), pp. 885–890.

[321] A. PORTER AND I. RAFOLS, *Is science becoming more interdisciplinary? measuring and mapping six research fields over time*, Scientometrics, 81 (2009), pp. 719–745.

[322] L. PU, S. YANG, A. XIA, AND F. JIN, *Optogenetics manipulation enables prevention of biofilm formation of engineered pseudomonas aeruginosa on surfaces*, ACS synthetic biology, 7 (2018), pp. 200–208.

[323] E. B. PURCELL AND S. CROSSON, *Photoregulation in prokaryotes*, Current opinion in microbiology, 11 (2008), pp. 168–178.

[324] M. A. RAHMAN, N. TAKAHASHI, K. F. SILIGA, N. K. NG, Z. WANG, AND A. T. OHTA, *Vision-assisted micromanipulation using closed-loop actuation of multiple microrobots*, Robotics and biomimetics, 4 (2017), pp. 1–10.

[325] M. RASMUSSEN, L. ODDERSHEDE, AND H. SIEGUMFELDT, *Optical tweezers cause physiological damage to escherichia coli and listeria bacteria*, Applied and environmental microbiology, 74 (2008), pp. 2441–2446.

[326] S. RAVINDRAN, *How diy technologies are democratizing science*, Nature, 587 (2020), pp. 509–511.

[327] G. K. REDDY, L. STEHNO-BITTEL, AND C. S. ENWEMEKA, *Laser photostimulation accelerates wound healing in diabetic rats*, Wound Repair and Regeneration, 9 (2001), pp. 248–255.

[328] R. J. REDFIELD, *Is quorum sensing a side effect of diffusion sensing?*, Trends in microbiology, 10 (2002), pp. 365–370.

[329] J. REGTMEIER, T. T. DUONG, R. EICHHORN, D. ANSELMETTI, AND A. ROS, *Dielectrophoretic manipulation of dna: Separation and polarizability*, Analytical chemistry, 79 (2007), pp. 3925–3932.

[330] A. REINA, A. J. COPE, E. NIKOLAIDIS, J. A. MARSHALL, AND C. SABO, *Ark: Augmented reality for kilobots*, IEEE Robotics and Automation letters, 2 (2017), pp. 1755–1761.

[331] N. A. REPINA, A. ROSENBLOOM, A. MUKHERJEE, D. V. SCHAFFER, AND R. S. KANE, *At light speed: advances in optogenetic systems for regulating cell signaling and behavior*, Annual review of chemical and biomolecular engineering, 8 (2017), pp. 13–39.

[332] C. W. REYNOLDS, *Flocks, herds and schools: A distributed behavioral model*, in Proceedings of the 14th annual conference on Computer graphics and interactive techniques, 1987, pp. 25–34.

[333] M. RIGHINI, A. S. ZELENINA, C. GIRARD, AND R. QUIDANT, *Parallel and selective trapping in a patterned plasmonic landscape*, Nature Physics, 3 (2007), pp. 477–480.

[334] M. ROBBINS, O. SIDDIQUI, T. FUCHSBERGER, G. GOODFELLOW, O. PAULSEN, C. F. KAMINSKI, T. EUSER, AND G. S. K. SCHIERLE, *Optogenie: an open-source device for the optogenetic stimulation of cells*, Journal of Open Hardware, 5 (2021).

[335] P. RØRTH, *Collective cell migration*, Annual Review of Cell and Developmental, 25 (2009), pp. 407–429.

[336] ——, *Fellow travellers: emergent properties of collective cell migration*, EMBO reports, 13 (2012), pp. 984–991.

[337] M. RUBENSTEIN, C. AHLER, AND R. NAGPAL, *Kilobot: A low cost scalable robot system for collective behaviors*, in 2012 IEEE International Conference on Robotics and Automation, IEEE, 2012, pp. 3293–3298.

[338] M. RUBENSTEIN, A. CABRERA, J. WERFEL, G. HABIBI, J. MCLURKIN, AND R. NAGPAL, *Collective transport of complex objects by simple robots: theory and experiments*, in Proceedings of the 2013 international conference on Autonomous agents and multi-agent systems, 2013, pp. 47–54.

[339] M. RUBENSTEIN, A. CORNEJO, AND R. NAGPAL, *Programmable self-assembly in a thousand-robot swarm*, Science, 345 (2014), pp. 795–799.

[340] M. RULLAN, D. BENZINGER, G. W. SCHMIDT, A. MILIAS-ARGEITIS, AND M. KHAMMASH, *An optogenetic platform for real-time, single-cell interrogation of stochastic transcriptional regulation*, Molecular cell, 70 (2018), pp. 745–756.

[341] S. SAEEDI, M. TRENTINI, M. SETO, AND H. LI, *Multiple-robot simultaneous localization and mapping: A review*, Journal of Field Robotics, 33 (2016), pp. 3–46.

[342] E. ŞAHIN, *Swarm robotics: From sources of inspiration to domains of application*, in International workshop on swarm robotics, Springer, 2004, pp. 10–20.

[343] M. S. SAKAR, D. NEAL, T. BOUDOU, M. A. BOROCHIN, Y. LI, R. WEISS, R. D. KAMM, C. S. CHEN, AND H. H. ASADA, *Formation and optogenetic control of engineered 3d skeletal muscle bioactuators*, Lab on a Chip, 12 (2012), pp. 4976–4985.

[344] S. SAND, S. ZHANG, M. MÜHLEGG, G. FALCONI, C. ZHU, T. KRÜGER, AND S. NOWAK, *Swarm exploration and navigation on mars*, in 2013 International Conference on Localization and GNSS (ICL-GNSS), IEEE, 2013, pp. 1–6.

[345] K. SASAKI, M. KOSHIOKA, H. MISAWA, N. KITAMURA, AND H. MASUHARA, *Pattern formation and flow control of fine particles by laser-scanning micromanipulation*, Optics letters, 16 (1991), pp. 1463–1465.

[346] N. SAVAGE, *Digital spatial light modulators*, Nature Photonics, 3 (2009), pp. 170–172.

[347] H. SAYAMA, *Robust morphogenesis of robotic swarms*, IEEE Computational Intelligence Magazine, 5 (2010), pp. 43–49.

[348] J. SCHINDELIN, I. ARGANDA-CARRERAS, E. FRISE, V. KAYNIG, M. LONGAIR, T. PIETZSCH, S. PREIBISCH, C. RUEDEN, S. SAALFELD, B. SCHMID, ET AL., *Fiji: an open-source platform for biological-image analysis*, Nature methods, 9 (2012), pp. 676–682.

[349] F. SCHMIDT, B. LIEBCHEN, H. LÖWEN, AND G. VOLPE, *Light-controlled assembly of active colloidal molecules*, The Journal of chemical physics, 150 (2019), p. 094905.

[350] E. SCHNEIDER AND H. STARK, *Optimal steering of a smart active particle*, EPL (Europhysics Letters), 127 (2019), p. 64003.

[351] N. SCHUERGERS, T. LENN, R. KAMPMANN, M. V. MEISSNER, T. ESTEVES, M. TEMERINAC-OTT, J. G. KORVINK, A. R. LOWE, C. W. MULLINEAUX, AND A. WILDE, *Cyanobacteria use micro-optics to sense light direction*, Elife, 5 (2016), p. e12620.

[352] T. D. SEELEY, *The wisdom of the hive: the social physiology of honey bee colonies*, Harvard University Press, 2009.

[353] T. D. SEELEY, S. CAMAZINE, AND J. SNEYD, *Collective decision-making in honey bees: how colonies choose among nectar sources*, Behavioral Ecology and Sociobiology, 28 (1991), pp. 277–290.

[354] G. SEMPO, S. CANONGE, C. DETRAIN, AND J.-L. DENEUBOURG, *Complex dynamics based on a quorum: Decision-making process by cockroaches in a patchy environment*, Ethology, 115 (2009), pp. 1150–1161.

[355] O. I. SENTÜRK, O. SCHAUER, F. CHEN, V. SOURJIK, AND S. V. WEGNER, *Red/far-red light switchable cargo attachment and release in bacteria-driven microswimmers*, Advanced Healthcare Materials, 9 (2020), p. 1900956.

[356] M. SITTI, H. CEYLAN, W. HU, J. GILTINAN, M. TURAN, S. YIM, AND E. DILLER, *Biomedical applications of untethered mobile milli/microrobots*, Proceedings of the IEEE, 103 (2015), pp. 205–224.

[357] M. SITTI AND D. S. WIERSMA, *Pros and cons: Magnetic versus optical microrobots*, Advanced Materials, 32 (2020), p. 1906766.

[358] I. SLAVKOV, D. CARRILLO-ZAPATA, N. CARRANZA, X. DIEGO, F. JANSSON, J. KAANDORP, S. HAUERT, AND J. SHARPE, *Morphogenesis in robot swarms*, Science Robotics, 3 (2018).

[359] A. SNEZHKO AND I. S. ARANSON, *Magnetic manipulation of self-assembled colloidal asters*, Nature materials, 10 (2011), pp. 698–703.

[360] C. A. SOLARI, R. E. MICHOD, AND R. E. GOLDSTEIN, *Volvox barberi, the fastest swimmer of the volvocales (chlorophyceae) 1*, Journal of phycology, 44 (2008), pp. 1395–1398.

[361] A. A. SOLOVEV, S. SANCHEZ, AND O. G. SCHMIDT, *Collective behaviour of self-propelled catalytic micromotors*, Nanoscale, 5 (2013), pp. 1284–1293.

[362] M. D. SOORATI, M. K. HEINRICH, J. GHOFRANI, P. ZAHADAT, AND H. HAMANN, *Photomorphogenesis for robot self-assembly: adaptivity, collective decision-making, and self-repair*, Bioinspiration & biomimetics, 14 (2019), p. 056006.

[363] F. SOTO, E. KARSHALEV, F. ZHANG, B. ESTEBAN FERNANDEZ DE AVILA, A. NOURHANI, AND J. WANG, *Smart materials for microrobots*, Chemical Reviews, (2021).

[364] W. W. SPRENGER, W. D. HOFF, J. P. ARMITAGE, AND K. J. HELLINGWERF, *The eubacterium ectothiorhodospira halophila is negatively phototactic, with a wavelength dependence that fits the absorption spectrum of the photoactive yellow protein.*, Journal of bacteriology, 175 (1993), pp. 3096–3104.

[365] S. K. SRIVASTAVA, G. CLERGEAUD, T. L. ANDRESEN, AND A. BOISEN, *Micromotors for drug delivery in vivo: The road ahead*, Advanced drug delivery reviews, 138 (2019), pp. 41–55.

[366] E. B. STEAGER, D. WONG, N. CHODOSH, AND V. KUMAR, *Optically addressing microscopic bioactuators for real-time control*, in 2015 IEEE International Conference on Robotics and Automation (ICRA), IEEE, 2015, pp. 3519–3524.

[367] H. STEEL, R. HABGOOD, C. L. KELLY, AND A. PAPACHRISTODOULOU, *In situ characterisation and manipulation of biological systems with chi. bio*, PLoS biology, 18 (2020), p. e3000794.

[368] P. S. STEWART AND J. W. COSTERTON, *Antibiotic resistance of bacteria in biofilms*, The lancet, 358 (2001), pp. 135–138.

[369] J. N. STIRMAN, M. M. CRANE, S. J. HUSSON, A. GOTTSCHALK, AND H. LU, *A multispectral optical illumination system with precise spatiotemporal control for the manipulation of optogenetic reagents*, Nature protocols, 7 (2012), p. 207.

[370] G. STOYCHEV, A. KIRILLOVA, AND L. IONOV, *Light-responsive shape-changing polymers*, Advanced Optical Materials, 7 (2019), p. 1900067.

[371] J. SUDD, *The transport of prey by ants*, Behaviour, 25 (1965), pp. 234–271.

[372] K. SUGAWARA, T. KAZAMA, AND T. WATANABE, *Foraging behavior of interacting robots with virtual pheromone*, in 2004 IEEE/RSJ International Conference on Intelligent Robots and Systems (IROS)(IEEE Cat. No. 04CH37566), vol. 3, IEEE, 2004, pp. 3074–3079.

[373] R. SUZUKI, J. KATO, M. D. GROSS, AND T. YEH, *Reactile: Programming swarm user interfaces through direct physical manipulation*, in Proceedings of the 2018 CHI Conference on Human Factors in Computing Systems, 2018, pp. 1–13.

[374] M. E. TAGA AND B. L. BASSLER, *Chemical communication among bacteria*, Proceedings of the National Academy of Sciences, 100 (2003), pp. 14549–14554.

[375] Y. TAO, H. F. CHAN, B. SHI, M. LI, AND K. W. LEONG, *Light: A magical tool for controlled drug delivery*, Advanced Functional Materials, 30 (2020), p. 2005029.

[376] A. TERO, S. TAKAGI, T. SAIGUSA, K. ITO, D. P. BEBBER, M. D. FRICKER, K. YUMIKI, R. KOBAYASHI, AND T. NAKAGAKI, *Rules for biologically inspired adaptive network design*, Science, 327 (2010), pp. 439–442.

[377] G. THALHAMMER, R. STEIGER, S. BERNET, AND M. RITSCH-MARTE, *Optical macro-tweezers: trapping of highly motile micro-organisms*, Journal of Optics, 13 (2011), p. 044024.

[378] G. THERAULAZ AND E. BONABEAU, *A brief history of stigmergy*, Artificial life, 5 (1999), pp. 97–116.

[379] G. THERAULAZ, E. BONABEAU, AND J. DENUEBOURG, *Response threshold reinforcements and division of labour in insect societies*, Proceedings of the Royal Society of London. Series B: Biological Sciences, 265 (1998), pp. 327–332.

[380] J. F. TRANIELLO AND R. B. ROSENGAUS, *Ecology, evolution and division of labour in social insects*, Animal behaviour, 53 (1997), pp. 209–213.

[381] R. L. TRELSTAD, E. D. HAY, AND J.-P. REVEL, *Cell contact during early morphogenesis in the chick embryo*, Developmental biology, 16 (1967), pp. 78–106.

[382] A. E. TURGUT, H. ÇELIKKANAT, F. GÖKÇE, AND E. ŞAHIN, *Self-organized flocking in mobile robot swarms*, Swarm Intelligence, 2 (2008), pp. 97–120.

[383] N. UEKI, S. MATSUNAGA, I. INOUYE, AND A. HALLMANN, *How 5000 independent rowers coordinate their strokes in order to row into the sunlight: Phototaxis in the multicellular green alga volvox*, BMC biology, 8 (2010), pp. 1–21.

[384] M. T. VALENTINE, N. R. GUYDOSH, B. GUTIÉRREZ-MEDINA, A. N. FEHR, J. O. ANDREASSON, AND S. M. BLOCK, *Precision steering of an optical trap by electro-optic deflection*, Optics letters, 33 (2008), pp. 599–601.

[385] J. K. VALLEY, A. JAMSHIDI, A. T. OHTA, H.-Y. HSU, AND M. C. WU, *Operational regimes and physics present in optoelectronic tweezers*, Journal of Microelectromechanical Systems, 17 (2008), pp. 342–350.

[386] J. K. VALLEY, S. NEALE, H.-Y. HSU, A. T. OHTA, A. JAMSHIDI, AND M. C. WU, *Parallel single-cell light-induced electroporation and dielectrophoretic manipulation*, Lab on a Chip, 9 (2009), pp. 1714–1720.

[387] S. VERMA, G. NOVATI, AND P. KOUMOUTSAKOS, *Efficient collective swimming by harnessing vortices through deep reinforcement learning*, Proceedings of the National Academy of Sciences, 115 (2018), pp. 5849–5854.

[388] T. VICSEK AND A. ZAFEIRIS, *Collective motion*, Physics reports, 517 (2012), pp. 71–140.

[389] K. VILLA, F. NOVOTNÝ, J. ZELENKA, M. P. BROWNE, T. RUML, AND M. PUMERA, *Visible-light-driven single-component bivo4 micromotors with the autonomous ability for capturing microorganisms*, ACS nano, 13 (2019), pp. 8135–8145.

[390] K. VILLA AND M. PUMERA, *Fuel-free light-driven micro/nanomachines: artificial active matter mimicking nature*, Chemical Society Reviews, 48 (2019), pp. 4966–4978.

[391] K. VISSCHER, S. P. GROSS, AND S. M. BLOCK, *Construction of multiple-beam optical traps with nanometer-resolution position sensing*, IEEE journal of selected topics in quantum electronics, 2 (1996), pp. 1066–1076.

[392] G. VIZSNYICZAI, G. FRANGIPANE, C. MAGGI, F. SAGLIMBENI, S. BIANCHI, AND R. DI LEONARDO, *Light controlled 3d micromotors powered by bacteria*, Nature communications, 8 (2017), pp. 1–7.

[393] G. VON MALTZAHN, J.-H. PARK, K. Y. LIN, N. SINGH, C. SCHWÖPPE, R. MESTERS, W. E. BERDEL, E. RUOSLAHTI, M. J. SAILOR, AND S. N. BHATIA, *Nanoparticles that communicate in vivo to amplify tumour targeting*, Nature materials, 10 (2011), pp. 545–552.

[394] J. M. WALTER, D. GREENFIELD, C. BUSTAMANTE, AND J. LIPHARDT, *Light-powering escherichia coli with proteorhodopsin*, Proceedings of the National Academy of Sciences, 104 (2007), pp. 2408–2412.

[395] G. WANDREY, C. BIER, D. BINDER, K. HOFFMANN, K.-E. JAEGER, J. PIETRUSZKA, T. DREPPER, AND J. BÜCHS, *Light-induced gene expression with photocaged iptg for induction profiling in a high-throughput screening system*, Microbial cell factories, 15 (2016), p. 63.

[396] H.-Y. WANG, C.-Y. CHEN, P.-Y. CHU, Y.-X. ZHU, C.-H. HSIEH, J.-J. LU, AND M.-H. WU, *Application of an optically induced dielectrophoresis (odep)-based microfluidic system for the detection and isolation of bacteria with heterogeneity of antibiotic susceptibility*, Sensors and Actuators B: Chemical, 307 (2020), p. 127540.

[397] L. WANG, A. KAEPPLER, D. FISCHER, AND J. SIMMCHEN, *Photocatalytic tio2 micromotors for removal of microplastics and suspended matter*, ACS applied materials & interfaces, 11 (2019), pp. 32937–32944.

[398] X. WANG, L. HE, Y. I. WU, K. M. HAHN, AND D. J. MONTELL, *Light-mediated activation reveals a key role for rac in collective guidance of cell movement in vivo*, Nature cell biology, 12 (2010), pp. 591–597.

[399] Y. WANG, P. BROWN, AND Y. XIA, *Swarming towards the target*, Nature Materials, 10 (2011), pp. 482–483.

[400] O. M. WANI, H. ZENG, AND A. PRIIMAGI, *A light-driven artificial flytrap*, Nature communications, 8 (2017), pp. 1–7.

[401] H. WEI, Y. CAI, H. LI, D. LI, AND T. WANG, *Sambot: A self-assembly modular robot for swarm robot*, in 2010 IEEE International Conference on Robotics and Automation, IEEE, 2010, pp. 66–71.

[402] M. WEITZMAN AND K. M. HAHN, *Optogenetic approaches to cell migration and beyond*, Current opinion in cell biology, 30 (2014), pp. 112–120.

[403] S. A. WEST, K. WINZER, A. GARDNER, AND S. P. DIGGLE, *Quorum sensing and the confusion about diffusion*, Trends in microbiology, 20 (2012), pp. 586–594.

[404] D. WEUSTER-BOTZ, *Parallel reactor systems for bioprocess development*, Technology transfer in biotechnology, (2005), pp. 125–143.

[405] R. C. WHYTOCK AND J. CHRISTIE, *Solo: an open source, customizable and inexpensive audio recorder for bioacoustic research*, Methods in Ecology and Evolution, 8 (2017), pp. 308–312.

[406] L. E. WICKERT, S. POMERENKE, I. MITCHELL, K. S. MASTERS, AND P. K. KREEGER, *Hierarchy of cellular decisions in collective behavior: Implications for wound healing*, Scientific reports, 6 (2016), pp. 1–9.

[407] B. WIJNEN, E. J. HUNT, G. C. ANZALONE, AND J. M. PEARCE, *Open-source syringe pump library*, PloS one, 9 (2014), p. e107216.

[408] A. WILDE AND C. W. MULLINEAUX, *Light-controlled motility in prokaryotes and the problem of directional light perception*, FEMS microbiology reviews, 41 (2017), pp. 900–922.

[409] A. F. WINFIELD, C. J. HARPER, AND J. NEMBRINI, *Towards dependable swarms and a new discipline of swarm engineering*, in International Workshop on Swarm Robotics, Springer, 2004, pp. 126–142.

[410] G. B. WITMAN, *Chlamydomonas phototaxis*, Trends in cell biology, 3 (1993), pp. 403–408.

[411] A. WIXFORTH, C. STROBL, C. GAUER, A. TOEGL, J. SCRIBA, AND Z. V. GUTTENBERG, *Acoustic manipulation of small droplets*, Analytical and bioanalytical chemistry, 379 (2004), pp. 982–991.

[412] J. WU, D. DELLAL, AND S. WASSERMAN, *Prokaryote playhouse: a low-cost, laser-cut acrylic incubator for optogenetic bacterial culture*, HardwareX, (2021), p. e00184.

[413] M. C. WU, *Optoelectronic tweezers*, Nature Photonics, 5 (2011), pp. 322–324.

[414] X. WU, X. XUE, J. WANG, AND H. LIU, *Phototropic aggregation and light-guided long-distance collective transport of colloidal particles*, Langmuir, 36 (2020), pp. 6819–6827.

[415] Y. I. WU, D. FREY, O. I. LUNGU, A. JAEHRIG, I. SCHLICHTING, B. KUHLMAN, AND K. M. HAHN, *A genetically encoded photoactivatable rac controls the motility of living cells*, Nature, 461 (2009), pp. 104–108.

[416] Y. XIE AND C. ZHAO, *An optothermally generated surface bubble and its applications*, Nanoscale, 9 (2017), pp. 6622–6631.

[417] L. XU, F. MOU, H. GONG, M. LUO, AND J. GUAN, *Light-driven micro/nanomotors: from fundamentals to applications*, Chemical Society Reviews, 46 (2017), pp. 6905–6926.

[418] M. XUAN, J. SHAO, C. GAO, W. WANG, L. DAI, AND Q. HE, *Self-propelled nanomotors for thermomechanically percolating cell membranes*, Angewandte Chemie International Edition, 57 (2018), pp. 12463–12467.

[419] J. YAN AND B. L. BASSLER, *Surviving as a community: antibiotic tolerance and persistence in bacterial biofilms*, Cell host & microbe, 26 (2019), pp. 15–21.

[420] M. YAZAWA, A. M. SADAGHIANI, B. HSUEH, AND R. E. DOLMETSCH, *Induction of protein-protein interactions in live cells using light*, Nature biotechnology, 27 (2009), pp. 941–945.

[421] B. YIGIT, Y. ALAPAN, AND M. SITTI, *Programmable collective behavior in dynamically self-assembled mobile microrobotic swarms*, Advanced Science, 6 (2019), p. 1801837.

[422] J. ZEMÁNEK, T. MICHÁLEK, AND Z. HURÁK, *Feedback control for noise-aided parallel micromanipulation of several particles using dielectrophoresis*, Electrophoresis, 36 (2015), pp. 1451–1458.

[423] H. ZENG, O. M. WANI, P. WASYLCZYK, AND A. PRIIMAGI, *Light-driven, caterpillar-inspired miniature inching robot*, Macromolecular rapid communications, 39 (2018), p. 1700224.

[424] C. ZHANG, K. KHOSHMANESH, A. MITCHELL, AND K. KALANTAR-ZADEH, *Dielectrophoresis for manipulation of micro/nano particles in microfluidic systems*, Analytical and bioanalytical chemistry, 396 (2010), pp. 401–420.

[425] J. ZHANG, J. GUO, F. MOU, AND J. GUAN, *Light-controlled swarming and assembly of colloidal particles*, Micromachines, 9 (2018), p. 88.

[426] J. ZHANG, Y. LUO, AND C. L. POH, *Blue light-directed cell migration, aggregation, and patterning*, Journal of Molecular Biology, (2020).

[427] J. ZHANG, Q. ZOU, AND H. TIAN, *Photochromic materials: more than meets the eye*, Advanced Materials, 25 (2013), pp. 378–399.

[428] K. ZHANG AND B. CUI, *Optogenetic control of intracellular signaling pathways*, Trends in biotechnology, 33 (2015), pp. 92–100.

[429] K. ZHANG, A. JIAN, X. ZHANG, Y. WANG, Z. LI, AND H.-Y. TAM, *Laser-induced thermal bubbles for microfluidic applications*, Lab on a Chip, 11 (2011), pp. 1389–1395.

[430] S. ZHANG, J. JUVERT, J. M. COOPER, AND S. L. NEALE, *Manipulating and assembling metallic beads with optoelectronic tweezers*, Scientific reports, 6 (2016), pp. 1–10.

[431] X. ZHANG, L. MA, AND Y. ZHANG, *High-resolution optical tweezers for single-molecule manipulation*, The Yale journal of biology and medicine, 86 (2013), p. 367.

[432] Y. ZHANG, K. YUAN, AND L. ZHANG, *Micro/nanomachines: from functionalization to sensing and removal*, Advanced Materials Technologies, 4 (2019), p. 1800636.

[433] Z. ZHANG, *A flexible new technique for camera calibration*, IEEE Transactions on pattern analysis and machine intelligence, 22 (2000), pp. 1330–1334.

[434] C. ZHAO, Y. XIE, Z. MAO, Y. ZHAO, J. RUFO, S. YANG, F. GUO, J. D. MAI, AND T. J. HUANG, *Theory and experiment on particle trapping and manipulation via optothermally generated bubbles*, Lab on a Chip, 14 (2014), pp. 384–391.

[435] J. ZHENG, B. DAI, J. WANG, Z. XIONG, Y. YANG, J. LIU, X. ZHAN, Z. WAN, AND J. TANG, *Orthogonal navigation of multiple visible-light-driven artificial microswimmers*, Nature communications, 8 (2017), pp. 1–7.

[436] L. ZHENG, L.-G. CHEN, H.-B. HUANG, X.-P. LI, AND L.-L. ZHANG, *An overview of magnetic micro-robot systems for biomedical applications*, Microsystem Technologies, 22 (2016), pp. 2371–2387.

[437] B. ZUO, M. WANG, B.-P. LIN, AND H. YANG, *Photomodulated tricolor-changing artificial flowers*, Chemistry of Materials, 30 (2018), pp. 8079–8088.